

**SECONDARY FORMATION OF ORGANIC AEROSOL:
INVESTIGATION OF THE DIURNAL VARIATIONS
OF ORGANIC AND ELEMENTAL CARBON**

**Barbara J. Turpin
B.S., California Institute of Technology, 1984**

**A dissertation submitted to the faculty
of the Oregon Graduate Center
in partial fulfillment of the
requirements for the degree
Doctor of Philosophy
in
Environmental Science and Engineering**

July, 1989

The dissertation "Secondary Formation of Organic Aerosol: Investigation of the Diurnal Variations of Organic and Elemental Carbon" by Barbara Jo Turpin has been examined and approved by the following Examination Committee:

James J. Muntzicker, Thesis Advisor
OGC Sr. Vice President, Professor

James F. Pankow
Department Chairman, Professor

Richard L. Johnson
Assistant Professor

Robert J. O'Brien
Adjunct Faculty, Portland State U.

William Fish
Assistant Professor

DEDICATION

Surely, if I won a gold medal in epee, I would dedicate it to Dave Younge and Jim Huntzicker for their understanding and encouragement. Likewise, I dedicate my dissertation to those who have helped me maintain my sanity and my enthusiasm for science by means of diversion.

Their efforts began around a fire on a foggy beach and spread to consume Tacoma, Mt. Rainier National Park, and crab cocktail. They journeyed with me through the House of Cats, Camels, and Couches, exploring the secrets of Rubio Canyon and the depths of the Huntington Gardens. Their dedication, encouragement, friendship and funding transformed my back-woods fencing hobby into a rewarding form of self-expression which is teaching me patience, concentration, the psychology of success, and how to ask "Where is the bathroom" in many languages. They have inspired me with song, sharpened me through daily banter, and strengthened me with the energy of periodic gatherings.

To all of you: gracias, dziekuje, koszonom, merci and thank you - don't stop now.

ACKNOWLEDGMENT

This research was made possible through funding from the California Air Resources Board (Contracts A5-149-32 and A732-072) and the Motor Vehicle Manufacturers Association (Contract OGC8725-7120C). Discussions with Ken Hart, Steve McDow, John Storey, Paul Roberts and Susanne Hering are gratefully appreciated. The many hours of GC/MS analyses performed by Mary Ligocki and Ken Hart, as well as the assistance provided in the field by Don Buchholz, John Rau, Doug Lawson, Fritz Nordby, Steve Gomez, Gervase McKay, Dave Finley and Janice Green were invaluable. The help provided in the laboratory by Allan Ryall, Gerry Boehme, Lorne Isabelle and Bill Asher and the help provided on the document by Julie Wilson, Barbara Ryall, Carol Hendrickson, Judi Irvine, Laura Maskell and Bob Marx are gratefully appreciated. The direction of my committee: Jim Pankow, Rick Johnson, Bob O'Brien and Bill Fish and the direction of the California Air Resources Board and the Coordinating Research Council in the development and implementation of CSMCS and SCAQS projects are gratefully acknowledged. Most of all, the direction, support, and friendship of my advisor, Jim Huntzicker, has made this research experience a rewarding one.

TABLE OF CONTENTS

	Page
Approval	iii
Dedication	iv
Acknowledgments	v
Table of Contents	vi
List of Tables	x
List of Figures	xiii
Glossary of Abbreviations	xxii
Glossary of Symbols	xxiv
Abstract	xxvi
Chapter 1. INTRODUCTION	1
Chapter 2. HANDLING AND THERMAL-OPTICAL CARBON ANALYSIS OF MANUALLY COLLECTED SAMPLES	9
Introduction	9
Sample Handling	9
Thermal-Optical Carbon Analysis Method	10
Blanks	13
External Standards	15
Uncertainties	16
Round Robin Study	16

Contents (continued):		Page
Chapter 3.	PRELIMINARY STUDY: AN INVESTIGATION OF LOS ANGELES MID-DAY PARTICULATE CARBON	19
	Introduction	19
	Experimental	20
	Results	24
	Summary	49
Chapter 4.	AN <u>IN SITU</u>, TIME-RESOLVED ANALYZER FOR AEROSOL ORGANIC AND ELEMENTAL CARBON	50
	Introduction	50
	The <u>In Situ</u> Carbon Analyzer	51
	Instrument Characterization	60
	Carbonaceous Species Methods Comparison Study Sampling	70
	CSMCS Data Treatment	71
	Comparison With Conventional Sampling and Analysis	72
	Ambient Measurements	78
Chapter 5.	INTERCOMPARISON OF PHOTOACOUSTIC AND THERMAL-OPTICAL METHODS FOR THE MEASUREMENT OF ATMOSPHERIC ELEMENTAL CARBON	85
	Introduction	85
	Photoacoustic Spectrometer	86
	Thermal-Optical Carbon Analyzer	88
	Ambient Sampling	89

Contents (continued)	Page
Results	89
Summary	90
Chapter 6. ORGANIC AEROSOL SAMPLING ARTIFACTS IN LOS ANGELES	93
Introduction	93
Filter Surface Area	95
Face Velocity Experiments	96
Results	101
CSMCS Dilution Experiment	124
SCAQS Dilution Experiment	130
Laboratory Experiments	141
Results	141
Summary	145
Chapter 7. GC/MS STUDY OF ORGANIC COMPOUNDS ON AEROSOL AND BACKUP FILTERS	152
Introduction	152
Thermal Desorption/Gas Chromatography/ Mass Spectroscopy	153
Results	154
Chapter 8. SECONDARY FORMATION OF ORGANIC AEROSOL: INVESTIGATION OF THE DIURNAL VARIATIONS OF ORGANIC AND ELEMENTAL CARBON IN THE LOS ANGELES BASIN	160
Introduction	160
Experimental	161

Contents (continued)	Page
SCAQS Meteorology	168
Primary and Secondary Organic Aerosol	170
Conclusion	187
Chapter 9. SUMMARY AND CONCLUSIONS	190
Summary	190
Conclusions	195
Recommendations	195
References	197
Appendix A. Ford Photoacoustic and OGC Thermal-Optical Elemental Carbon Data Used for Intercomparison	202
Appendix B. GC/MS Results	204
Appendix C. SCAQS Bromine and Lead Concentrations	213
Appendix D. Data Validation Tests for SCAQS <u>In Situ</u> Data	221
Appendix E. SCAQS Organic Carbon, Elemental Carbon, and Ozone Concentrations with Meteorological Data at Claremont, California, June 12 - September 2, 1987 and at Long Beach, California, November 6 - December 13, 1987.	224
Vita	257

LIST OF TABLES

	Page
Table 2.1. Laboratory Carbon Analysis Time Sequence	12
Table 2.2. Laboratory Carbon Analyzer Uncertainties	17
Table 3.1. Site Specific Ozone and Secondary Organic Carbon Data	25
Table 3.2. Correlations Between Pasadena Data	28
Table 3.3. Average Organic Carbon Values	48
Table 4.1. Regression Results for <u>In Situ</u> Carbon Analyzer Flame Ionization Detector Response (counts/counts in calibration peak) as a Function of Mass of Methane Injected (μgC)	62
Table 4.2. Regression Results for Comparison of <u>In Situ</u> and Manual Methods	77
Table 6.1. BET Surface Area Measurements	97
Table 6.2. Regression Results for Comparison of Two-Port (43 cm/s) and Face Velocity Sampler (40 cm/s) Backup Filters	104
Table 6.3. Regression Results for Comparison of Face Velocity Sampler Backup Filters	112
Table 6.4. Regression Results for Comparison of Face Velocity Sampler Front Filters	119
Table 6.5. Comparison of the Face Velocity Dependence of Carbon Loading for Portland and CSMCS Glendora, California, Experiments	121

Tables (continued)	Page
Table 6.6. Regression Results for Comparison of 20 cm/s Quartz - Quartz Front Filter (QQF(20)) and 40 cm/s Quartz - Quartz Front Plus Backup Filter (QQF(40) + QQB(40)) Concentrations ($\mu\text{gC}/\text{m}^3$)	123
Table 6.7. Regression Results for Comparison of Teflon - Quartz Backup Filter Data of Different Face Velocities but the Same Exposed Surface Area	125
Table 6.8. Percentage of Input Air Stripped of Aerosol	127
Table 6.9. CSMCS Dilution Experiment Organic Carbon Loadings ($\mu\text{gC}/\text{cm}^2$)	128
Table 6.10. Relative Artifact Contributions Determined from Dilution Experiment	131
Table 6.11. Comparison of SCAQS Dilution Experiment Final Backup Filter Concentrations	134
Table 6.12. Results of SCAQS Dilution Experiment	140
Table 6.13. Regression Results for the Laboratory Vapor Artifact Experiment: Aerosol Loading (μg) as a Function of Collection Time (min)	144
Table 6.14. Regression Results for Comparison of Adsorbed Vapor and Particulate Organic Carbon Loadings ($\mu\text{gC}/\text{cm}^2$)	150
Table 7.1. Comparison of QQ Front and Backup Filters with TQ Backups for the Major Compound Classes	156
Table 7.2. Averages for Alkanes: QQF, TQB, and QQF/TQB (ng/m^3)	158
Table 8.1. Coefficients of Determination (R^2) for Selected SCAQS Data	174
Table 8.2. Summary Data for August 25 - 31	176
Table 8.3. Summary of Data for November 17 - 19	185

Tables (continued)		Page
Table A.1.	Ford Photoacoustic and OGC Thermal-Optical Elemental Carbon Data Used For Intercomparison	202
Table B.1.	Grand Averages (ng/m³)	204
Table B.2.	Daytime Averages CSMCS GC/MS (ng/m³)	207
Table B.3.	Nighttime Averages CSMCS GC/MS (ng/m³)	210
Table C.1.	Retention Of Pollutants From Previous Days As Indicated By Lead And Br/Pb	220
Table D.1.	Level I Validation	222

LIST OF FIGURES

	Page
Figure 2.1. Typical output for laboratory thermal-optical carbon analyzer.	14
Figure 3.1. Schematic of the Los Angeles Basin showing 1984 field study sites.	22
Figure 3.2. Comparison of standard normal variates of secondary organic carbon and elemental carbon concentrations at Pasadena, California, July 5 - September 27, 1984.	30
Figure 3.3. Comparison of standard normal variates of secondary organic carbon and lead concentrations at Pasadena, California, July 5 - September 27, 1984.	31
Figure 3.4. Comparison of standard normal variates of elemental carbon and lead concentrations at Pasadena, California, July 5 - September 27, 1984.	32
Figure 3.5. Comparison of standard normal variates of secondary organic carbon and ozone concentrations at Pasadena, California, July 5 - September 27, 1984.	34
Figure 3.6. Comparison of standard normal variates of nitrate and ozone concentrations at Pasadena, California, July 5 - September 27, 1984.	35
Figure 3.7. Comparison of standard normal variates of secondary organic carbon and nitrate concentrations at Pasadena, California, July 5 - September 27, 1984.	36
Figure 3.8. Ambient ratios of organic to elemental carbon for particles under 2.0 μm in diameter at Lennox, California, July 5 - September 27, 1984.	38
Figure 3.9. Ambient ratios of organic to elemental carbon for particles under 2.0 μm in diameter at Pasadena, California, July 5 - September 27, 1984.	39

Figures (continued)	Page
Figure 3.10. Ambient ratios of organic to elemental carbon for particles under 2.0 μm in diameter at Azusa, California, July 5 - September 27, 1984.	40
Figure 3.11. Ambient ratios of organic to elemental carbon for particles under 2.0 μm in diameter at Upland, California, July 5 - September 27, 1984.	41
Figure 3.12. Ambient ratios of organic to elemental carbon for particles under 2.0 μm in diameter at San Bernardino, California, July 5 - September 27, 1984.	42
Figure 3.13. Total organic carbon concentrations and maximum and minimum primary organic carbon concentration estimates ($\mu\text{gC}/\text{m}^3$) for particles under 2.0 μm in diameter at Lennox, California, July 5 - September 27, 1984.	43
Figure 3.14. Total organic carbon concentrations and maximum and minimum primary organic carbon concentration estimates ($\mu\text{gC}/\text{m}^3$) for particles under 2.0 μm in diameter at Pasadena, California, July 5 - September 27, 1984.	44
Figure 3.15. Total organic carbon concentrations and maximum and minimum primary organic carbon concentration estimates ($\mu\text{gC}/\text{m}^3$) for particles under 2.0 μm in diameter at Azusa, California, July 5 - September 27, 1984.	45
Figure 3.16. Total organic carbon concentrations and maximum and minimum primary organic carbon concentration estimates ($\mu\text{gC}/\text{m}^3$) for particles under 2.0 μm in diameter at Upland, California, July 5 - September 27, 1984.	46
Figure 3.17. Total organic carbon concentrations and maximum and minimum primary organic carbon concentration estimates ($\mu\text{gC}/\text{m}^3$) for particles under 2.0 μm in diameter at San Bernardino, California, July 5 - September 27, 1984.	47
Figure 4.1. <u>In situ</u> carbon analyzer analytical unit with tubing diagram, top view.	52
Figure 4.2. <u>In situ</u> carbon analyzer analytical unit, side view.	53
Figure 4.3. Schematic of <u>in situ</u> carbon analyzer.	54
Figure 4.4. Filter mounting system for <u>in situ</u> carbon analyzer.	56

Figures (continued)	Page
Figure 4.5. Typical output for <u>in situ</u> carbon analyzer.	59
Figure 4.6. <u>In situ</u> carbon analyzer methane injection experiment instrument response (flame ionization detector counts/counts in calibration peak) as a function of mass of carbon injected (μgC).	61
Figure 4.7. Typical <u>in situ</u> carbon analyzer output for a sucrose aerosol collection.	66
Figure 4.8. Comparison of optical absorbance ($-\text{Ln}(I/I_0)$) and elemental carbon loading ($\mu\text{gC}/\text{cm}^2$) for the <u>in situ</u> carbon analyzer.	69
Figure 4.9. Comparison of <u>in situ</u> and manual sampler results ($\mu\text{gC}/\text{m}^3$) for total particulate carbon.	74
Figure 4.10. Comparison of <u>in situ</u> and manual sampler results ($\mu\text{gC}/\text{m}^3$) for particulate organic carbon.	75
Figure 4.11. Comparison of <u>in situ</u> and manual sampler results ($\mu\text{gC}/\text{m}^3$) for elemental carbon.	76
Figure 4.12. Twelve hour average concentrations ($\mu\text{gC}/\text{m}^3$) of particulate organic (OC), elemental (EC), and total carbon (TC) for particles under $2.5 \mu\text{m}$ in diameter at Glendora, California, August 12-21, 1986.	79
Figure 4.13. Total particulate carbon concentrations ($\mu\text{gC}/\text{m}^3$) for particles under $2.5 \mu\text{m}$ in diameter at Glendora, California, August 12-21, 1986.	80
Figure 4.14. Concentrations of ozone (pphm), particulate organic carbon ($\mu\text{gC}/\text{m}^3$), and particulate elemental carbon ($\mu\text{gC}/\text{m}^3$) at Glendora, California, August 19, 1986.	82
Figure 4.15. Concentrations of ozone (pphm), particulate organic carbon ($\mu\text{gC}/\text{m}^3$) at Glendora, California, August 20, 1986.	83
Figure 5.1. Comparison of elemental carbon concentrations ($\mu\text{gC}/\text{m}^3$) measured by Ford Motor Company photoacoustic spectrometer and Oregon Graduate Center <u>in situ</u> thermal-optical carbon analyzer.	91
Figure 6.1. Six port filter sampler used in face velocity experiment.	98

Figures (continued)	Page
Figure 6.2. Aerosol filter holder with annular masks used in face velocity experiment.	100
Figure 6.3. Comparison of quartz fiber backup filters behind Teflon front filters for two-port (43 cm/s) and 40 cm/s face velocity samples.	102
Figure 6.4. Comparison of quartz fiber backup filters behind quartz fiber front filters for two-port (43 cm/s) and 40 cm/s face velocity samples.	103
Figure 6.5. Organic carbon concentrations ($\mu\text{gC}/\text{m}^3$) on quartz fiber backup filters behind Teflon front filters for face velocities of 20, 40 and 80 cm/s.	105
Figure 6.6. Organic carbon concentrations ($\mu\text{gC}/\text{m}^3$) on quartz fiber backup filters behind quartz fiber front filters for face velocities of 20 and 40 cm/s.	106
Figure 6.7. Comparison of organic carbon concentrations ($\mu\text{gC}/\text{m}^3$) at face velocities of 20 and 40 cm/s for quartz fiber backup filters behind Teflon front filters.	107
Figure 6.8. Comparison of organic carbon concentrations ($\mu\text{gC}/\text{m}^3$) at face velocities of 40 and 80 cm/s for quartz fiber backup filters behind Teflon front filters.	108
Figure 6.9. Comparison of organic carbon concentrations ($\mu\text{gC}/\text{m}^3$) at face velocities of 20 and 40 cm/s for quartz fiber backup filters behind quartz fiber front filters.	109
Figure 6.10. Comparison of organic carbon concentrations ($\mu\text{gC}/\text{m}^3$) for quartz fiber backup filters behind quartz fiber front filters (QQ) and quartz fiber backup filters behind Teflon front filters (TQ) at a face velocity of 20 cm/s.	110
Figure 6.11. Comparison of organic carbon concentrations ($\mu\text{gC}/\text{m}^3$) for quartz fiber backup filters behind quartz fiber front filters (QQ) and quartz fiber backup filters behind Teflon front filters (TQ) at a face velocity of 40 cm/s.	111

Figures (continued)	Page
Figure 6.12. Twelve hour average concentrations ($\mu\text{gC}/\text{m}^3$) of particulate organic (OC), elemental (EC), and total carbon (TC) in particles under $1.0 \mu\text{m}$ in diameter at Glendora, California, August 12-21, 1986.	114
Figure 6.13. Comparison of elemental carbon concentrations ($\mu\text{gC}/\text{m}^3$) for quartz fiber front filters at face velocities of 20 and 40 cm/s.	116
Figure 6.14. Comparison of organic carbon concentrations ($\mu\text{gC}/\text{m}^3$) for quartz fiber front filters at face velocities of 20 and 40 cm/s.	117
Figure 6.15. Comparison of "artifact corrected," particulate organic carbon concentrations (POC) ($\mu\text{gC}/\text{m}^3$) at face velocities of 20 and 40 cm/s.	118
Figure 6.16. Comparison of organic carbon concentrations ($\mu\text{gC}/\text{m}^3$) on 20 cm/s quartz-quartz front filters (QQF(20)) and on the sum of 40 cm/s quartz-quartz front and backup filters (QQF(40) + QQB(40)).	122
Figure 6.17. Southern California Air Quality Study dilution experiment organic carbon concentrations ($\mu\text{gC}/\text{m}^3$), December 5, 2200 hours - December 6, 1000 hours, 1987.	136
Figure 6.18. Southern California Air Quality Study dilution experiment organic carbon concentrations ($\mu\text{gC}/\text{m}^3$), December 7, 1000-2200 hours, 1987.	137
Figure 6.19. Southern California Air Quality Study dilution experiment organic carbon concentrations ($\mu\text{gC}/\text{m}^3$), December 9, 1000-2200 hours, 1987.	138
Figure 6.20. Southern California Air Quality Study dilution experiment organic carbon concentrations ($\mu\text{gC}/\text{m}^3$), December 9, 2200 hours - December 10, 1000 hours, 1987.	139
Figure 6.21. Aerosol total carbon and adsorbed vapor loadings (μg) as a function of collection time (min) in laboratory vapor saturation experiment.	142
Figure 6.22. Expanded view of adsorbed vapor loading (μg) as a function of collection time (min) in laboratory vapor saturation experiment.	143

Figures (continued)	Page
Figure 6.23. Adsorbed vapor as a function of particulate organic carbon loading ($\mu\text{gC}/\text{cm}^2$) for 20 cm/s Carbonaceous Species Methods Comparison Study face velocity samples.	146
Figure 6.24. Adsorbed vapor as a function of particulate organic carbon loading ($\mu\text{gC}/\text{cm}^2$) for 40 cm/s Carbonaceous Species Methods Comparison Study face velocity samples.	147
Figure 6.25. Adsorbed vapor as a function of particulate organic carbon loading ($\mu\text{gC}/\text{cm}^2$) for Carbonaceous Species Methods Comparison Study two-port samples.	148
Figure 6.26. Adsorbed vapor as a function of particulate organic carbon loading ($\mu\text{gC}/\text{cm}^2$) for Carbonaceous Species Methods Comparison Study <u>in situ</u> carbon analyzer samples.	149
Figure 8.1. <u>In situ</u> carbon analyzer laser signal ($-\text{Ln}I/I_0$) as a function of oven temperature (C) for a typical Southern California Air Quality Study instrument blank analysis.	165
Figure 8.2. Optical absorbance ($-\text{Ln}I/I_0$) as a function of elemental carbon loading ($\mu\text{gC}/\text{cm}^2$) for August, 1987, Southern California Air Quality Study data.	166
Figure 8.3. Optical absorbance ($-\text{Ln}I/I_0$) as a function of elemental carbon loading ($\mu\text{gC}/\text{cm}^2$) for November and December, 1987, Southern California Air Quality Study data.	167
Figure 8.4. Schematic of the Los Angeles Basin showing Southern California Air Quality Study sampling sites and streamlines describing the most frequent afternoon surface winds during July (Blumenthal et al, 1974).	169
Figure 8.5. Histogram of time of daily particulate elemental carbon maximum at Claremont, California for Southern California Air Quality Study summer data, 1987.	172
Figure 8.6. Histogram of time of daily particulate organic carbon maximum at Claremont, California for Southern California Air Quality Study summer data, 1987.	173
Figure 8.7. Concentrations of organic and elemental carbon ($\mu\text{gC}/\text{m}^3$), ozone (pphm) and b_{scat} (10^{-4} m^{-1}) for August 25-31, 1987 at Claremont, California.	175

Figures (continued)	Page
Figure 8.8. Coefficients of determination (R^2) between organic and elemental carbon concentrations on August 25-31, 1987 at Claremont, California.	178
Figure 8.9. Estimates of primary and secondary organic aerosol ($\mu\text{gC}/\text{m}^3$) for August 28, 1987 at Claremont, California assuming a primary organic/elemental carbon ratio of 1.4.	181
Figure 8.10. Estimates of primary and secondary organic aerosol ($\mu\text{gC}/\text{m}^3$) for August 28, 1987 at Claremont, California assuming a primary organic/elemental carbon ratio of 2.4.	182
Figure 8.11. Concentrations of organic and elemental carbon ($\mu\text{gC}/\text{m}^3$) for November 17-19, 1987 at Long Beach, California.	184
Figure 8.12. Ratios of organic to elemental carbon at Long Beach, California on November 17-19, 1987.	186
Figure 8.13. Estimates of primary and secondary organic aerosol ($\mu\text{gC}/\text{m}^3$) for August 28, 1987 at Claremont, California assuming that the ambient organic/elemental carbon ratio at Long Beach, California on November 17 describes the primary organic/elemental carbon ratio at Claremont, California on August 28.	188
Figure C.1. Lead concentrations ($\mu\text{g}/\text{m}^3$) and bromine/lead ratios for particles under $2.5 \mu\text{m}$ in diameter at Claremont, California, June 1987.	215
Figure C.2. Lead concentrations ($\mu\text{g}/\text{m}^3$) and bromine/lead ratios for particles under $2.5 \mu\text{m}$ in diameter at Claremont, California, July 1987.	216
Figure C.3. Lead concentrations ($\mu\text{g}/\text{m}^3$) and bromine/lead ratios for particles under $2.5 \mu\text{m}$ in diameter at Claremont, California, August and September, 1987.	217
Figure C.4. Lead concentrations ($\mu\text{g}/\text{m}^3$) and bromine/lead ratios for particles under $2.5 \mu\text{m}$ in diameter at Long Beach, California, November and December, 1987.	218
Figure E.1. Explanation of meteorological symbols.	225
Figure E.2. Total amount of sky coverage (N).	226

Figures (continued)	Page
Figure E.3. Wind speed symbols (ff).	227
Figure E.4. Precipitation symbols (present weather (ww)).	228
Figure E.5. OC, EC, ozone and meteorological data June 15-17, 1987 in Claremont, California.	229
Figure E.6. OC, EC, ozone and meteorological data June 18-20, 1987 in Claremont, California.	230
Figure E.7. OC, EC, ozone and meteorological data June 21-23, 1987, in Claremont, California.	231
Figure E.8. OC, EC, ozone and meteorological data June 24-26, 1987 in Claremont, California.	232
Figure E.9. OC, EC, ozone and meteorological data June 26-28, 1987 in Claremont, California.	233
Figure E.10. OC, EC, ozone and meteorological data July 1-3, 1987 in Claremont, California.	234
Figure E.11. OC, EC, ozone and meteorological data July 6-8, 1987 in Claremont, California.	235
Figure E.12. OC, EC, ozone and meteorological data July 9-11, 1987 in Claremont, California.	236
Figure E.13. OC, EC, ozone and meteorological data July 12-14, 1987 in Claremont, California.	237
Figure E.14. OC, EC, ozone and meteorological data July 15-17, 1987 in Claremont, California.	238
Figure E.15. OC, EC, ozone and meteorological data July 18-20, 1987 in Claremont, California.	239
Figure E.16. OC, EC, ozone and meteorological data July 21-23, 1987 in Claremont, California.	240
Figure E.17. OC, EC, ozone and meteorological data July 24-26, 1987 in Claremont, California.	241
Figure E.18. OC, EC, ozone and meteorological data July 27-29, 1987 in Claremont, California.	242

Figures (continued)	Page
Figure E.19. OC, EC, ozone and meteorological data August 17-19, 1987 in Claremont, California.	243
Figure E.20. OC, EC, ozone and meteorological data August 20-22, 1987 in Claremont, California.	244
Figure E.21. OC, EC, ozone and meteorological data August 23-25, 1987 in Claremont, California.	245
Figure E.22. OC, EC, ozone and meteorological data August 26-28, 1987 in Claremont, California.	246
Figure E.23. OC, EC, ozone and meteorological data August 29-31, 1987 in Claremont, California.	247
Figure E.24. OC, EC, ozone and meteorological data September 1-3, 1987 in Claremont, California.	248
Figure E.25. OC, EC, ozone and meteorological data November 6-8, 1987 in Long Beach, California.	249
Figure E.26. OC, EC, ozone and meteorological data November 11-13, 1987 in Long Beach, California.	250
Figure E.27. OC, EC, ozone and meteorological data November 16-18, 1987 in Long Beach, California.	251
Figure E.28. OC, EC, ozone and meteorological data November 18-20, 1987 in Long Beach, California.	252
Figure E.29. OC, EC, ozone and meteorological data December 2-4, 1987 in Long Beach, California.	253
Figure E.30. OC, EC, ozone and meteorological data December 5-7, 1987 in Long Beach, California.	254
Figure E.31. OC, EC, ozone and meteorological data December 9-11, 1987 in Long Beach, California.	255
Figure E.32. OC, EC, ozone and meteorological data December 10-12, 1987 in Long Beach, California.	256

GLOSSARY OF ABBREVIATIONS

ACHEX	Aerosol Characterization Experiment
BV	ball valve
CSMCS	Carbonaceous Species Methods Comparison Study
D	12 hour daytime samples
DQQ	port containing a quartz fiber filter followed by a quartz fiber filter in which a fraction of the input air has been stripped of particles
ESCA	x-ray photoelectron spectroscopy
EC	elemental carbon
EMSI	Environmental Monitoring and Services, Inc.
FID	flame ionization detector
GC/MS	gas chromatography/mass spectroscopy
i.d.	inner diameter
N	12 hour nighttime samples
OC	organic carbon
OC(20)	organic carbon collected at a face velocity of 20 cm/s
OC(40)	organic carbon collected at a face velocity of 40 cm/s
OGC	Oregon Graduate Center
PAH	polycyclic aromatic hydrocarbon
PDT	Pacific daylight time
POC	particulate organic carbon
pphm	parts per hundred million

PST	Pacific standard time
QQ	port containing a quartz fiber filter followed by a quartz fiber filter
QQB	quartz fiber backup filter in QQ combination
QQF	quartz fiber front filter in QQ combination
QTO	port containing a Teflon filter between two quartz fiber filters
SCAQS	Southern California Air Quality Study
SNV	standard normal variate
SV	solenoid valve
TC	total carbon
TD/GC/MS	thermal desorption/gas chromatography/mass spectroscopy
TQ	port containing a Teflon filter followed by a quartz fiber filter
TQQ	port containing a Teflon filter followed by two quartz fiber filters
TQB	quartz fiber backup filter in TQ combination
XRF	x-ray fluorescence
1/3TQQ	port containing a quartz fiber filter followed by a quartz fiber filter where 1/3 of the input air has been stripped of particles
2/3TQQ	port containing a quartz fiber filter followed by a quartz fiber filter where 2/3 of the input air has been stripped of particles
μgC	micrograms of Carbon

GLOSSARY OF SYMBOLS

A	adsorbed vapor
b	extinction coefficient ($\text{cm}^2/\mu\text{g}$)
C	concentration on filter ($\mu\text{g}/\text{cm}^2$)
C_i	compound specific gas-particle partitioning coefficient ($\text{torr cm}^3 \text{ cm}^{-2}$)
d_p	particle diameter
I	intensity of transmitted light through sample
I_0	intensity of transmitted light through reference
K	compound specific constant
K_0	organic contamination from dilution system
n	number of samples
P	particulate organic carbon
p	gas phase partial pressure
p_0	saturation vapor pressure
Q_1	enthalpy for desorption directly from surface
Q_v	enthalpy of vaporization of the liquid
R	correlation coefficient
R^2	coefficient of determination
Re	Reynolds number
S	surface area for sorption
t	student's t-test value
T	factor describing the effect of the addition of a Teflon filter on the final backup filter concentrations

u	fluid velocity through jet (cm s^{-1})
v	volume of gas sorbed
V	volatilized organic material
w	jet diameter
X	p/p_0 ; gas phase partial pressure/saturation vapor pressure
α	fraction of input air which has not been stripped of particles
Δp	pressure drop (inches H_2O)
λ	wavelength
ϕ	fraction of compound which is in the particulate phase
σ	standard deviation
θ	concentration of surface area ($\text{cm}^2 \text{cm}^{-3}$)
ν	kinematic viscosity of the fluid ($\text{cm}^2 \text{s}^{-1}$)

ABSTRACT

Secondary Formation of Organic Aerosol: Investigation of the Diurnal Variations of Organic and Elemental Carbon

Barbara J. Turpin, Ph.D.

Oregon Graduate Center, 1989

Supervising Professor: James J. Huntzicker

Although carbonaceous species comprise a large fraction of urban aerosol, the contributions of primary and secondary sources to carbonaceous aerosol are not well understood. The purpose of this research was to establish a method of identifying primary and secondary organic aerosol through the use of time-resolved organic and elemental carbon measurements.

Because of the need to obtain improved time-resolution, low detection limits, and minimal influence from sampling artifacts, an *in situ* carbon analyzer was developed, characterized, and compared with other methods. The instrument combines the sampling function of a conventional filter sampler with the analytical function of a thermal-optical carbon analyzer. Field experiments were conducted in Los Angeles to investigate volatilization and adsorption sampling artifacts. Some ambient filter samples were also analyzed for specific organic compounds using direct thermal desorption/gas chromatography/mass spectroscopy.

The in situ carbon analyzer measured particulate organic and elemental carbon in the Los Angeles Basin during the Carbonaceous Species Methods Comparison Study in 1986 and the Southern California Air Quality Study in 1987. Organic and elemental carbon concentrations showed strong diurnal variations. Peak concentrations occurred during the daylight hours in the summer and at night in the fall. The maximum concentrations observed in the winter were two to three times higher than the summer maxima. On several summer days in 1987 the diurnal profiles of organic and elemental carbon were quite similar. Good correlations, comparable to those observed during the fall, were observed between organic and elemental carbon, suggesting that the organic aerosol on those days was principally primary. Comparison of the diurnal profiles of organic carbon with those of elemental carbon and ozone provided evidence for considerable secondary formation of organic aerosol during three sampling periods in 1987: July 11 - 13, July 25 - 29, and August 27 - 31. At the height of the August 27 - 31 episode secondary formation accounted for roughly 50% to 70% of the organic aerosol at 1700 hours (PDT).

CHAPTER 1. INTRODUCTION

Elevated particulate concentrations in urban areas result not only from direct particulate emissions but also from the condensation of products of gas phase, photochemical reactions. Aerosols emitted directly as particles are known as primary whereas those formed in the atmosphere are referred to as secondary aerosols. Although carbonaceous species comprise a large fraction of urban aerosol (Shah et al., 1986), the relative contributions of primary and secondary components of carbonaceous aerosol have long been disputed. The formation of secondary aerosol is believed to result from the gas phase oxidation of such precursors as olefins, cyclic olefins, di-olefins, and aromatics (Grosjean, 1977). Products with low volatility either nucleate or condense on the surfaces of pre-existing particles. As a result, secondary aerosols are found mainly in the accumulation mode (particle diameter between 0.1 and 1.0 μm) (Whitby et al., 1972). Particles in this size range scatter light effectively and are capable of penetration deep into the lungs. Gas-to-particle conversion of sulfur and nitrogen compounds has been observed in the atmosphere, and at times these secondary processes are responsible for high concentrations of particulate mass (Grosjean, 1977). The ability of specific organic compounds to form aerosols has been demonstrated in smog chamber experiments involving sunlight irradiation of specific gaseous components (Groblicki and Nebel, 1971; O'Brien et al., 1975;

Heisler and Friedlander, 1977; McMurry and Grosjean, 1985; Stern et al., 1987). However, the extent of secondary formation of organic aerosols in the atmosphere is not well understood because of the many compounds whose interactions must be taken into consideration.

A variety of approaches has been used to estimate the magnitude of secondary organic aerosol formation. These have ranged from detailed organic analysis of aerosol to simpler measurements such as aerosol organic carbon or the organic oxygen content of aerosol.

Appel et al. (1976; 1979) used a sequential solvent extraction scheme to obtain estimates of primary organic carbon, secondary organic carbon, and elemental carbon in summertime samples from the Los Angeles basin. Although this method of distinguishing between the various types of carbon is somewhat arbitrary, the correlation between secondary organic aerosol and ozone (an indicator of photochemical activity) was highly significant whereas correlation of primary organic aerosol with ozone was statistically insignificant.

Grosjean and Friedlander (1975) examined the diurnal variation of gas-particle distribution factors to identify times when secondary aerosol formation was significant. The distribution factor is the mass fraction of total atmospheric organic carbon (exclusive of methane and acetylene) in the particulate phase. Distribution factors which show distinct peaks at mid-day, when photochemical activity is high, indicate gas-to-particle conversion. Organic aerosol concentrations and organic gas-particle distribution factors showed very similar diurnal behaviors for several days during three Los Angeles smog episodes. Friedlander (1973) and Gartrell and Friedlander (1975) used chemical mass

balance techniques and estimated that secondary organic aerosol comprised about 9% of total Pasadena aerosol.

Measurement of individual organic compounds in aerosol has also provided useful information concerning the distribution between primary and secondary organic carbon. Primary organic compounds include alkanes, alkenes, substituted benzenes, styrenes, and phenols. Secondary formation of aerosols containing a variety of difunctionally substituted alkane derivatives has been demonstrated in smog chamber experiments, and these compounds have been identified in some atmospheric samples (Grosjean, 1977; Grosjean et al., 1978; Cronn et al., 1975; O'Brien et al., 1975; Knights et al., 1975). Knights et al. (1975) found similarity between the diurnal profiles of several dicarboxylic acids and ozone, indicating photochemical formation. O'Brien et al. (1975) collected summertime Los Angeles area aerosols with a highly oxygenated organic fraction unlike that observed in vehicle exhaust. In contrast, X-ray photoelectron spectroscopy (ESCA) was applied to West Covina, California, samples by Novakov (1982) with the conclusion that only a minor fraction of this aerosol was composed of oxygenated organic compounds. However, a later study in the same laboratory using a different analytical technique found one organic aerosol sample from Riverside, California, at the eastern edge of the Los Angeles basin which was highly oxygenated (Benner et al., 1984).

Because of the complexity of carbonaceous aerosol many investigators have found it useful to separate it into organic (OC) and elemental (EC) classes. The latter is also called black carbon or graphitic carbon and results predominantly from combustion processes. For this reason it is a good tracer for primary

organic aerosol. Particulate organic carbon is formed by a variety of processes, including combustion and secondary formation.

Huntzicker et al. (1986) examined the correlation of OC with EC in the Ohio River Valley. After correction for the inherent correlation resulting from common meteorological dispersion, the correlation between OC and EC was still quite high, suggesting that combustion was the principal source of organic aerosol in that region. A similar method used by Wolff et al. (1983) led to the same conclusion regarding Denver aerosol during the November-December 1978 period.

Several investigators (Wolff et al., 1983; Novakov, 1982; Gray et al., 1986; Grosjean, 1984; Chu and Macias, 1981) have used the OC/EC ratio or a variant ratio to investigate the importance of primary and secondary organic aerosol. In such an approach, elevated ratios are considered to be indicative of secondary formation. Of course it is necessary to exclude other causes of elevated ratios such as local, atypical sources of primary carbonaceous aerosol. Support for the use of EC as a tracer for primary OC is provided in the Los Angeles Basin emission inventory developed by Gray (1986) for carbonaceous aerosol in Los Angeles. For particles smaller than 10 μm in aerodynamic diameter, 60% of OC and 89% of EC resulted from combustion, and the primary TC/EC ratio (TC = OC + EC) derived from the inventory was 3.4 (OC/EC = 2.4).

In 1982 Gray et al. (1986) conducted a year-long study in the Los Angeles basin in which 24-hr filter samples were taken every sixth day at several sites. The TC/EC ratio showed little seasonal dependence and a yearly average of 2.6 in downtown Los Angeles. This is comparable to that observed in Los Angeles

during winter, peak morning traffic periods (Conklin et al., 1981) and implies that on an annual basis the secondary component of the downtown aerosol is negligible. The yearly average TC/EC ratio increased a small, but statistically significant amount moving downwind to the sites farthest removed from the principal core of emissions and reached a high of 3.0 at Azusa and 2.9 at Rubidoux. This could represent a secondary component as large as 38%.

Grosjean (1984) used a similar approach in a study in the Los Angeles area although his results included sampling periods as short as two hours. OC/EC ratios for 2-hr and 24-hr samples during periods of peak photochemical activity averaged 10.3 and 8.5 respectively, suggesting significant secondary formation.

Novakov (1982) measured total carbon and optical attenuation on particle-laden filters for several urban centers. The optical attenuation is assumed to be caused predominantly by elemental carbon. Statistical analysis showed a correlation (R^2) of 72% between optical attenuation and total carbon for 24-hr samples at all sites. On an annual average basis the primary contribution to total carbon ranged from 97% in New York City to 62% for Fremont, California. Although reduced EC/TC ratios suggested the presence of secondary organic carbon in cities like Fremont, no correlation between the EC/TC ratio and ozone was found for the California sites.

Wolff et al. (1983) measured organic and elemental carbon at several urban sites. Although the seasonal dependence of EC/TC suggested some influence of secondary processes, no relationship between EC/TC and ozone concentration was found.

Chu and Macias (1981) examined the use of both elemental carbon and lead as tracers for primary carbon. As noted above, elemental carbon is considered to be a good tracer of primary carbonaceous aerosol. Since 90% of elemental carbon and 60% of primary total carbon are from mobile sources (Gray, 1986), lead should also be a reasonable tracer of primary carbonaceous aerosol. From emission inventory considerations the C/Pb ratio was estimated to be between 4 and 7 for primary Los Angeles aerosol in 1973. During the California Aerosol Characterization Experiment (ACHEX) C/Pb ratios in Los Angeles were greater than 7 on 40% of the days, indicating substantial secondary formation on those days. Two to six hour samples showed definite peaks in the C/Pb ratio in the early afternoon. The highest ratios were observed inland at Riverside and West Covina. Analysis of 6 hour St. Louis samples yielded summer OC/EC ratios averaging 4.3 and winter ratios averaging 1.8, again suggesting a summertime secondary contribution.

Chu and Macias (1981) noted that secondary organic aerosol could not be detected in the C/Pb ratio using 24 hour composites rather than samples of higher time resolution. If secondary formation is only important during mid-day, its impact on C/Pb and OC/EC ratios would be greatly diluted in a 24 hour average.

In summary, despite the rather large literature on secondary organic aerosol, no clear picture has emerged. It does appear, however, that such aerosol is important only during those times of year when photochemical activity is high. Moreover, there is likely to be a strong diurnal variation in secondary organic aerosol concentrations owing to the diurnal behavior of photochemical activity.

Therefore, an understanding of organic aerosol formation will require time-resolved data.

The purpose of this research was to establish a method of identifying primary and secondary organic aerosol through the use of organic and elemental carbon measurements. Because of the need to obtain improved time-resolution, low detection limits, and minimal influence from sampling artifacts, development of an in situ carbon analyzer was continued. A statistical characterization of the instrument took place in the laboratory, and field comparisons were made with (1) manual sampling and laboratory thermal-optical analysis and (2) the Ford Motor Company photoacoustic spectrometer. A series of artifact experiments were performed in the Los Angeles Basin using a variety of manual filter samplers, and some of these filters were analyzed by direct thermal desorption/gas chromatography/mass spectroscopy as well as thermal-optical carbon analysis. These investigations ensured that proper correction would be made for vapor related sampling artifacts in the in situ carbon analyzer. All field experiments were conducted during the Carbonaceous Species Methods Comparison Study (CSMCS) in Glendora, California, in August 1986 or the Southern California Air Quality Study (SCAQS) in Claremont, California (June - September, 1987) and Long Beach, California (November - December, 1987). The in situ carbon analyzer measured organic and elemental carbon during both studies, and sampling was conducted for bromine and lead during SCAQS. Because of the central importance of the Oregon Graduate Center (OGC) thermal-optical carbon analyzer to this work, a detailed discussion of the analytical sequence and quality assurance procedures is included in Chapter 2.

The study presented in Chapter 3 was conducted prior to the beginning of thesis research and provides the impetus for this dissertation.

CHAPTER 2: HANDLING AND THERMAL-OPTICAL CARBON ANALYSIS OF MANUALLY COLLECTED SAMPLES

INTRODUCTION

All quartz fiber filter samples collected manually during the course of this research were analyzed for organic and elemental carbon using the OGC laboratory thermal-optical carbon analyzer. Filter preparation and sample handling are described below as well as the quality assurance measures followed and the uncertainties obtained. The laboratory thermal-optical carbon analyzer electronics and software were rebuilt between the 1986 and 1987 field studies, and the analysis procedure has been altered somewhat since the original publications (Huntzicker et al., 1982; Johnson et al., 1981). Therefore a description of the current analytical sequence is included.

SAMPLE HANDLING

Prior to sampling all quartz fiber filters were heat-cleaned at 500 C in air for at least two hours and stored in petri dishes lined with aluminum foil. The aluminum foil was pre-cleaned at 380 C. At the end of the sampling period the filters were returned to the petri dishes and immediately stored at -10 C until analysis. A blank filter was assigned to each sampling day and was treated in

exactly the same manner with respect to filter preparation, handling, and analysis as the analytical filters collected on that day. Flow readings and pressure drops were recorded at the beginning and end of each sampling period. A dry test meter was used to calibrate all filter sampler flow rotameters, and a counter in line with each pump monitored collection time.

THE THERMAL-OPTICAL CARBON ANALYSIS METHOD

The OGC laboratory thermal-optical carbon analyzer is described in detail by Huntzicker et al. (1982) and Johnson et al. (1981). Briefly, it is a thermal volatilization-combustion technique in which the reflectance of 633 nm He-Ne laser light from the filter sample is used to correct for the pyrolysis of organic carbon which occurs during analysis. Organic carbon is volatilized by heating the sample in two steps to 470 C and 610 C in pure helium. The volatilized organic carbon is oxidized to CO₂, reduced to CH₄, and measured by a flame ionization detector (FID). The oven temperature is then reduced to 420 C, and oxygen is added to achieve a composition of approximately 2% O₂ in 98% He. Elemental carbon is then combusted by stepping the temperature to 750 C (through 510, 550, 590, and 670 C). When elemental carbon combustion is complete, the oven temperature is reduced to 280 C. Two calibrations follow, both accomplished by automatic injection of a known amount of methane. The first is performed in a O₂-He atmosphere and the second in pure He. FID response is somewhat sensitive to carrier gas composition, and dual calibrations improve the accuracy of the analysis.

During organic analysis some organic carbon is pyrolytically converted to elemental carbon causing the filter to darken. Unless a correction is made for this effect, the elemental carbon fraction can be seriously over-estimated. This correction is accomplished by measuring the optical reflectance of the filter continuously throughout the analysis. As pyrolysis occurs, the reflectance decreases. With the addition of oxygen, elemental carbon removal begins, and the reflectance starts to increase. The point at which the filter reflectance reaches its pre-pyrolysis value is taken to be the split point between OC and EC. All carbon measured before this point (as represented by the FID signal) is considered organic and after, elemental. A complicating factor in making this correction is that the FID signal lags the reflectance signal by the transit time of the carrier gas from the volatilization-oxidation oven to the FID. To achieve an accurate pyrolysis correction, it is necessary to align the FID and reflectance signals by measuring the transit time. This is accomplished by measuring the time between sample insertion and FID response for clean filter punches doped with sucrose.

The laboratory carbon analyzer is controlled by an Apple IIe computer equipped with a Sunset Laboratory I/O board and a Grappler printer card. Prior to the Southern California Air Quality Study of 1987 a Commodore computer controlled the laboratory carbon analyzer. The computer directs the valve switching and temperature control sequences, records temperature, laser, and FID signals, plots the analysis, and presents results in terms of organic and elemental carbon loadings ($\mu\text{gC}/\text{cm}^2$). The time sequence for valve switching and temperature control is given in Table 2.1, and a typical output is shown in

TABLE 2.1. LABORATORY CARBON ANALYSIS TIME SEQUENCE

ELAPSED TIME (SEC.)	OVEN TEMP. (C)	VALVE CHANGES
0	280	system has been purged with He; FID on line; atmosphere is pure He
200	470	organic carbon removal begins
400	610	organic carbon removal continues
680	420	organic carbon removal complete; oven temp. reduced
1000	420	oxygen introduced
1140	510	elemental carbon oxidation begins
1240	550	elemental carbon oxidation cont.
1340	590	elemental carbon oxidation cont.
1440	670	elemental carbon oxidation cont.
1540	750	elemental carbon oxidation cont.
1840	280	elemental carbon oxidation complete; oven temperature reduced
1880	280	CH ₄ calibration loop switched on line; calibration in O ₂ -He
1920	280	CH ₄ calibration loop switched off line
2120	280	carrier gas switched to pure He
2140	280	CH ₄ calibration loop switched on line; calibration in He
2180	280	CH ₄ calibration loop switched off line
2410	280	FID switched off line
2414	280	analysis complete

Figure 2.1. In this figure the FID and reflectance signals have been aligned. Table 2.1 describes the regular analysis program which distinguishes between organic and elemental carbon fractions. A short analysis program can be run for total carbon alone. In this program the sample is combusted at 800 C in a 2% O₂-98% He atmosphere followed by an internal CH₄ calibration.

BLANKS

For each day of operation of the laboratory carbon analyzer at least one instrument blank and punches from one field blank were run. The instrument blank measurement was used to ensure that the system was working properly and was not contaminated. Blank subtraction used an average of all field blanks run during the analysis of that sample set. It was performed by dividing the analysis into eight sections plus the division established by the organic-elemental carbon split and subtracting the blank value from the sample value on a section by section basis.

Blank subtraction could be accomplished in one of two ways. If the instrument blank dominated, the mass of carbon measured in the field blank analysis would be independent of the number of punches used (or the mass of carbon on the blank per cm² would be inversely proportional to the number of punches used), and the blank should be subtracted on a mass basis. Alternatively, if the filter blank dominated, the blank value expressed in μgC/cm² would be independent of the number of punches used. Carbonaceous Methods Species Comparison Study blanks were analyzed with 32 long and short analysis runs. Analyses were examined by paired t-test to determine whether the 1, 2, and

FIGURE 2.1

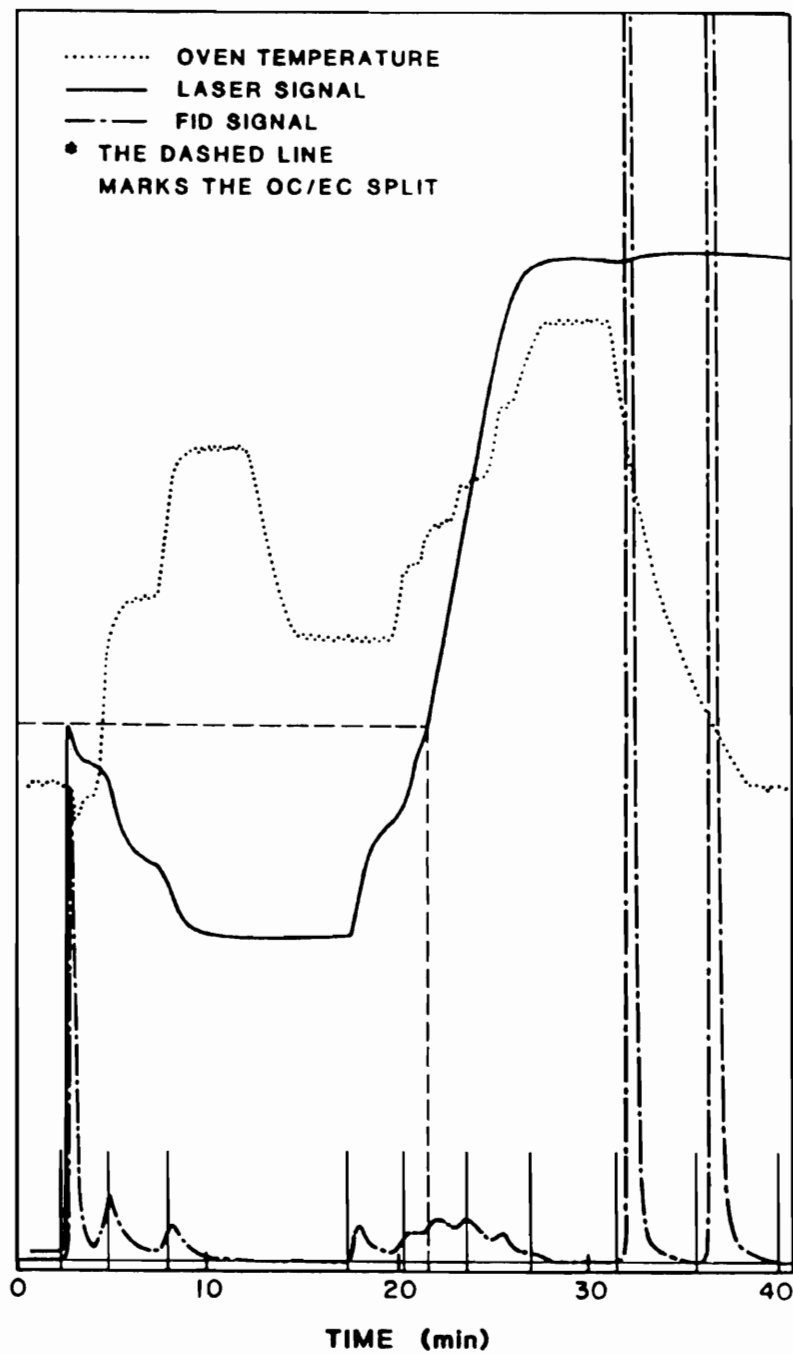


Figure 2.1. Typical output for laboratory thermal-optical carbon analyzer. Oven temperature, optical reflectance, and flame ionization detector. The dashed line at about 21.3 minutes is the split point between organic and elemental carbon.

3 punch samples could be sub-sets of the same population when expressed as μgC and as $\mu\text{gC}/\text{cm}^2$. The results were consistent with the dominance of the filter blank, indicating that subtraction on a mass per surface area basis would be optimal. The detection limits (3σ) for laboratory carbon analysis during CSMCS were 1.4 and 1.3 $\mu\text{gC}/\text{cm}^2$ for long and short analysis program runs respectively.

Twenty-two long and short analyses of Southern California Air Quality Study blanks were run using 2 and 4 punches. Results of paired t-tests on 2 and 4 punch runs indicated that the instrument blank dominated for the long analysis program, and the filter blank dominated for the short analysis program. As a result, blank subtraction was performed on a mass basis (μg) for front filters (long analysis program) and on a mass per surface area basis ($\mu\text{g}/\text{cm}^2$) for backup filters (short analysis program). The detection limits (3σ) for SCAQS laboratory carbon analysis were 0.5 μgC and 0.4 $\mu\text{gC}/\text{cm}^2$ for long and short analysis programs respectively.

EXTERNAL STANDARDS

External standards were prepared from a sucrose solution containing 5 g of carbon/liter deionized water. Filter punches were heat-cleaned in the carbon analyzer oven, then cooled in place and doped with enough solution to give 10 to 35 μg of carbon.

The accuracy of the sucrose solution approach was checked with a second external standard. Ten CH_4 samples containing between 2 and 25 μg of carbon were injected into the laboratory carbon analyzer. The ratio of methane to sucrose responses was 1.01 ± 0.05 . Thus, there was no difference in the results at

the 95% confidence level, validating our external calibration method. The linearity of instrument response was verified by the good fit ($R^2 = 99.3\%$) between mass of carbon injected and instrument response over the range studied in the CH_4 experiment.

UNCERTAINTIES

The accuracy of total carbon measurements was $\pm 2\%$, as determined by the uncertainty in instrument response to external sucrose standards. Measures of precision were based on replicate filter analyses of at least 10% of all samples in each data set and were determined by one-way analysis of variance. They represent combined instrument uncertainties and variations in aerosol deposition over the filter area. They are presented in Table 2.2.

ROUND ROBIN STUDY

A round robin interlaboratory comparison was conducted during CSMCS. It evaluated the overall uncertainty of carbonaceous aerosol monitoring through (1) nine days of simultaneous sampling using the range of sampling and analysis methods applied by eight different research groups and (2) interlaboratory analysis of aliquots of "reference" aerosol samples. The second study is described in detail by Countess (1989), and the OGC participation will be discussed here.

Twenty aliquots of samples collected on 8" x 10" Pallflex QAST quartz-fiber Hi-Vol filters were distributed to 13 laboratories by Environmental Monitoring and Services, Inc. (EMSI) for blind analysis. The sample sets included ambient CSMCS samples, automotive exhaust samples, ambient Medford, Oregon samples

TABLE 2.2. LABORATORY CARBON ANALYZER UNCERTAINTIES

	CSMCS ROUND ROBIN SAMPLES	CSMCS TWO PORT & FACE VELOCITY SAMPLES	SCAQS DILUTION EXPERIMENT SAMPLES
ORGANIC CARBON (OC)	8.4%	4.3%	4.4%
ELEMENTAL CARBON (EC)	6.9%	7.5%	3.3%
TOTAL CARBON (TC)	7.0%	4.6%	3.8%
TOTAL CARBON FROM BACKUP FILTERS		6.7%	3.7%
NUMBER OF REPLICATES	16	14	6
NUMBER OF REPLICATES FOR BACKUP FILTERS		38	8

dominated by wood smoke emissions, an ambient sample treated to significantly reduce the organic fraction, an organic aerosol sample generated in a smog chamber, and a sample blank. Three aliquots from each of four ambient samples were given to all participants, to provide a blind measure of precision.

The measures of precision for the OGC results, based on blind analysis of the four ambient samples submitted in triplicate are: organic carbon, 7.4%; elemental carbon, 6.2%; total carbon, 7.4% (Countess, 1989). These are consistent with our estimates determined by replicate analysis of sample aliquots. The lack of an absolute standard for organic and elemental carbon makes it impossible to evaluate the accuracy of the participants' performance. However, the spread in the values reported indicates the uncertainty with which carbonaceous aerosol is measured. The coefficient of variance (standard deviation/mean) for total carbon ranged from 4.2% for the ambient CSMCS sample to 14.1% for the unleaded automotive exhaust sample (Countess, 1989). Countess expressed the uncertainty in the split between organic and elemental carbon as the variation in the EC to TC ratio. Excluding the organic aerosol sample, the coefficient of variation of this ratio ranged from 10% for the diesel sample to 83% for the heavily loaded wood smoke sample. The precision for elemental carbon, calculated from his numbers, ranges from 24% to 85% for the diesel and wood smoke samples respectively with an uncertainty of 34% for the ambient samples. Therefore, although the agreement is good for total carbon, interlaboratory agreement regarding the split between organic and elemental carbon is still fairly poor.

CHAPTER 3. PRELIMINARY STUDY

AN INVESTIGATION OF LOS ANGELES MID-DAY PARTICULATE CARBON

INTRODUCTION

As discussed in Chapter 1, several investigators have used the ratio of organic carbon to elemental carbon (OC/EC) or a related ratio to investigate the extent of secondary formation (Gray et al., 1984; Novakov, 1982; Wolff et al., 1981). In such an approach, ambient ratios greater than those observed for primary aerosol are considered indicative of secondary formation. However, an estimate of the primary OC/EC ratio is needed to proceed with an analysis of this type.

Atmospheric sampling conducted in downtown Los Angeles, California, during winter, peak morning traffic periods (Conklin et al., 1981), and a comprehensive emissions inventory for the Los Angeles basin (Gray, 1986) yielded mean OC/EC ratios of 1.7 and 2.4 respectively. A monitoring program comprised of 24 hour samples (Gray et al., 1986), conducted for one year, resulted in mean OC/EC ratios of 1.4 and 1.6 for Lennox and downtown Los Angeles respectively. These locations are near the ocean, and pollutants are mostly fresh. Little seasonal dependence was seen in the ratio, indicating that secondary formation did not contribute significantly to these 24 hour average OC concentrations. Thus, ambient data and emissions information indicate the primary OC/EC ratio in the Los Angeles Basin should fall in the range of 1.4 to 2.4. Unfortunately, the

current study did not contain data taken at times of low photochemical activity, so an internal check of the primary ratio estimate was not possible.

Emissions ratios differ considerably from source to source (Cass et al., 1982). Thus, the primary ratio will be influenced by meteorology, diurnal and seasonal fluctuations in emissions, and the influence of local sources. Because of the sea breeze the inland sites in the Los Angeles Basin receive a more representative mixture of sources. Confidence in the estimates of the primary ratio is enhanced in areas where there are no large local sources. Such is the case in Pasadena and San Bernardino, which are northeast of downtown Los Angeles.

Because secondary organic aerosol is formed as a product in the general photochemical smog sequence, significant secondary organic aerosol formation should be accompanied by elevated ozone concentrations and should roughly correlate with other photochemically produced secondary aerosols of local origin (e.g. nitrate). Although secondary organic aerosol formation is expected to be accompanied by elevated ozone concentrations, conditions which result in high ozone concentrations might not be sufficient to generate secondary organic aerosol because aerosol formation will also depend upon the presence of organic precursors.

EXPERIMENTAL

This sampling program examined the Los Angeles aerosol at times when photochemical activity was at a maximum. Four hour filter samples were collected at five Los Angeles Basin locations (Lennox, Pasadena, Azusa, Upland and San Bernardino) from 1000 to 1400 hours every six days from July 5 to

September 27, 1984. Lennox is near the ocean on the western edge of the basin. Pasadena, Azusa, Upland and San Bernardino are along the northern edge of the basin from west to east as shown in Figure 3.1. A cyclone impactor at each sampler inlet removed particles with aerodynamic diameters larger than $2.0 \mu\text{m}$, and fine aerosol was collected on quartz fiber filters. The system operated at a flow rate of 10 l/min and a filter face velocity of 17 cm/s. Quartz fiber filters were heat treated for at least 1 hour at 600 C prior to use. Following collection, they were placed in air tight petri dishes lined with heat treated aluminum foil and chilled for storage. Nuclepore and Teflon filter samples were taken concurrently and analyzed for sulfates and nitrates by ion chromatography (Nuclepore) and for trace elements by x-ray fluorescence (Teflon). Quartz fiber filter samples were analyzed for organic and elemental carbon using the OGC thermal-optical carbon analyzer (see Chapter 2).

Instrument blanks, field blanks, and external sucrose standards were analyzed daily during sample analysis. The blanks yielded detection limits (3σ) of $0.4 \mu\text{gC}/\text{m}^3$ and $0.2 \mu\text{gC}/\text{m}^3$ for OC and EC respectively. Replicate analysis of 17% of the sample set provided the data for the determination of uncertainties. The 95% confidence interval was $0.4 \mu\text{gC}/\text{m}^3$ for EC, $0.8 \mu\text{gC}/\text{m}^3$ for total OC, and $0.5 - 0.9 \mu\text{gC}/\text{m}^3$ for primary OC using the minimum and maximum values selected for the primary OC/EC ratio.

The compatibility of the measurements used to estimate the primary OC/EC ratio and the measurements of this study must be carefully assessed because of the poor agreement between methods of organic and elemental carbon determination. In none of the studies, including this one, were OC concentrations

FIGURE 3.1

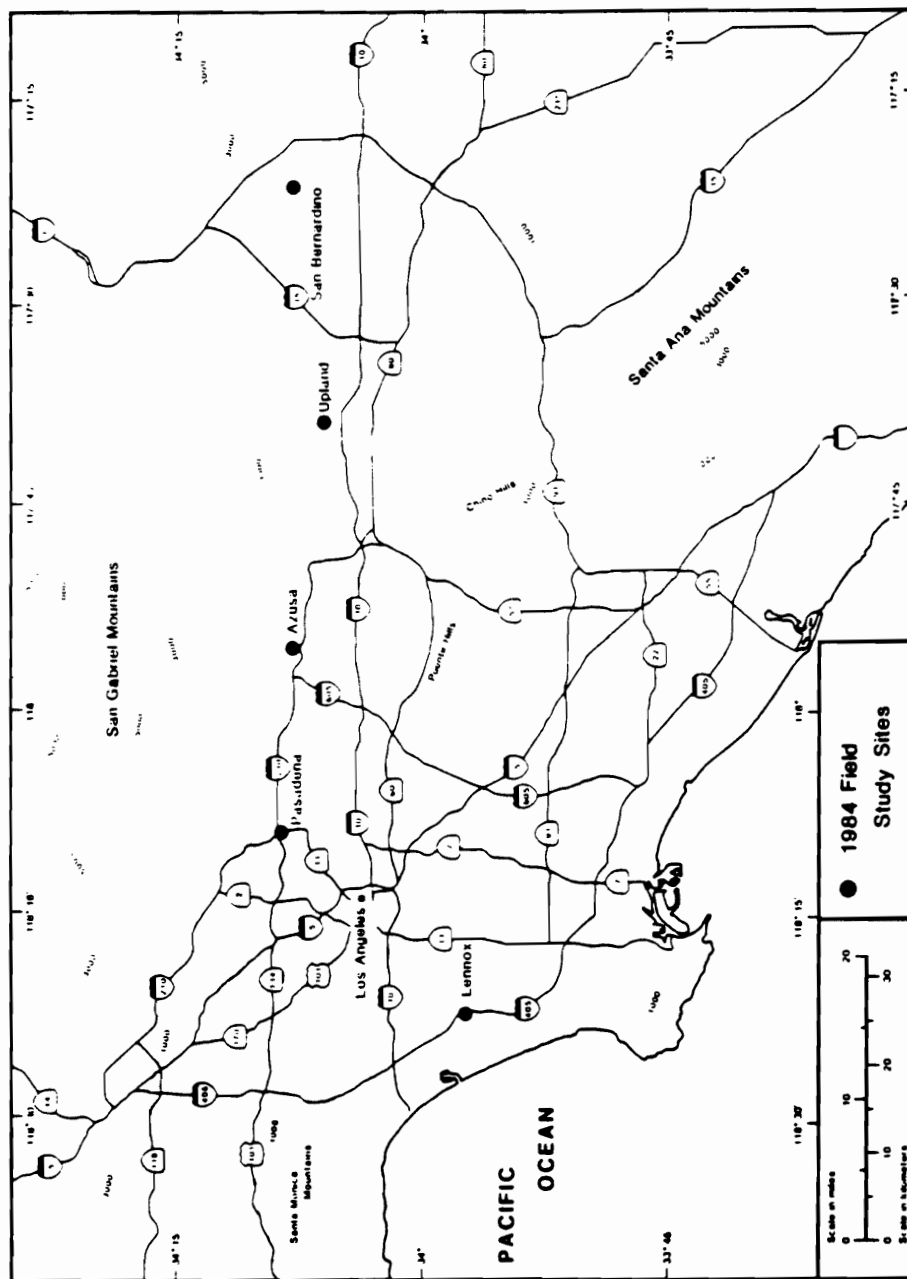


Figure 3.1. Schematic of the Los Angeles Basin showing 1984 field study sites.

corrected for vapor adsorption artifacts on the quartz fiber filters. However, because the fractional contribution of adsorbed vapor to organic aerosol loading decreases with increased loading and increased filter face velocity (McDow and Huntzicker, 1989; McDow, 1986, Chapter 6), it is important to compare the effect of the vapor artifact on the OC/EC ratios observed in each study. A least squares fit of adsorbed vapor as a function of particulate organic carbon loading ($\mu\text{gC}/\text{cm}^2$) for Los Angeles basin samples collected at a face velocity of 20 cm/s in 1986 (Turpin and Huntzicker, 1988) was used to estimate the contribution of adsorbed vapor for the average organic carbon loading observed for the current study and for the study of Gray et al. (1986). (Gray et al. (1986) collected samples at a face velocity of 18 cm/s, but loadings were about three times as great as the current study.) Thus, relative to the conditions of the current study, the primary ratios suggested by the Gray et al. (1986) study were underestimated by a factor of 1.5. Adjusted to the current study, the primary OC/EC ratios derived from the Gray et al. (1986) study became 2.1 and 2.4 based on Lennox and downtown Los Angeles data respectively, which still fall within the range (1.4 - 2.4) used for the primary ratio.

Of the three data sets used to estimate the primary ratio, the Gray data, which were also analyzed by the OGC thermal-optical carbon analyzer, are probably the most compatible with the current study. The same sampling medium was used for the Conklin study, but collection was at a much higher face velocity, and the samples were analyzed for total carbon by gamma ray analysis of light elements and for elemental carbon by reflectance. The emissions inventory is a compilation of data from many sources.

RESULTS

The secondary component of the organic aerosol can be estimated from equations 3.1 and 3.2.

$$OC_{\text{sec}} = OC_{\text{tot}} - OC_{\text{pri}} \quad \text{and} \quad (3.1)$$

$$OC_{\text{pri}} = EC \times (OC/EC)_{\text{pri}} \quad (3.2)$$

where

- OC_{sec} = secondary OC
- OC_{tot} = measured OC
- OC_{pri} = primary OC
- EC = measured EC
- $(OC/EC)_{\text{pri}}$ = primary ratio estimate

Table 3.1 shows the average hour of peak ozone concentration for each site over the period of this study. The ozone peak for Pasadena was at noon, in the middle of the sampling period. Because filter samples were only taken from 1000 to 1400 hours, it is not possible to determine the exact time when secondary OC peaks occurred. However, insight into the temporal relationship between ozone and secondary OC maxima is provided by the following reasoning. Mid-day secondary OC concentrations in Pasadena exceeded the average mid-day secondary OC concentration computed over all sites on 89 percent of the sampling days. Moving downwind, through Azusa, Upland, and San Bernardino the number of above-average secondary OC concentrations decreased, and the time of peak ozone concentration increased from 1200 to 1440 hours. This suggests that the secondary OC peak had moved past the temporal sampling

TABLE 3.1. SITE SPECIFIC OZONE AND SECONDARY ORGANIC CARBON DATA

The first column indicates the percentage of sampling days where the secondary OC estimate at that site is higher than the average computed over all sites.

	<i>% of days secondary OC higher than intersite avg</i>	<i>time of peak ozone</i>
Lennox	8%	1330
Pasadena	89%	1210
Azusa	50%	1300
Upland	50%	1400
San Bernardino	5%	1440

window at the eastern sites. Within the 1000 to 1400 hour window the highest ozone concentrations were found in Azusa whereas the highest secondary OC concentrations were found in Pasadena. Since peak ozone concentrations in Pasadena occurred about one hour before those in Azusa, the data suggest a lag time on the order of one hour between the ozone maximum and the secondary organic aerosol maximum. This conclusion has subsequently been supported by SCAQS ozone and in situ carbon analyzer data which suggest a time lag of 1.5 ± 1.0 hours. Therefore, the Pasadena site will be the focus of this study because both ozone and secondary OC peaks should be included within the sampling period.

In the sampling program of Gray et al. (1986) 24-hour samples were taken at Lennox. A very high correlation was observed between OC and EC ($R=0.99$), and the ratio of total to elemental carbon showed little seasonal dependence. This indicated that secondary formation did not have a significant impact in Lennox when averaged over 24 hour periods. In contrast, the Pasadena 4 hour mid-day samples showed a much lower correlation between OC and EC ($R=0.78$), and OC correlated equally well with ozone ($R=0.78$). Thus the presence of organic carbon was explained equally well by common origin with the primary tracer, EC, and with the secondary tracer, ozone.

The conclusion that secondary formation contributes significantly to mid-day summer Los Angeles organic aerosol concentrations would be supported if episodes identified with secondary formation corresponded with elevated nitrate and ozone concentrations. The correlation coefficients (R) of linear least squares fits between Pasadena concentrations of a variety of variables are given in

Table 3.2. The 1000 - 1400 hour average concentrations were used for all data except ozone. Two entries for ozone are given, one using the peak ozone concentration which occurred at about 1200 hours and the other using the 0900 - 1300 hour average concentration to take into consideration the apparent one hour time lag between ozone and secondary organic aerosol formation. The 1000 - 1400 hour and 0800 - 1200 hour averages yield similar results. No correlation between secondary OC and the primary tracers, lead and EC, was observed. The correlation between secondary OC and ozone was not statistically significant ($R=0.27$), and the correlation with nitrate was modest ($R=0.72$) but significant at a 95% level of confidence. The correlation between nitrate and ozone was also not statistically significant ($R=0.26$), and in fact, secondary OC acted similarly to nitrate with respect to the other variables in the table.

The lack of strong correlations is not surprising because the chemical and dynamical processes involved in secondary aerosol formation are quite complex, and it is unlikely that linear expressions can adequately describe the relationships between such photochemical products as ozone, nitrate, and secondary OC. Therefore, a simple sign test might be more appropriate than a linear regression. In this test, variables are expressed in terms of their standard normal variates (SNV), and correlations are sought between the signs of those values.

The standard normal variate is defined as:

$$\text{SNV} = (X - X_{\text{AVG}})/\sigma \quad (3.3)$$

where X = concentration ($\mu\text{g}/\text{m}^3$)
 X_{AVG} = avg. concentration at that site
 σ = standard deviation of the concentrations at that site

A data set presented in the form of standard normal variates has a mean of zero and a standard deviation of one. The purpose of a non-parametric sign test (Chatfield, 1983) is to determine whether or not the signs of two variables are positively or negatively correlated to a certain level of significance. If (a_1, a_2, \dots, a_n) and (b_1, b_2, \dots, b_n) represent two sample sets between which there is no sign correlation, then roughly half of the products $(a_i b_i)$ will be positive. More precisely, the fraction of products that are positive will follow a binomial distribution. The level of significance of an observed number of positive products is the probability of observing at least that many positive products in a sample set which follows a binomial distribution.

The standard normal variates of Pasadena secondary OC and EC, secondary OC and lead, and EC and lead are plotted for each sampling day in Figures 3.2 - 3.4 respectively. At the 90% confidence level a negative sign correlation was observed between secondary OC and lead, and secondary OC and EC were uncorrelated. This indicates that the organic aerosol defined as secondary could not be explained as primary organic aerosol by correlation with these primary tracers. A positive sign correlation significant at the 95% confidence level was

FIGURE 3.2

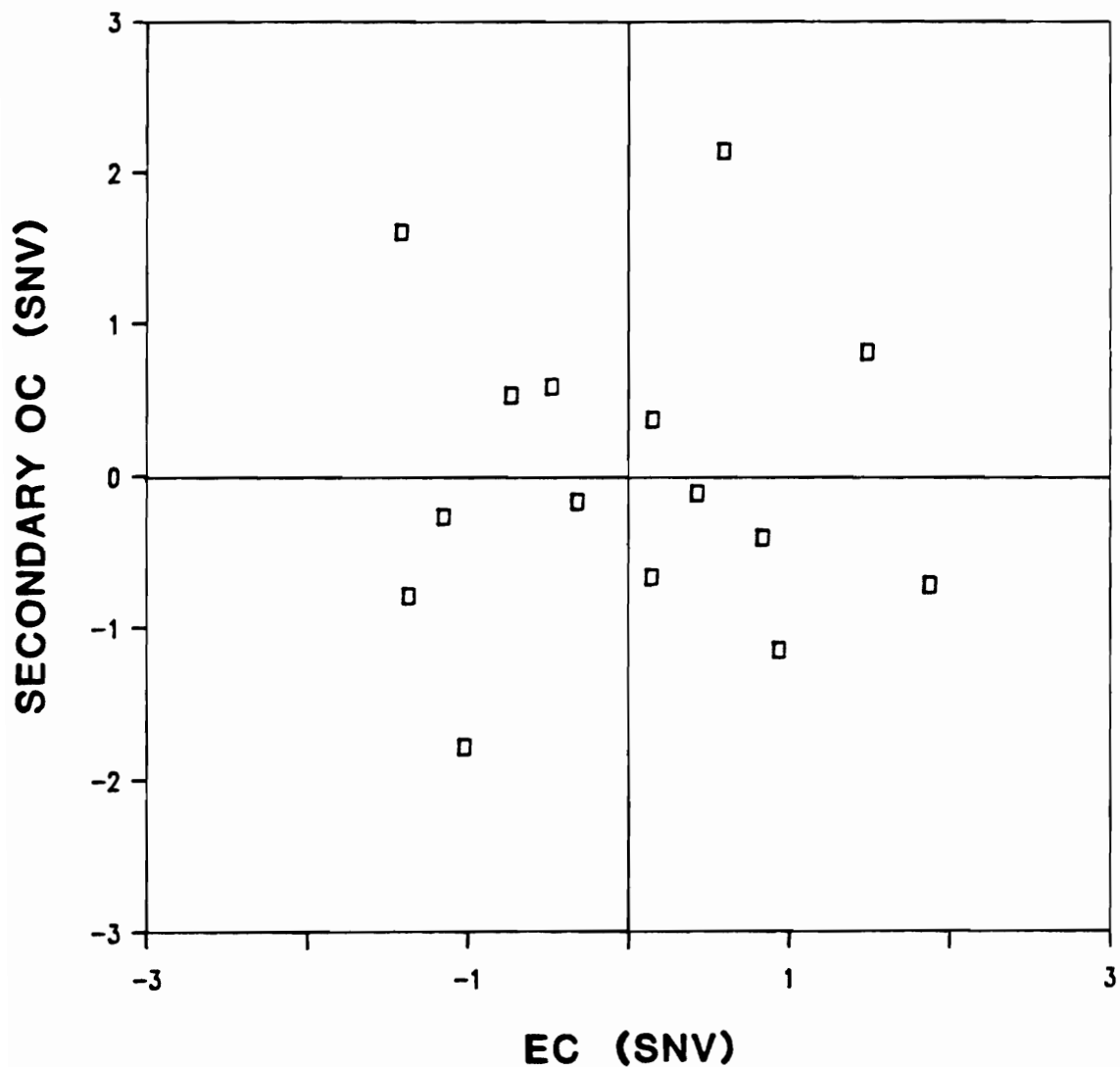


Figure 3.2. Comparison of standard normal variates of secondary organic carbon and elemental carbon concentrations at Pasadena, California, July 5 - September 27, 1984. A data set presented in the form of standard normal variates has zero mean and a standard deviation of one.

FIGURE 3.3

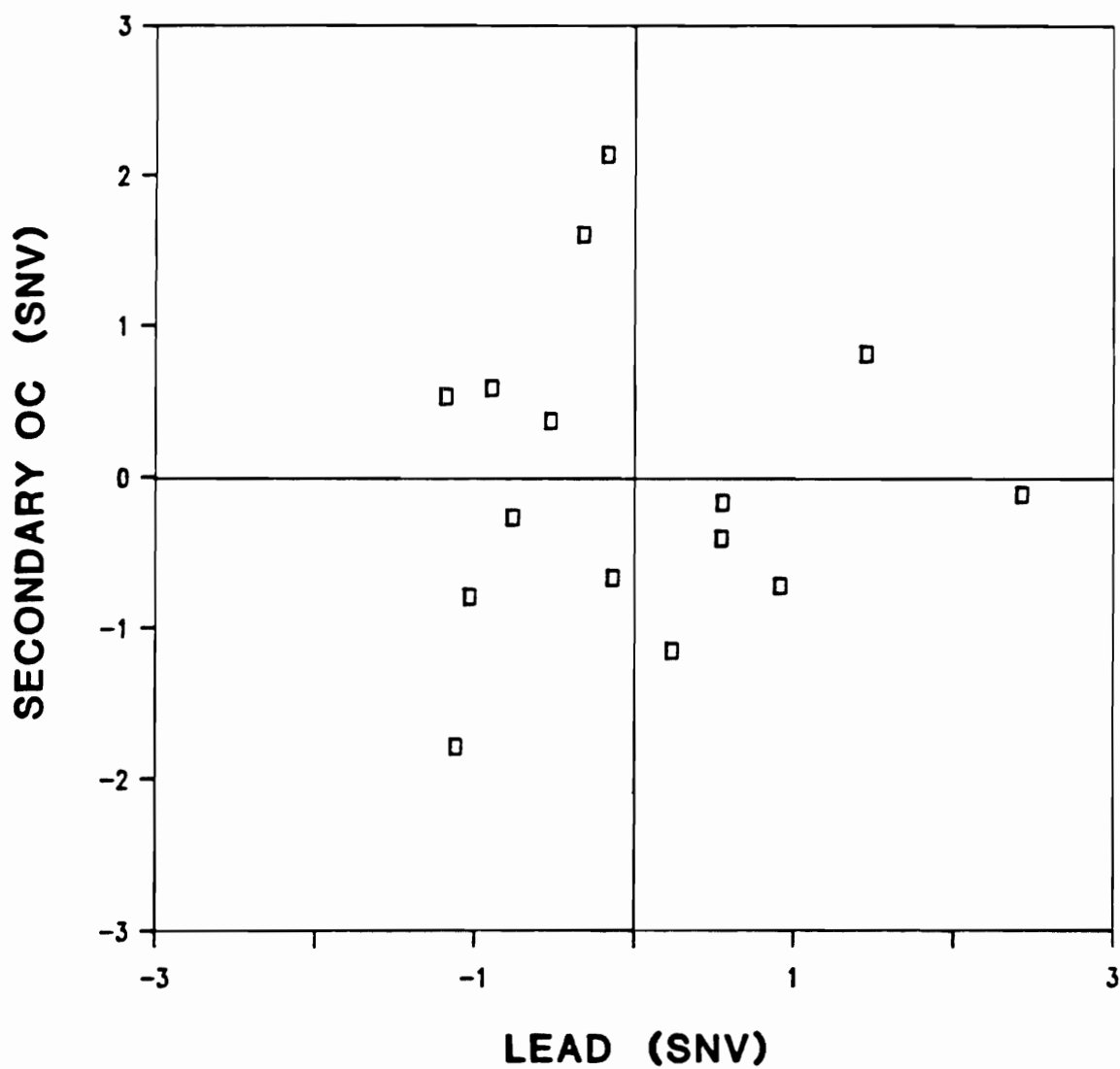


Figure 3.3. Comparison of standard normal variates of secondary organic carbon and lead concentrations at Pasadena, California, July 5 - September 27, 1984. A data set presented in the form of standard normal variates has zero mean and a standard deviation of one.

FIGURE 3.4

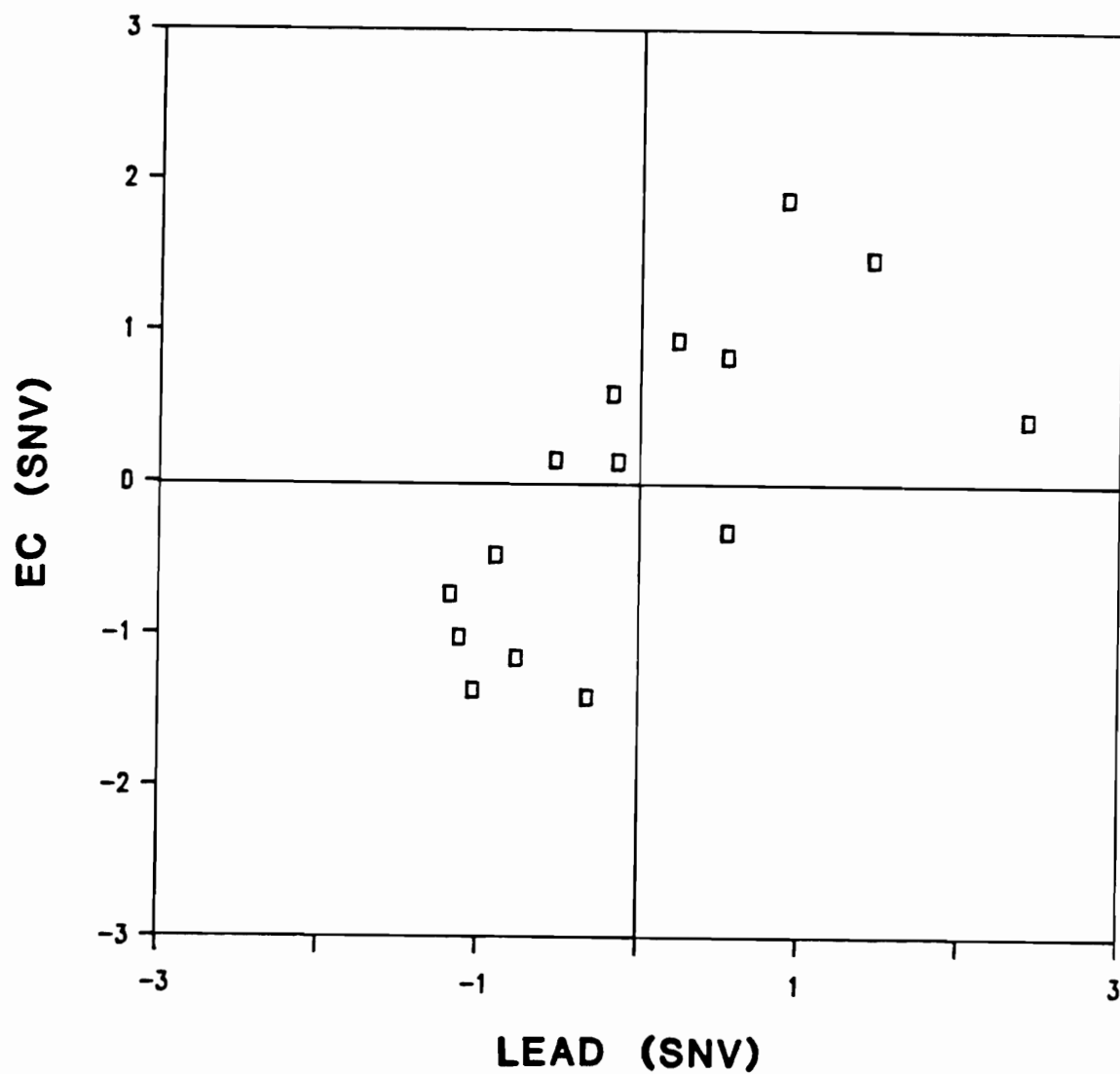


Figure 3.4. Comparison of standard normal variates of elemental carbon and lead concentrations at Pasadena, California, July 5 - September 27, 1984. A data set presented in the form of standard normal variates has zero mean and a standard deviation of one.

observed between SNV's for lead and EC. A strong correlation between lead and elemental carbon is expected in an area like Pasadena where both lead and EC are primarily from motor vehicles.

Figure 3.5 shows the SNV's of secondary OC and ozone for the Pasadena data. Because formation of organic aerosol requires the presence of several compounds, only a general correlation can be expected between secondary OC and any one photochemical indicator. Higher than average secondary OC concentrations were accompanied by higher than average ozone concentrations as expected on all days but one, August 28. On 10 of 15 days secondary OC and ozone were either both positive or both negative, and the positive ozone - secondary OC sign correlation was significant at the 90% confidence level.

Figure 3.6 shows the SNV's of Pasadena nitrate and ozone. Nitrate, like secondary OC, is a photochemically generated secondary aerosol component. Higher than average nitrate concentrations were accompanied by higher than average ozone concentrations on all but two days, and on 11 of 15 days nitrate and ozone were either both positive or both negative. The positive ozone - nitrate sign correlation was significant at the 95% confidence level.

Although the positive sign correlation between secondary OC and ozone is only fair, the positive secondary OC - nitrate correlation is quite good as shown in Figure 3.7. SNV values showed a positive sign correlation on 12 of 15 days which was significant at the 99% confidence level as determined by a non-parametric sign test. This is consistent with the statistically significant linear correlation result discussed above. Because nitrate is a photochemically

FIGURE 3.5

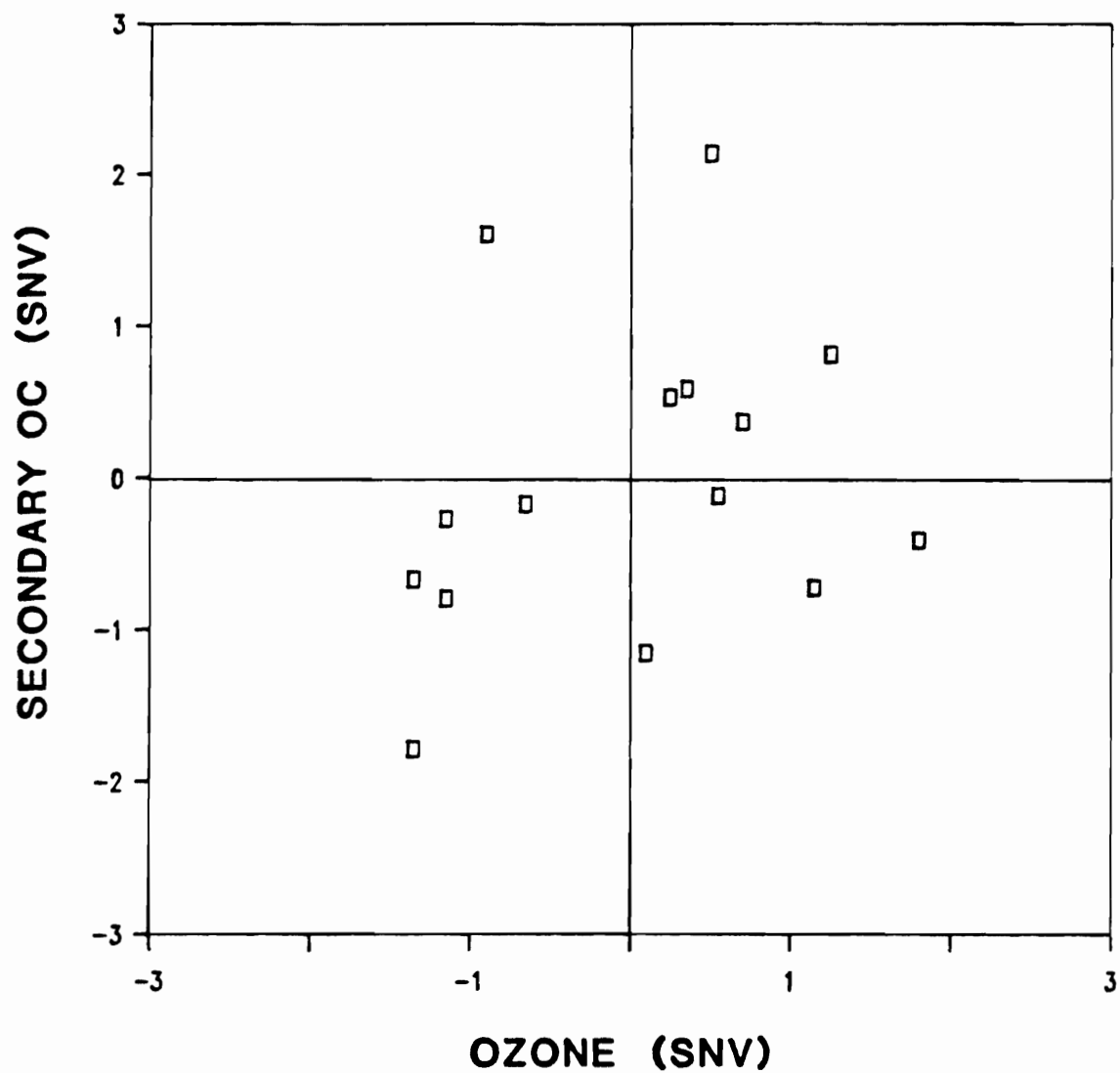


Figure 3.5. Comparison of standard normal variates of secondary organic carbon and ozone concentrations at Pasadena, California, July 5 - September 27, 1984. A data set presented in the form of standard normal variates has zero mean and a standard deviation of one.

FIGURE 3.6

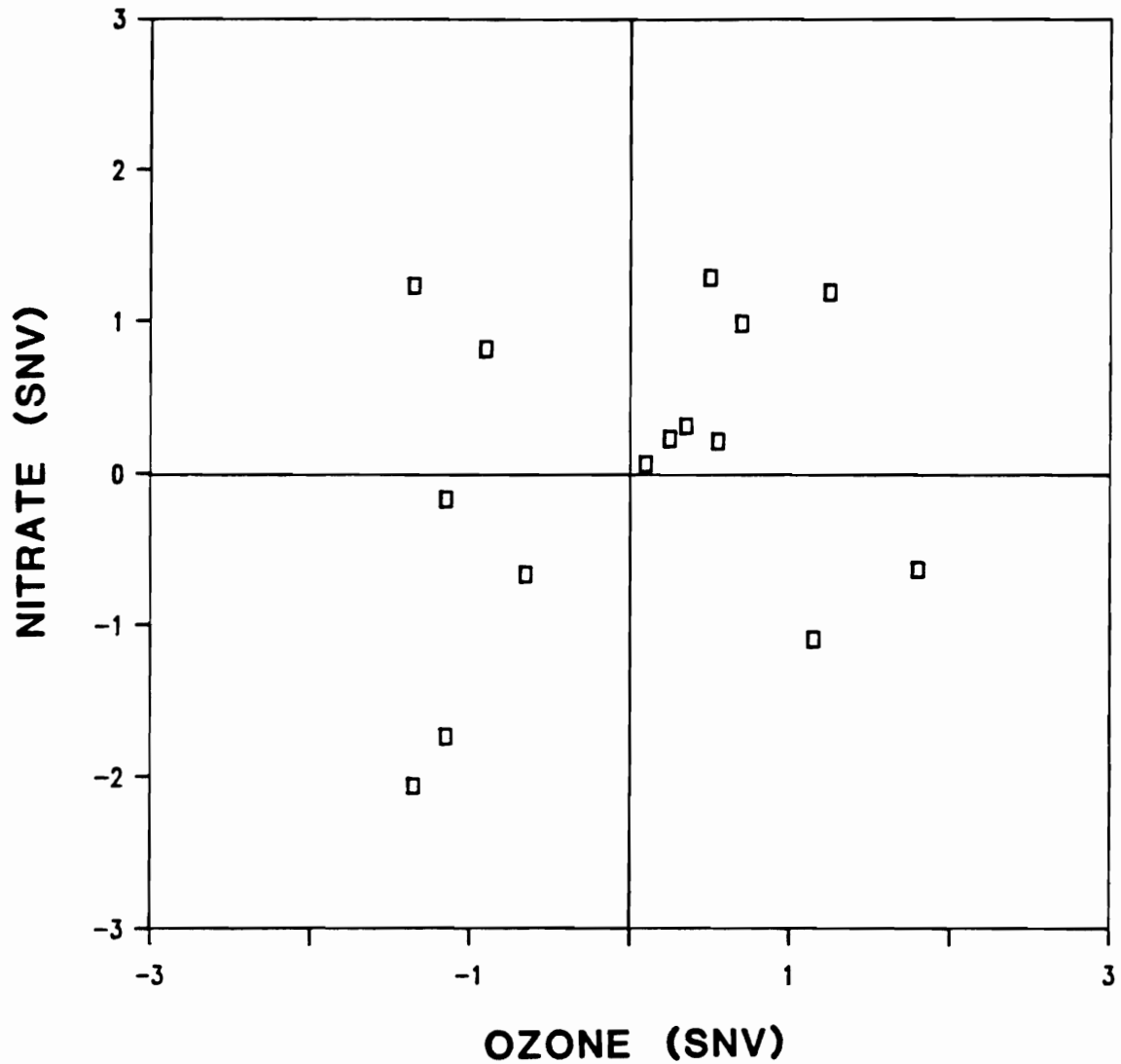


Figure 3.6. Comparison of standard normal variates of nitrate and ozone concentrations at Pasadena, California, July 5 - September 27, 1984. A data set presented in the form of standard normal variates has zero mean and a standard deviation of one.

FIGURE 3.7

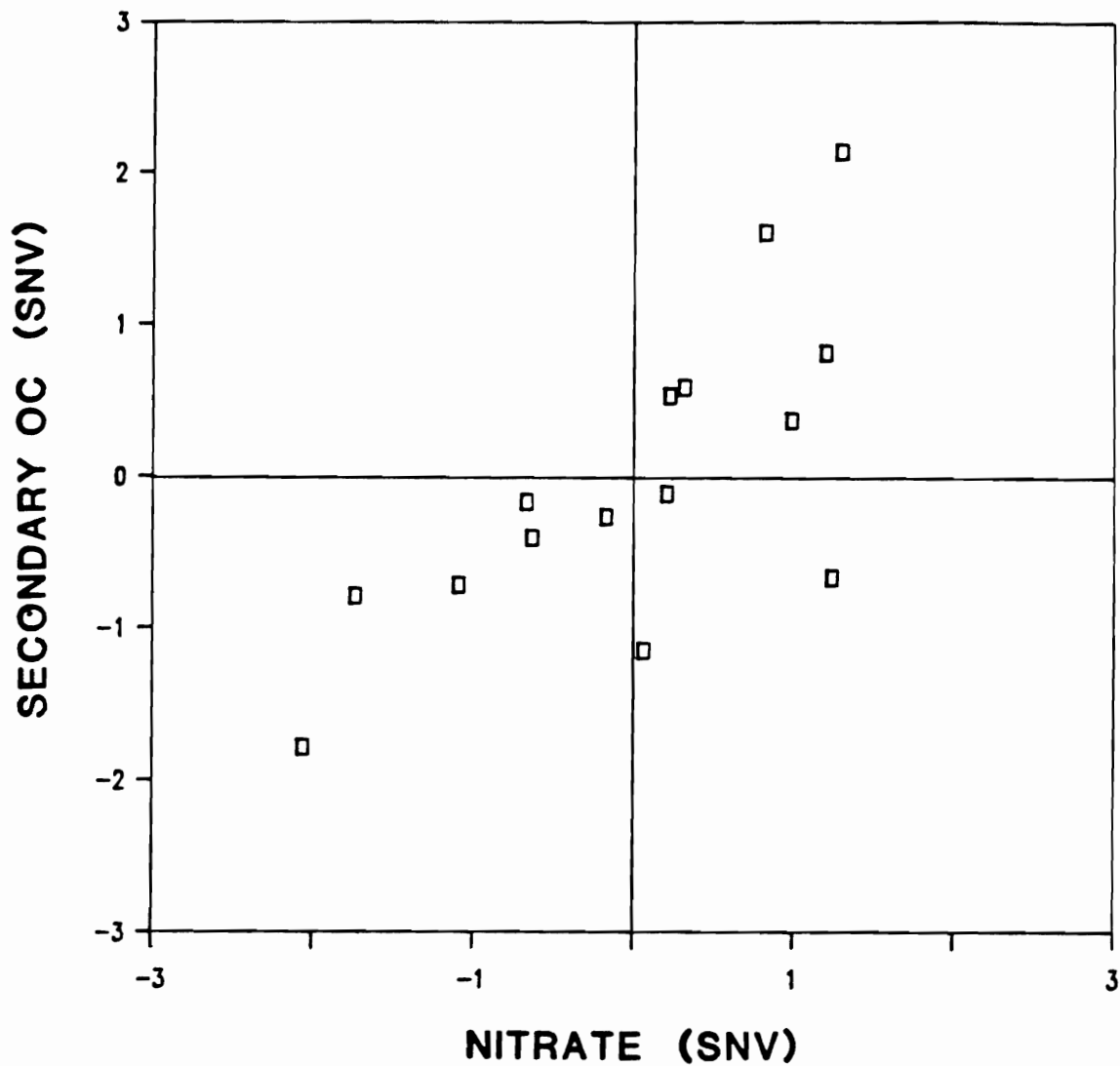


Figure 3.7. Comparison of standard normal variates of secondary organic carbon and nitrate concentrations at Pasadena, California, July 5 - September 27, 1984. A data set presented in the form of standard normal variates has zero mean and a standard deviation of one.

generated secondary aerosol component, these correlations support our definition of secondary organic aerosol.

Despite large uncertainties resulting from manual sampling and limitations in the analytical method, OC/EC ratios were significantly greater than the primary ratio at 95% confidence levels on most sampling days at all sites. Figures 3.8 - 3.12 show OC/EC for each site; the range in which the primary ratio falls is shown for comparison. OC/EC ratios ranged from 1.5 to 16.2 with an intersite average of 4.9, which is substantially higher than the primary ratio.

The total organic carbon concentrations for each site are shown in Figures 3.13 - 3.17 with the minimum and maximum concentrations which can be attributed to primary aerosol. Results suggest that a significant amount of secondary organic aerosol formation took place on most days, particularly in Pasadena, Upland and San Bernardino. Site averages are presented in Table 3.3. Each entry is presented as a range of values to take into account the uncertainty in the primary OC/EC ratio. Large secondary contributions were seen in Pasadena on August 28 and San Bernardino, the eastern most site, on Sept 15 where 10 - 11 $\mu\text{gC}/\text{m}^3$ and 14 - 16 $\mu\text{gC}/\text{m}^3$, respectively, were attributed to secondary formation. The contributions of primary and secondary sources vary considerably from day to day. August 10 in Lennox was a day when apparently all the organic aerosol observed during the mid-day period was of primary origin. However, under mid-day, summer conditions, secondary formation appears to be responsible for roughly half of the organic aerosol in the Los Angeles basin.

FIGURE 3.8

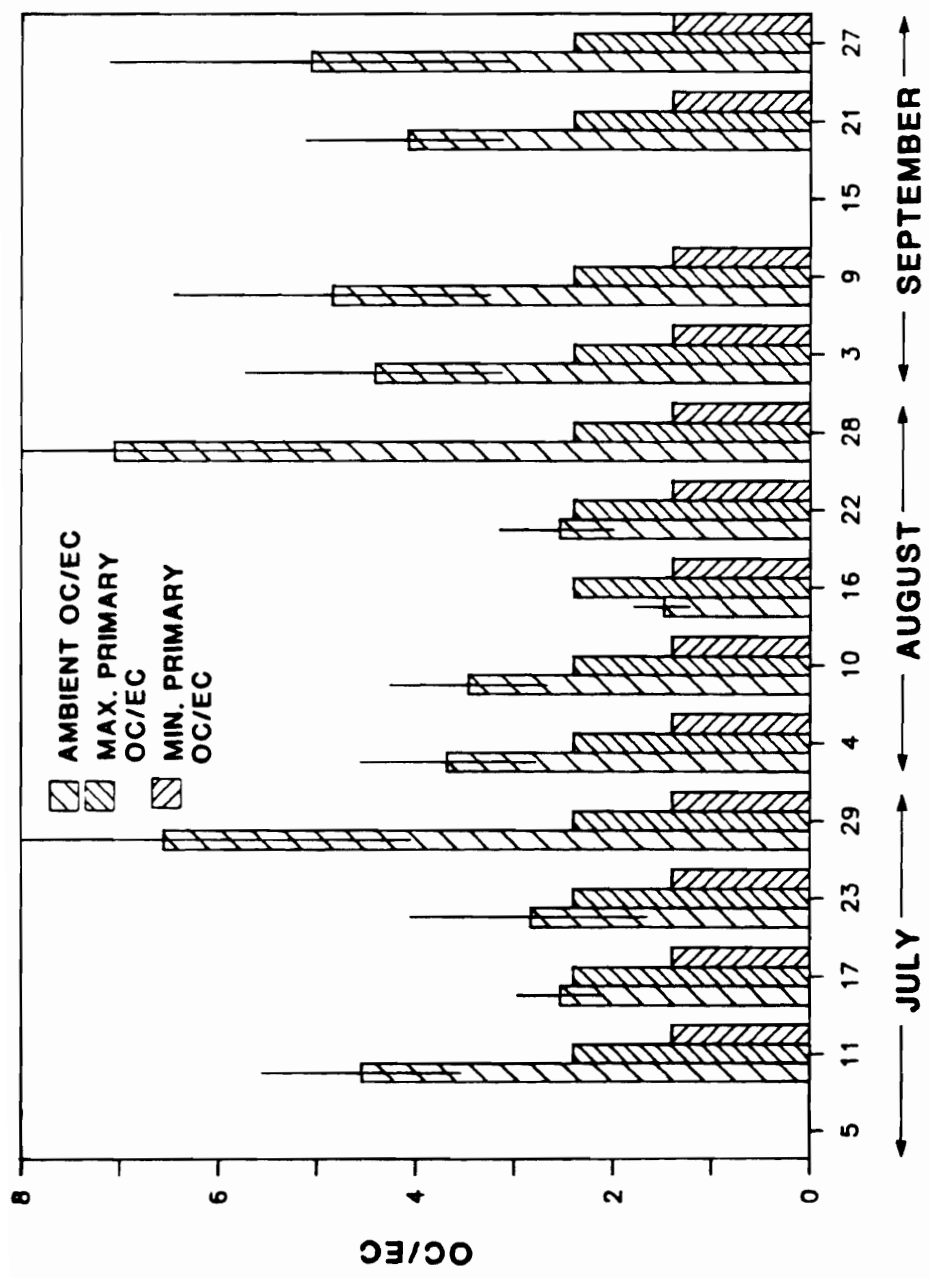


Figure 3.8. Ambient ratios of organic to elemental carbon for particles under 2.0 μm in diameter at Lennox, California, July 5 - September 27, 1984. Shown with maximum and minimum estimates of the primary organic to elemental carbon ratio. Error bars are 95% confidence limits.

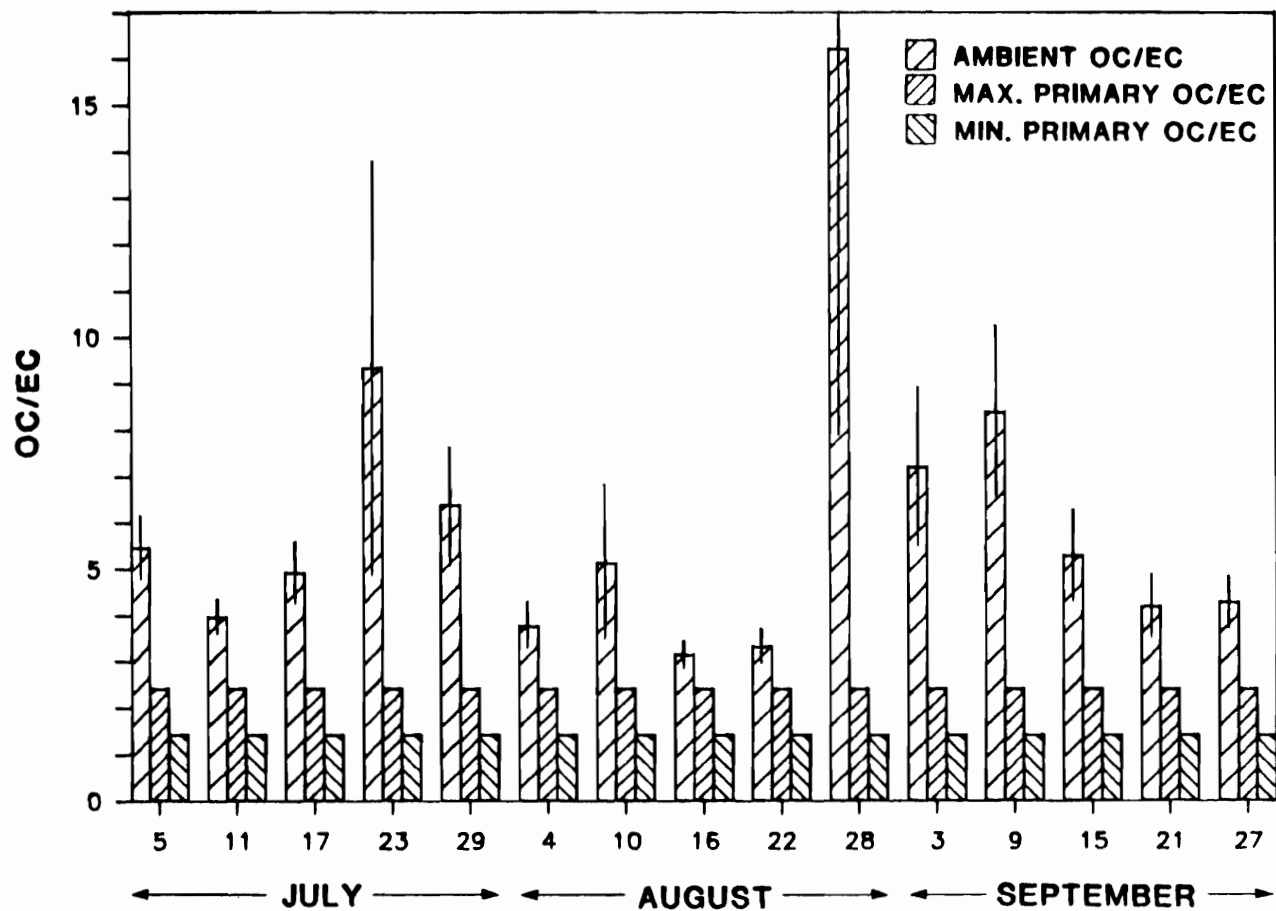


Figure 3.9. Ambient ratios of organic to elemental carbon for particles under $2.0 \mu\text{m}$ in diameter at Pasadena, California, July 5 - September 27, 1984. Shown with maximum and minimum estimates of the primary organic to elemental carbon ratio. Error bars are 95% confidence limits.

FIGURE 3.9

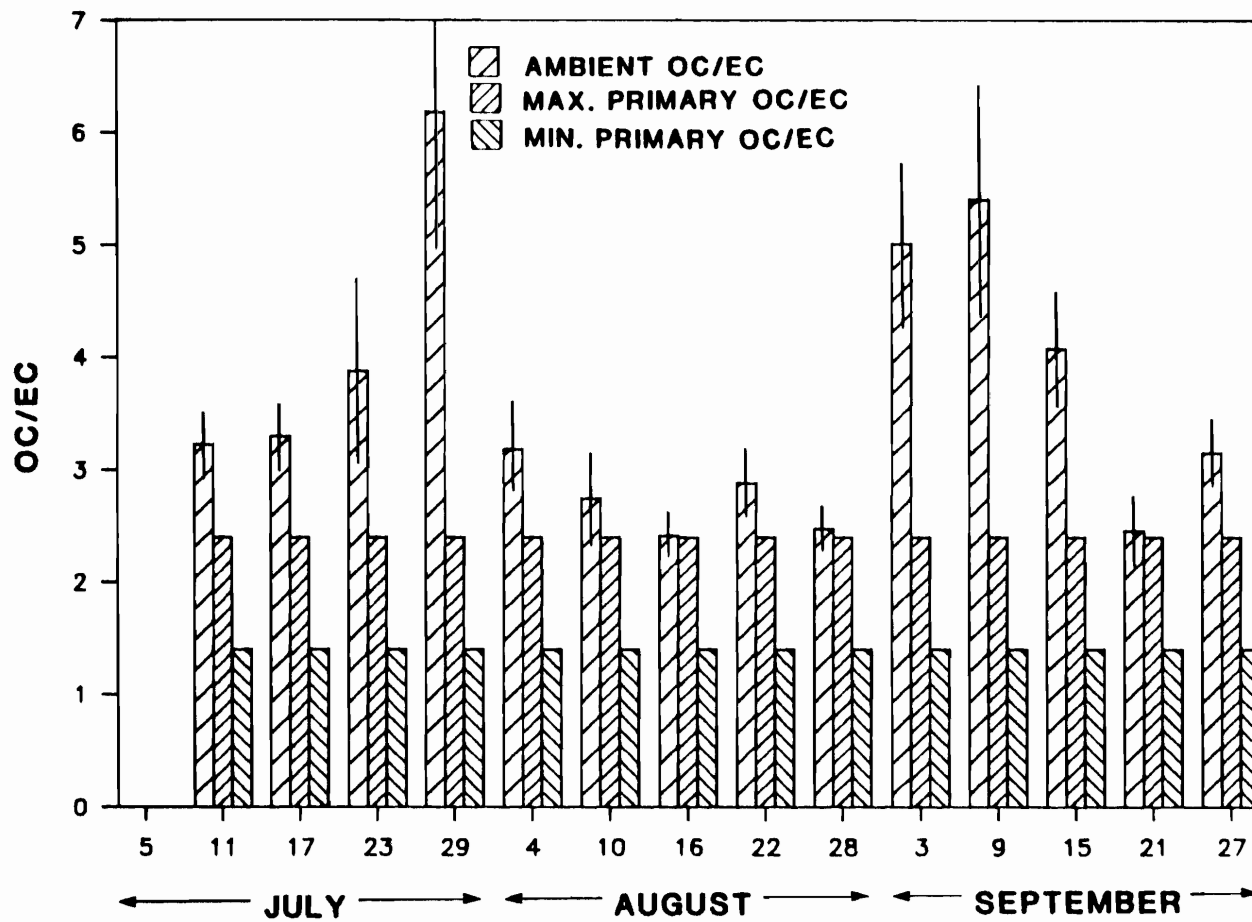


Figure 3.10. Ambient ratios of organic to elemental carbon for particles under $2.0 \mu\text{m}$ in diameter at Azusa, California, July 5 - September 27, 1984. Shown with maximum and minimum estimates of the primary organic to elemental carbon ratio. Error bars are 95% confidence limits.

FIGURE 3.10

FIGURE 3.11

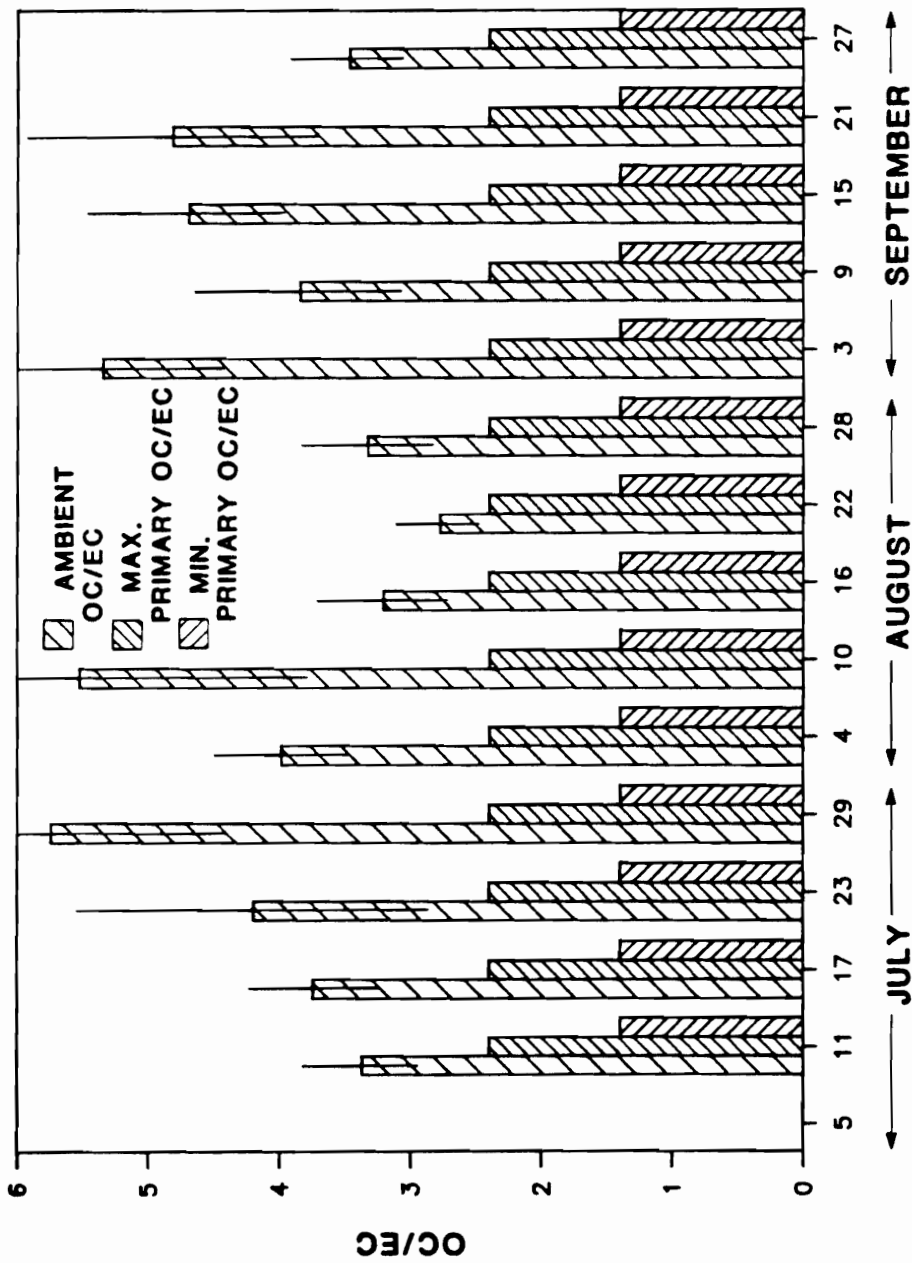


Figure 3.11. Ambient ratios of organic to elemental carbon for particles under 2.0 μm in diameter at Upland, California, July 5 - September 27, 1984. Shown with maximum and minimum estimates of the primary organic to elemental carbon ratio. Error bars are 95% confidence limits.

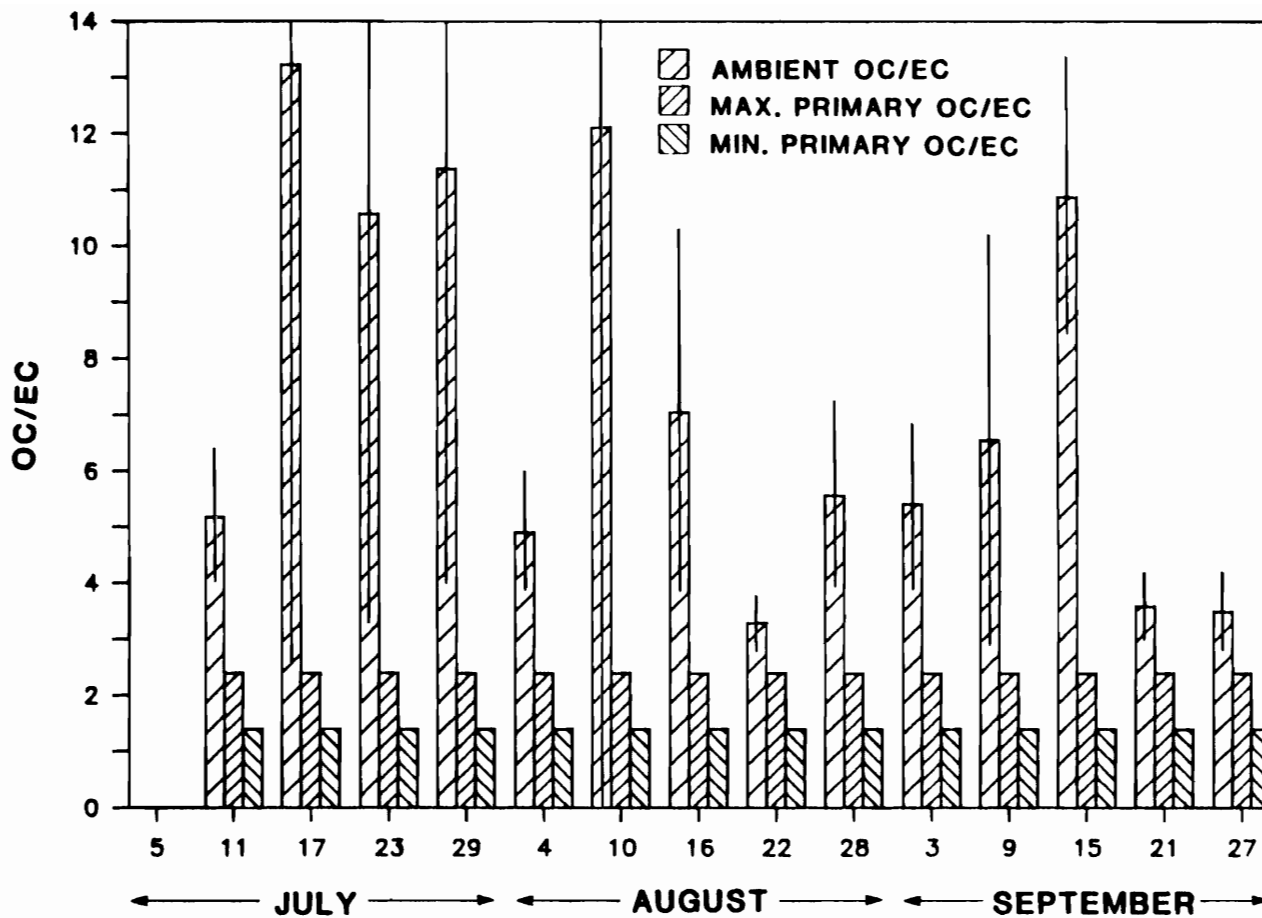


Figure 3.12. Ambient ratios of organic to elemental carbon for particles under $2.0 \mu\text{m}$ in diameter at San Bernardino, California, July 5 - September 27, 1984. Shown with maximum and minimum estimates of the primary organic to elemental carbon ratio. Error bars are 95% confidence limits.

FIGURE 3.12

FIGURE 3.13

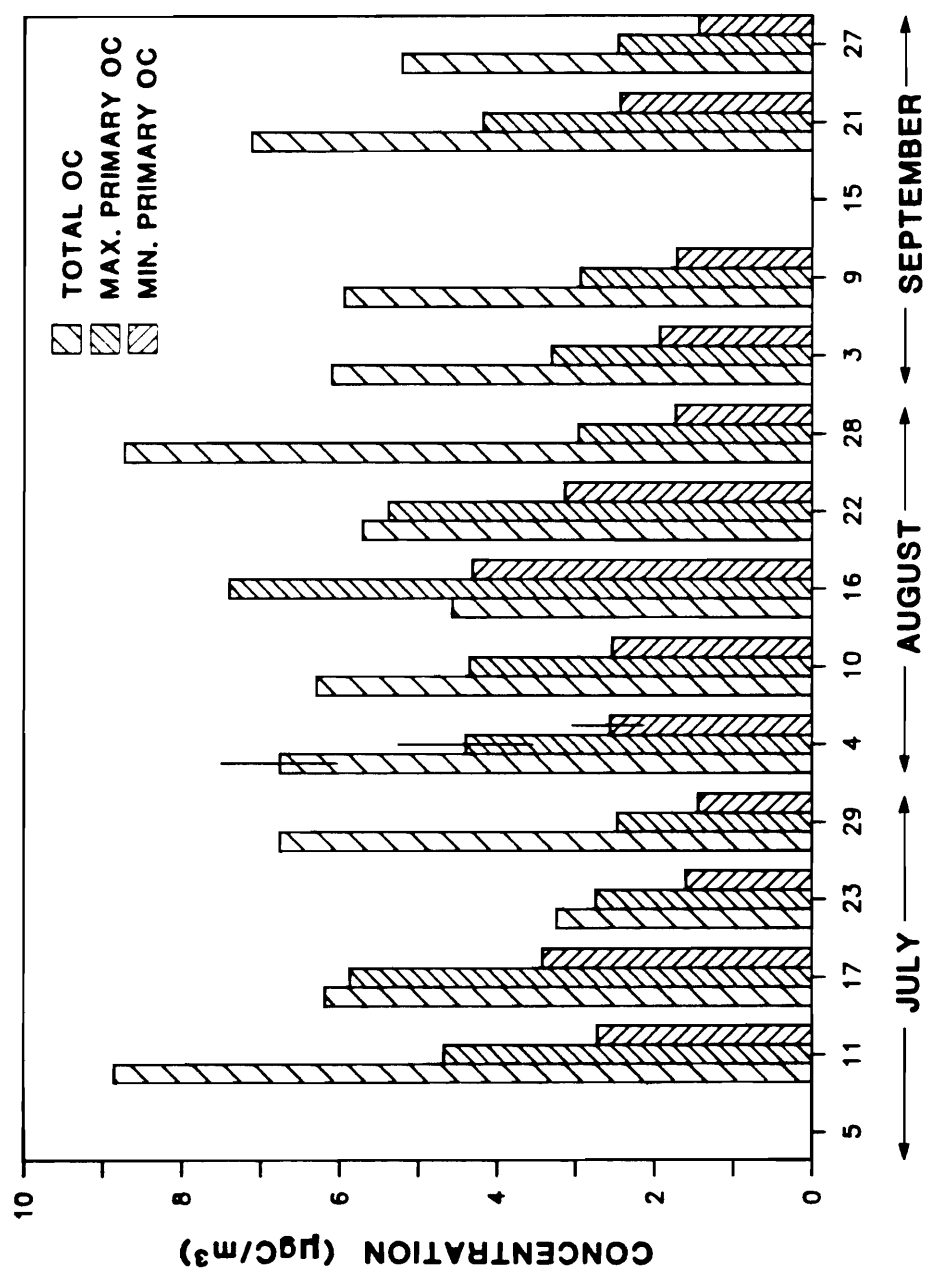


Figure 3.13. Total organic carbon concentrations and maximum and minimum primary organic carbon concentration estimates ($\mu\text{gC}/\text{m}^3$) for particles under $2.0 \mu\text{m}$ in diameter at Lennox, California, July 5 - September 27, 1984. Error bars are 95% confidence limits.

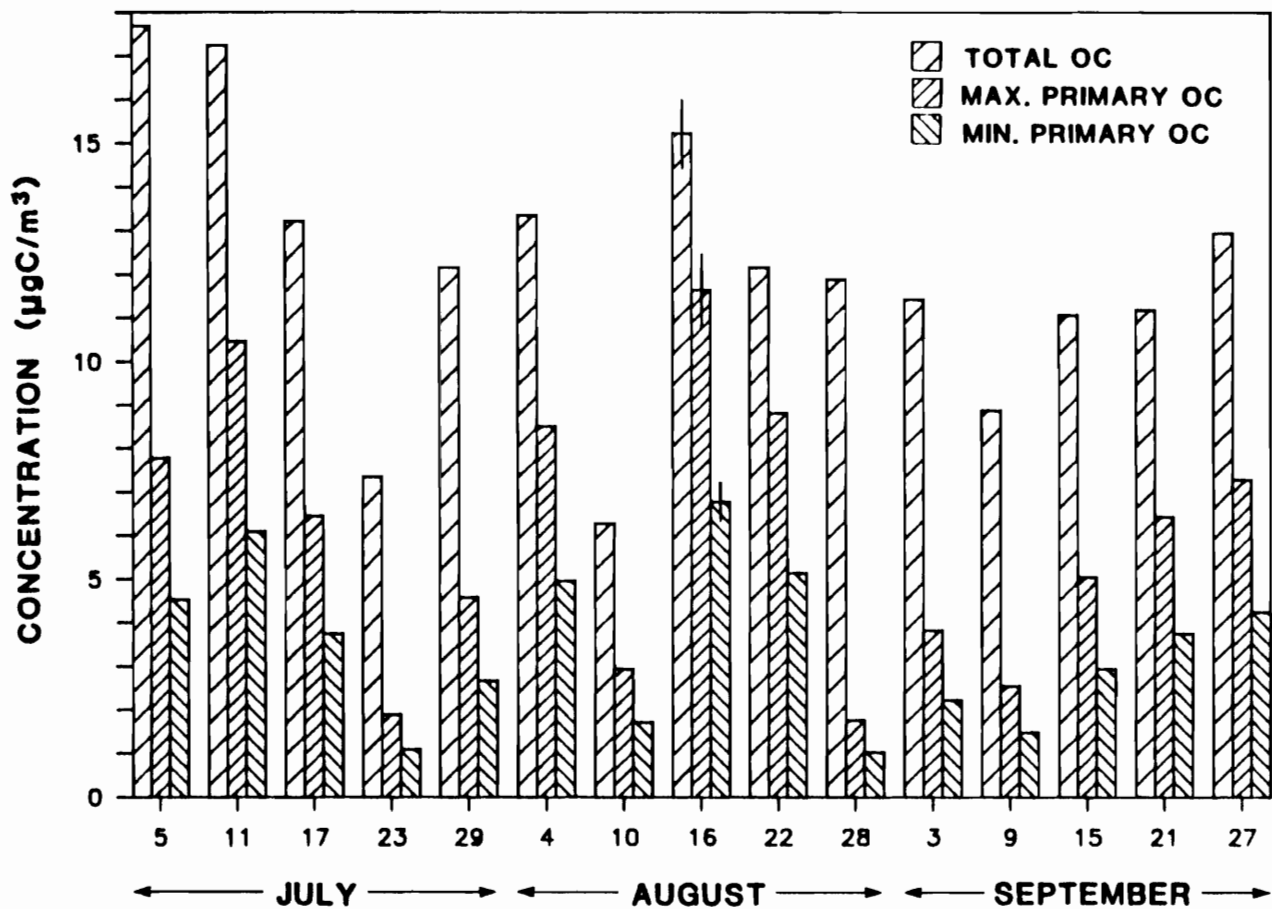


Figure 3.14. Total organic carbon concentrations and maximum and minimum primary organic carbon concentration estimates ($\mu\text{gC}/\text{m}^3$) for particles under $2.0 \mu\text{m}$ in diameter at Pasadena, California, July 5 - September 27, 1984. Error bars are 95% confidence limits.

FIGURE 3.14

FIGURE 3.15

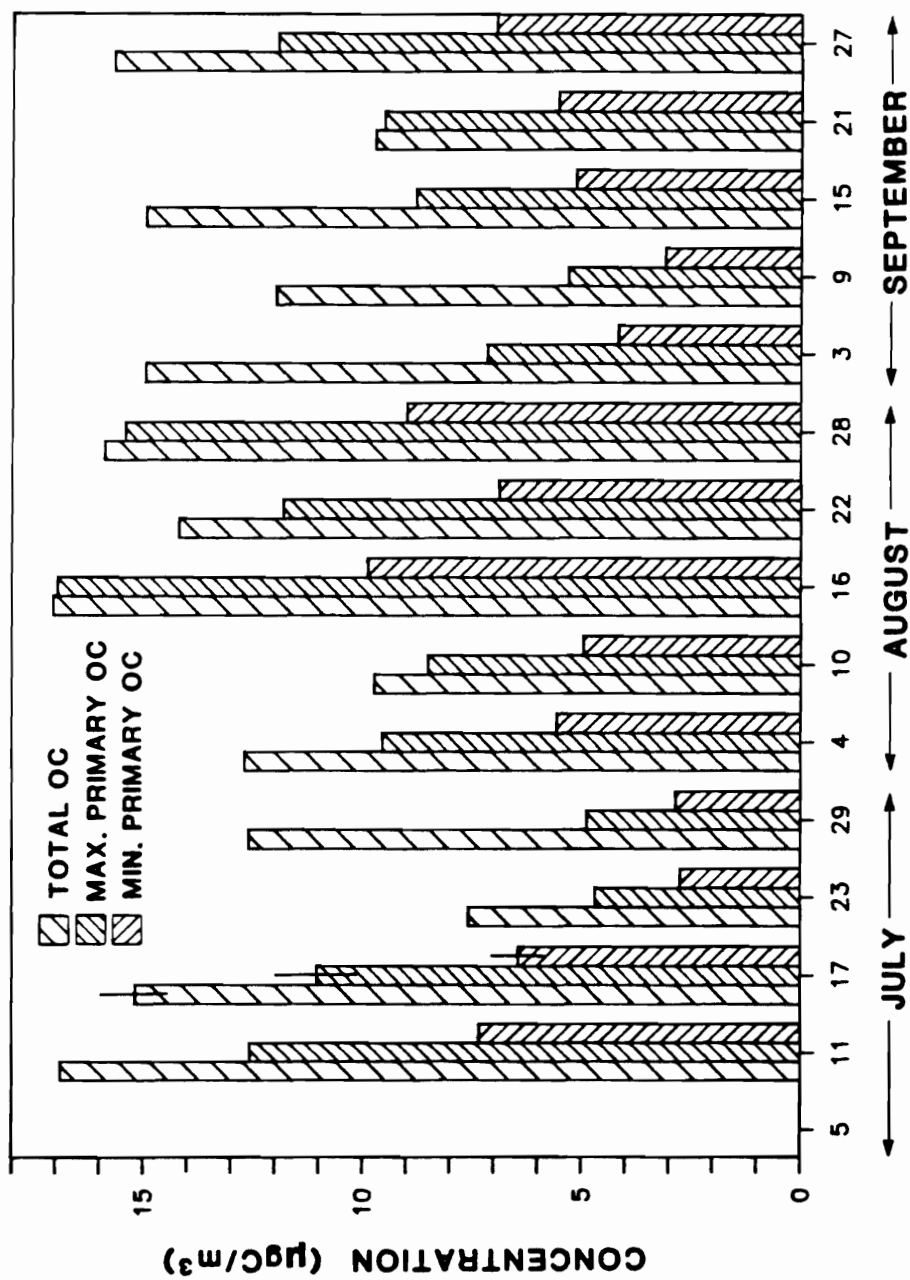


Figure 3.15. Total organic carbon concentrations and maximum and minimum primary organic carbon concentration estimates ($\mu\text{gC}/\text{m}^3$) for particles under $2.0 \mu\text{m}$ in diameter at Azusa, California, July 5 - September 27, 1984. Error bars are 95% confidence limits.

FIGURE 3.16

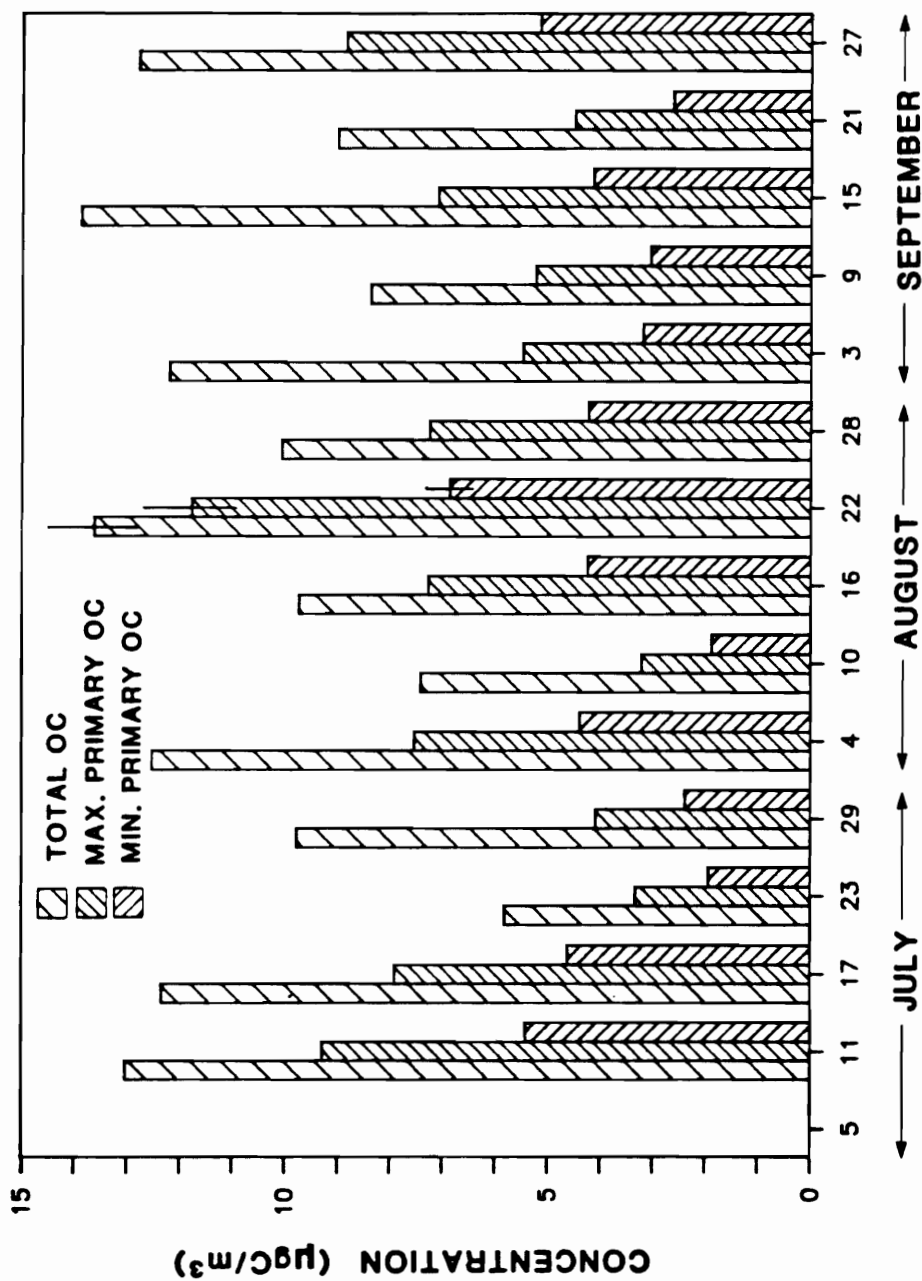


Figure 3.16. Total organic carbon concentrations and maximum and minimum primary organic carbon concentration estimates ($\mu\text{gC}/\text{m}^3$) for particles under $2.0 \mu\text{m}$ in diameter at Upland, California, July 5 - September 27, 1984. Error bars are 95% confidence limits.

FIGURE 3.17

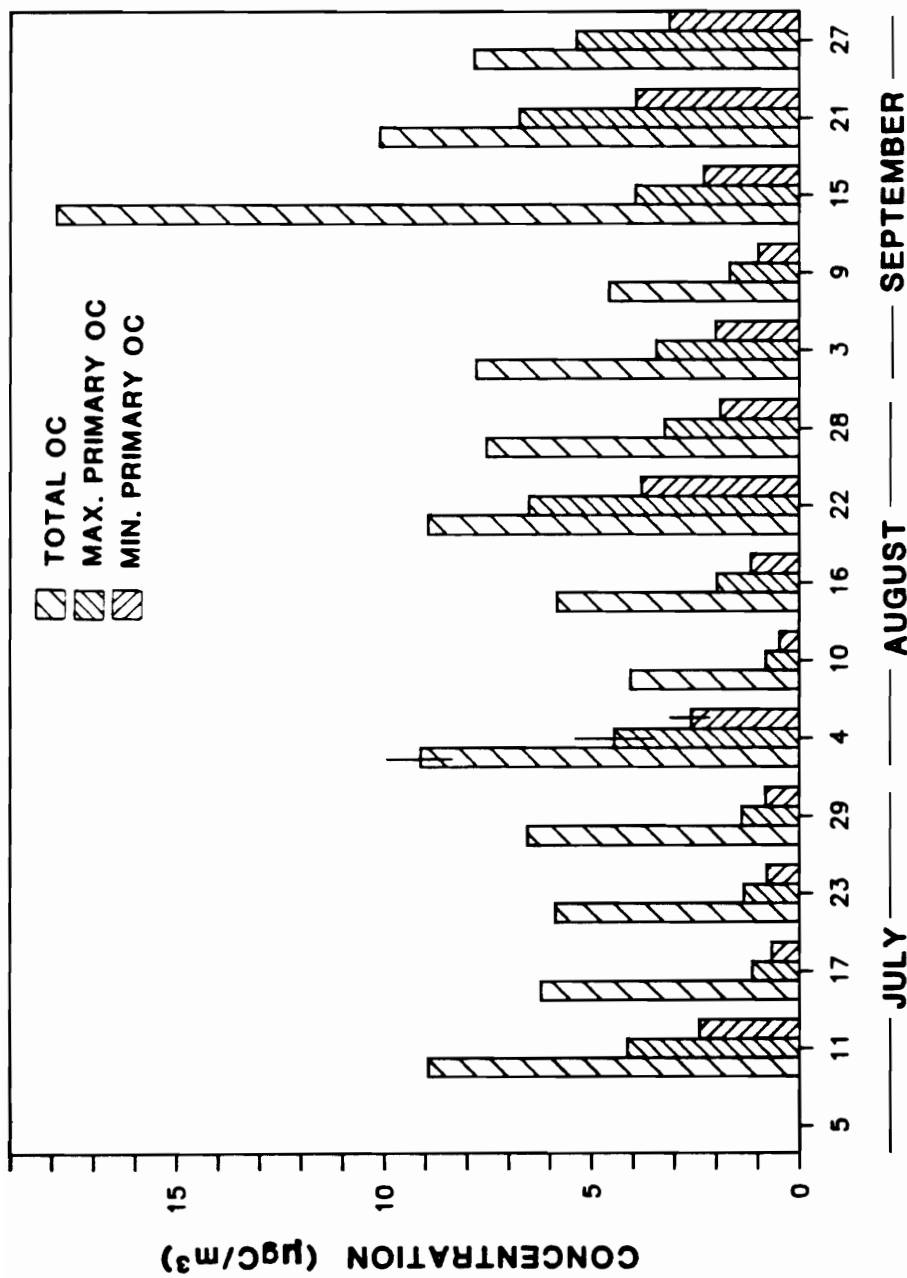


Figure 3.17. Total organic carbon concentrations and maximum and minimum primary organic carbon concentration estimates ($\mu\text{gC}/\text{m}^3$) for particles under $2.0 \mu\text{m}$ in diameter at San Bernardino, California, July 5 - September 27, 1984. Error bars are 95% confidence limits.

TABLE 3.3. AVERAGE ORGANIC CARBON VALUES

Average percent secondary refers to the percent of total organic carbon which can be attributed to secondary formation averaged over all sampling days at that site.

	TOTAL O.C. ($\mu\text{gC}/\text{m}^3$)	TOTAL E.C. ($\mu\text{gC}/\text{m}^3$)	PRIMARY O.C. ($\mu\text{gC}/\text{m}^3$)	AVG PERCENT SECONDARY (%)
LENNOX	6.3	1.7	2 - 4	31 - 60
PASADENA	12.1	2.5	4 - 6	53 - 72
AZUSA	13.5	4.1	6 - 10	28 - 58
UPLAND	10.8	2.8	4 - 7	39 - 65
SAN B.	8.0	1.4	2 - 3	60 - 76

SUMMARY

Aerosol sampling during photochemically active times across the Los Angeles Basin has provided evidence of secondary formation of organic aerosol in the ambient atmosphere. Mid-day, total organic carbon concentrations correlated equally well with elemental carbon, a tracer for primary organic aerosol, and with ozone, an indicator of photochemical activity. Ratios of ambient OC/EC exceeded the primary ratio estimates on most sampling days at all sites, and it was possible to estimate the secondary OC component on the basis of ambient data and primary OC/EC ratios. The resultant secondary OC showed a statistically significant linear correlation with aerosol nitrate, another secondary component, but the linear correlation with ozone, a presumed precursor, was not statistically significant. Because of the complexity of the chemistry the lack of correlation between product and precursor was not surprising. The use of a non-parametric sign test, which does not impose a linear model on the data, revealed a fair correlation between secondary OC and ozone and an excellent correlation between secondary OC and nitrate.

Secondary organic aerosol so defined appears to have contributed roughly half of the organic aerosol in the Los Angeles basin during mid-day summer conditions. It is quite possible that secondary aerosol concentrations are not significant compared to primary aerosol when averaged over a 24 hour period. However, a contribution of this magnitude to mid-day aerosol concentrations can be expected to have a significant impact on visibility and health. Additional research is needed to evaluate the variability of the primary ratio and explore the time dependence of carbonaceous aerosol concentrations.

CHAPTER 4. AN IN SITU, TIME-RESOLVED ANALYZER FOR AEROSOL ORGANIC AND ELEMENTAL CARBON

INTRODUCTION

Although secondary formation of organic aerosols has been demonstrated in smog chamber experiments involving selected organic compounds and oxides of nitrogen (e.g., Heisler and Friedlander, 1977; McMurry and Grosjean, 1985), there is considerable uncertainty concerning the importance of secondary organic aerosol formation in the ambient atmosphere. Progress in understanding this problem has been hampered by the lack of adequate time resolution in conventional filter sampling methods for organic aerosol. These methods involve the collection of aerosol by drawing ambient air through filters which are then transported to the laboratory for analysis at a later time. Sample handling, volatilization loss during storage, and limitations in the analytical method contribute to high detection limits. To overcome these problems, long sampling periods are usually required, and consequently, most of the concentration data for carbonaceous aerosol are in the form of 12 or 24 hour averages. Because atmospheric chemistry is dynamic on the time scale of minutes to hours, a great deal of information is lost in these long averaging periods. In particular, diurnal cycles which could be associated with secondary formation processes, have been difficult to resolve.

Filter sampling for organic aerosol is complicated by two additional problems. Adsorption of organic vapors on the sampling filter comprises a positive artifact, and volatilization, which removes material from the filter, is a negative artifact (Cadle et al., 1983; McDow, 1986; McDow and Huntzicker, 1989). The latter can occur either when the collected particulate material is exposed to a pressure drop during sampling, and/or when there is a change in ambient air quality causing a redistribution of material between gas and particulate phases. McDow and Huntzicker (1989) have shown that the correction for vapor adsorption can be approximated with a two-port, parallel sampler. This technique has been incorporated into the in situ carbon analyzer and is described below.

THE IN SITU CARBON ANALYZER

Because of the need to obtain improved time resolution, low detection limits, and minimal influence from sampling artifacts, an in situ carbon analyzer was developed. This instrument combines the sampling function of a conventional filter sampler with the analytical function of a thermal-optical carbon analyzer (Huntzicker et al., 1982; Johnson et al., 1981). The instrument has been packaged as several independent units to facilitate rapid assembly in the field. In addition, the analytical unit is open-sided (components are mounted on stacked platforms) allowing modification for alternate experiments. The layout of the analytical unit is shown in Figure 4.1 and 4.2, and Figure 4.3 is an operational schematic.

The sampling system consists of two independent filter samplers which provide for the collection of aerosol and the determination of the vapor

FIGURE 4.1

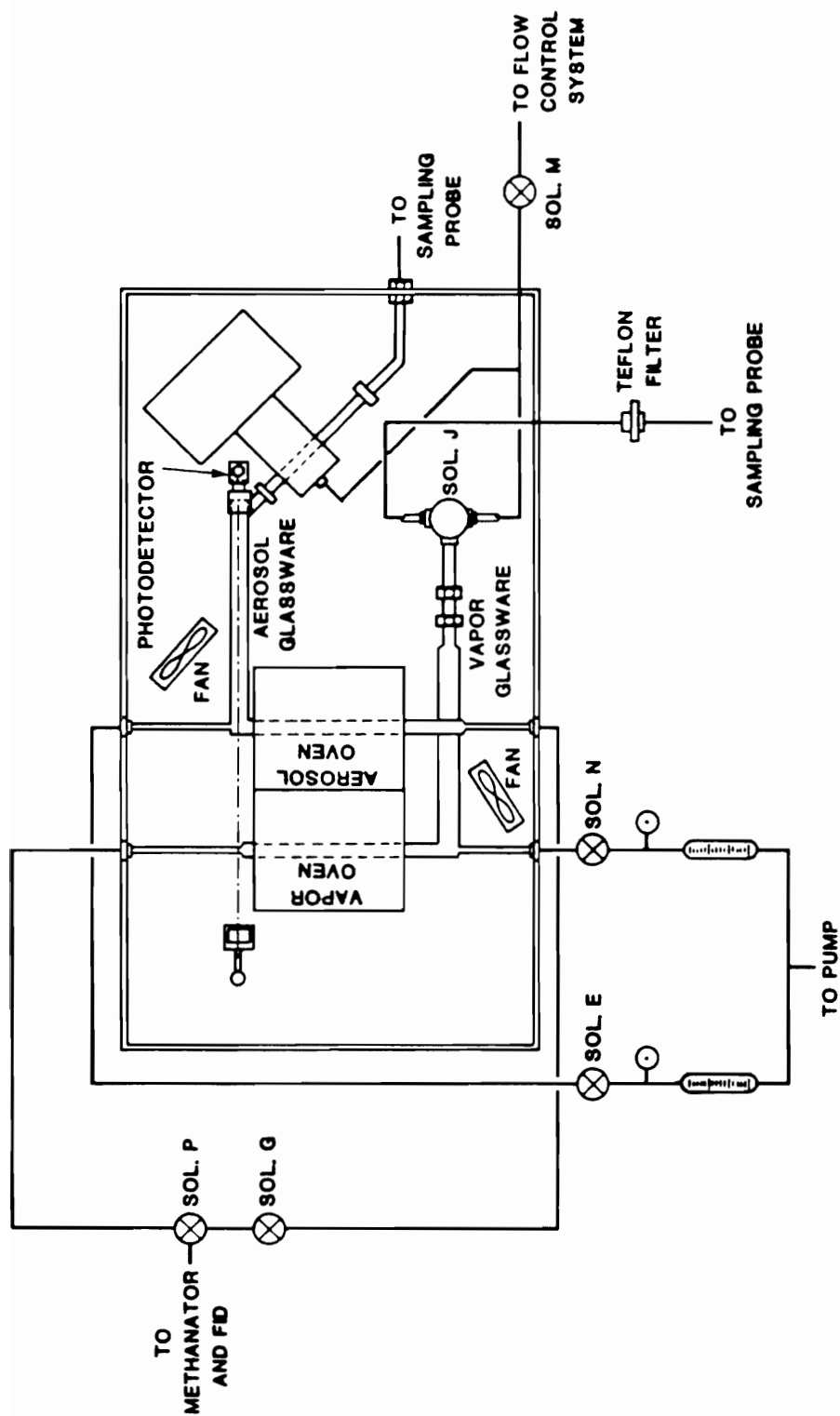


Figure 4.1. In situ carbon analyzer analytical unit with tubing diagram, top view. Fans point to locations in glassware where quartz fiber filter disks are mounted. SOL: solenoid valve.

FIGURE 4.2

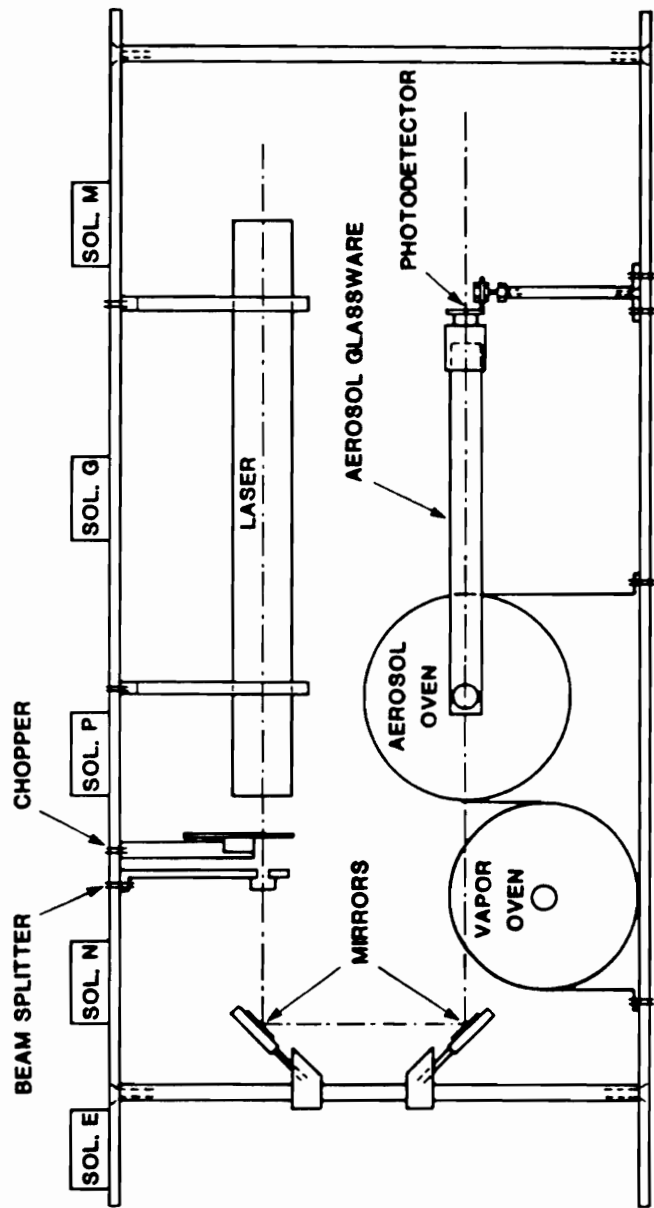


Figure 4.2. *In situ* carbon analyzer analytical unit, side view.

SOL: solenoid valve.

FIGURE 4.3

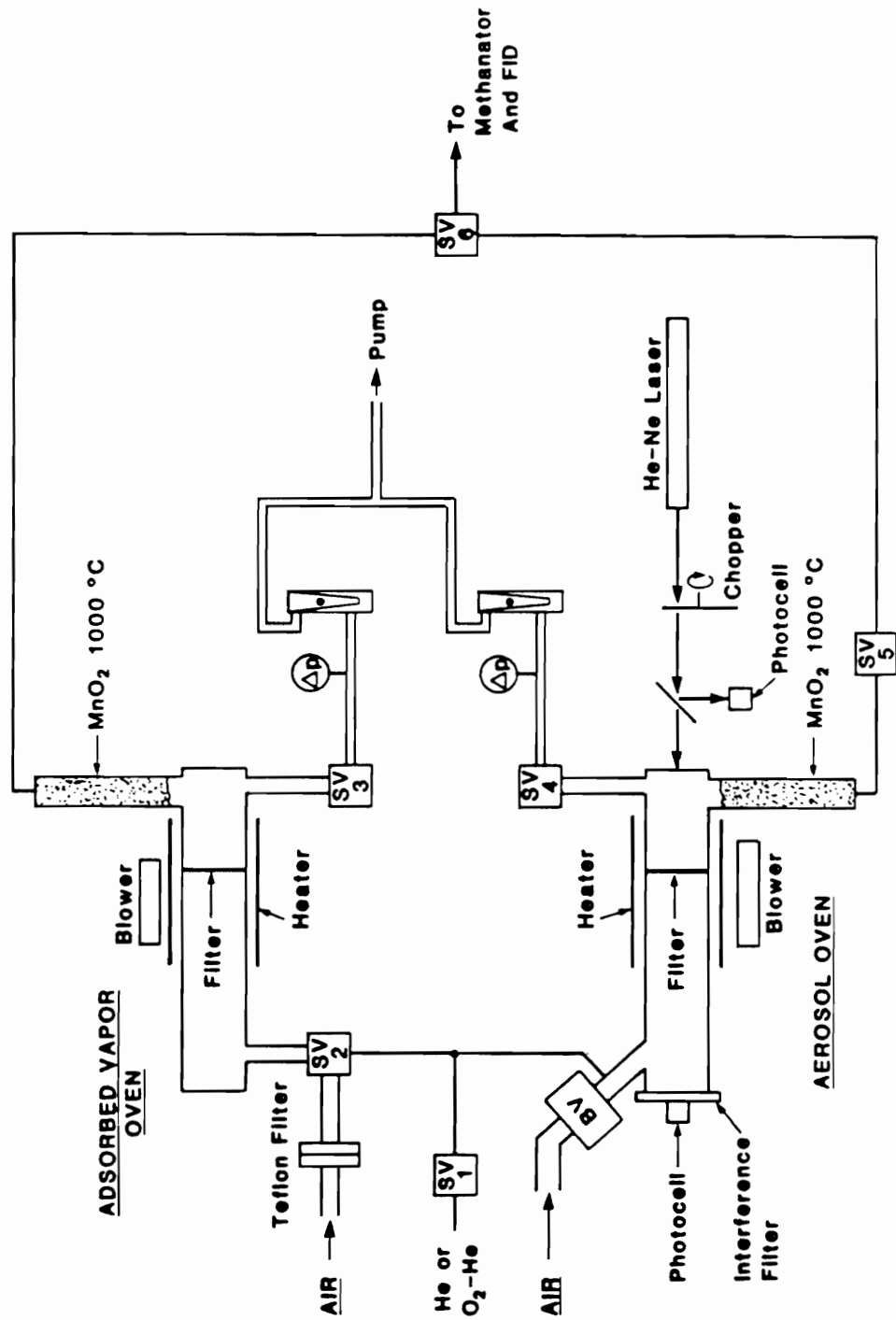


Figure 4.3. Schematic of *in situ* carbon analyzer. BV: ball valve; SV1-SV6: solenoid valves.

adsorption artifact (see Chapter 6). In each sampler two back-to-back, circular disks (1.5 cm diameter) of a quartz fiber filter (Pallflex QAOT) are mounted inside the carbon analyzer as shown in Figure 4.4. (Two filter disks are necessary to prevent rupture during sampling.) In the aerosol-side sampler ambient air is drawn through a 2.5 μm cut-point Marple (1974) impactor with a jet Reynolds number of 3700 (Marple and Liu, 1975). The quartz fiber filters which follow collect the fine fraction of the aerosol and whatever organic vapor adsorbs on the filters. Between the impactor and the filters is a ball valve (BV) which is used to isolate the system from the atmosphere during the analytical part of the cycle. A ball valve is used for this application to permit the unimpeded flow of aerosol into the instrument during the sampling part of the cycle.

On the vapor side a Teflon filter (Gelman Teflon ringed, 47 mm diameter, 2 μm pore size filter) is mounted upstream of the quartz fiber filters. The Teflon filter removes the particulate material but because of its low surface area adsorbs a relatively small amount of organic vapors in comparison to a quartz fiber filter. The quartz fiber filter behind the Teflon filter collects only adsorbable organic vapors and provides an estimate of the amount of organic vapor adsorbing on the quartz fiber aerosol filter. The concentration of organic aerosol can then be estimated by subtracting the organic carbon concentration on the Teflon - quartz backup filter from the organic carbon concentration on the quartz fiber aerosol filter. A Teflon solenoid valve (SV2) isolates the vapor side from the atmosphere during analysis. Both sampling lines draw from a common manifold, and the flow in both sides is maintained at 8.5 l/min. This sampling rate corresponds to a filter face velocity of 80 cm/s. Because collection periods are short and the

FIGURE 4.4

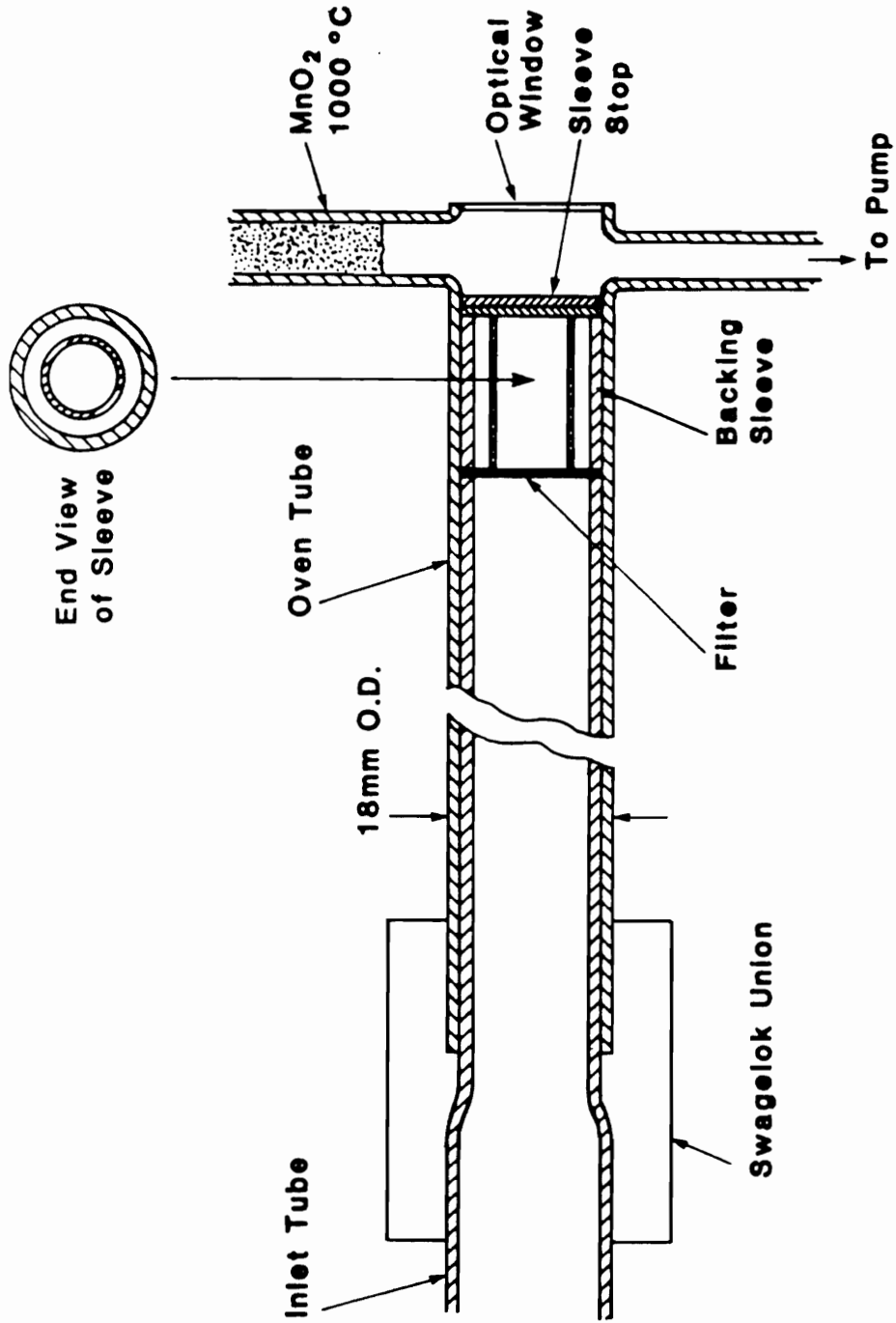


Figure 4.4. Filter mounting system for *in situ* carbon analyzer. The backing sleeve provides a support on which the two back-to-back quartz fiber filter disks are mounted.

major aerosol components (including sulfates and nitrates) are removed during the analytical part of each operating cycle, only a minimal buildup of pressure drop occurs during sampling. This minimizes the volatilization artifact.

Correction is made for adsorption.

Ambient air is drawn through the filters with a pump for a preset period of time. At the end of the sampling period the aerosol-side ball valve (BV), the vapor-side solenoid valve (SV2), and the pump solenoid valves (SV3, SV4) close, and the instrument is converted to a carbon analyzer similar in design to the OGC laboratory carbon analyzer (Huntzicker et al., 1982; Johnson et al., 1981). After purging the system with helium, the vapor side is analyzed by rapid heating to 650 C. Adsorbed organic vapors are volatilized and oxidized to CO₂ in a 1000 C MnO₂ bed. The CO₂ is reduced to CH₄ in a 500 C nickel-firebrick methanator and measured in a flame ionization detector (FID). At the completion of the adsorbed vapor measurement a solenoid valve (SV6) switches, and the filters from the aerosol side of the instrument are analyzed. The first step in this process involves heating to 650 C in a helium atmosphere to volatilize adsorbed organic vapors and particulate organic carbon. At the completion of this process the temperature is reduced to about 350 C, and the atmosphere is changed to 2% O₂-98% He to oxidize elemental carbon. The temperature is increased in steps to 750 C, ensuring complete removal of elemental carbon. In the final step of the analysis, a known amount of methane is introduced for internal calibration.

During organic carbon volatilization some organic carbon is pyrolytically converted to elemental carbon (i.e., charring). Correction for pyrolytic conversion is accomplished by monitoring the transmittance of a chopped 633 nm He-Ne

laser light through the aerosol-side filters during the analysis. Figure 4.5a shows the laser transmittance for a typical analysis. At the beginning of the analysis the transmittance through the loaded filters is measured. As the aerosol-side temperature is raised and organic material is removed, pyrolysis occurs; this results in a darkening of the filters and a decrease in transmittance. When oxygen is added, elemental carbon begins to oxidize, and the transmittance increases until the filters are clean. The point at which the transmittance regains its initial value is considered to be the split between organic and elemental carbon. This split is shown in Figure 4.5 by the long line extending upwards from the time axis. All material prior to the split is considered organic and after, elemental. Some temperature dependence has been observed in the laser system as seen by the increase in transmittance when the temperature of the aerosol-side oven is reduced at the end of the analysis. The influence of this effect on the results is small and can be minimized experimentally or corrected in the computations.

Figure 4.5b shows the time behavior of the FID during the carbon analysis. The first peak corresponds to adsorbed organic vapor on the vapor-side quartz fiber filters. The second and third peaks represent material removed from the aerosol filters before and after the addition of oxygen. The final peak is the calibration. The temperature profile of the aerosol-side oven is shown in Figure 4.5c; the vapor-side oven temperature is not shown.

System control, analysis, and data acquisition are all accomplished by an Apple II-Plus computer. At the end of each analysis the computer performs the

FIGURE 4.5

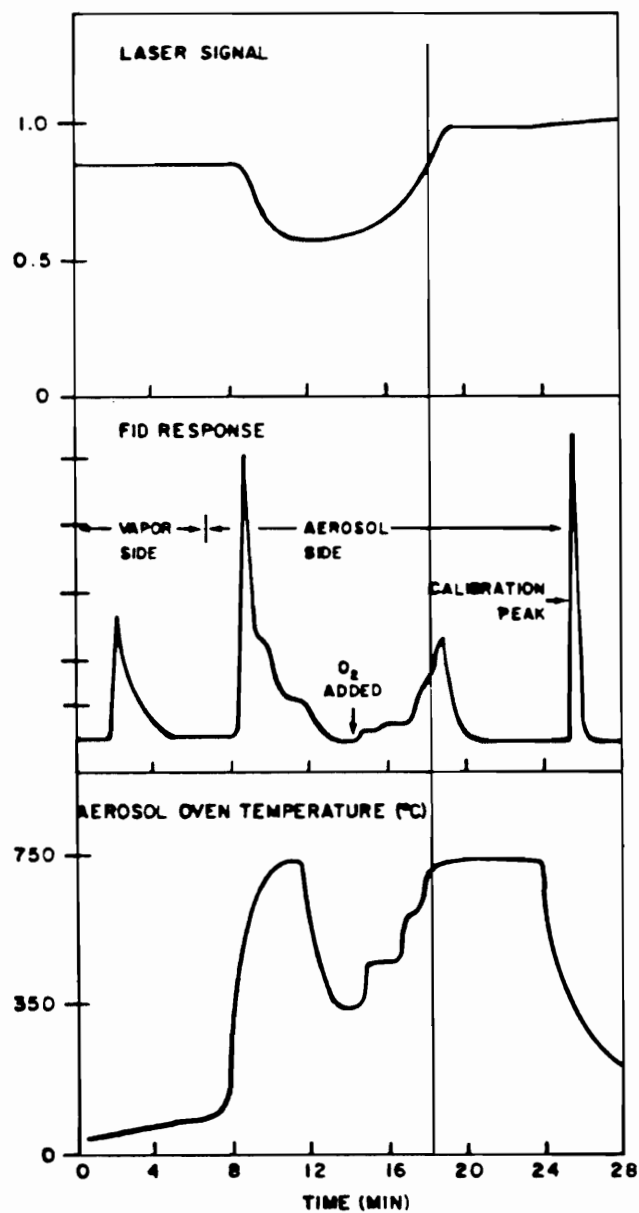


Figure 4.5. Typical output for in situ carbon analyzer.

- (a) Optical transmittance; (b) flame ionization detector;
 (c) temperature of aerosol-side oven. The vertical line occurring at about 18.5 minutes is the split point between organic and elemental carbon.

pyrolysis correction, integrates the peaks, corrects for the vapor adsorption artifact, and presents the results in $\mu\text{gC}/\text{m}^3$.

INSTRUMENT CHARACTERIZATION

The analytical precision for total carbon (i.e., particulate + adsorbed vapor) was estimated by multiple injections of a known amount of CH_4 into the aerosol oven and measurement of the instrument response using the standard analysis program of the in situ analyzer. Ten injections of 180 μl of 5.39% CH_4 in He were made, and the resultant coefficient of variation was 1.3%. The corresponding detection limit (3σ) was 0.2 μg .

The accuracy of the CH_4 injection approach was checked by cross-calibrating against the laboratory thermal-optical carbon analyzer. In this experiment the response of the laboratory analyzer to CH_4 injections and to known amounts of sucrose deposited on quartz fiber filter disks was measured. The latter involved 10 injections ranging between 2 and 25 μgC . The ratio of the methane to sucrose responses was 1.01 ± 0.05 . Thus, there was no difference between the two approaches at a 95% level of confidence, and it can be concluded that the methane injection method is a valid calibration for the in situ analyzer. The methane injection experiment also demonstrated the linearity of the in situ analyzer response over the range studied. A linear regression between the mass of carbon injected and the instrument response gave a very good fit ($R^2=99.5\%$) as shown in Figure 4.6. Regression results are given in Table 4.1.

To check for consistency between the aerosol and vapor sides of the instrument, a set of experiments was run in which both sides were pre-filtered

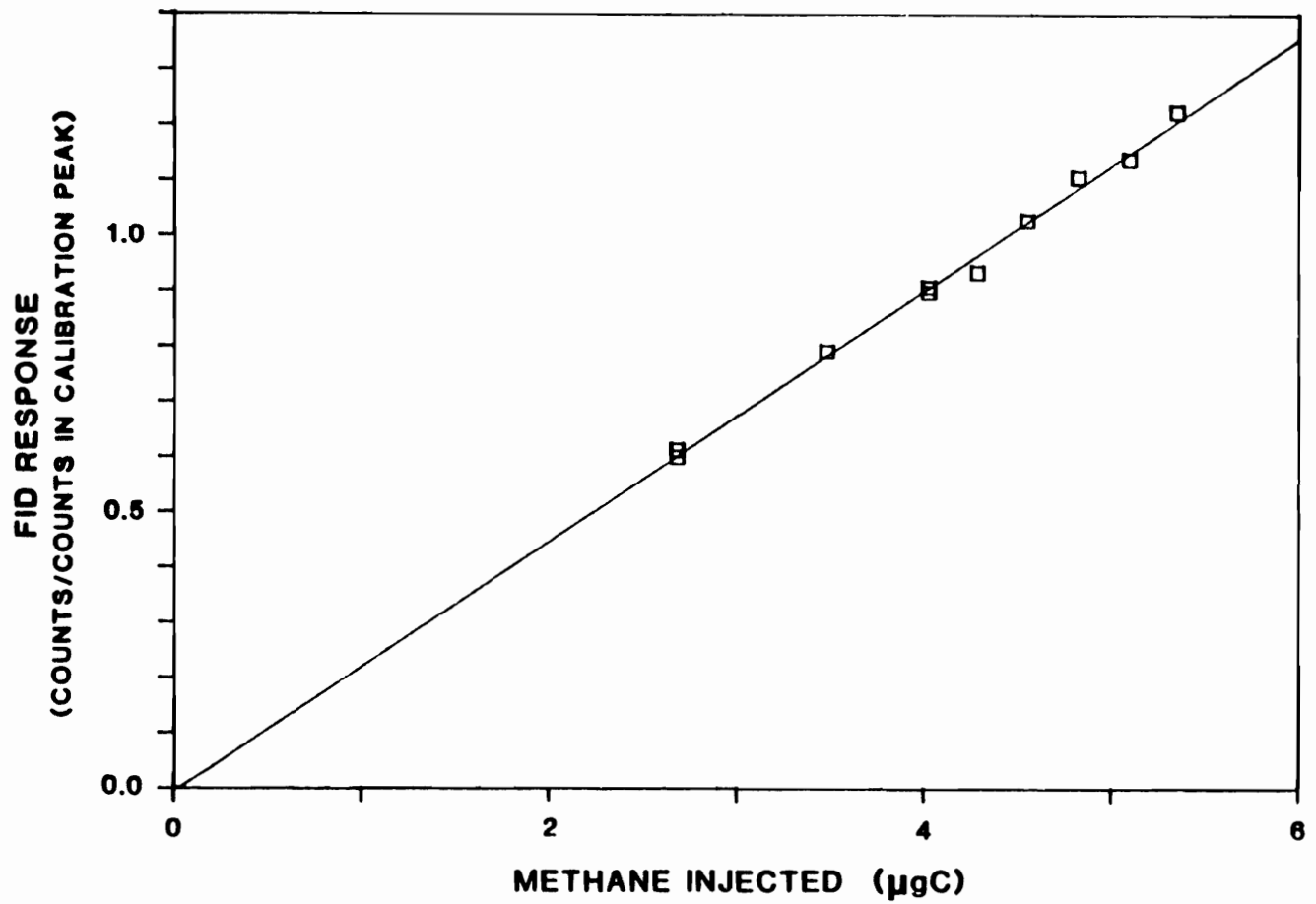


FIGURE 4.6

Figure 4.6. In situ carbon analyzer methane injection experiment and instrument response (flame ionization detector counts/counts in calibration peak) as a function of mass of carbon injected (µgC). The solid line is the linear least squares fit of Table 4.1. FID Response = $(-0.006 \pm 0.05) + (0.23 \pm 0.01) * \text{Methane Injected}$ ($R^2 = 99.5\%$)

TABLE 4.1. REGRESSION RESULTS FOR IN SITU CARBON ANALYZER FLAME IONIZATION DETECTOR RESPONSE (counts/counts in calibration peak) AS A FUNCTION OF MASS OF METHANE INJECTED (μgC).

Uncertainties are 95% confidence intervals. The number of samples comprising the regression is indicated by n, and R^2 is the percentage of the variance explained by the regression.

$$(\text{FID RESPONSE}) = a + b(\text{METHANE INJECTED})$$

	a	b	R^2	n
LINEAR REGRESSION	-0.006 ± 0.05	0.23 ± 0.01	99.5%	10

with a Teflon filter. In this configuration the analytical filters in both sides collect adsorbable organic vapor and should be equivalent. Eight runs involving the sampling of ambient air for periods of either three or eight hours were made at OGC. A two-sided t-test showed no significant difference between the two sides with 95% confidence intervals. The pooled standard deviation of the difference between the two sides was $0.068 \mu\text{gC}/\text{m}^3$, which was equivalent to a coefficient of variation of 2.2%. Because total aerosol carbon is determined by the difference between the two sides, the compounded analytical precision for the measurement of total aerosol carbon with the in situ analyzer was 3.1%.

Since each in situ analysis uses the whole sample, it is not possible to determine separate analytical precisions for organic and elemental carbon. However, results from replicate analysis of 16 ambient filter samples using the laboratory carbon analyzer should provide some insight. One-way analysis of variance on the results gave the following standard deviations: total carbon, 7.0%; organic carbon, 8.4%; and elemental carbon 6.9%. In situ analyzer uncertainties for both total carbon (1.3%) and total particulate carbon (3.1%) are less than the total carbon uncertainty for the laboratory analyzer (7%). It is likely that the precision uncertainties for organic and elemental carbon in the in situ analyzer are also less than for the laboratory analyzer, and they are probably comparable to those observed for total particulate carbon.

The FID baseline can be evaluated at several points during the analysis. Because the FID response varies with carrier gas composition, slight shifts in the baseline can occur. The optimal baseline subtraction procedure minimizes the difference between the analytical blank and the estimated baseline continuously.

This, however, is not practical. The baseline subtraction scheme which was chosen was that which minimized the difference between the baseline and the FID signal of a series of instrument blanks on a point by point basis. The baseline for the vapor-side material is sampled prior to its removal and the baseline is sampled separately for the He and O₂-He sections of the aerosol-side analysis and for the CH₄ calibration.

The transit time between the sampling filters and the FID was determined experimentally by aligning the initial increase in optical transmittance of the laser signal and the arrival of CO₂ from the oxidation of elemental carbon at the FID. (The increase in the laser signal results from the oxidative removal of elemental carbon.) Good agreement was found between the experimentally determined transit time and the expected transit time calculated from flow conditions. The laser signal responds immediately to the removal of material from the filters whereas the FID signal is delayed by the transit time. Proper correction for the pyrolytic conversion of organic to elemental carbon requires that these signals be aligned.

The accuracy of the split between organic (OC) and elemental carbon (EC) is dependent upon the accuracy of the pyrolysis correction. The pyrolysis correction is based on the following assumptions: (1) elemental carbon is the only component of the sample which affects the optical transmittance and either (2) the pyrolytically generated EC and the original EC have the same extinction coefficient (optical absorbance/EC loading) or (3) the pyrolytically generated EC is removed first.

The first assumption was tested with a sucrose aerosol experiment. A 10 g/l sucrose solution was nebulized, deionized in a ^{85}Kr charge nebulizer, aged in continuous flow chambers, and sampled at 9 l/min with the in situ carbon analyzer. Analysis of 9 samples containing 15 to 90 μg of carbon showed that the presence of significant amounts of light scattering particles on the filters did not affect the transmittance. The transmittance through the loaded filters (initial laser signal) was almost identical to the transmittance through the clean filters (final laser signal), and although a large fraction of the organic material underwent pyrolysis, the sample was properly reported as entirely organic. The negligible effect of the deposited particles on the transmittance probably resulted because light scattering from the quartz fibers of the filters themselves overwhelmed that from the deposited particles. Sampling and analysis of sucrose aerosol used only the aerosol-side sampler, and a typical sucrose aerosol analysis is shown in Figure 4.7. Assumption (1) has not been adequately tested for samples containing colored compounds such as might be present in wood smoke.

Insight into the second and third assumptions was provided by the following observations. Quartz fiber filters which have been used to collect the fine particle fraction of ambient aerosol exhibit a grayish color on their front surface, and the shade depends on the amount of particulate matter collected. The back side of the filter, however, is white. If the filter is subjected to laboratory carbon analysis only up to the end of the organic analysis (i.e. vaporization in a He atmosphere without O_2) and then removed from the analyzer, both the front and back sides exhibit a grayish color. This suggests that during organic carbon analysis some of the volatilized carbon undergoes a surface chemical reaction

FIGURE 4.7

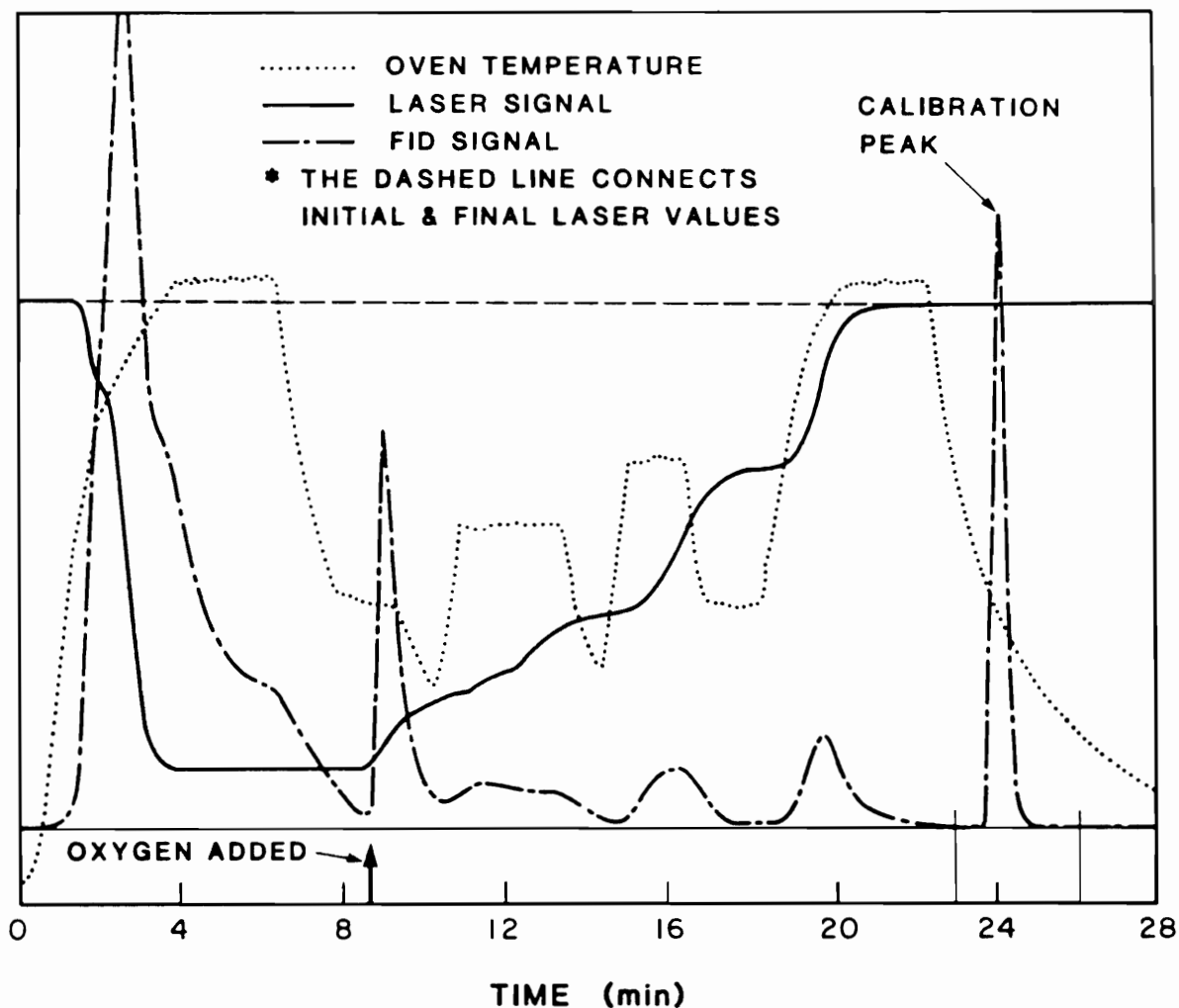


Figure 4.7. Typical *in situ* carbon analyzer output for a sucrose aerosol collection. Optical transmittance, flame ionization detector, and oven temperature. Adsorbed vapor was not measured in this experiment. The dashed line is drawn horizontally from the initial laser transmittance signal.

with the quartz fibers to produce a thin film of elemental carbon on the quartz fiber filters. Because elemental carbon is now distributed throughout the filter - rather than only near the front surface, the back of the filter appears gray.

This film of pyrolytically generated elemental carbon has a much larger surface area per mass of carbon than the original EC and would therefore be expected to oxidize much more rapidly than the original EC when O₂ is introduced during the analysis. This would suggest that assumption (3) applies. This conclusion is supported by the fact that during a sucrose analysis (Figure 4.7) almost all of the pyrolytically generated EC is removed at a temperature below that at which the OC-EC split occurs in an ambient analysis. Because of the size and morphological dependence of optical absorption this "thin film" model also suggests that the pyrolytically generated elemental carbon and original elemental carbon should exhibit different optical absorbances (i.e., assumption (2) is invalid). The validity of assumptions (1) and (3) and the good agreement of in situ EC measurements with an independent method discussed in Chapter 5 suggest that the pyrolysis correction procedure is accurate.

The response of optical absorbance to elemental carbon loading was investigated by sampling a black ink aerosol and a sucrose aerosol generated in the laboratory. The black ink aerosol was generated from a solution of 2.9 g/l of Staedtler mars 745 black drawing ink (Hogan, 1985), and the sucrose aerosol was generated from a solution of 10 g/l sucrose. The solution was nebulized, deionized in a ⁸⁵Kr charge neutralizer, aged in continuous flow chambers, and sampled at 9 l/min with the in situ carbon analyzer. Twelve black ink aerosol samples and eight samples of sucrose aerosol were collected. The sucrose aerosol

samples were entirely organic, but the analyses were used to observe the optical absorbance as a function of loading for pyrolytically generated elemental carbon. Beer's law adapted for particles on filters is $I = I_0 \exp(-bC)$ where I and I_0 are the intensities of transmitted light for the sample and blank, C is the concentration ($\mu\text{gC}/\text{cm}^2$), and b is the extinction coefficient ($\text{cm}^2/\mu\text{g}$). As shown in Figure 4.8, optical absorbance ($-\ln(I/I_0)$) varied linearly with elemental carbon loading to about $25 \mu\text{gC}$ ($14 \mu\text{gC}/\text{cm}^2$) for the black ink aerosol and $20 \mu\text{gC}$ ($11 \mu\text{gC}/\text{cm}^2$) for the elemental carbon generated pyrolytically from the sucrose aerosol. Beyond this point increases in the filter loading had a diminishing affect on the absorbance. The breakdown of Beer's law occurs at a high enough loading that it will not affect the sensitivity of the pyrolysis correction in the range in which the instrument is operated. The data also suggest that the extinction coefficient for the elemental carbon pyrolytically generated from sucrose aerosol ($0.5 \text{ cm}^2/\mu\text{g}$) is higher than the extinction coefficient for the black ink EC ($0.3 \text{ cm}^2/\mu\text{g}$). (These numbers represent the extinction coefficients observed for the particle-loaded filters in the standard in situ carbon analyzer configuration which are not necessarily the same as the extinction coefficients for the ambient aerosol.)

In another experiment, black ink aerosol was collected until the filter was perfectly black, i.e., no further decrease in the transmittance was observed. The transmittance through this filter was not zero. This "light pipe" effect was observed through an optical microscope by Gundel et al. (1984) who hypothesized that some of the fibers were acting like optical fibers transporting light through the filter. The in situ carbon analyzer transmittance has been adjusted to read

FIGURE 4.8

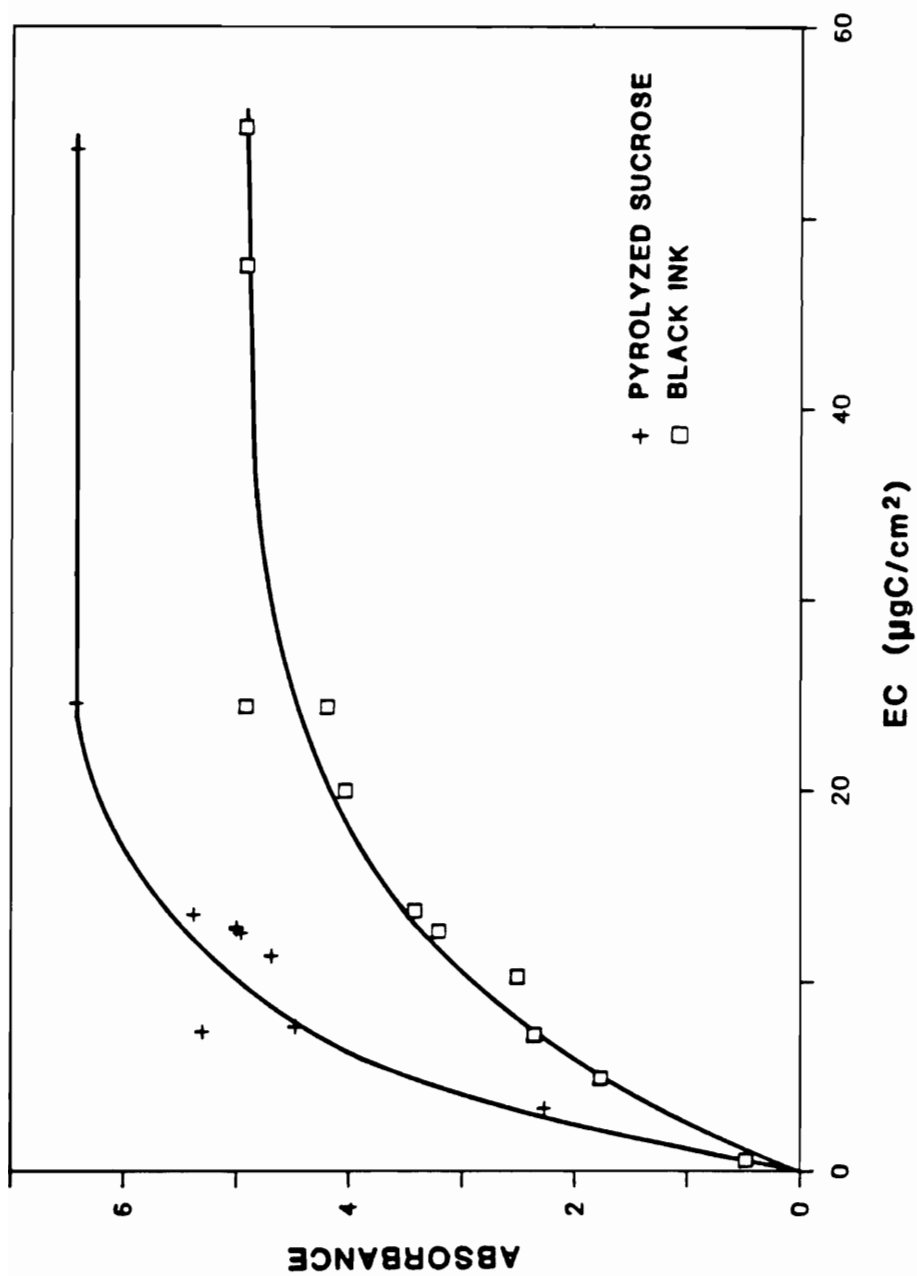


Figure 4.8. Comparison of optical absorbance ($-\ln(I/I_0)$) and elemental carbon loading ($\mu\text{gC}/\text{cm}^2$) for the in situ carbon analyzer. Elemental carbon was from a pyrolyzed sucrose aerosol and a black ink aerosol. I and I_0 are the intensities of transmitted light for the sample 2 blank respectively.

zero through a perfectly black filter (a filter loaded until the transmittance ceased to decrease).

CARBONACEOUS SPECIES METHODS COMPARISON STUDY SAMPLING

Organic and elemental carbon concentrations were measured by the in situ carbon analyzer and by manual sampling during CSMCS in Glendora, California, in August, 1986. The in situ carbon analyzer was assembled in a trailer provided by the California Air Resources Board. Ambient air was sampled at 8.5 l/min through a 2.54 cm diameter manifold extending 1 meter above the roof and capped with a rain shield and bug screen. It operated on a cycle ranging from 90 to 180 minutes. Analysis time accounted for 40 minutes of that cycle. A quality assurance check was made on the sampling system by making collections in which both sampling ports were pre-filtered with a Teflon filter. Instrument blanks were measured every evening by setting the program to collect for zero minutes followed by carbon analysis. A three-peak internal calibration program was also run daily. This program was identical to the normal analysis program except that the methane calibration loop was switched on-line during the vapor-side analysis, again during the He segment of the aerosol-side analysis, and during the final stages of the O₂-He segment (i.e., the elemental carbon part of the cycle). Because the instrument response differed by as much as 10% between these three conditions, appropriate response factors were incorporated into the data output.

CSMCS DATA TREATMENT

In situ carbon analyzer instrument blanks during the CSMCS were not significantly different from zero with 95% confidence limits, and therefore no blank subtraction was needed. The response factors determined by the three-peak internal calibration program exhibited no diurnal behavior but did appear to be affected somewhat when carrier gas cylinders were changed and when flows were adjusted. Therefore the response factors for each sampling run were estimated using the closest three-peak calibration to either side of the sampling run under consideration unless a change in carrier gas or a flow adjustment had taken place.

A slight temperature dependence was observed in the laser signal of the blank and calibration runs. The laser signal decreased somewhat with increasing oven temperature, but the relationship between laser signal and oven temperature was path dependent. It should be noted that the optical transmittance of laser light through the quartz fiber sampling filter is used to determine the OC-EC split, and this split always occurs between 17 and 20 minutes into the analysis. Therefore, the initial laser signal and the average signal between 17 and 20 minutes in the blank and three-peak calibration runs were used to adjust the initial laser value in the sample runs to the equivalent value at the temperature at which the OC-EC split occurred. The correction, which was applied to the data, was about 3% and did not significantly alter the results.

Several quality control measures were applied to the CSMCS data. The program calculates OC, EC and TC separately, and these were individually entered into data spreadsheets. The sums (OC + EC) were compared with TC

values to check for typographical errors and errors in spreadsheet data manipulations. A search for outliers was conducted by examining graphs of optical absorbance vs. elemental carbon loading and OC-EC split time vs. elemental carbon loading. The graphical output of each analysis was examined visually to verify that the transit time and integration limits were correct, that the FID signal did not saturate, and that the carbon loading was sufficient to obtain an accurate OC-EC split.

COMPARISON WITH CONVENTIONAL SAMPLING AND ANALYSIS

During CSMCS, manual samples were collected with a two-port sampler. A laminar flow field was developed in each sampling port by attaching a 25 cm long, 3.7 cm i.d. aluminum tube to the filter holder inlet. This was capped with a rain shield and an insect screen and shaded from the sun. One port contained a 2.5 μm cut-point Marple (1974) impactor with a jet Reynolds number of 7400 (Marple and Liu, 1975; the Reynolds number for a round jet impactor is uw/ν where u is the fluid velocity through the jet (cm/s), w is the jet diameter, and ν is the kinematic viscosity of the fluid (cm^2/s)). The boundary layer thickness in the impactor jet decreases with Reynolds number (Re) up to a Reynolds number of about 3000 above which little change is observed. Thus, operating above $\text{Re} = 3000$ results in a sharp particle cut-off efficiency curve. The impactor was situated about half way down the tube followed by a 47 mm quartz fiber filter (Pallflex QAOT) for aerosol collection. The second port contained a 47 mm Teflon filter (Zefluor, 2 μm pore size) followed by a quartz fiber filter for the vapor adsorption estimate. Both ports sampled ambient air at a flow rate of 25

l/min which was equivalent to a filter face velocity of about 43 cm/s. The impactor surface was cleaned and coated daily with Apiezon N vacuum grease to reduce bounce (Cheng and Yeh, 1979; Esmen et al., 1978). For the first two days of the study 4-hour samples were collected during the day and an 8-hour sample at night. For the remaining 7 days 12 hour samples were collected. The samples were analyzed for OC, EC and TC using the laboratory thermal-optical carbon analyzer described in Chapter 2. They were also analyzed by direct thermal desorption GC/MS (see Chapter 7). Midway through the sampling program a third port was added to this sampler to accommodate a sampling artifact experiment (see Chapter 6).

Figures 4.9 - 4.11 compare in situ concentrations for total, organic and elemental particulate carbon with manual sampler concentrations. In situ results are composites of measured values, averaged over the collection period of the manual sampler. Linear regression fits with 95 percent confidence intervals are given in Table 4.2 for total, organic and elemental particulate carbon comparisons. The fits are quite good for total and elemental carbon ($R^2=92\%$ and 98% respectively). For organic carbon, however, the regression was significant only within 90% confidence intervals despite the fact that $R^2=85\%$. This resulted from the small number of samples available for comparison and the inherent variability in the measurement. (Unfortunately, less samples were available for the organic and elemental carbon comparisons because of a malfunction in the optical transmittance system during the first week of the study.)

FIGURE 4.9

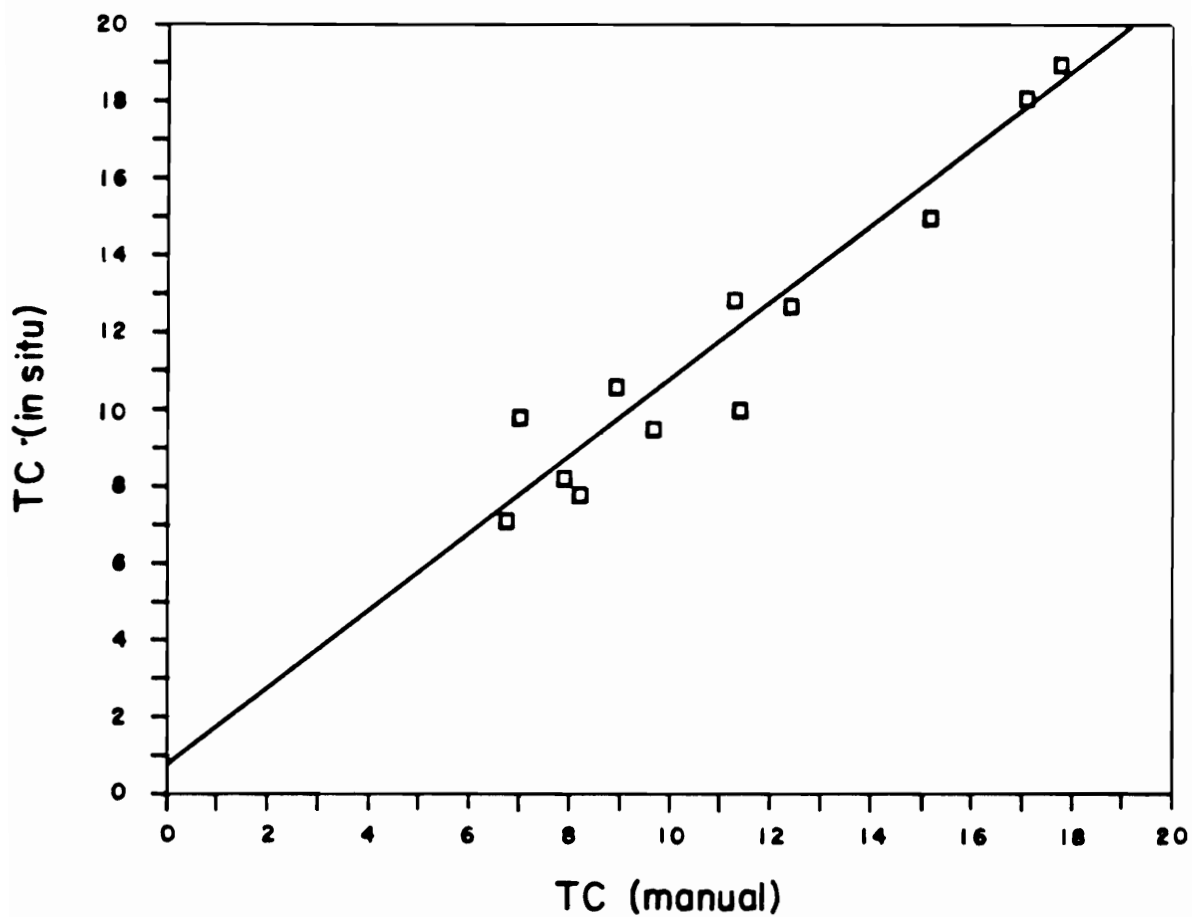


Figure 4.9. Comparison of in situ and manual sampler results ($\mu\text{gC}/\text{m}^3$) for total particulate carbon. The solid line is the linear least squares fit of Table 4.2. In Situ = $(0.8 \pm 2) + (1.0 \pm 0.2) * \text{Manual}$ ($R^2 = 92\%$).

FIGURE 4.10

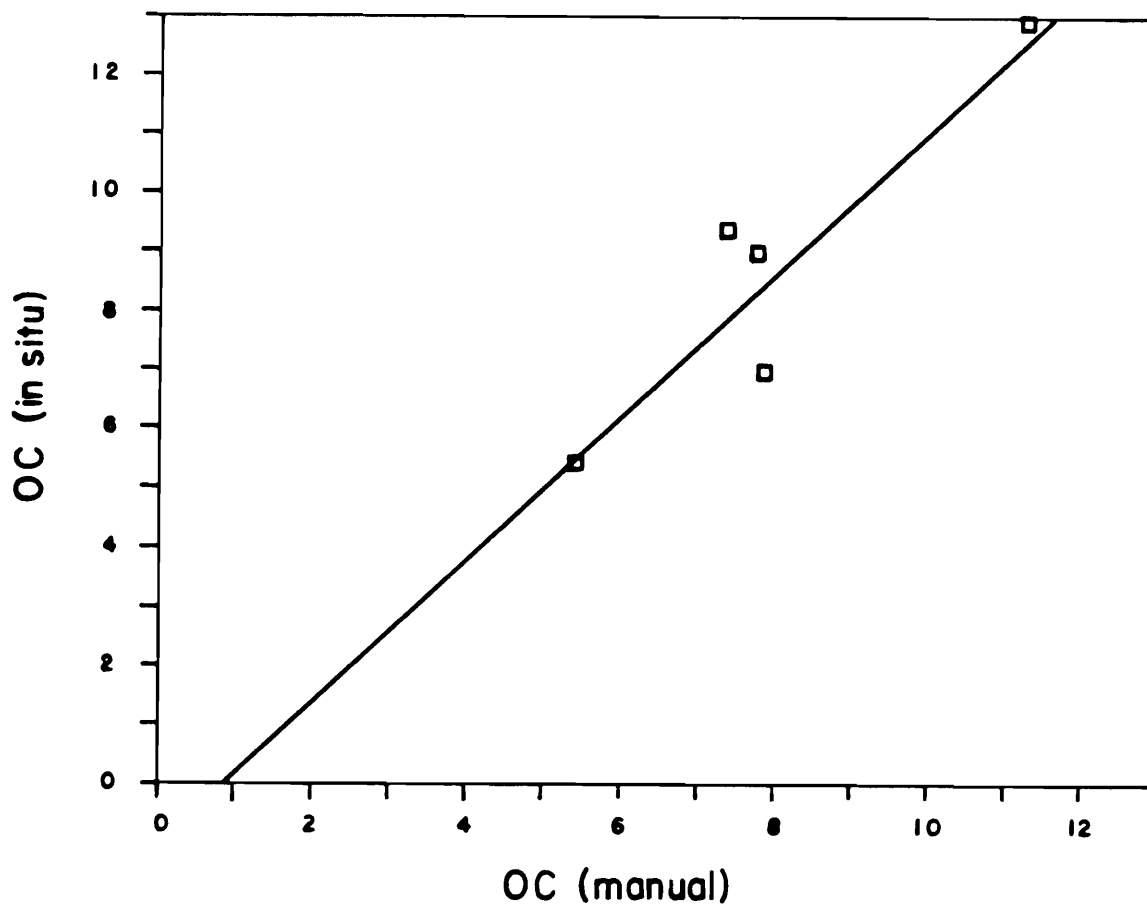


Figure 4.10. Comparison of in situ and manual sampler results ($\mu\text{gC}/\text{m}^3$) for particulate organic carbon. The solid line is the linear least squares fit of Table 4.2. In Situ = $(-0.9 \pm 6) + (1.2 \pm 0.7) \cdot \text{Manual}$ ($R^2 = 85\%$).

FIGURE 4.11

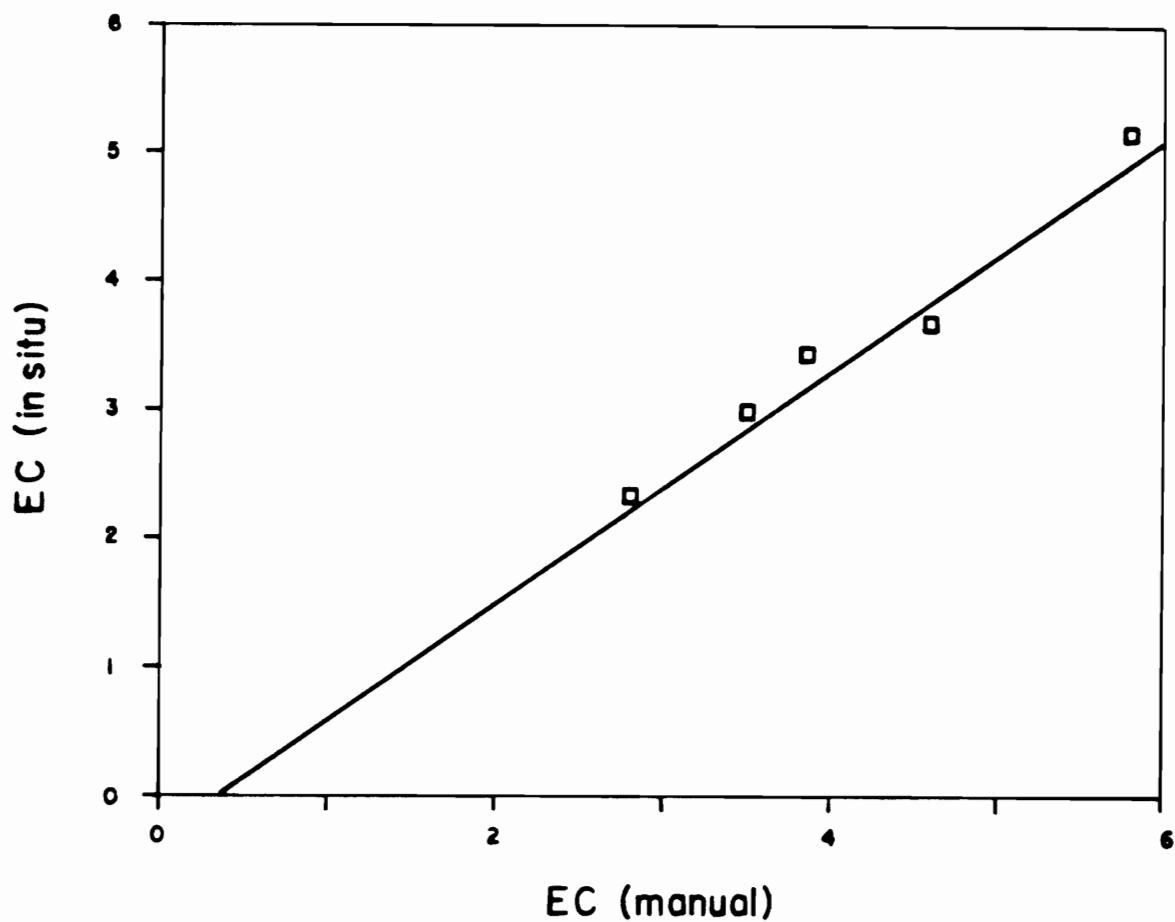


Figure 4.11. Comparison of in situ and manual sampler results ($\mu\text{gC}/\text{m}^3$) for elemental carbon. The solid line is the linear least squares fit of Table 4.2. In Situ = $(-0.2 \pm 1) + (0.9 \pm 0.3)*\text{Manual}$ ($R^2 = 98\%$).

TABLE 4.2. REGRESSION RESULTS FOR COMPARISON OF IN SITU AND MANUAL METHODS.

Uncertainties are 95% confidence intervals for total and elemental carbon and 90% for organic carbon. The number of samples comprising the regression is indicated by n, and R² is the percentage of the variance explained by the regression.

$$\text{In Situ} = a + b (\text{Manual})$$

	a	b	R ²	n
Total Carbon	0.8 ± 2	1.0 ± 0.2	92%	12
Organic Carbon	-0.9 ± 6	1.2 ± 0.7	85%	5
Elemental Carbon	-0.2 ± 1	0.9 ± 0.3	98%	5

A paired, two-sided t-test showed no significant difference between in situ and manual sampler results for total, organic or elemental carbon at the 95% confidence level. However, for elemental carbon a single-sided t-test indicated that the in situ values were significantly less than the manual sampler values. The magnitude of that difference was about 14 percent. The most likely cause of this discrepancy relates to the different optical systems used in the in situ and laboratory analyzers for the pyrolysis correction. The former uses optical transmittance, but the latter uses optical reflectance. The observed difference is probably a fundamental one resulting from the different types of optical measurements and is still under investigation. Despite the lower level of confidence in the in situ - manual comparison for organic carbon, it is reasonable to conclude that since good agreement is seen for particulate total and elemental carbon (apart from the systematic deviation for the later) the in situ analyzer also provides reliable results for aerosol organic carbon.

AMBIENT MEASUREMENTS

Twelve hour average CSMCS particulate OC, EC and TC data are plotted in Figure 4.12, and total aerosol carbon data with two hour time resolution are plotted in Figure 4.13. Despite the gaps in the data which occurred during calibration and service periods, strong diurnal variations are seen for total, organic, and elemental carbon with peak concentrations occurring during the daylight hours. The vapor artifact comprised 20 to 50% of the organic material on the manual samples and 30 to 60% of the organic material on the in situ samples. The larger in situ artifact is probably a result of the double filter

FIGURE 4.12

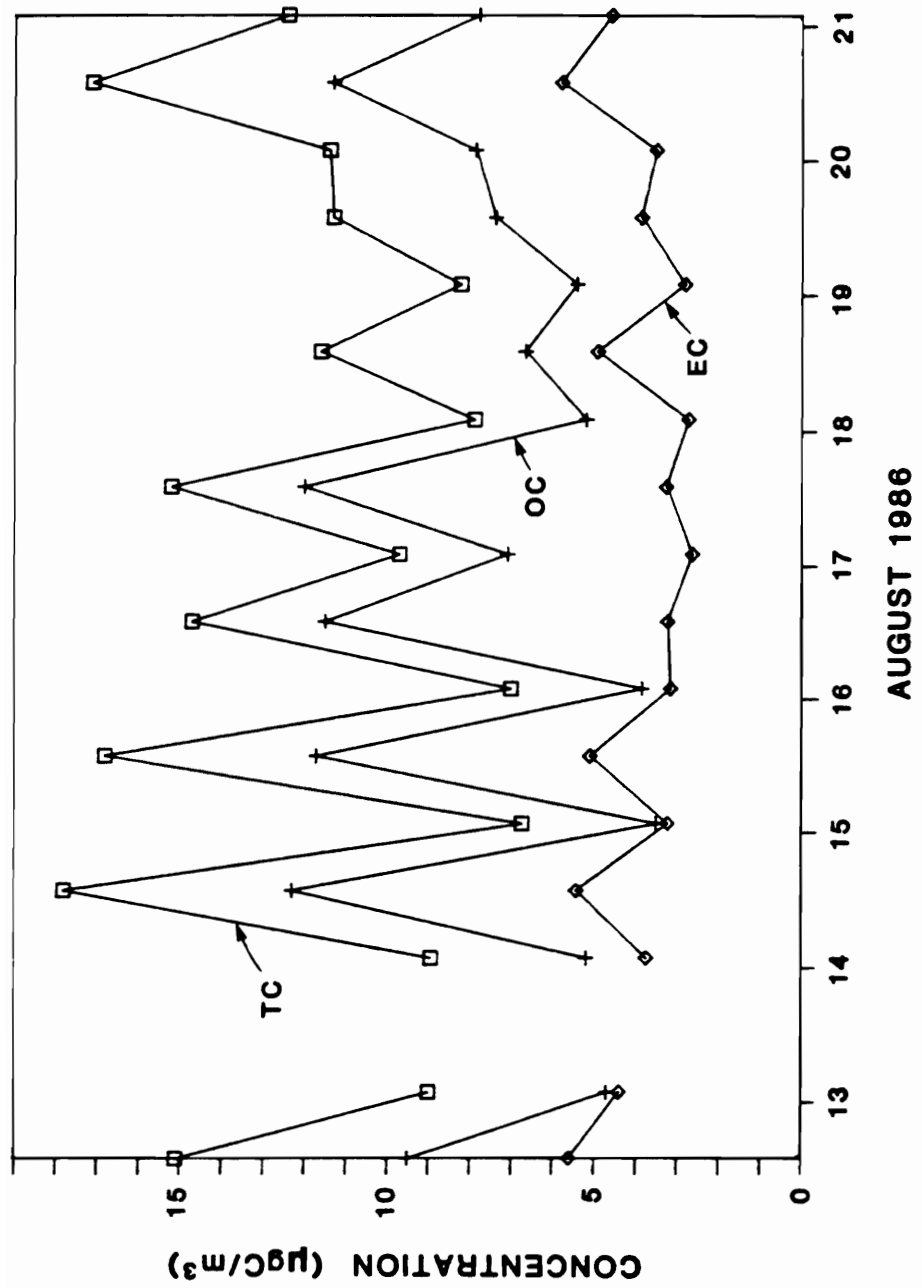


Figure 4.12. Twelve hour average concentrations ($\mu\text{gC}/\text{m}^3$) of particulate organic (OC), elemental (EC), and total carbon (TC) for particles under $2.5 \mu\text{m}$ in diameter at Glendora, California, August 12-21, 1986. Sample times were 08:00-20:00 and 20:00-08:00. The x-axis is marked with the August sampling date.

FIGURE 4.13

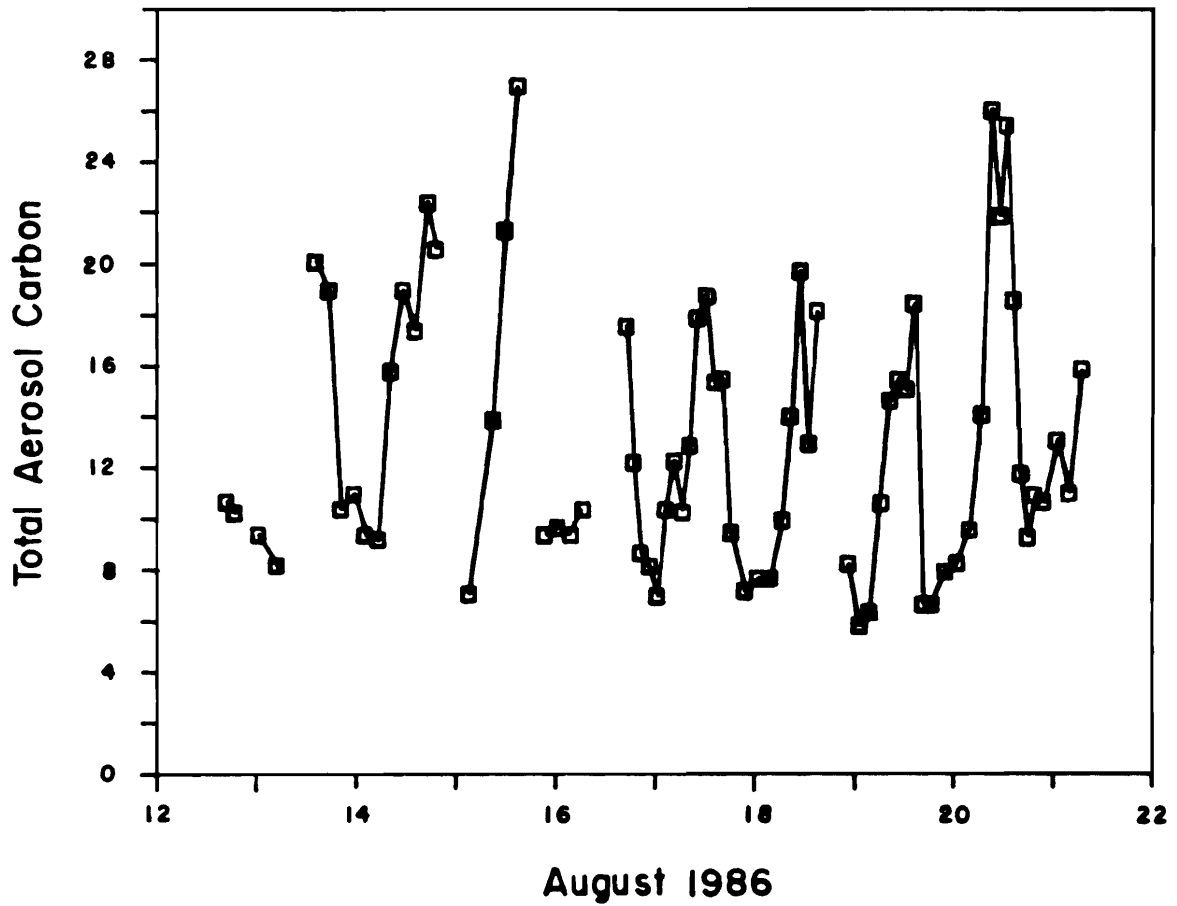


Figure 4.13. Total particulate carbon concentrations ($\mu\text{gC}/\text{m}^3$) for particles under $2.5 \mu\text{m}$ in diameter at Glendora, California, August 12-21, 1986.

arrangement and short sampling periods employed by the instrument (see Chapter 6). In addition, 30 to 50% of the material removed after the addition of oxygen during in situ carbon analysis was pyrolyzed organic material. Thus, both corrections were significant.

Concentrations of particulate organic and elemental carbon and ozone, an indicator of atmospheric photochemical activity, are plotted for August 19 and 20 in Figures 4.14 and 4.15. Ozone data are from the California Air Resources Board Haagen-Smit Laboratory. Each data point represents the midpoint of the sampling period. On both days mid-day temperatures exceeded 32 C, and there was a strong ground-based inversion on the morning of August 20.

On August 19 ozone peaked at about 1400 hours (PDT) at a concentration of about 23 pphm, indicating "moderate" photochemical smog. Both organic and elemental carbon exhibited similar diurnal patterns with their peaks broadly distributed over much of the mid-day. Because elemental carbon is a tracer for primary, combustion-generated aerosol, it is likely that the organic aerosol on this day was principally primary. The in situ data do not provide evidence for a strong secondary component on August 19.

The situation of August 20, however, is quite different. Elemental carbon showed a distinct maximum at about 0900 (PDT) which corresponded with the highest carbon monoxide concentrations recorded during the study -- 4 ppm as a 1 hour average. These pollutant levels were probably a result of the accumulation of local emissions during the morning inversion. Organic carbon experienced a secondary maximum at the same time, and the ratio of OC to EC was 1.3. A low ratio such as this is indicative of a primary aerosol. However, as

FIGURE 4.14

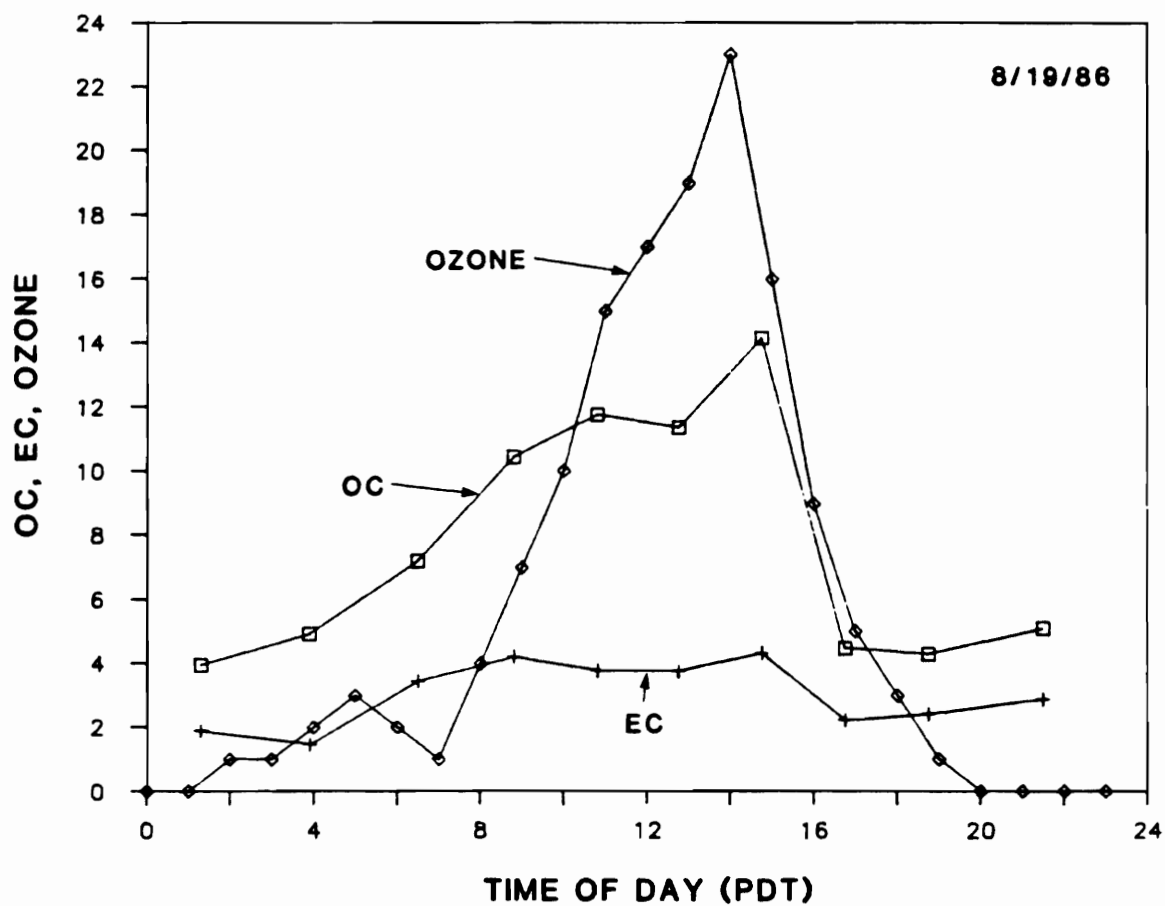


Figure 4.14. Concentrations of ozone (pphm), particulate organic carbon ($\mu\text{gC}/\text{m}^3$), and particulate elemental carbon ($\mu\text{gC}/\text{m}^3$) at Glendora, California, August 19, 1986.

FIGURE 4.15

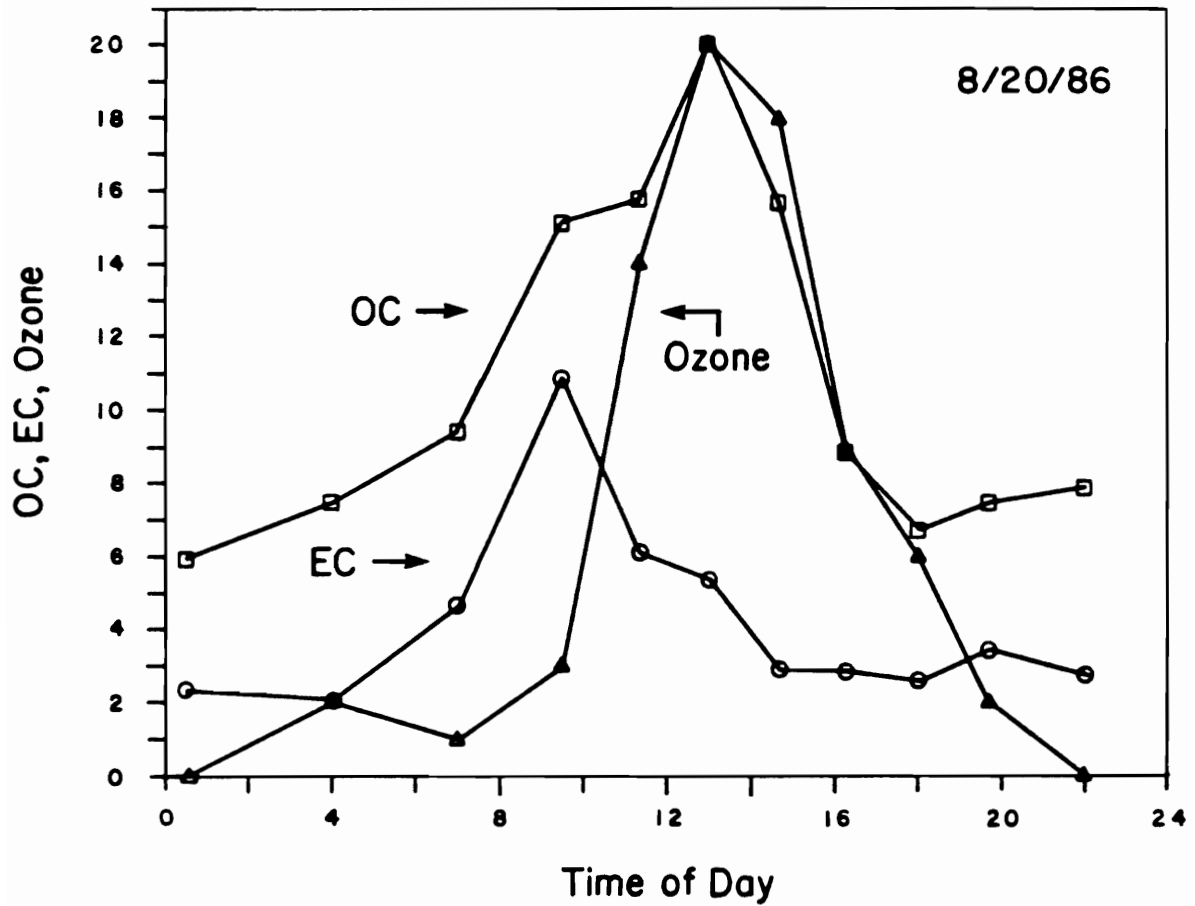


Figure 4.15. Concentrations of ozone (pphm), particulate organic carbon ($\mu\text{gC}/\text{m}^3$), and particulate elemental carbon ($\mu\text{gC}/\text{m}^3$) at Glendora, California, August 20, 1986.

the day proceeded, the elemental carbon concentration fell sharply, and the concentrations of organic carbon and ozone rose sharply and reached their maxima in early afternoon. At about this time the ratio of organic to elemental carbon also reached its maximum (5.2). These observations strongly suggest a secondary origin for the afternoon peak in organic carbon.

Investigation of the roles of primary and secondary processes in the formation of organic aerosol is continuing. The in situ carbon analyzer was used in the Southern California Air Quality Study in Claremont, California (summer, 1987), and in Long Beach, California (fall, 1987), and these data are discussed in Chapter 8.

**CHAPTER 5. INTERCOMPARISON OF PHOTOACOUSTIC
AND THERMAL-OPTICAL METHODS FOR THE MEASUREMENT
OF ATMOSPHERIC ELEMENTAL CARBON**

INTRODUCTION

Elemental carbon is present in significant concentrations in atmospheric aerosols (Shah et al., 1986; Gray et al., 1984) and contributes to visibility reduction by optical absorption. Many different methods for the analysis of elemental carbon exist, but agreement between methods has been poor (see Round Robin Study Chapter 2). Elemental carbon data from the OGC time-resolved thermal-optical carbon analyzer (in situ carbon analyzer) and the Ford Scientific Research Laboratory photoacoustic spectrometer have been compared. The two methods are based on different operational principles for both sampling and analysis of elemental carbon aerosol.

Elsewhere, the Ford and OGC methodologies have both been characterized as "in situ" methods. In the case of the Ford instrument "in situ" refers to the direct analysis of the aerosol in its natural suspended state without the use of a collection medium. In the case of the OGC instrument "in situ" refers to the direct analysis of the filter-collected aerosol in its sampling configuration without sample handling. The term "in situ" has not been used further in this chapter to avoid confusion from the different usages.

Elemental carbon measurements made by Ford and OGC in Claremont, California during SCAQS intensive sampling days have been compared. Ford carried out a similar comparison to validate the photoacoustic method first in Dearborn, Michigan (Adams et al., 1989a) and then in Claremont California during SCAQS (Adams et al., 1989b). However, for the Ford validation studies, the thermal-optical analysis of high volume filter samples was carried out only after the filters were first solvent-extracted to remove interfering organic carbon. In contrast, this chapter compares the photoacoustic method with filter samples which were collected and analyzed without solvent extraction, requiring the thermal-optical carbon analyzer to properly determine the split between organic and elemental carbon.

PHOTOACOUSTIC SPECTROMETER

The Ford photoacoustic spectrometer measures the optical absorption ($\lambda = 514.5 \text{ nm}$) of elemental carbon aerosol in a continuously flowing atmospheric sample in real-time, i.e., with 30 second time resolution. This optical absorption (m^{-1}) is divided by the appropriate value for the absorption cross-section for elemental carbon, $10 \text{ m}^2/\text{g}$ (Japar et al., 1984; Adams et al., 1989b), to convert to concentration (g/m^3). The principle of operation of this type of spectrometer is based on the photoacoustic effect (Pao, 1977; Rosencwaig, 1980). Radiation from a laser beam is absorbed by the sample and transferred as heat energy to the surrounding gas. An increase in pressure in the sample cell results. By modulating the laser beam, the oscillating pressure forms a sound wave which can

be detected with a microphone. The microphone signal is directly proportional to the optical absorption.

The Ford photoacoustic spectrometer has been described and characterized, and its measurement of elemental carbon has been validated elsewhere (Adams, 1988; Adams et al., 1989a; Adams et al., 1989b). The instrument has several distinctive features: 1) optical absorption (visible, wavelength = 514.5 nm) for elemental carbon aerosol is measured directly (elemental carbon concentration can be determined from the optical absorption); 2) measurements are continuous with 30 second resolution; and 3) measurements are made on the aerosol itself rather than on particles collected on some medium. The microphone signal of the instrument is conveniently calibrated with NO_2 , a visible light absorbing gas with an absorption coefficient of $0.316 \text{ m}^2/\text{g}$ at 514.5 nm and 22 C (Terhune and Anderson, 1977). Elemental carbon and NO_2 are the principal species which absorb visible light in the atmosphere. Interference due to atmospheric NO_2 has been eliminated by removing the NO_2 with a MnO_2 -coated denuder (Adams et al., 1986) at the inlet of the sampling cell. A description of the instrument set-up and procedures used during SCAQS has been given by Adams et al. (1989b).

Validation of the photoacoustic method was accomplished by correlating the optical absorption data with elemental carbon concentrations determined thermal-optically (Sunset Laboratory, Forest Grove, Oregon) for solvent extracted filter samples collected over corresponding time periods (Adams et al., 1989b). The least squares fit between the optical absorption in 10^{-5}m^{-1} (y) and the thermal-optical elemental carbon concentration in $\mu\text{g}/\text{m}^3$ (x) was $y = 10.06(\pm 0.56)x + 2.7(\pm 5.6)$ with a correlation coefficient (R) of 0.945 (n = 41). The good fit

suggests that both methods were measuring elemental carbon with high precision. The slope of the regression line is an independent determination of the absorption coefficient for elemental carbon. The agreement between this value and the accepted value of $9.5 (\pm 1.5) \text{ m}^2/\text{g}$ at 514.5 nm (Japar et al., 1984) is the basis for presuming the accuracy of the photoacoustic method. The method has a precision of $\pm 6\%$ and a detection limit of $0.3 \mu\text{gC}/\text{m}^3$.

THERMAL-OPTICAL CARBON ANALYZER

The Oregon Graduate Center time-resolved thermal-optical carbon analyzer measures both organic and elemental particulate carbon. It is described in detail in Chapter 4. The analytical precision for total carbon, expressed as a coefficient of variation, was 1.3%, and the corresponding detection limit (3σ) was $0.2 \mu\text{g}$. Comparable precision is expected for organic and elemental carbon based on our experience with the laboratory carbon analyzer (Turpin and Huntzicker, 1988; Huntzicker et al., 1982; Johnson et al., 1981). However, since each analysis uses the whole sample, these values have not been determined.

During this sampling program the carbon analyzer sampled ambient air at 8.7 l/min for 80 minutes followed by a 40 minute analysis. An instrument blank and a separate calibration program were run daily during sampling. Each analysis was calibrated internally by injection of a known amount of methane during each analysis run.

AMBIENT SAMPLING

Sampling days were SCAQS intensive study days, selected on the basis of predictions of low level or surface inversions with high concentrations of ozone or PM10 (particulate matter $<10 \mu\text{m}$). Eleven days in 1987 were selected: June 19, June 24 - 25, July 13 - 15, August 27 - 29, and September 2 - 3. The 80 minute collection period of the OGC carbon analyzer cycle was centered on each odd hour (i.e., 0620 - 0740 PDT). The calibration and instrument blank determinations took up one late night sampling period. The Ford instrument operated continuously except for the time required for calibrations and baseline checks. Each calibration took one hour, and calibrations were run at 0000, 0500, 1000 and 1700 PDT. Baseline checks were carried out during the first 5-10 minutes of every hour. The Ford data were processed as hourly averages (i.e., the ~50 minutes of continuous measurements between baseline checks).

RESULTS

Averages of the Ford data over sampling periods of ~100 minutes with sampling midpoints on each odd hour are listed in Appendix A with the 80 minute OGC averages having similar sampling midpoints. The Ford averages compile data within 50-55 minutes of the midpoint compared with 40 minutes for the OGC averages. If significant changes occurred in ambient concentrations between the beginning and end of the segment, a small difference in the sampling midpoints of Ford and OGC averages could significantly alter the comparison. To minimize this problem, all data with sampling midpoints offset from the hour by more than 5 minutes were excluded. Because differences between the

sampling periods of the two sets of data could be an important source of variability in the comparison, the best agreement should be seen when changes in ambient concentrations are gradual. For this reason the sample period from 1400 to 1600 hours on September 2 was excluded because it was clear from the Ford data that a large change in concentration had occurred over this period, and it would not be reflected equally by the OGC and Ford sampling periods.

Figure 5.1 compares Ford and OGC elemental carbon concentrations. The solid line represents the linear regression of Equation (4.1), and the uncertainties in Equation (4.1) correspond to the standard error.

$$\text{FORD} = (0.92 \pm 0.06) * \text{OGC} + (0.30 \pm 0.74) \quad (4.1)$$

$$R = 0.905 \quad n = 59$$

The fit is quite good ($R=0.905$). Moreover, the ratio of the mean Ford value to the mean OGC value ($\mu\text{g}/\text{m}^3$) is 1.01, and a two sided t-test shows no significant difference between Ford and OGC values at the 95% confidence level.

SUMMARY

Two independent measurement methods for elemental carbon in ambient aerosols compared well. The methods are based on different physical properties of elemental carbon. One method uses filter collection and thermal analysis to measure organic and elemental carbon and makes an appropriate correction for the pyrolytic conversion of organic to elemental carbon. The other method, based on the photoacoustic effect, measures the optical absorption of the

FIGURE 5.1

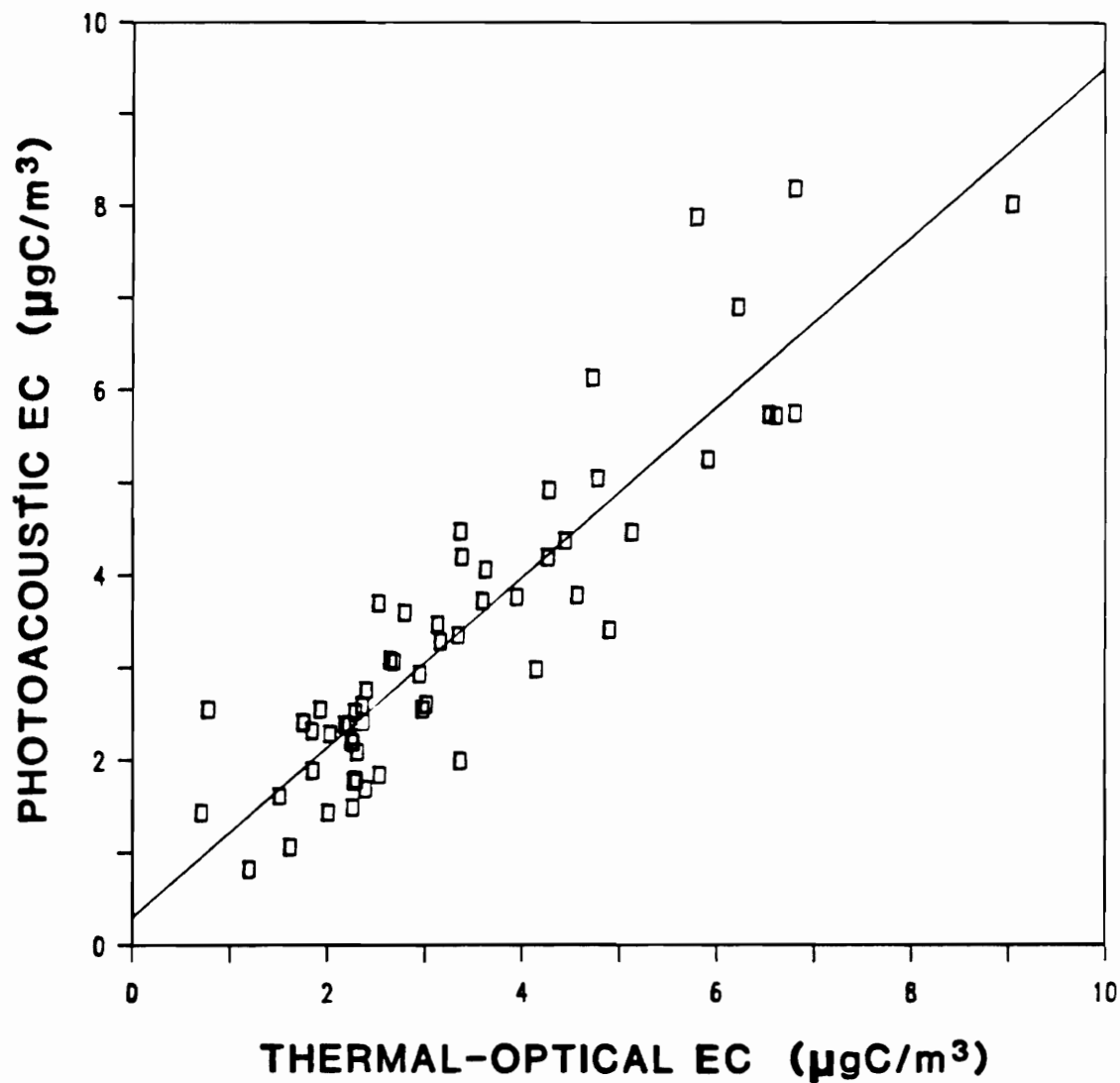


Figure 5.1. Comparison of elemental carbon concentrations ($\mu\text{gC}/\text{m}^3$) measured by Ford Motor Company photoacoustic spectrometer and Oregon Graduate Center in situ thermal-optical carbon analyzer. The solid line is the linear least squares fit of Equation 4.1. Ford = $(0.30 \pm 0.74) + (0.92 \pm 0.06) \cdot \text{OGC}$ ($R = 0.905$).

elemental carbon aerosol in its suspended atmospheric state. Calibration of optical absorption is done with NO_2 and the independently measured absorption coefficient of aerosol elemental carbon. Historically, agreement between different methods of elemental carbon determination has been poor. The agreement of these two independent methods greatly increases the confidence in the measurements made by both methods. Additionally, it adds confidence to the method of pyrolysis correction used by the in situ carbon analyzer to determine the split between organic and elemental carbon.

CHAPTER 6. ORGANIC AEROSOL SAMPLING ARTIFACTS IN LOS ANGELES

INTRODUCTION

Filter sampling for organic aerosol is complicated by two artifact errors. Adsorption of organic vapors on the sampling filter comprises a positive artifact, and volatilization, which removes material from the filter, is a negative artifact (Cadle et al., 1983; McDow, 1986). The importance of adsorption is evidenced by the presence of significant concentrations of organic carbon on backup filters behind primary aerosol filters which are essentially 100% efficient in removing particles (Cadle et al., 1983). At equilibrium adsorption can be described in terms of gas-particle partitioning concepts. According to BET theory (Brunauer et al., 1938) the volume of gas sorbed in a single component system is:

$$v = C_b SX / ((1 - X)(1 + (C_b - 1)X)) \quad (6.1)$$

where

- v = volume of gas sorbed
- $C_b = K \exp((Q_1 - Q_v)/RT)$
- K = compound specific constant
- Q_1 = enthalpy for desorption directly from surface
- Q_v = enthalpy of vaporization of the liquid
- R = gas constant
- T = temperature
- S = surface area for sorption
- X = p/p_0
- p = gas phase partial pressure
- p_0 = saturation vapor pressure

The gas-particle partitioning fraction derived from this theory, assuming less than monolayer coverage, (Pankow, 1987; Junge, 1977; Yamasaki et al.,1982) is:

$$\phi_i = C_i\theta / (C_i\theta + p_{0i}) \quad (6.2)$$

where:

ϕ_i = fraction of compound i found
in the adsorbed phase

C_i = compound specific constant
(torr cm³ cm⁻²)

θ = concentration of filter surface
area for adsorption (cm² cm⁻³)

p_{0i} = saturation vapor pressure of
compound i

In the atmosphere the situation is more complex because there are many adsorbing species present. Also, it is likely that greater than monolayer coverage occurs routinely.

Volatilization can occur when the collected particulate material is exposed to a pressure drop during sampling causing the concentrations of organic compounds, and therefore the equilibrium value of ϕ , to decrease near the filter surface. Additionally, a change in ambient air quality can cause a redistribution of material between the gas and particulate phases, resulting in a weighted average filter sample which gives more weight to ambient conditions toward the end of the sampling period. These sampling artifacts are not well understood and therefore inhibit attempts to accurately assess aerosol concentrations.

If adsorption was the dominant artifact, then effective correction would be accomplished by subtracting the estimated artifact, as measured on the backup

filter, from the quartz fiber front filter. If volatilization was dominant, the estimated artifact would be added to the front filter concentration to produce a more accurate measure of organic aerosol. Experiments performed by McDow and Huntzicker (1989) in the Portland area have shown that the concentration of organic carbon collected both on quartz fiber front filters and on the quartz fiber backup filters behind them decreases with increasing filter face velocity. (The face velocity is the volumetric flow rate divided by the exposed surface area of the filter.) Elemental carbon concentrations show no face velocity dependence. In addition, at a face velocity of 40 cm/s the concentration of organic carbon on quartz fiber backup filters behind Teflon front filters was about a factor of 2 greater than on quartz fiber backup filters behind quartz fiber front filters. Finally, when the concentrations of organic carbon on quartz fiber backup filters behind Teflon front filters were subtracted from the concentrations of organic carbon on quartz fiber (front) filters in the Portland experiments, the face velocity dependence of the apparent aerosol organic carbon concentration was greatly reduced. These results suggest that adsorption of organic vapors is the dominant artifact in the sampling of organic aerosol.

FILTER SURFACE AREA

Three quartz fiber filters (Gelman QAOT), glass fiber filters (Gelman A-E, 61631), and Zeflour Teflon filters (2 μm pore, Gelman P5PJ047) were weighed and analyzed by Micromeritics (Norcross, Georgia) for BET surface area in krypton. The filters were baked out prior to weighing, the Teflon filters at 250 C, glass fiber filters at 420 C, and quartz fiber filters at 700 C.

Table 6.1 presents BET filter surface area in m^2 BET surface area/ m^2 filter for the three types of filters. The experiment which follows uses 47 mm quartz fiber filters which have been masked down to 7.6 cm^2 , 3.7 cm^2 , and 1.9 cm^2 giving BET filter surface areas of 0.096 m^2 , 0.047 m^2 , and 0.024 m^2 . In comparison, the surface area of particulate material collected on a filter after a 12 hour collection at 9 l/m is about 0.003 m^2 (assuming an ambient aerosol concentration of $100 \mu\text{g}/\text{m}^3$ and a specific particle surface area of $5 \text{ m}^2/\text{g}$; McDow and Huntzicker, 1989). Thus, the surface area added to the filter through the addition of particles is small. In addition, assuming the particles are in equilibrium with the atmosphere at the time of collection, a change in the vapor adsorbed to these particles should only occur with a change in atmospheric conditions. For these reasons, the presence of particulate material on the sampling filter should not significantly affect the adsorbed vapor artifact.

FACE VELOCITY EXPERIMENTS

Face velocity experiments were performed in Glendora, California during CSMCS to investigate the importance of organic sampling artifacts under Los Angeles conditions. Use of a six-port filter sampler, shown in Figure 6.1, permitted simultaneous collection of six filter samples from a common manifold. Laminar flow was maintained in the manifold by drawing air out through the bottom of the manifold as well as through the sampling ports. Impactors installed

TABLE 6.1. BET SURFACE AREA MEASUREMENTS

Filter surface area expressed in m^2 surface area/ m^2 filter. Uncertainties are $\pm 1\sigma$. Measurements made by Micromeritics in Norcross, Georgia for BET surface area in krypton.

FILTER TYPE	SURFACE AREA (m^2/m^2 filter)
QUARTZ FIBER FILTERS (Gelman QAOT)	126 ± 9
GLASS FIBER FILTERS (Gelman A-E, 61631)	125 ± 7
ZEFLUOR TEFLON MEMBRANE FILTERS (2 μm pore, Gelman P5PJ047)	26 ± 2

FIGURE 6.1

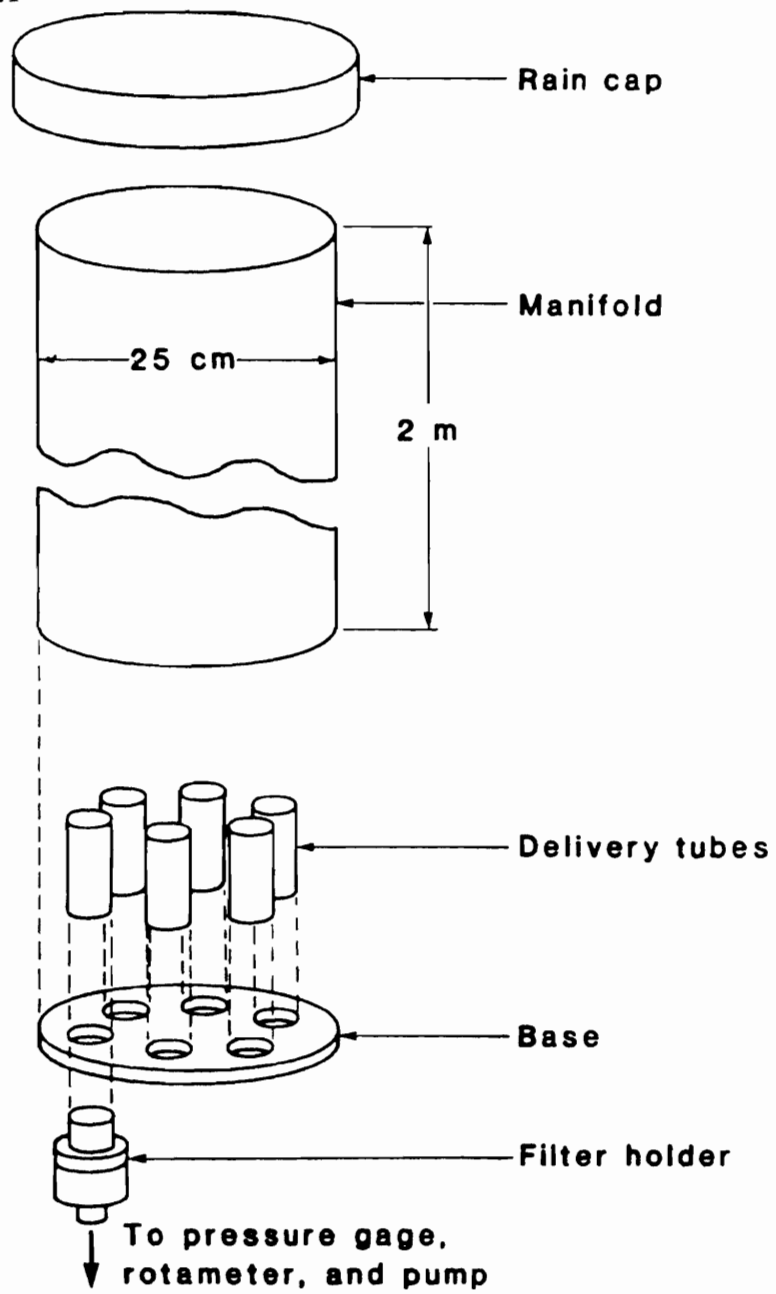


Figure 6.1. Six port filter sampler used in face velocity experiment.

at the delivery tube inlets removed all particles larger than $1.0 \mu\text{m}$. A sharp particle cut-off efficiency curve was ensured by operating at a Reynolds number of 7000 (Marple and Liu, 1975). Three of the filter holders contained a quartz fiber (Pallflex QAOT) front filter followed by a quartz fiber backup filter (designated QQ), and the other three contained a Teflon (Zefluor, $2 \mu\text{m}$ pore size) filter followed by a quartz fiber filter (designated TQ). The TQ combination was used to estimate the amount of vapor adsorption artifact on the QQ front filter. All QQ and TQ combinations sampled air at 9 l/min , but three different face velocities (20 , 40 , and 80 cm/s) were used for the three sets of QQ and TQ filters. Different face velocities were achieved by reducing the filter areas with annular masks as shown in Figure 6.2.

The face velocity sampler collected 12 hour samples on a standard CSMCS schedule, with filter changes at 0800 and 2000 PDT. Impactors were cleaned and regreased with Apiezon N vacuum grease daily. Care was taken to shade the filter holders from the sun. Filters from the 80 cm/s QQ sampling port were not used in this analysis because they did not seat properly in the filter holder.

The sample handling and quality assurance procedures used were those described in Chapter 2, and all samples were analyzed on the OGC laboratory thermal-optical carbon analyzer (see Chapter 2). The accuracy of total carbon measurements was 2%, and the measures of precision are listed in Table 2.2. A consistency check was performed between this sampler and a two-port filter sampler operated concurrently by OGC (see Chapter 4). The face velocity sampler operated with a particle cut-point of $1.0 \mu\text{m}$ instead of the $2.5 \mu\text{m}$ cut-point used in the other samplers and so aerosol values could not be compared.

FIGURE 6.2

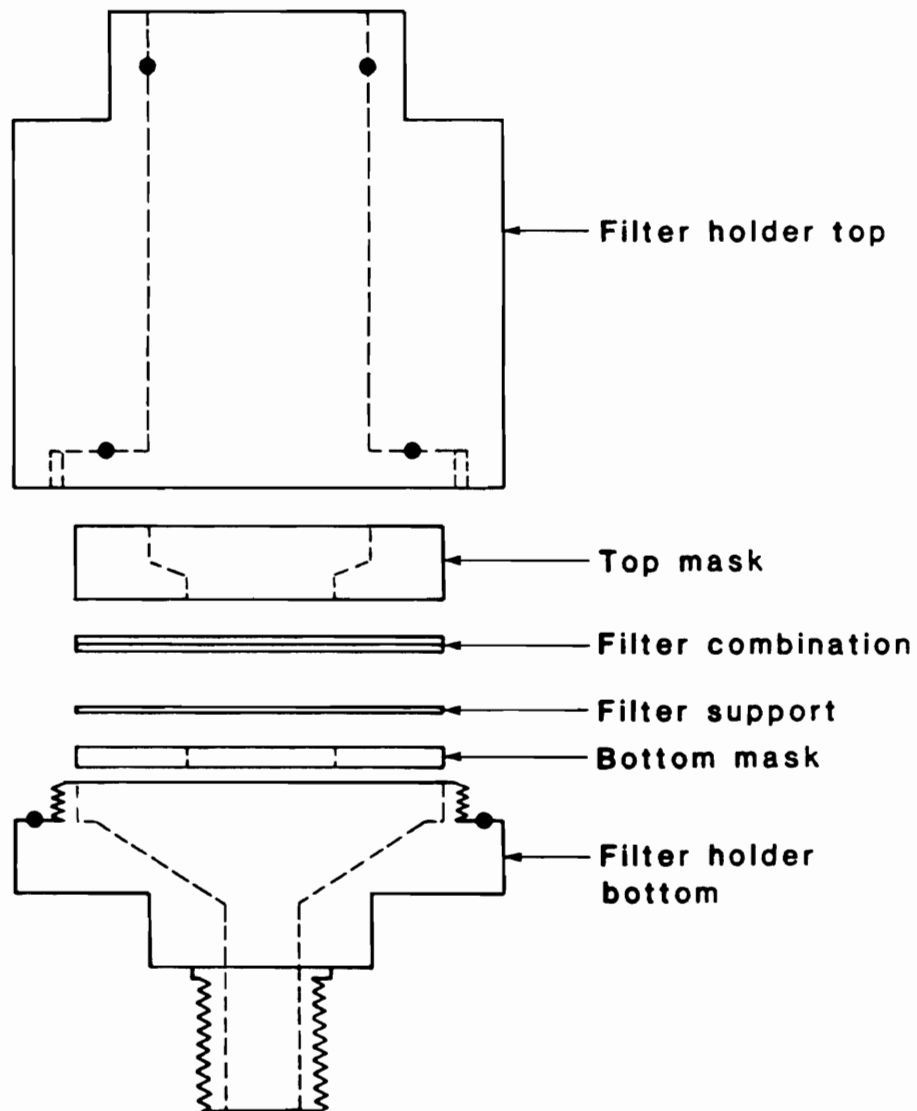


Figure 6.2. Aerosol filter holder with annular masks used in face velocity experiment. The solid black circles are O-rings.

However, 40 cm/s TQ and QQ backup filter concentrations from the face velocity sampler were compared with two-port backup filter concentrations. The two-port sampler operated at a face velocity of 43 cm/s. The comparisons are shown in Figures 6.3 and 6.4 with regression results in Table 6.2. A two-sided paired t-test shows no significant difference between samplers for either TQ or QQ backups at the 95% confidence level. However, the agreement is better for TQ backups than QQ backups and so is the least squares fit ($R^2 = 91\%$ for TQ and $R^2 = 80\%$ for QQ). The good agreement between backup filter results not only serves as a quality control check between samplers, but it also validates the use of 40 cm/s face velocity sampler TQ backup carbon concentrations to correct for vapor adsorption in two-port samples when the corresponding two-port TQ backups were not available.

RESULTS

The measured concentrations ($\mu\text{gC}/\text{m}^3$) of organic carbon collected on the backup filters are shown in Figures 6.5 and 6.6. Figures 6.7 - 6.11 and Table 6.3 present comparisons in terms of x-y plots and regressions. A strong diurnal variation is apparent with the peak loadings occurring during the day. A substantial decrease in measured concentration is observed with increasing face velocity (decreasing exposed filter surface area) for both TQ and QQ backup filters (TQB and QQB). In addition, the measured concentrations of organic carbon on 40 cm/s TQ backup filters are about 1.4 times greater than the concentrations measured on QQ backup filters. QQ backup filter loadings averaged $3.2 \mu\text{gC}/\text{cm}^2$. In comparison, in McDow's (1986) Portland experiment

FIGURE 6.3

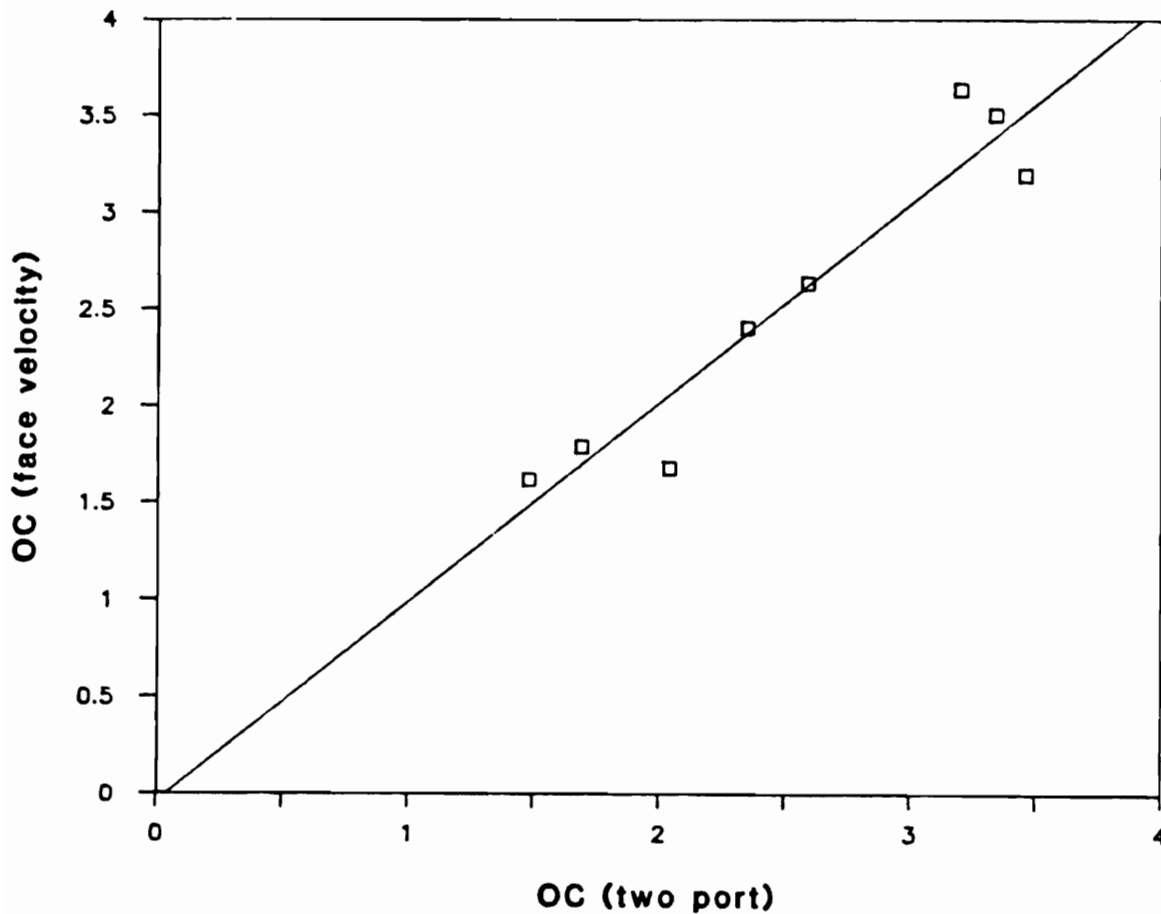


Figure 6.3. Comparison of quartz fiber backup filters behind Teflon front filters for two-port (43 cm/s) and 40 cm/s face velocity samples. The solid line is the linear least squares fit of Table 6.2. Face Velocity = $(-0.04 \pm 0.9) + (1.0 \pm 0.3) * \text{Two Port}$ ($R^2 = 91\%$).

FIGURE 6.4

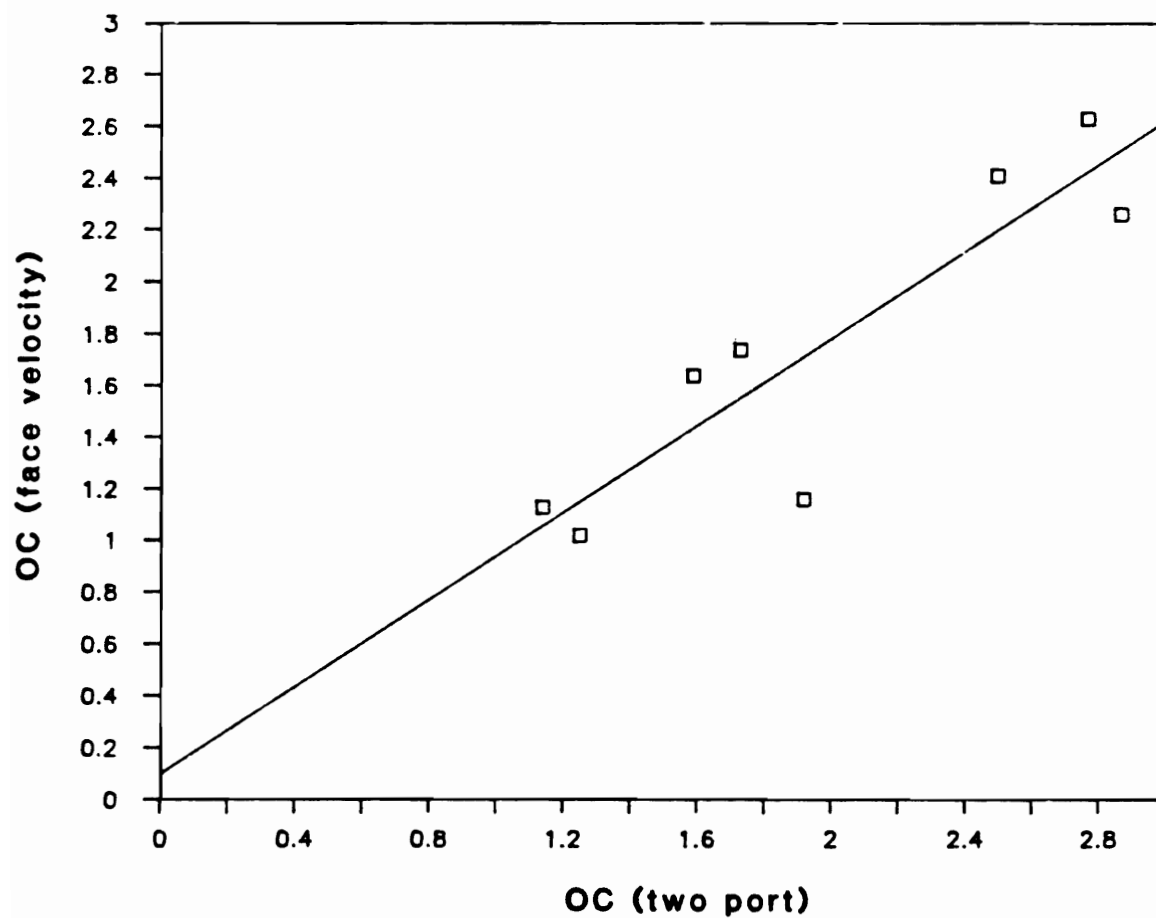


Figure 6.4. Comparison of quartz fiber backup filters behind quartz fiber front filters for two-port (43 cm/s) and 40 cm/s face velocity samples. The solid line is the linear least squares fit of Table 6.2. Face Velocity = $(0.10 \pm 0.9) + (0.8 \pm 0.4) * \text{Two Port}$ ($R^2 = 80\%$).

TABLE 6.2. REGRESSION RESULTS FOR COMPARISON OF TWO-PORT (43 cm/s) AND FACE VELOCITY SAMPLER (40 cm/s) BACKUP FILTERS.

Uncertainties are 95% confidence intervals. The number of samples comprising the regression is indicated by n, and R² is the percentage of the variance explained by the regression.

$$(\text{FACE VELOCITY}) = a + b (\text{TWO PORT})$$

	a	b	R ²	n
TQ BACKUP - TC	-0.04 ± 0.9	1.0 ± 0.3	91%	8
QQ BACKUP - TC	0.10 ± 0.9	0.8 ± 0.4	80%	8

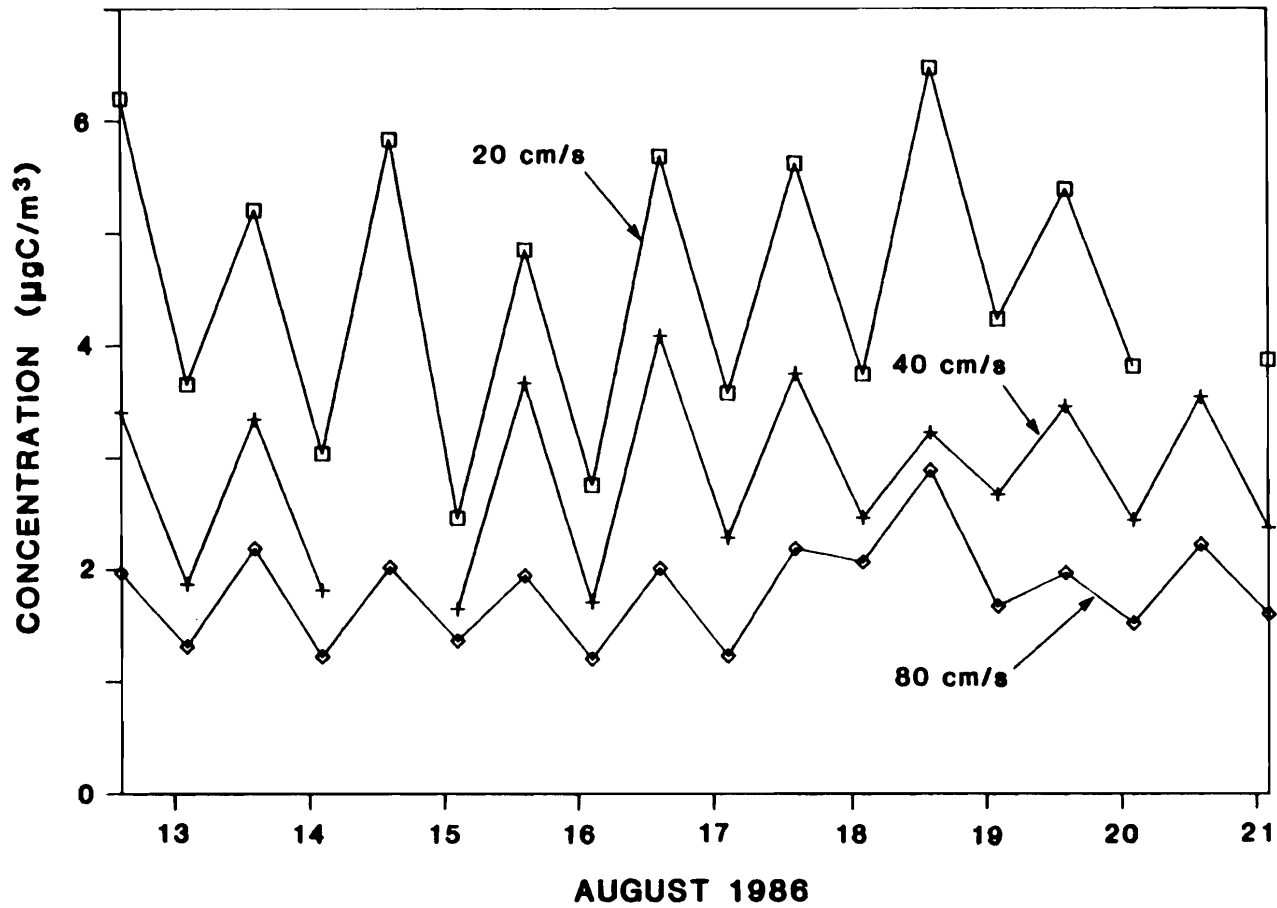


Figure 6.5. Organic carbon concentrations ($\mu\text{gC}/\text{m}^3$) on quartz fiber backup filters behind Teflon front filters for face velocities of 20, 40 and 80 cm/s. Sample times were 08:00-20:00 and 20:00-08:00. The x-axis is marked with the August sampling date.

FIGURE 6.5

FIGURE 6.6

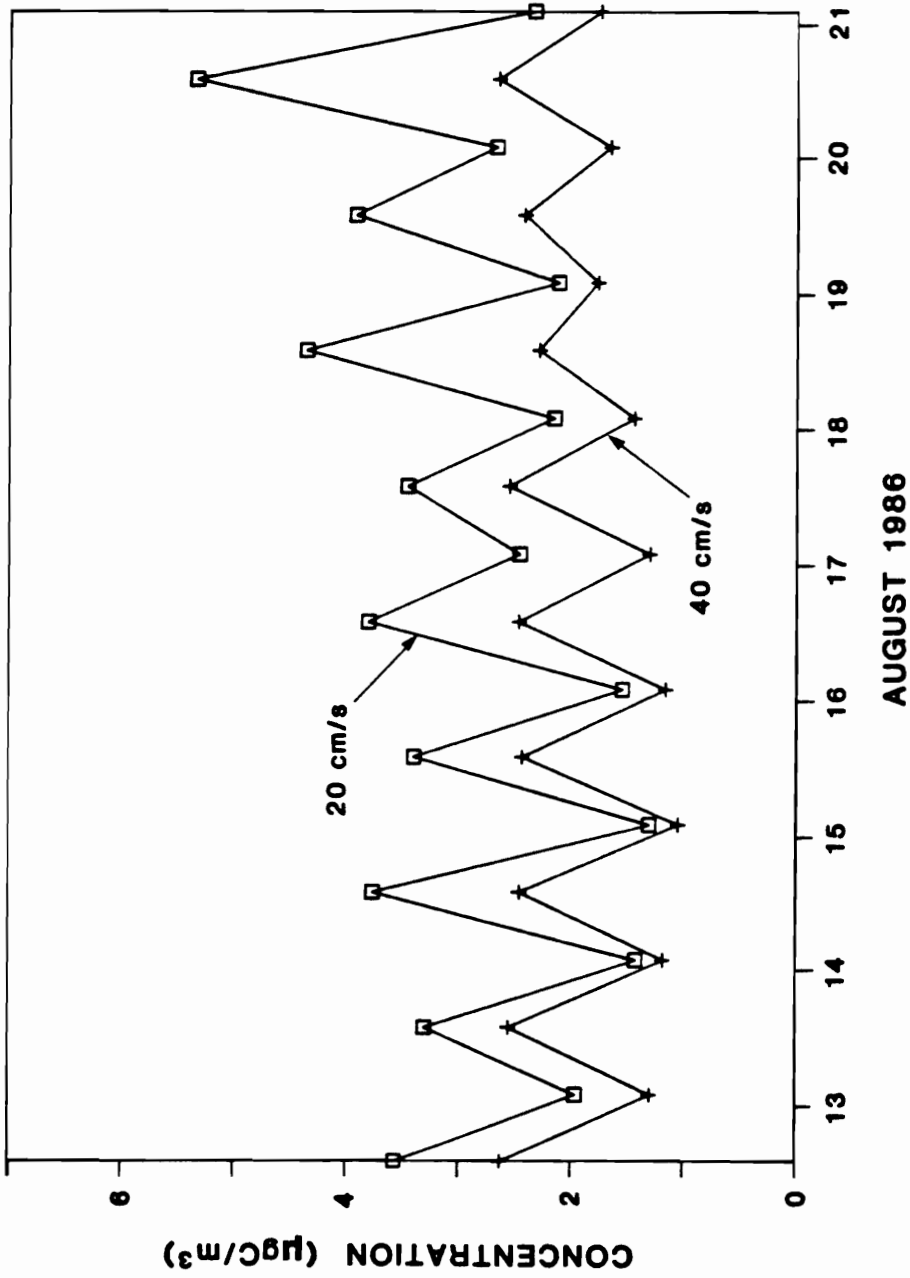


Figure 6.6. Organic carbon concentrations ($\mu\text{gC}/\text{m}^3$) on quartz fiber backup filters behind quartz fiber front filters for face velocities of 20 and 40 cm/s. Sample times were 08:00-20:00 and 20:00-08:00. The x-axis is marked with the August sampling date.

FIGURE 6.7

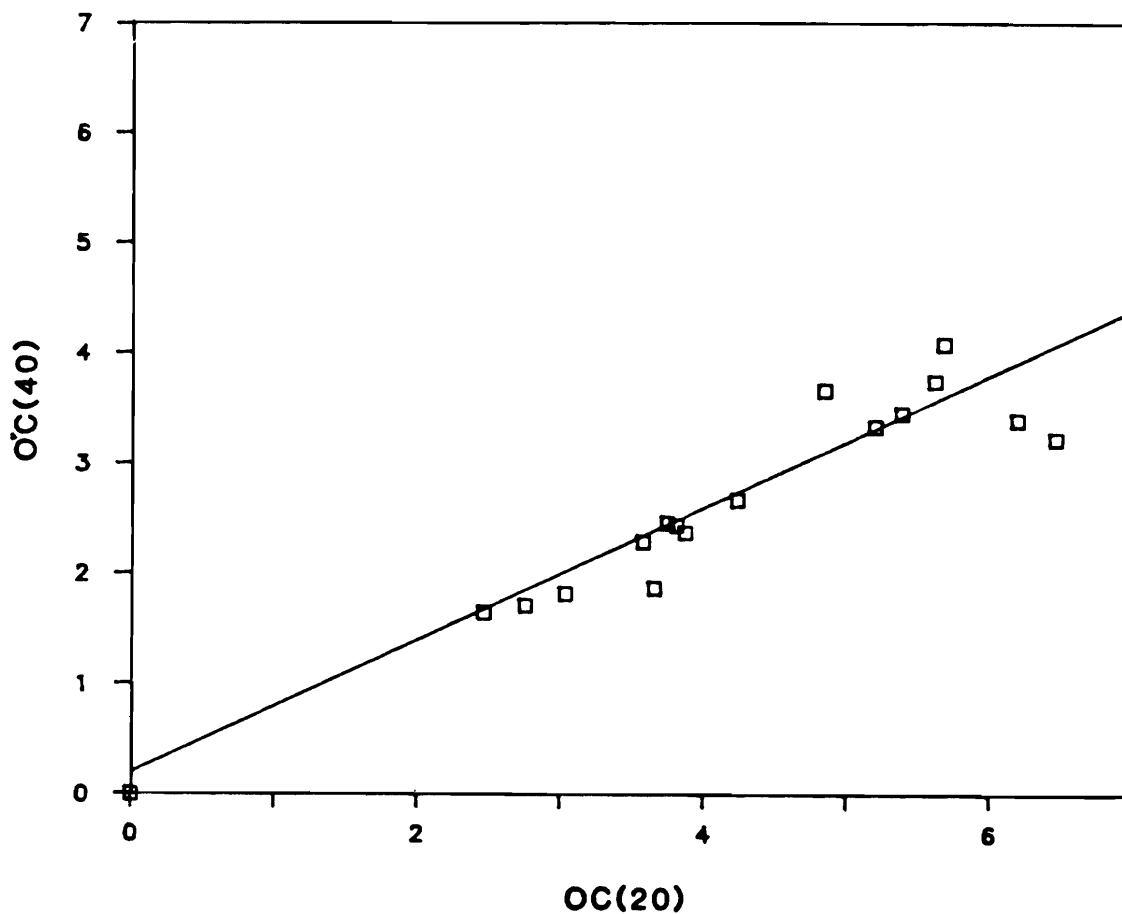


Figure 6.7. Comparison of organic carbon concentrations ($\mu\text{gC}/\text{m}^3$) at face velocities of 20 and 40 cm/s for quartz fiber backup filters behind Teflon front filters. The solid line is the linear least squares fit of Table 6.3. $\text{OC}(40) = (0.2 \pm 0.8) + (0.6 \pm 0.2) \cdot \text{OC}(20)$ ($R^2 = 80\%$).

FIGURE 6.8

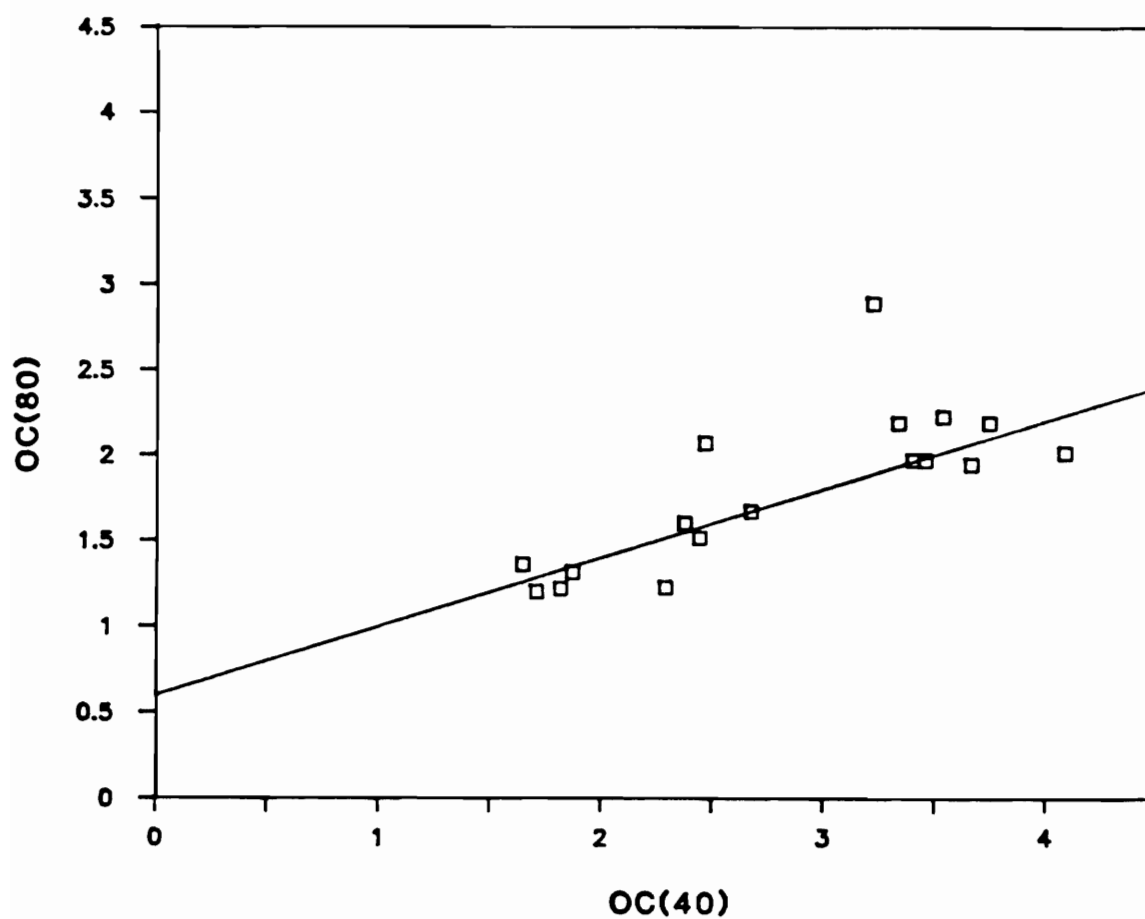


Figure 6.8. Comparison of organic carbon concentrations ($\mu\text{gC}/\text{m}^3$) at face velocities of 40 and 80 cm/s for quartz fiber backup filters behind Teflon front filters. The solid line is the linear least squares fit of Table 6.3. $\text{OC}(80) = (0.6 \pm 0.7) + (0.4 \pm 0.2) \cdot \text{OC}(40)$ ($R^2 = 54\%$).

FIGURE 6.9

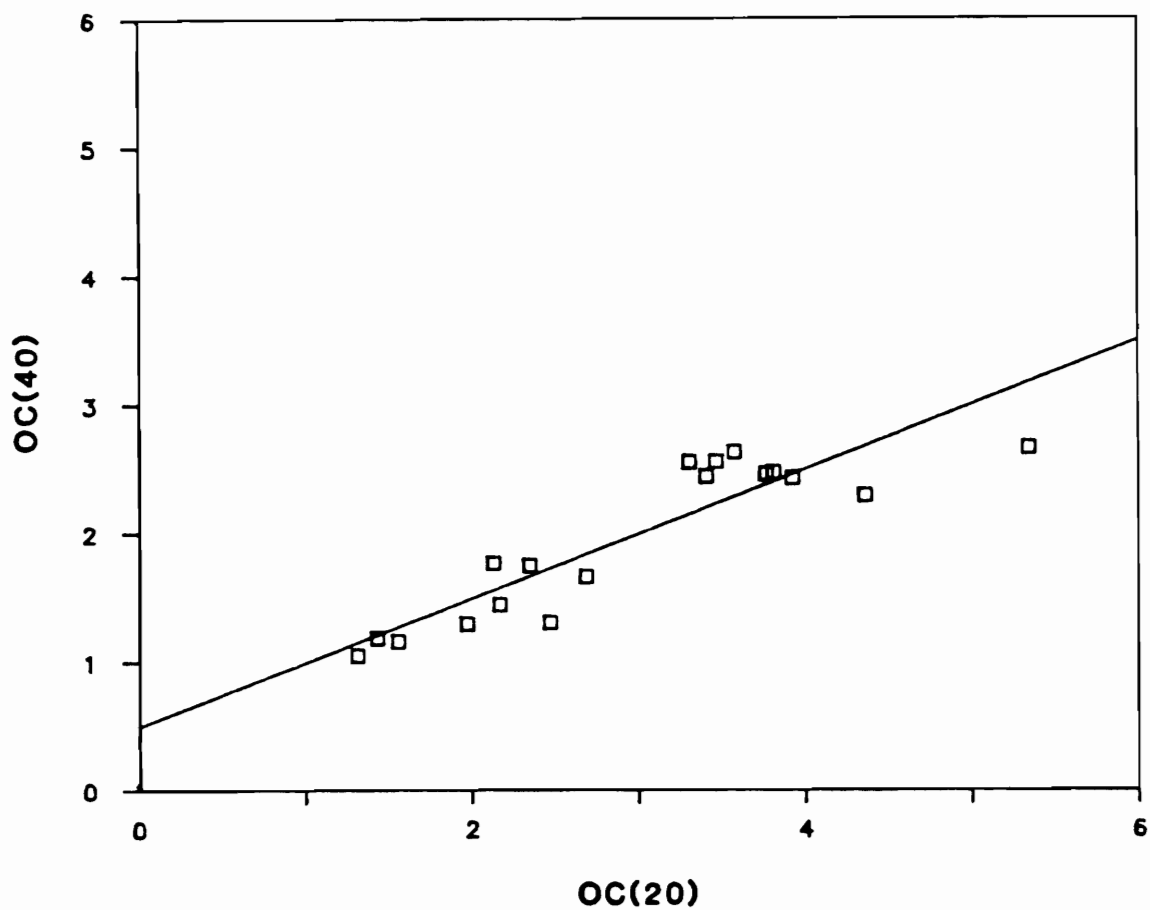


Figure 6.9. Comparison of organic carbon concentrations ($\mu\text{gC}/\text{m}^3$) at face velocities of 20 and 40 cm/s for quartz fiber backup filters behind quartz fiber front filters. The solid line is the linear least squares fit of Table 6.3. $\text{OC}(40) = (0.5 \pm 0.4) + (0.5 \pm 0.1) \cdot \text{OC}(20)$ ($R^2 = 80\%$).

FIGURE 6.10

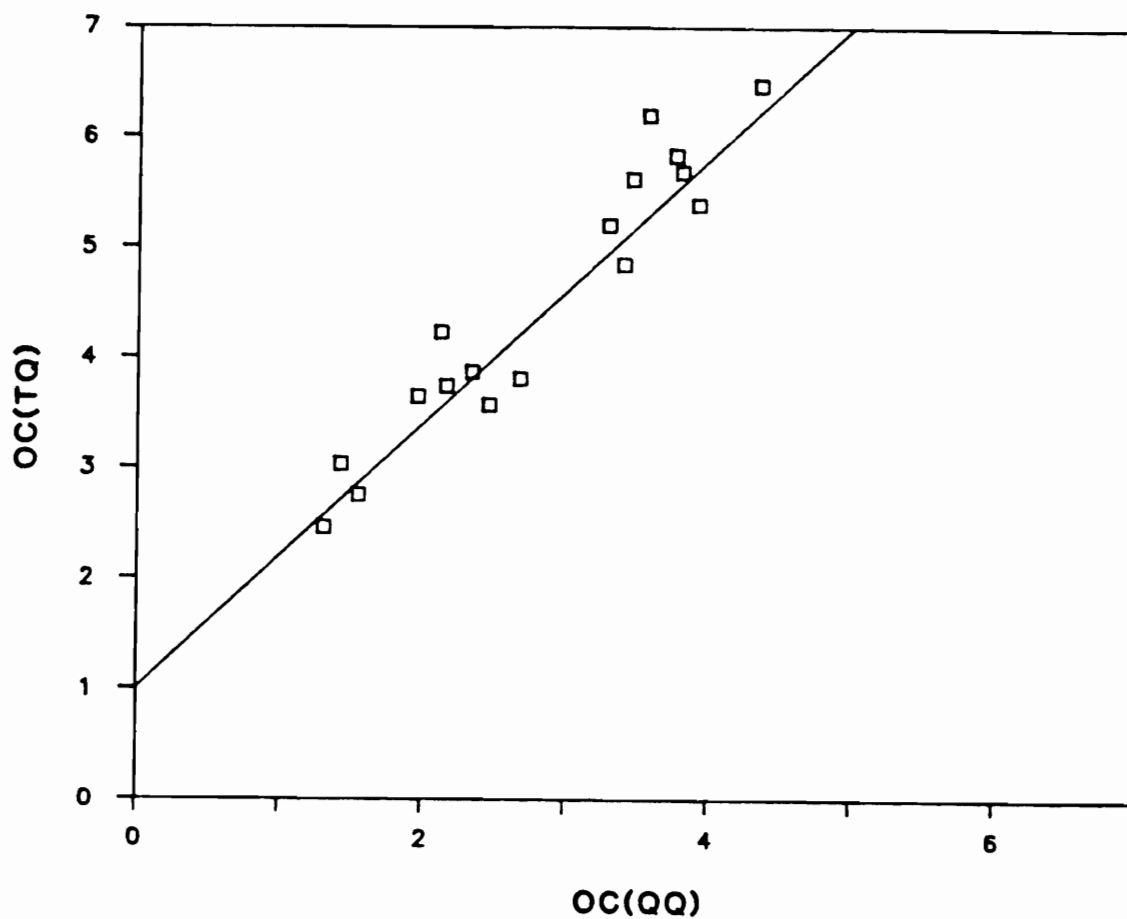


Figure 6.10. Comparison of organic carbon concentrations ($\mu\text{gC}/\text{m}^3$) for quartz fiber backup filters behind quartz fiber front filters (QQ) and quartz fiber backup filters behind Teflon front filters (TQ) at a face velocity of 20 cm/s. The solid line is the linear least squares fit of Table 6.3. $\text{OC}(\text{TQ}) = (1.0 \pm 0.6) + (1.2 \pm 0.2) \cdot \text{OC}(\text{QQ})$ ($R^2 = 92\%$).

FIGURE 6.11

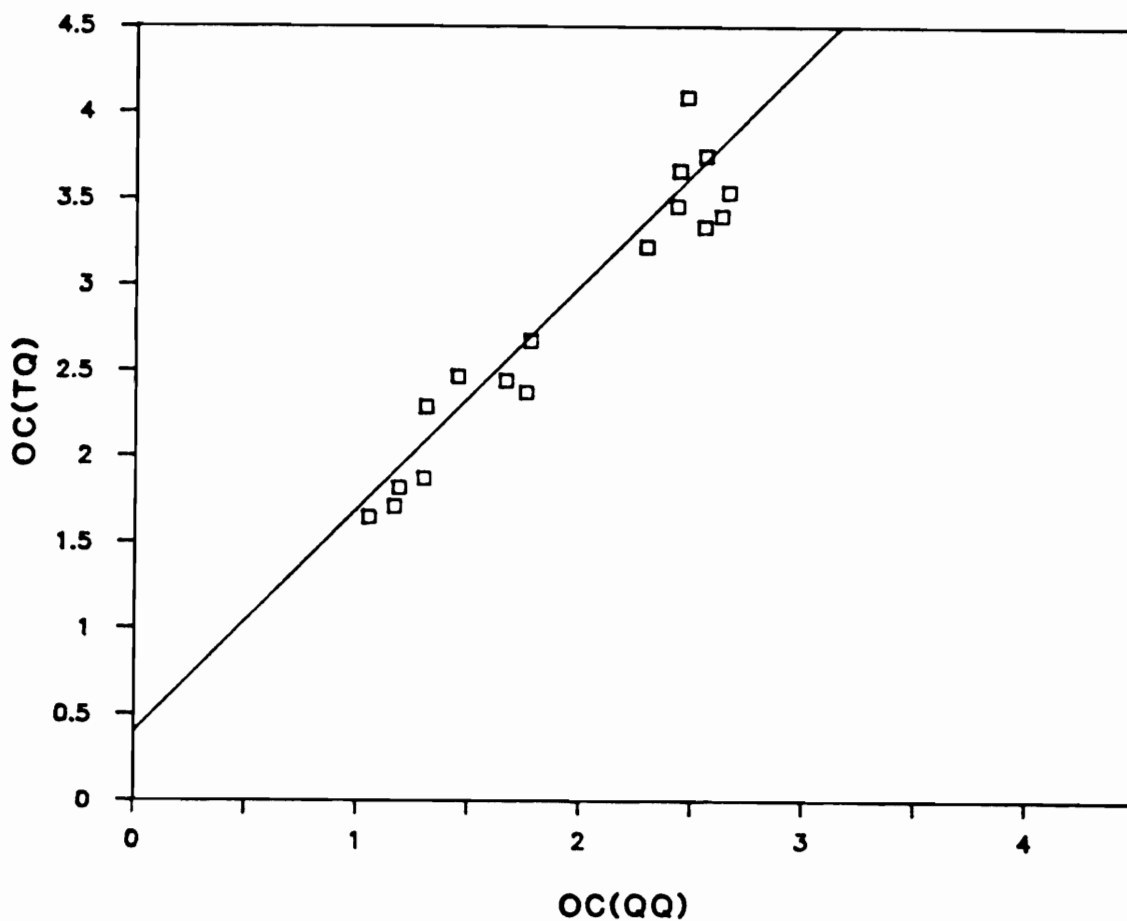


Figure 6.11. Comparison of organic carbon concentrations ($\mu\text{gC}/\text{m}^3$) for quartz fiber backup filters behind quartz fiber front filters (QQ) and quartz fiber backup filters behind Teflon front filters (TQ) at a face velocity of 40 cm/s. The solid line is the linear least squares fit of Table 6.3. $\text{OC}(\text{TQ}) = (0.4 \pm 0.5) + (1.3 \pm 0.2) \cdot \text{OC}(\text{QQ})$ ($R^2 = 90\%$).

TABLE 6.3. REGRESSION RESULTS FOR COMPARISON OF FACE VELOCITY SAMPLER BACKUP FILTERS.

The percentage of the variance explained by the regression of Y on 1 predictor in X is given by R^2 . The ratio is mean value of X/mean value of Y.

$$Y = a + bX$$

X	Y	RATIO (X/Y)	R^2
TQB(20)	TQB(40)	1.6	80%
TQB(40)	TQB(80)	1.6	54%
TQB(20)	TQB(80)	2.5	73%
QQB(20)	QQB(40)	1.5	80%
QQB(20)	TQB(20)	0.6	92%
QQB(40)	TQB(40)	0.7	90%

organic carbon concentrations on TQ backup filters were a factor of 2 greater than QQ backups for an average QQ backup loading of $2.5 \mu\text{gC}/\text{cm}^2$. This observation and the diurnal variation of backup filter concentrations are corroborated by the two-port sampler results.

Lower concentrations on QQ backups can be explained by the difference in adsorption capacities for Teflon and quartz fiber filters and can only exist if equilibrium has not yet been reached between the gas phase and adsorbed phase in the region of the QQ front filter. The Teflon filter adsorbs little because of its low surface area. The quartz fiber filter, however, has a large surface area and adsorbs a significant amount of organic vapors, reducing the concentration of adsorbable vapors which reaches the QQ backup filter until the gas phase/adsorbed phase distribution of organic vapor in the region of the front filter has reached equilibrium. If organic carbon was in equilibrium between gas and adsorbed phases on both Teflon and quartz fiber front filters then the concentration of gas phase organic carbon behind both front filters would be the same, and TQ and QQ backup filters would be identical. Since this is not the case, the TQ backup filter provides a better estimate of the vapor adsorption artifact present on the QQ front filter. Adsorption corrected, "particulate" concentrations of OC, EC, and TC found in particles less than $1.0 \mu\text{m}$ in diameter are plotted in Figure 6.12. Particulate OC and TC concentrations were obtained by subtracting each TQ backup from the corresponding QQ front filter value.

In Portland, McDow (1986) performed an experiment in which one port contained a QQ and one a QTQ (Teflon filter, inserted between two quartz fiber filters) filter combination to determine whether contamination from the Teflon

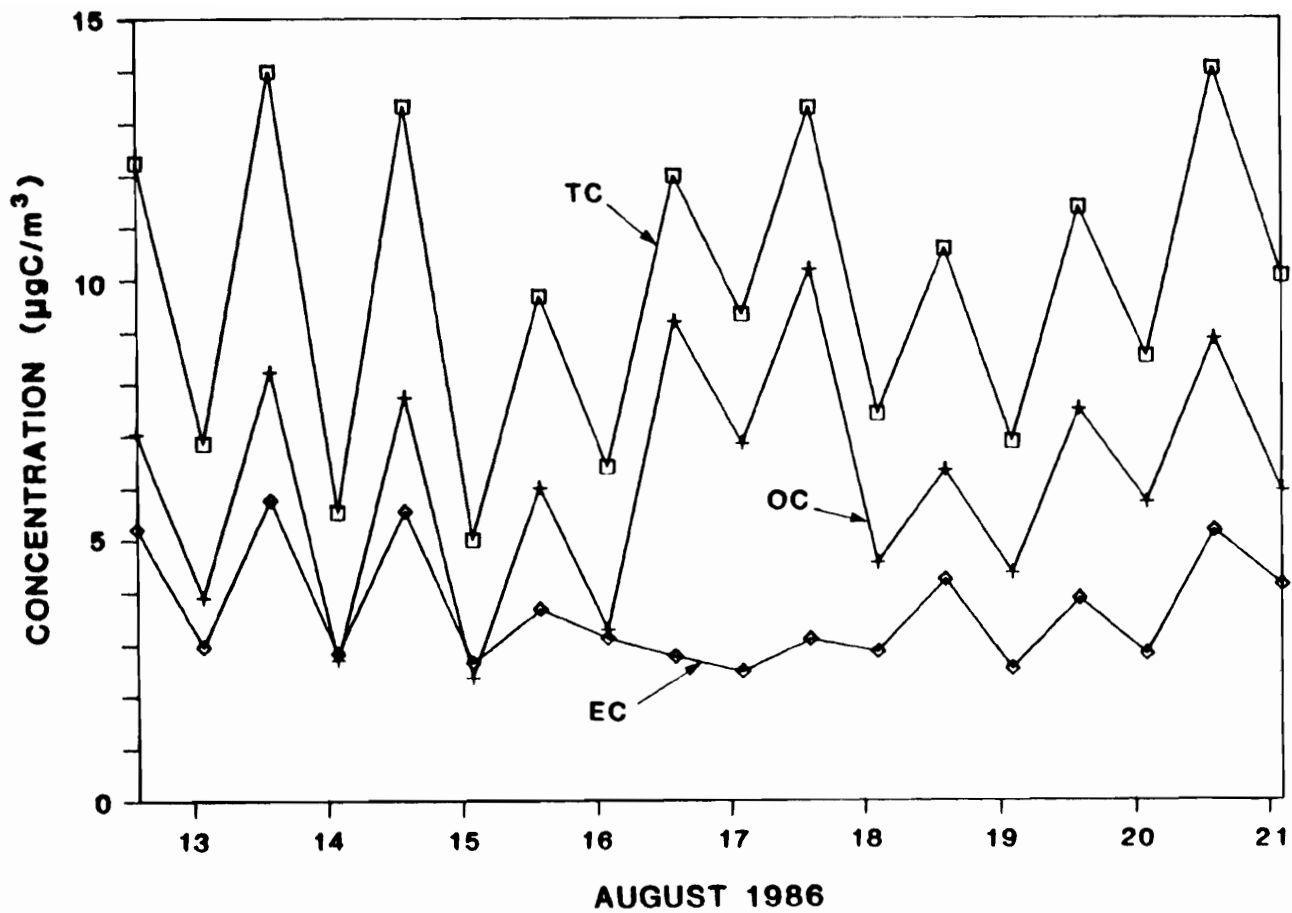


Figure 6.12. Twelve hour average concentrations ($\mu\text{gC}/\text{m}^3$) of particulate organic (OC), elemental (EC), and total carbon (TC) in particles under $1.0 \mu\text{m}$ in diameter at Glendora, California, August 12-21, 1986. Sample times were 08:00-20:00 and 20:00-08:00. The x-axis is marked with the August sampling date.

FIGURE 6.12

filter might be responsible for the difference between TQ and QQ backup results. Carbon loadings on the final quartz filters agreed within $0.10 \mu\text{gC}/\text{cm}^2$, which is much lower than the differences observed on the TQ and QQ backups. An additional experiment of McDow (1986) demonstrated that slightly more material was present on QQ backups than on TQQ final backups collected simultaneously indicating that some vapor adsorbed on the Teflon filter. Neither result can be explained by contamination from Teflon filters. These results were corroborated by QQ and TQQ filter data from the 1987 dilution experiment, discussed later in this chapter.

The front filter results are presented in Figures 6.13 - 6.15. Linear regression results are listed in Table 6.4. Elemental carbon measurements are not affected by sampling artifacts and therefore provide a good quality control check. A two-sided paired t-test showed no significant difference between 20 and 40 cm/s elemental carbon concentrations at the 95% confidence level. The 20 cm/s face velocity OC values are higher than the 40 cm/s values not only at the 95 but also at the 99% confidence level as demonstrated by a single sided t-test. When the measured concentrations of organic carbon on the TQ backup filters are subtracted from the corresponding apparent OC concentrations on the QQ front filters, the face velocity dependence is virtually eliminated. A two-sided t-test shows no significant difference between 20 and 40 cm/s vapor-corrected OC values at 95% confidence levels. These results confirm that adsorption of organic vapors is the dominant artifact in the sampling of organic aerosol in Los Angeles as well as Portland.

FIGURE 6.13

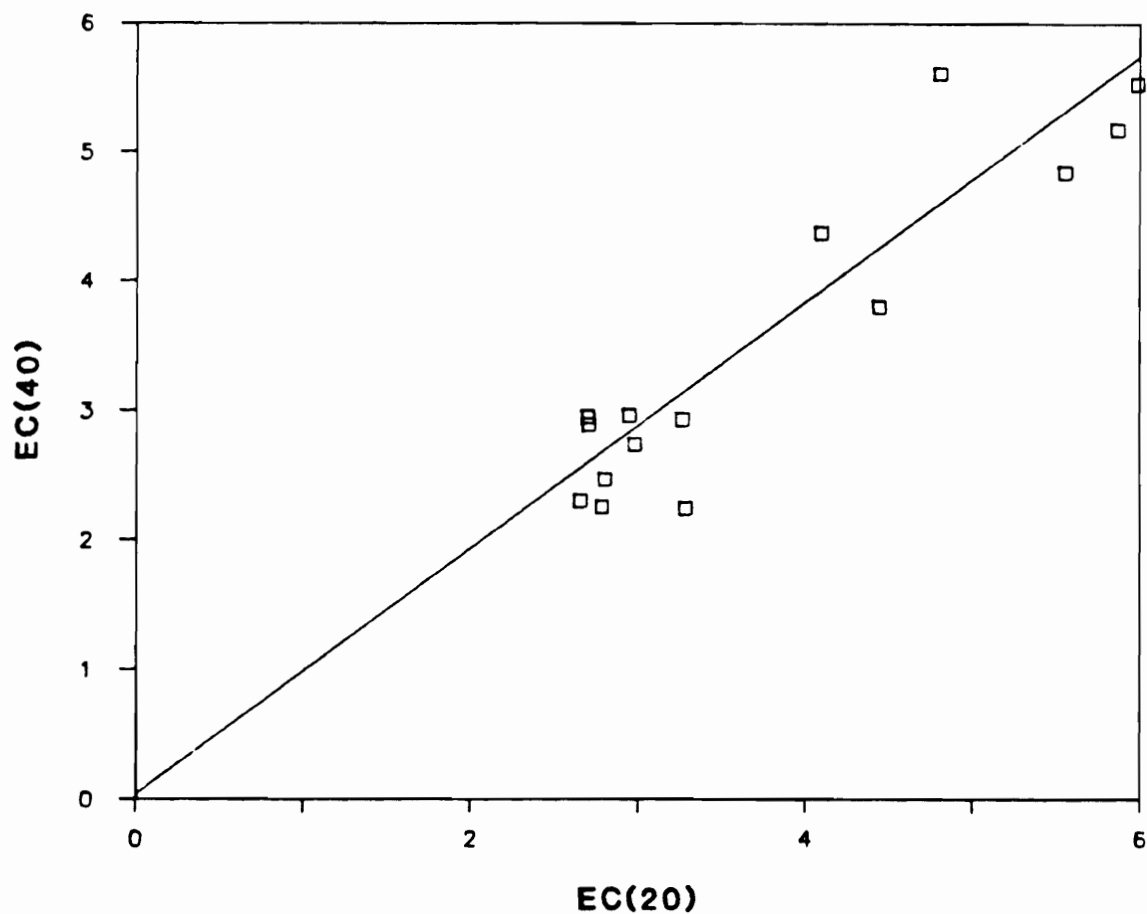


Figure 6.13. Comparison of elemental carbon concentrations ($\mu\text{gC}/\text{m}^3$) for quartz fiber front filters at face velocities of 20 and 40 cm/s. The solid line is the linear least squares fit of Table 6.4. $\text{EC}(40) = (0.04 \pm 0.9) + (0.93 \pm 0.2) \cdot \text{EC}(20)$ ($R^2 = 85\%$).

FIGURE 6.14

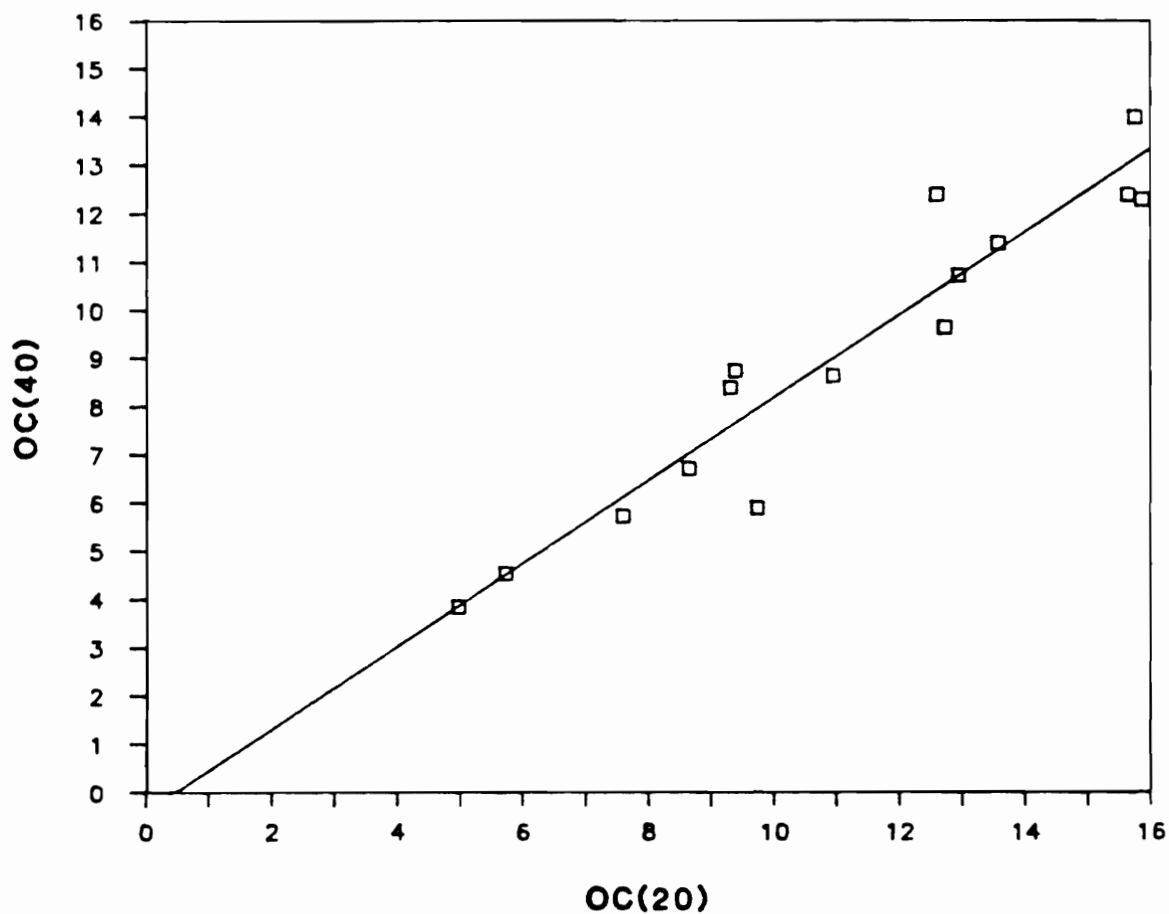


Figure 6.14. Comparison of organic carbon concentrations ($\mu\text{gC}/\text{m}^3$) for quartz fiber front filters at face velocities of 20 and 40 cm/s. The solid line is the linear least squares fit of Table 6.4. $\text{OC}(40) = (-0.4 \pm 2) + (0.86 \pm 0.2) \cdot \text{OC}(20)$ ($R^2 = 91\%$).

FIGURE 6.15

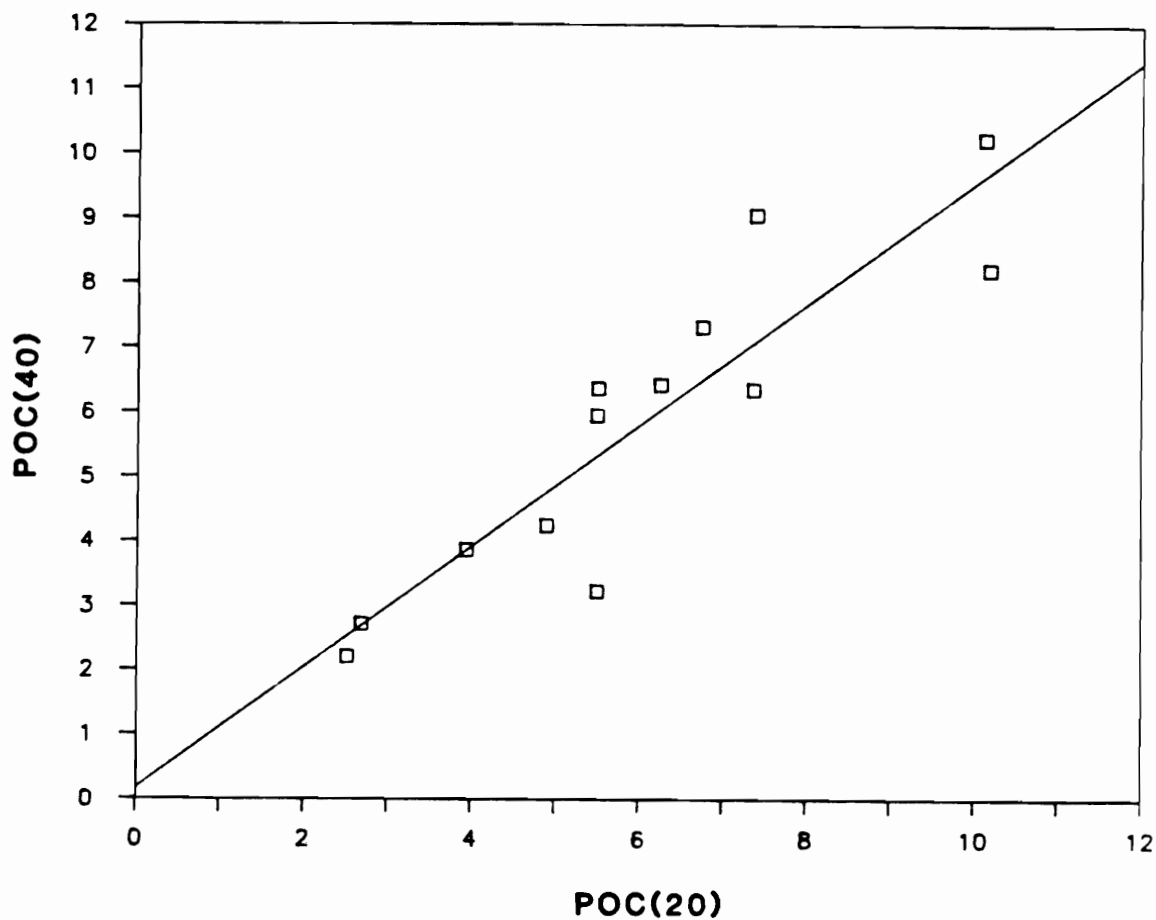


Figure 6.15. Comparison of "artifact corrected," particulate organic carbon concentrations (POC) ($\mu\text{gC}/\text{m}^3$) at face velocities of 20 and 40 cm/s. Correction for vapor adsorption is accomplished by subtracting the quartz fiber backup filter behind the Teflon filter from the quartz fiber front filter. The solid line is the linear least squares fit of Table 6.4. $\text{POC}(40) = (0.2 \pm 2) + (0.94 \pm 0.3) * \text{POC}(20)$ ($R^2 = 81\%$).

TABLE 6.4. REGRESSION RESULTS FOR COMPARISON OF FACE VELOCITY SAMPLER FRONT FILTERS.

Uncertainties are 95% confidence intervals. The number of samples comprising the regression is indicated by n, R^2 is the percentage of the variance explained by the regression, and the ratio expressed is the ratio of mean 20 cm/s to mean 40 cm/s concentrations. A one sided t-test shows that 20 cm/s uncorrected OC concentrations are significantly larger than 40 cm/s uncorrected OC concentrations with 95% confidence ($t = 7.1$). Elemental carbon and vapor corrected organic carbon (POC) are not significantly different ($t_{EC} = 1.9$; $t_{POC} = 0.6$) at the two face velocities.

$$(40 \text{ cm/s}) = a + b (20 \text{ cm/s})$$

	a	b	RATIO (20)/(40)	R2	n
EC	0.04 ± 0.9	0.93 ± 0.2	1.07	85%	15
UNCORRECTED OC	-0.4 ± 2	0.86 ± 0.2	1.22	91%	15
CORRECTED OC	0.2 ± 2	0.94 ± 0.3	1.03	81%	13

A comparison with the results of McDow (1986) for Portland experiments which included both 20 and 40 cm/s face velocity sampling ports is shown in Table 6.5. Carbon concentrations in the two experiments are comparable. The ratio of 20 to 40 cm/s uncorrected organic carbon concentrations is larger for the Glendora samples than for the Portland samples. For an average organic aerosol concentration of $6 \mu\text{gC}/\text{m}^3$ at a face velocity of 40 cm/s about 30% of the organic material deposited on the filter was attributed to vapor adsorption in the Glendora experiment. This compares with 10 to 15% at the same face velocity and average organic aerosol concentration of $7 \mu\text{gC}/\text{m}^3$ in Portland. As in the CSMCS experiments, the face velocity dependence in the Portland experiments was greatly reduced by backup filter subtraction. These results suggest that adsorbed vapor played a more significant role in the sampling of organic carbon in the conditions present during the CSMCS in Glendora, California, than in typical Portland conditions.

Because face velocity is a function of exposed surface area, the master variable controlling adsorption at constant gas phase concentrations could be either face velocity or surface area. Figure 6.16 compares 20 cm/s quartz - quartz front filter concentrations (QQF(20)) with the sum of 40 cm/s quartz - quartz front and backup filters (QQF(40)+QQB(40)). Regression results are given in Table 6.6. Together the 40 cm/s filters have the same exposed surface area as the single 20 cm/s front filter, but they have twice the face velocity. A two-sided paired t-test showed no significant difference between the two quantities with 95% confidence limits, and the ratio of mean QQF(20) to mean (QQF(40) + QQB(40)) was 1.005. However, a large fraction of this material is

TABLE 6.5. COMPARISON OF THE FACE VELOCITY DEPENDENCE OF CARBON LOADING FOR PORTLAND AND CSMCS GLENDORA, CALIFORNIA, EXPERIMENTS.

Ratios are of the mean 20 cm/s face velocity concentration to the mean 40 cm/s face velocity concentration. POC corresponds to particulate organic carbon which refers to the vapor-corrected concentrations. Organic aerosol concentrations in the two experiments are similar. The numbers in parenthesis for Portland are ratios of 15 cm/s face velocity concentrations to 40 cm/s concentrations.

	RATIOS OF THE MEANS	
	PORTLAND	GLENDORA (CSMCS)
EC(20)/EC(40)	0.95 (0.91)	1.07
OC(20)/OC(40)	1.09 (1.14)	1.22
POC(20)/POC(40)	(0.99)	1.03

FIGURE 6.16

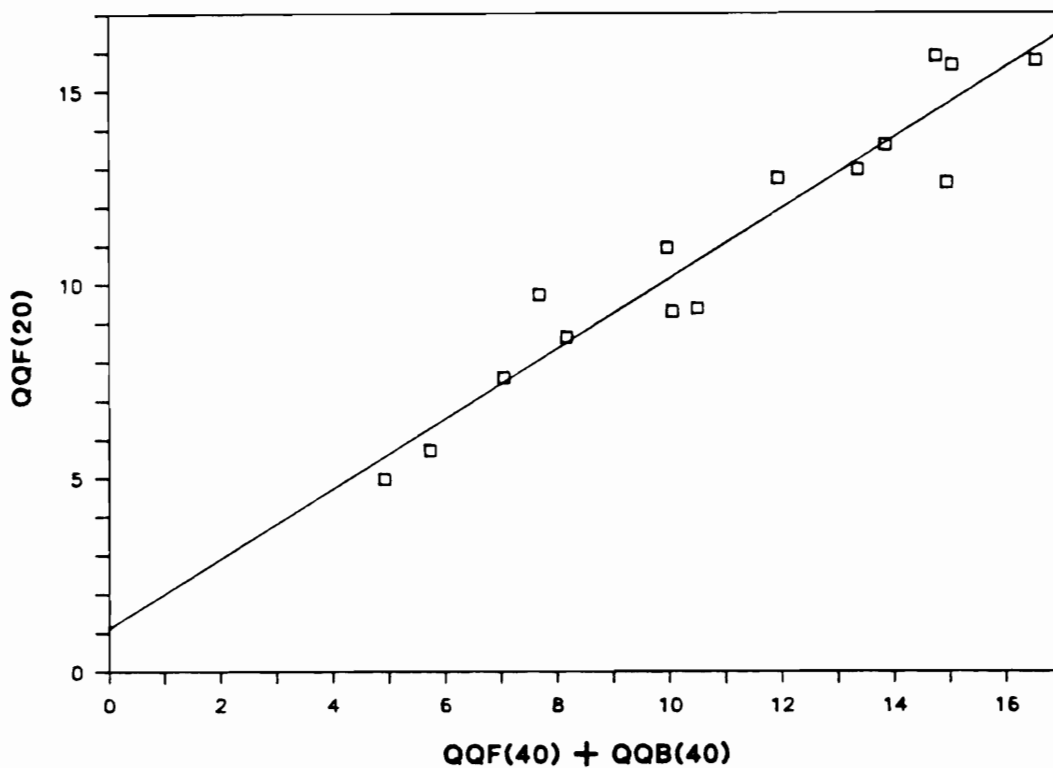


Figure 6.16. Comparison of organic carbon concentrations ($\mu\text{gC}/\text{m}^3$) on 20 cm/s quartz-quartz front filters (QQF(20)) and on the sum of 40 cm/s quartz-quartz front and backup filters (QQF(40) + QQB(40)). The solid line is the linear least squares fit of Table 6.6. $\text{QQF}(20) = (1.1 \pm 1.9) + (0.9 \pm 0.2) * (\text{QQF}(40) + \text{QQB}(40))$ ($R^2 = 92\%$).

TABLE 6.6. REGRESSION RESULTS FOR COMPARISON OF 20 cm/s QUARTZ - QUARTZ FRONT FILTER (QQF(20)) AND 40 cm/s QUARTZ - QUARTZ FRONT PLUS BACKUP FILTER (QQF(40) + QQB(40)) CONCENTRATIONS ($\mu\text{gC}/\text{m}^3$)

Uncertainties are 95% confidence intervals. The number of samples comprising the regression is n, and R^2 is the percentage of the variance explained by the regression.

$$(\text{QQF}(20)) = a + b (\text{QQF}(40) + \text{QQB}(40))$$

	a	b	R^2	n
LINEAR REGRESSION	1.1 ± 1.9	0.9 ± 0.2	92%	15

particulate, artificially improving the comparison. Table 6.7 displays the results when TQ backup filters were used for a similar test. The apparent organic carbon concentrations on 20 cm/s TQ backups were compared with 40 cm/s TQ backups multiplied by two and with 80 cm/s TQ backups multiplied by four. In addition, 40 cm/s TQ backups were compared with 80 cm/s TQ backups multiplied by two. A two sided t-test showed that in two of the three comparisons the quantities being compared were significantly different with 95% confidence. Thus these results are inconclusive regarding the relative role of surface area and face velocity in determining the magnitude of the vapor sampling artifact at a given organic carbon concentration.

CSMCS DILUTION EXPERIMENT

The two-port sampler which was used in the CSMCS to collect manual samples for comparison with the in situ carbon analyzer (see Chapter 4) was modified at 2000 hours (PDT) on August 15, 1986 to include a third port. In this configuration the sampler could investigate the relative importance of adsorption and volatilization artifacts in an experiment of Susanne Hering's design. All ports operated at 25 l/min, and large particles were removed with a 2.5 μ m cut-point impactor. One port contained a TQ filter combination, and two held QQ filter combinations. In one of the two QQ ports a fraction of the input air was stripped of aerosol by drawing it through a Teflon pre-filter with a bellows pump and re-injecting it into the sample stream; these samples are designated DQQ. By altering the sampling conditions in this way the loadings in the three ports

TABLE 6.7. REGRESSION RESULTS FOR COMPARISON OF TEFLON - QUARTZ BACKUP FILTER DATA OF DIFFERENT FACE VELOCITIES BUT THE SAME EXPOSED SURFACE AREA

Uncertainties are 95% confidence intervals. The number of samples comprising the regression is n, R² is the percentage of the variance explained by the regression, and t is the student's t-test value comparing data in x with that in y.

$$Y = a + bX$$

Y	X	a	b	R ²	n	t
TQB(20)	2xTQB(40)	0.6±1.2	0.7±0.2	81%	16	1.88
TQB(40)	2xTQB(80)	0.4±1.1	0.7±0.3	59%	17	4.25
TQB(20)	4xTQB(80)	0.3±1.4	0.6±0.2	73%	17	7.23

resulted from different combinations of three unknowns: adsorbed organic vapor, volatilized organic material, and organic aerosol.

The fraction of the input air which was stripped of aerosol ($1-\alpha$) is given in Table 6.8. Dilution experiment data are shown in Table 6.9. Elemental carbon concentrations again provide a good quality assurance check because they are not subject to sampling artifacts. When the DQQ (front filter) elemental carbon values were compared with the QQ (front filter) EC values multiplied by the fraction of unstripped air (α) entering the DQQ port (DQQ vs α QQ), good agreement was found except for the two runs on August 16 and August 20. This discrepancy might have been the result of the loss of dilution air out the sampler inlet. The questionable runs were excluded from the analysis.

Because Teflon and quartz fiber filters are essentially 100% effective at collection of particulate material, the presence of organic carbon on TQ and QQ backup filters demonstrated that adsorption occurs. The set of equations developed to describe the influence of adsorption, volatilization and particulate loading on the filter loading are based on a gas phase - adsorbed phase equilibrium model. According to BET theory (Equation 6.1) an increase in the pressure drop would decrease the partial pressure of the organic ($X_2 < X_1$) and volatilization would occur to bring the fraction of sorbed organic carbon to a new equilibrium. Volatilization would be expressed as $(v_1 - v_2)$ where v_1 and v_2 are the volumes of gas sorbed at equilibrium for $t=1$ and $t=2$ conditions respectively. Therefore, volatilization would be proportional to particle surface area. Evidence was presented earlier in the chapter suggesting that gas phase - adsorbed phase partitioning on quartz fiber filters is not typically in equilibrium. Further

TABLE 6.8. PERCENTAGE OF INPUT AIR STRIPPED OF AEROSOL

AUGUST, 1986	%
15(N)	19.3
16(D)	19.0
16(N)	19.7
17(D)	20.4
17(N)	19.6
18(D)	39.2
18(N)	47.4
19(D)	48.7
19(N)	71.2
20(D)	72.9
20(N)	18.7

TABLE 6.9. CSMCS DILUTION EXPERIMENT ORGANIC CARBON LOADINGS ($\mu\text{gC}/\text{cm}^2$)

The uncertainty for organic carbon is $\pm 4.3\%$ as a coefficient of variation. (D): 0800-2000 hour sample; (N): 2000-0800 hour sample; QQF: quartz-quartz front filter concentration in port which sampled undiluted ambient air; QQB: quartz-quartz backup filter concentration in port which sampled undiluted ambient air; DQ: quartz front filter concentration in port which sampled ambient air a fraction of which was stripped of particles; $(1-\alpha)$: fraction of ambient air which was stripped of particles in DQ port; TQB: quartz fiber filter concentration in port which sampled 100% particle-free ambient air.

DATE	QQF	QQB	DQ	TQB	$(1-\alpha)$
8/15 (N)	9.5	1.9	8.9	2.5	0.19
8/16 (D)	24.7	4.4	23.0	6.2	0.19
8/16 (N)	17.1	2.7	15.2	3.3	0.20
8/17 (D)	26.5	5.0	22.8	6.2	0.20
8/17 (N)	13.8	2.8	11.2	4.2	0.20
8/18 (D)	18.2	5.2	15.4	6.1	0.39
8/18 (N)	14.7	3.2	10.9	4.8	0.47
8/19 (D)	18.9	4.8	16.4	5.6	0.49
8/19 (N)	19.8	3.1	10.8	4.6	0.71
8/20 (D)	25.4	4.9	17.5	5.8	0.73
8/20 (N)	18.4	3.0	16.9	4.1	0.19

interpretation of these results will require a better understanding of how equilibrium is approached.

When it was assumed that volatilization was proportional to particle loading (to reflect particle surface area) the following equations resulted:

$$QQF = (P - V) + A \quad (6.3)$$

$$DQQF = \alpha(P - V) + A + K_o \quad (6.4)$$

$$TQB = A \quad (6.5)$$

where P represents particulate organic carbon; A, adsorption; V, volatilization; α , the fraction of unstripped ambient air, and K_o , the amount of organic contamination originating in the dilution system. Equations 6.3 and 6.4 are not independent, and as a result these equations could only be solved for (P - V) and A.

A contamination term is included in the above models because GC/MS results from DQQ backup filters showed strong phthalate peaks which were undoubtedly associated with contamination. The source of the contamination is not known but is most likely the bellows pump or some other component of the dilution system. The degree of contamination on the DQQ front filter can be estimated by comparing DQQ and QQ backup filters. These filters are exposed to the same concentration of organic vapor assuming that (1) redistribution between vapor and particulate phases between the dilution sampler inlet and the front filter is small; and (2) volatilization of particulate material from the front filter is small. The difference in DQQ and QQ backup filter organic carbon loadings was $1.5 \mu\text{gC}/\text{cm}^2$ on average. Because the first quartz fiber filter in a QQ or DQQ pair depletes the air of adsorbable vapor, this difference is a lower

limit. An upper limit can be obtained by multiplying this estimate by the ratio TQB/QQB. This yields an average upper limit contamination estimate of 2.0 $\mu\text{gC}/\text{cm}^2$ or 15% on the DQQ front filter.

Table 6.10 presents (P - V) and two estimates of adsorbed vapor from solution of the equations above. The poor agreement between adsorption estimates suggests that this simplified model is not adequate to describe the experiment. Uncertainty because of contamination in the dilution port prompted the development of a similar experiment for the Southern California Air Quality Study in 1987.

SCAQS DILUTION EXPERIMENT

In December 1987, during the fall segment of SCAQS, a second dilution experiment was conducted at the Long Beach site. Four sampling ports collected filter samples with different combinations of the three unknowns: adsorbed organic vapor, volatilized organic material, and organic aerosol. The use of four ports yielded an over-determined set of equations, enabling a better assessment of model fit. All ports operated at 30 l/min, and large particles were removed with a cyclone. Samples were collected roughly from 1000 - 2200 hours (D) and 2200 - 1000 hours (N). Each port contained a QQ filter combination, but in one port all input air was stripped of aerosol by drawing it through a Teflon filter (referred to as TQQ). In two of the remaining ports roughly 2/3 and 1/3 of the input air was stripped of aerosol by drawing it through a Teflon filter (referred to as 2/3TQQ and 1/3TQQ). The quartz fiber filters in the final port collected unfiltered ambient air (referred to as QQ).

TABLE 6.10. RELATIVE ARTIFACT CONTRIBUTIONS
DETERMINED FROM CSMCS DILUTION EXPERIMENT

Values describe particulate material minus that volatilized (P - V) and two estimates of adsorbed organic vapor (A) from solutions of the three equations: $A(1) = TQB$; $A(2) = (DQQF - \alpha QQF - K_0)/(1 - \alpha)$. The second estimate of adsorption involves the contamination term and therefore both low (1.5) and high (2.0) contamination estimates have been included. Values are filter loadings in $\mu\text{gC}/\text{cm}^2$.

	(P-V)	A(1)	A(2) low K_0	A(3) high K_0
August 15(N)	7.0	2.5	-1.7	-4.3
August 17(D)	20.3	6.2	1.4	-1.1
August 17(N)	9.6	4.2	-7.3	-9.8
August 18(D)	12.0	6.1	7.1	5.9
August 18(N)	10.0	4.8	3.4	2.4
August 19(D)	13.3	5.6	10.7	9.6
August 19(N)	15.2	4.6	5.1	4.4

During the first collection, made December 5 from 1000 to 2200 hours, three of the ports were run without Teflon filters to check for contamination in the system. The fourth port was being used in another experiment. The coefficient of variation of the front filter OC values from the three ports was 2.9%, and it was 1.2% for the OC values on the backup filters. These uncertainties are comparable to the analytical uncertainties for the dilution experiment samples (4.4% for front filter OC and 3.7% for backup filter OC), and it was therefore concluded that the system was not contaminated.

A check for consistency between elemental carbon concentrations measured on front filter samples collected concurrently was also used as a quality control test. The elemental carbon values obtained from the 1/3TQQ and the 2/3TQQ front filters were compared with the QQ front filter EC values multiplied by the fraction of unstripped air (α) entering the 1/3TQQ or 2/3TQQ port (i.e. 1/3TQQ vs α QQ). A one way analysis of variance comparing the two partially pre-filtered ports with α QQ identified three outliers: the 2/3TQQ and 1/3TQQ samples collected from 1000 to 2200 hours, December 8, and the 2/3TQQ sample collected from 2200 to 1000 hours beginning December 7. These runs have been excluded from the analysis.

In this, as in other experiments, OC concentrations on TQ backup filters were significantly greater than those on QQ backup filters with 95% levels of confidence, determined using a paired t-test. The ratio of the mean TQ backup to the mean QQ backup was 1.6. If the difference between TQ and QQ backup concentrations was the result of contamination from the Teflon filter, then the TQQ final backup concentration would exceed the QQ backup concentration.

Table 6.11 compares the final backup filters from the four ports. The table lists the difference between the mean backup filter concentration for the port listed above and the mean backup filter concentration for the port listed to the left. In none of these comparisons was contamination suggested. The values in parenthesis are the t values from the student's t-test. A two-sided t-test showed no significant difference between the backup filter values from any two ports with 95% confidence levels.

A set of equations was constructed to estimate the effect of the Teflon filter on the backup filter concentrations in the ports:

$$1/3TQQB = QQB + (1-\alpha_{1/3})T \quad (6.6)$$

$$2/3TQQB = QQB + (1-\alpha_{2/3})T \quad (6.7)$$

$$TQQB = QQB + T \quad (6.8)$$

where B refers to the final backup filter, $(1-\alpha_{1/3})$ is the fraction of the input air which passed through the Teflon filter in the 1/3TQQ port, $(1-\alpha_{2/3})$ is the fraction of input air which passed through the Teflon filter in the 2/3TQQ port, and T represents the effect of the Teflon filter on the final backup filter concentrations. A positive value of T would suggest contamination from the Teflon filter. A negative value would suggest that some adsorption of vapors took place on the Teflon filter and that this affected the TQQB filter concentration because gas phase - adsorbed phase partitioning had not reached equilibrium. The dilution experiment data were applied to these three equations, and T was estimated as

TABLE 6.11. COMPARISON OF SCAQS DILUTION EXPERIMENT FINAL BACKUP FILTER CONCENTRATIONS.

Values represent the mean final backup filter OC concentration of the port listed to the left subtracted from the mean final backup filter OC concentration of the port listed above. A positive difference would suggest contamination of the backup filter by the Teflon front filter. The values in the parenthesis are the t values from the student's t-test comparing the two sets of backup filter data. No significant difference was observed between any two sets of backup filter data.

	QQ	1/3TQQ	2/3TQQ	TQQ
QQ	0.00 (0.0)	0.00 (1.3)	-0.05 (0.0)	-0.14 (0.8)
1/3TQQ		0.00 (0.0)	-0.04 (1.2)	-0.13 (1.1)
2/3TQQ			0.00 (0.0)	-0.09 (0.9)
TQQ				0.00 (0.0)

$-0.1 \pm 0.3 \mu\text{gC}/\text{m}^3$ which is not significantly different from zero with 95% confidence intervals according to results from a two-sided paired t-test.

The dilution experiment data were interpreted in the same way as the CSMCS dilution data, assuming volatilization was proportional to loading. Figures 6.17 - 6.20 show the OC concentrations on front and back quartz fiber filters for the four runs which were used in the analysis. The pressure drops across the QQ filter combinations at the end of the sampling period were about 0, 0.5, 1.5, and 70 inches H₂O for samples with 15, 30, 33, and 53 $\mu\text{gC}/\text{cm}^2$ of OC respectively. The sample containing 53 $\mu\text{gC}/\text{cm}^2$ was collected the night of December 9, which was quite damp. The heavy loading of particulate pollutants and water probably was responsible for the large pressure drop. Final backup filters in the four ports were not significantly different. This confirms that adsorption on a quartz fiber filter is independent of the particle loading on the filter (or impactor cut-point used upstream). It follows that a several port sampler which collects ambient aerosol on quartz fiber filters following impactors of different size cuts can use the same (TQ backup) adsorption estimate. Three different estimates of adsorption and an estimate of (P - V) are shown in Table 6.12. These results clearly demonstrate the inability of the model to adequately describe the experiment. Although the experiments have generated some interesting data, further work is needed to develop an adequate model describing the effects of adsorption and volatilization on filter loading.

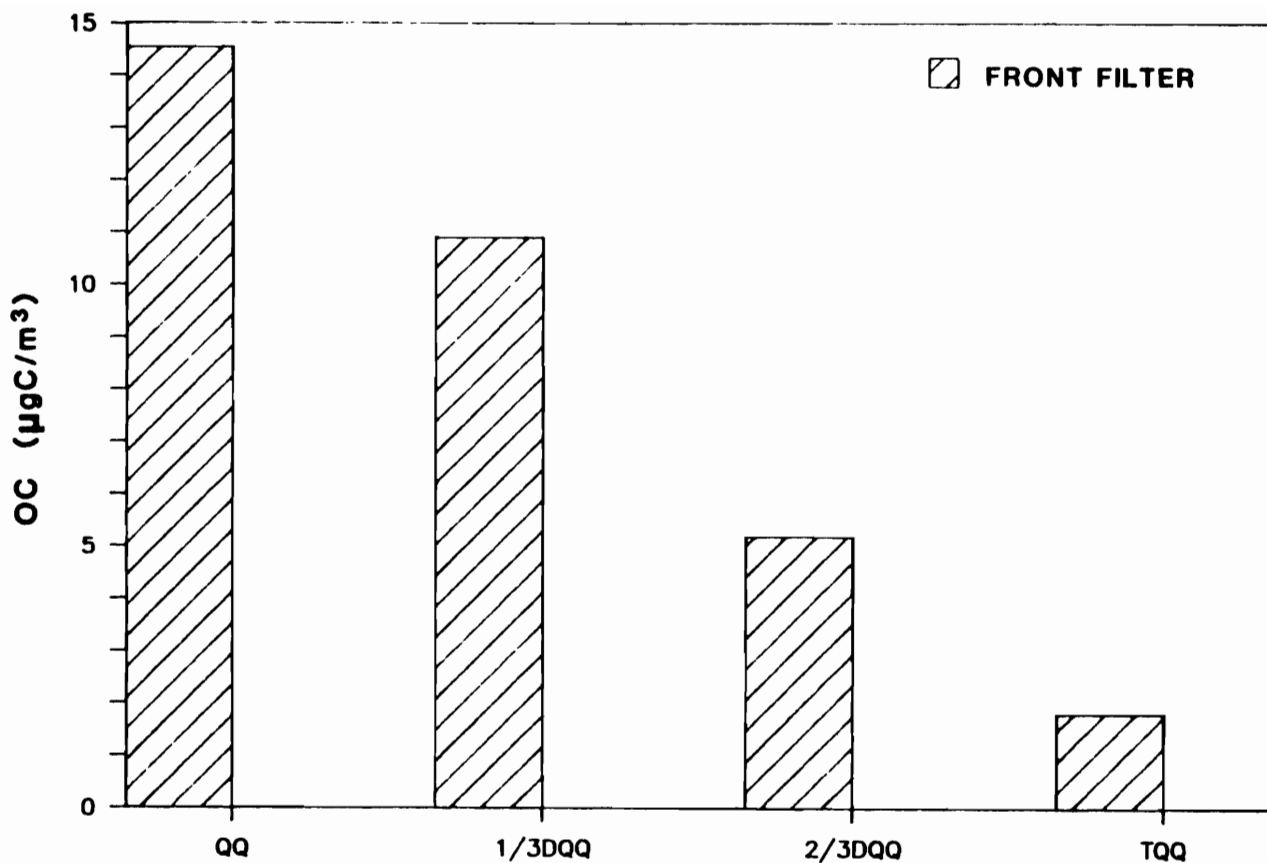


Figure 6.17. Southern California Air Quality Study dilution experiment organic carbon concentrations ($\mu\text{gC}/\text{m}^3$), December 5, 2200 hours - December 6, 1000 hours, 1987. QQ: quartz fiber filter followed by a quartz fiber filter sampling ambient air; 1/3DQQ: quartz fiber filter followed by quartz fiber filter sampling 2/3 ambient air and 1/3 particle-free ambient air; 2/3DQQ: quartz fiber filter followed by quartz fiber filter sampling 1/3 ambient air and 2/3 particle-free ambient air; TQQ: Teflon filter followed by two quartz fiber filters (quartz fiber filters sample particle-free ambient air).

FIGURE 6.17

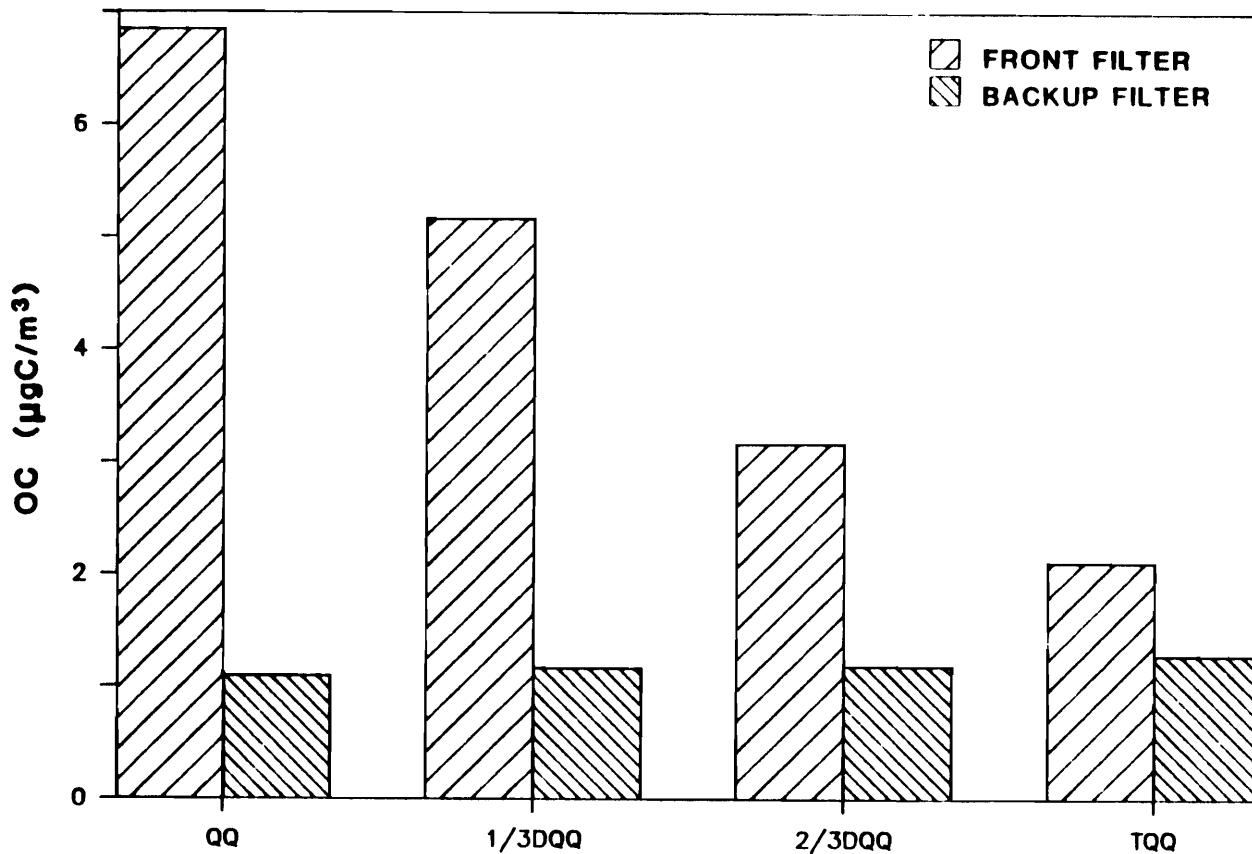


Figure 6.18. Southern California Air Quality Study dilution experiment organic carbon concentrations ($\mu\text{gC}/\text{m}^3$), December 7, 1000-2200 hours, 1987. QQ: quartz fiber filter followed by a quartz fiber filter sampling ambient air; 1/3DQQ: quartz fiber filter followed by quartz fiber filter sampling 2/3 ambient air and 1/3 particle-free ambient air; 2/3DQQ: quartz fiber filter followed by quartz fiber filter sampling 1/3 ambient air and 2/3 particle-free ambient air; TQQ: Teflon filter followed by two quartz fiber filters (quartz fiber filters sample particle-free ambient air).

FIGURE 6.18

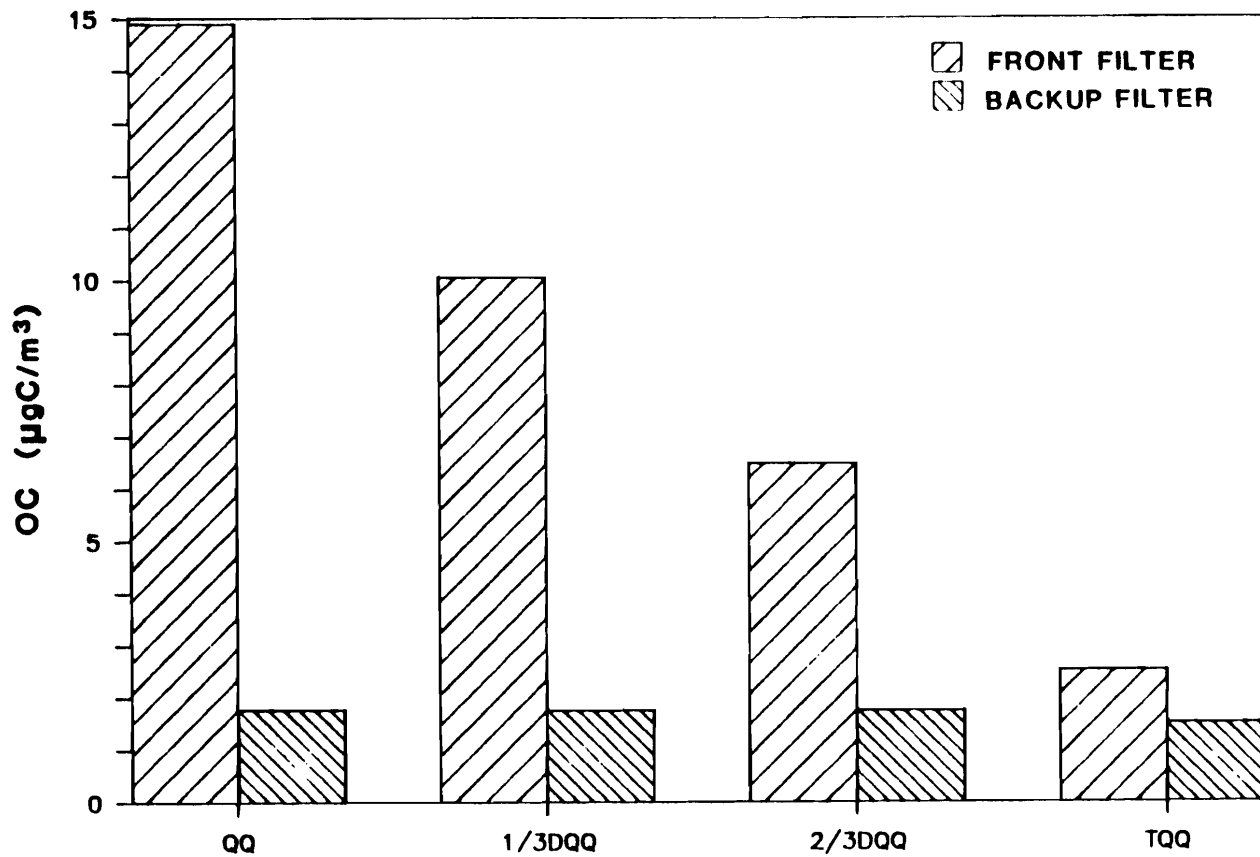


Figure 6.19. Southern California Air Quality Study dilution experiment organic carbon concentrations ($\mu\text{gC}/\text{m}^3$), December 9, 1000-2200 hours, 1987. QQ: quartz fiber filter followed by a quartz fiber filter sampling ambient air; 1/3DQQ: quartz fiber filter followed by quartz fiber filter sampling 2/3 ambient air and 1/3 particle-free ambient air; 2/3DQQ: quartz fiber filter followed by quartz fiber filter sampling 1/3 ambient air and 2/3 particle-free ambient air; TQQ: Teflon filter followed by two quartz fiber filters (quartz fiber filters sample particle-free ambient air).

FIGURE 6.19

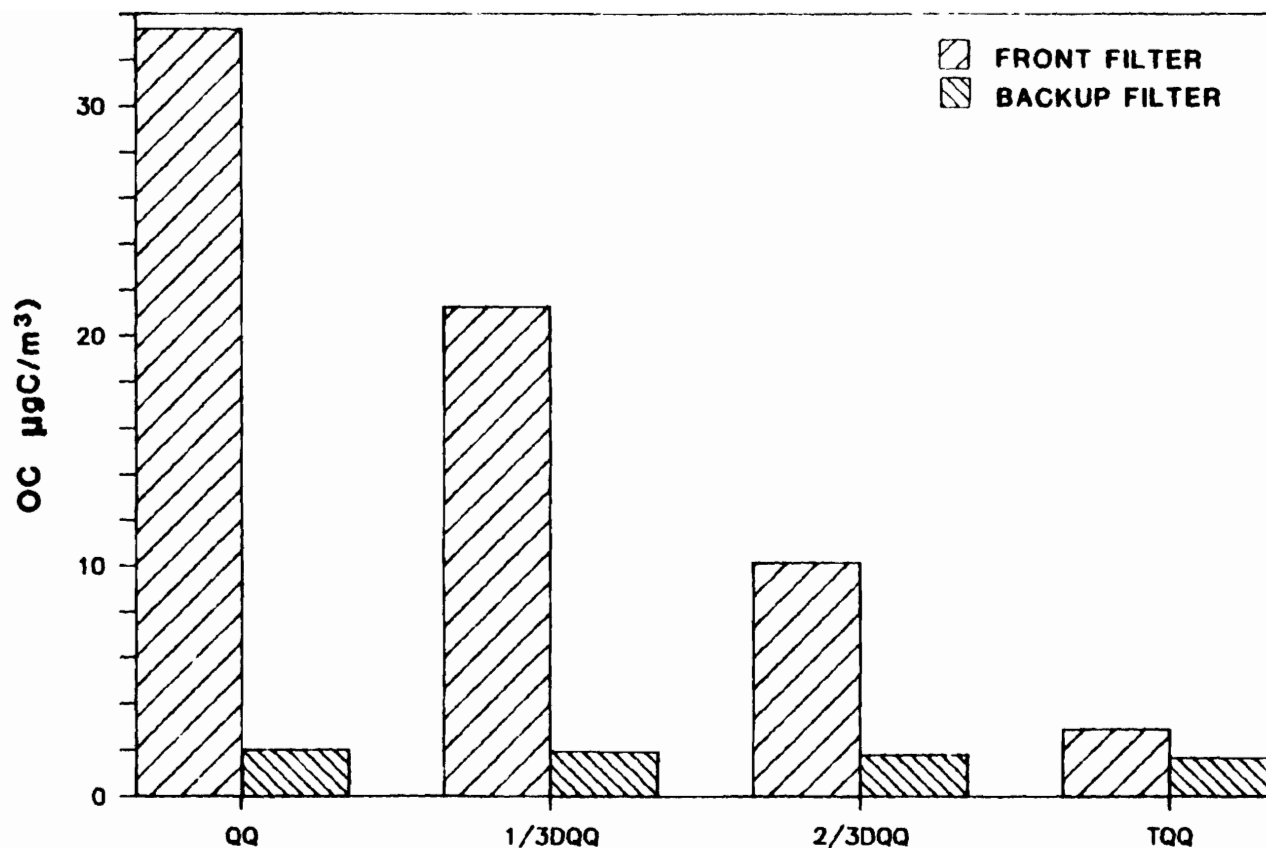


Figure 6.20. Southern California Air Quality Study dilution experiment organic carbon concentrations ($\mu\text{gC}/\text{m}^3$), December 9, 2200 hours - December 10, 1000 hours, 1987. QQ: quartz fiber filter followed by a quartz fiber filter sampling ambient air; 1/3DQQ: quartz fiber filter followed by quartz fiber filter sampling 2/3 ambient air and 1/3 particle-free ambient air; 2/3DQQ: quartz fiber filter followed by quartz fiber filter sampling 1/3 ambient air and 2/3 particle-free ambient air; TQQ: Teflon filter followed by two quartz fiber filters (quartz fiber filters sample particle-free ambient air).

FIGURE 6.20

TABLE 6.12. RESULTS OF SCAQS DILUTION EXPERIMENT

Values describe particulate material minus volatilization (P-V) and three estimates for adsorption based on solutions of the four equations: A(1) = TQB; A(2) = $(D_{1/3}QQF - \alpha_{1/3}QQF)/(1 - \alpha_{1/3})$; A(3) = $(D_{2/3}QQF - \alpha_{2/3}QQF)/(1 - \alpha_{2/3})$. Values are filter loadings in $\mu\text{gC}/\text{cm}^2$.

	(P-V)	A(1)	A(2)	A(3)
December 5(N)	29.0	4.1	1.5	-1.3
December 7(D)	10.4	4.6	1.1	3.9
December 9(D)	25.2	5.2	-4.2	6.4
December 9(N)	48.2	4.6	-18.2	3.4

LABORATORY EXPERIMENTS

A laboratory experiment was conducted in which a relatively constant concentration of organic vapor in air with a low aerosol content was sampled by the in situ carbon analyzer with varying collection times. Air from a pure air generator (AADCO 737) flowed into a sampling chamber at a flow rate of 22 l/min where it was sampled by aerosol and vapor side sampling inlets. On the vapor side a Teflon pre-filter removed all particles so that only adsorbed vapor was collected on the quartz fiber sampling filter whereas on the aerosol side, both aerosol and adsorbed vapor was collected on the quartz fiber sampling filter. Aerosol concentrations were determined by subtracting the vapor side result from the aerosol side result. The "clean air" generator provided a only a moderately constant source with aerosol concentrations which varied from 4.5 to 8.5 $\mu\text{gC}/\text{m}^3$. Despite the variation, the results clearly indicate an approach toward equilibrium vapor adsorption.

RESULTS

The results of the 8 run experiment are presented as mass loading vs collection time in Figure 6.21 with an expanded view of vapor loadings in Figure 6.22. The excellent correlation between aerosol loading and collection time ($R^2 = 98.9\%$), expressed by the linear regression results in Table 6.13, demonstrates that source variability did not influence the results. Aerosol collection doubled with doubling of collection time while the marginal increase in vapor loading diminished with increased sampling duration. Increases in vapor loading became insignificant for collection times longer than 200 minutes suggesting that the

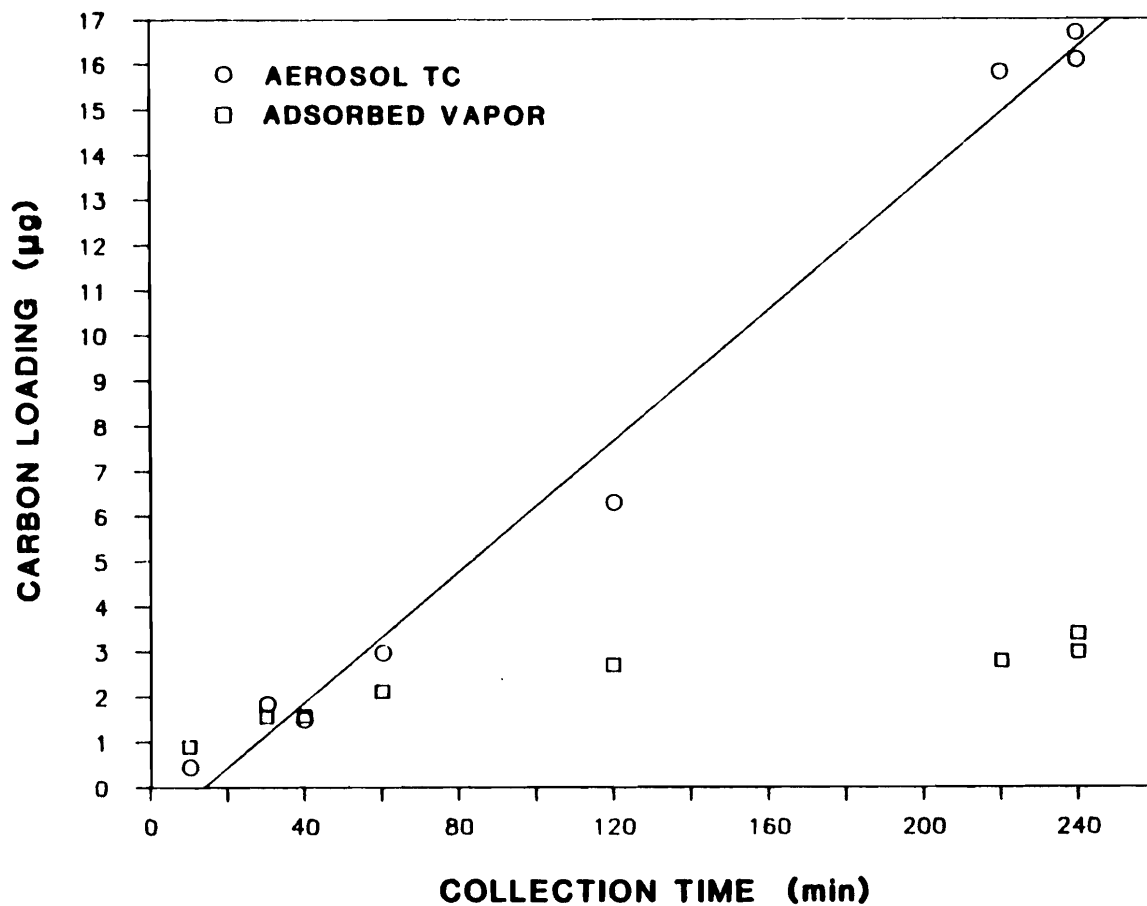


Figure 6.21. Aerosol total carbon and adsorbed vapor loadings (μg) as a function of collection time (min) in laboratory vapor saturation experiment. The filter area is 1.77 cm^2 . The solid line is the linear least squares fit for aerosol total carbon of Table 6.13. Aerosol TC = $(-1.0 \pm 1.2) + (0.07 \pm 0.008) \cdot \text{Collection Time}$ ($R^2 = 99\%$).

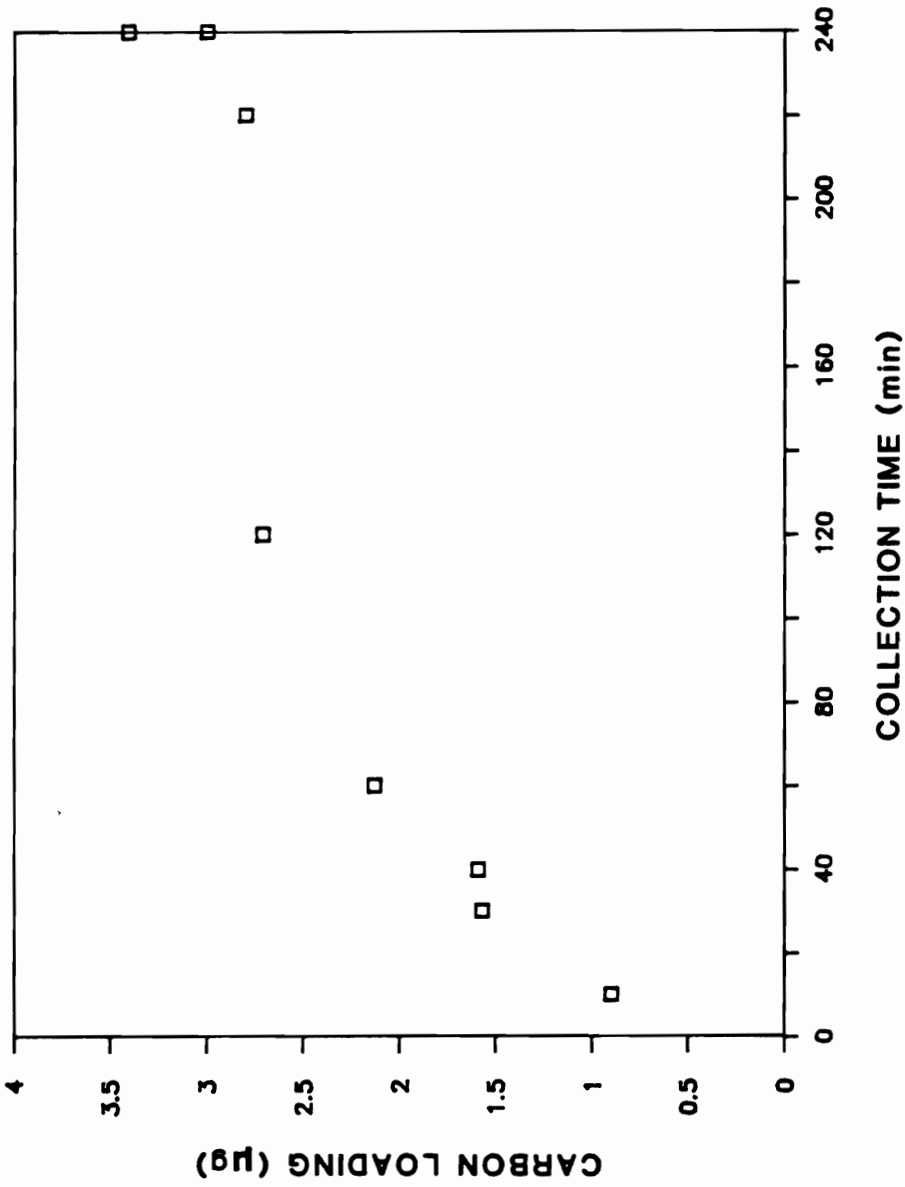


FIGURE 6.22

Figure 6.22. Expanded view of adsorbed vapor loading (μg) as a function of collection time (min) in laboratory vapor saturation experiment. The filter area is 1.77 cm^2 .

TABLE 6.13. REGRESSION RESULTS FOR THE LABORATORY VAPOR ARTIFACT EXPERIMENT: AEROSOL LOADING (μg) AS A FUNCTION OF COLLECTION TIME (min).

Uncertainties are 95% confidence intervals. The number of samples comprising the regression is indicated by n, and R^2 is the percentage of the variance explained by the regression.

$$(\text{AEROSOL TC}) = a + b (\text{COLLECTION TIME})$$

	a	b	R^2	n
LINEAR REGRESSION	-1.0 ± 1.2	0.07 ± 0.008	99%	8

partitioning between gas phase and adsorbed phase organic carbon had reached equilibrium. The 1.5 cm diameter double filter adsorbed 4 μg of organic carbon. The gas phase concentration was not measured. This experiment suggests that longer sampling durations will reduce the percentage of collected organic material which is adsorbed vapor and that it takes a significant amount of time for partitioning to reach equilibrium.

CSMCS data showed that adsorbed vapor loadings increased with increasing particulate organic carbon concentrations, suggesting an increase in adsorbed vapor loadings with increasing gas phase organic carbon concentrations.

Adsorbed vapor ($\mu\text{gC}/\text{cm}^2$) is plotted as a function of particulate organic carbon loading ($\mu\text{gC}/\text{cm}^2$) for the CSMCS two-port, *in situ* and face velocity samples in Figures 6.23 - 6.26. Regressions are presented in Table 6.14. All samples within each sample set were collected using the same face velocity, sample duration and exposed filter surface area. The linear dependence of adsorbed vapor loading on the organic carbon concentration suggests that adsorption was limited by the gas-phase organic carbon concentration and not by filter capacity. Multilayer sorption is likely to occur on the filter, and no evidence was found to indicate that the filter has a limited capacity for adsorption.

SUMMARY

Taken as a whole, these ambient South Coast Air Basin results are consistent with those obtained in Portland by McDow (1986). They suggest (1) that at the loadings of interest adsorption is the dominant artifact in the sampling of organic aerosol, (2) that the organic carbon collected on a quartz fiber filter behind a

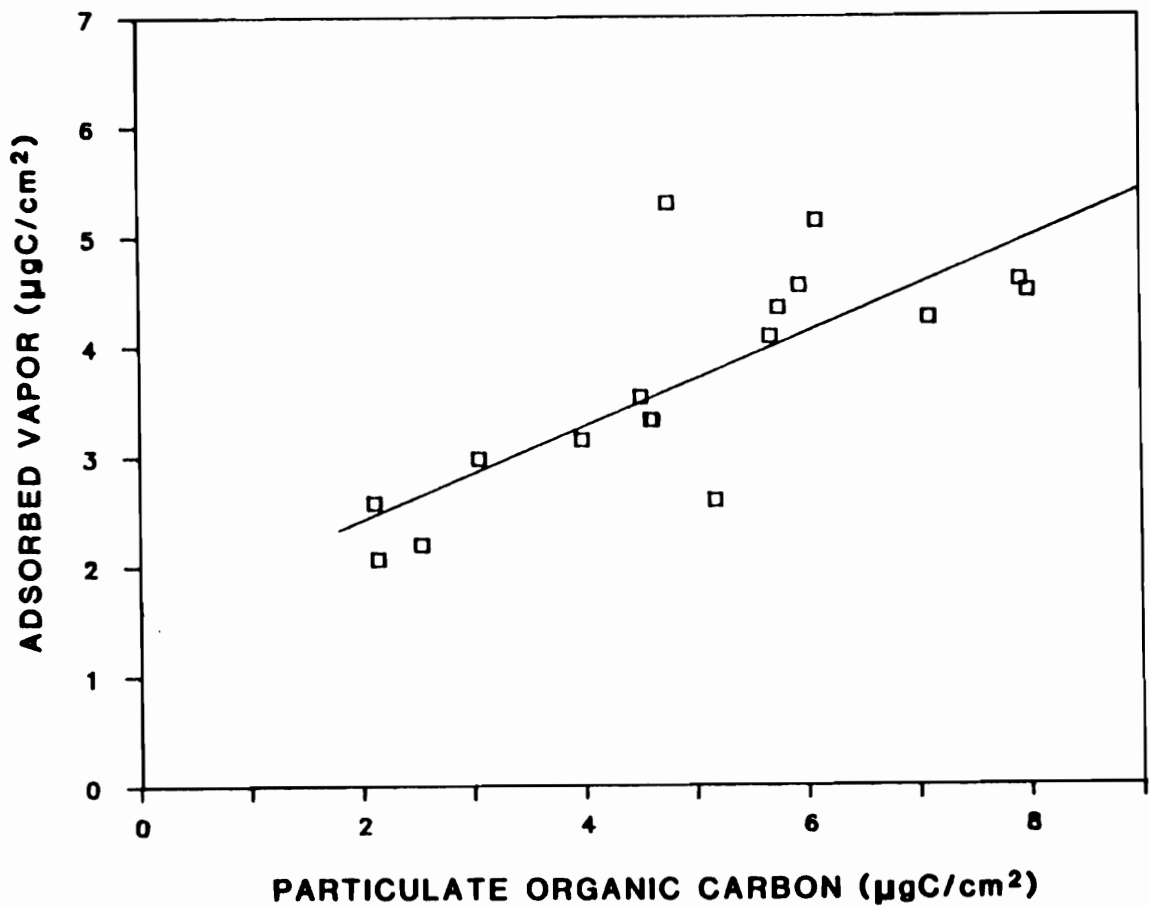


Figure 6.23. Adsorbed vapor as a function of particulate organic carbon loading ($\mu\text{gC}/\text{cm}^2$) for 20 cm/s Carbonaceous Species Methods Comparison Study face velocity samples. The solid line is the linear least squares fit of Table 6.14. Adsorbed Vapor = $(1.6 \pm 1.0) + (0.43 \pm 0.2) \cdot \text{POC}$ ($R^2 = 60\%$).

FIGURE 6.23

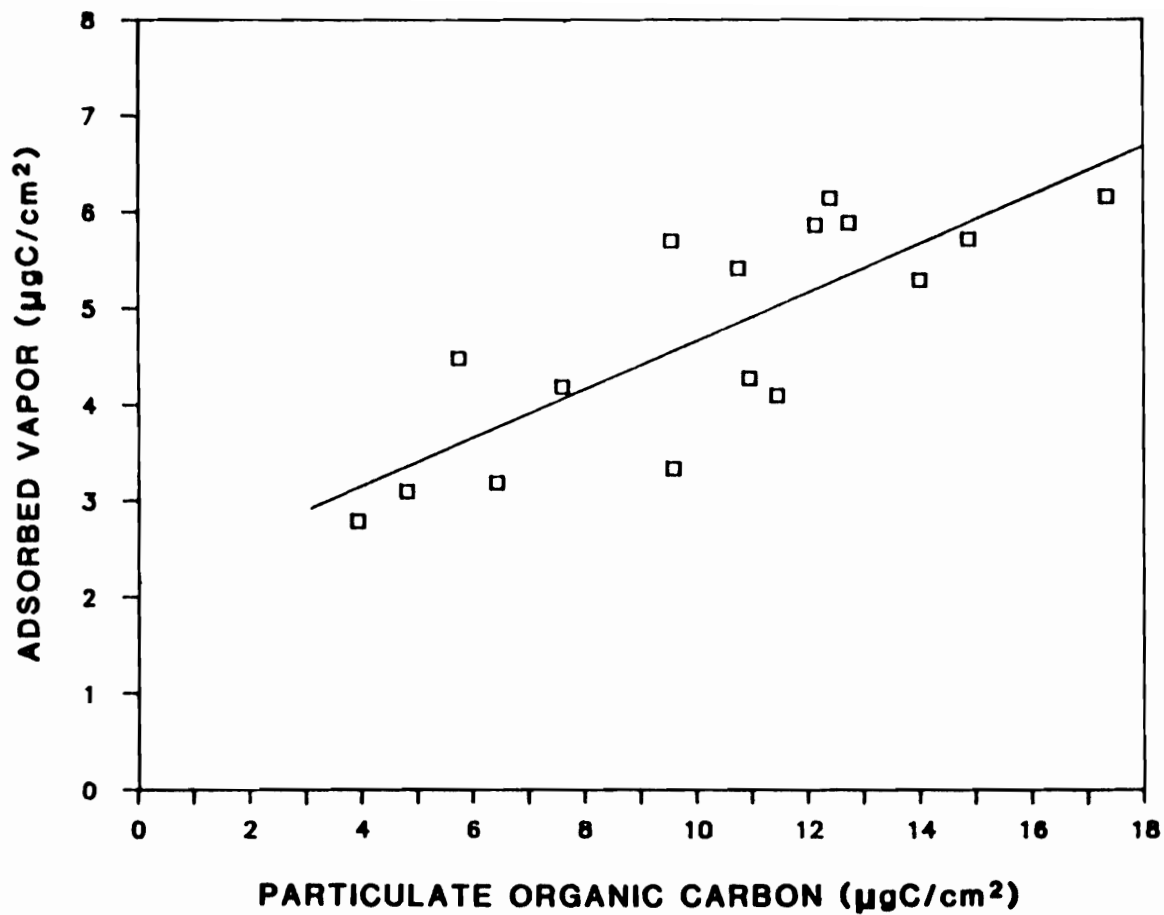


FIGURE 6.24

Figure 6.24. Adsorbed vapor as a function of particulate organic carbon loading ($\mu\text{gC}/\text{cm}^2$) for 40 cm/s Carbonaceous Species Methods Comparison Study face velocity samples. The solid line is the linear least squares fit of Table 6.14. Adsorbed Vapor = $(2.2 \pm 1.2) + (0.25 \pm 0.1) \cdot \text{POC}$ ($R^2 = 64\%$).

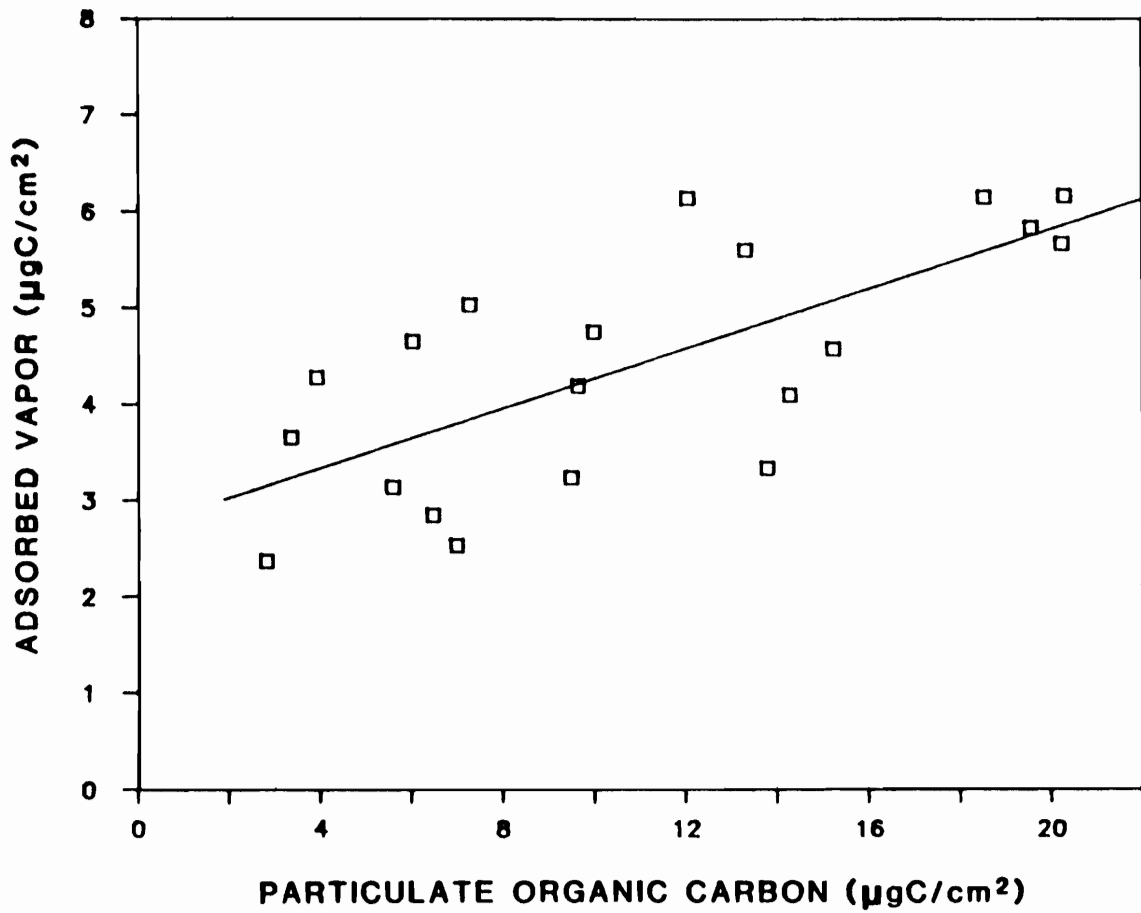


FIGURE 6.25

Figure 6.25. Adsorbed vapor as a function of particulate organic carbon loading ($\mu\text{gC}/\text{cm}^2$) for Carbonaceous Species Methods Comparison Study two-port samples. The solid line is the linear least squares fit of Table 6.14. Adsorbed Vapor = $(2.7 \pm 0.9) + (0.16 \pm 0.08) \cdot \text{POC}$ ($R^2 = 51\%$).

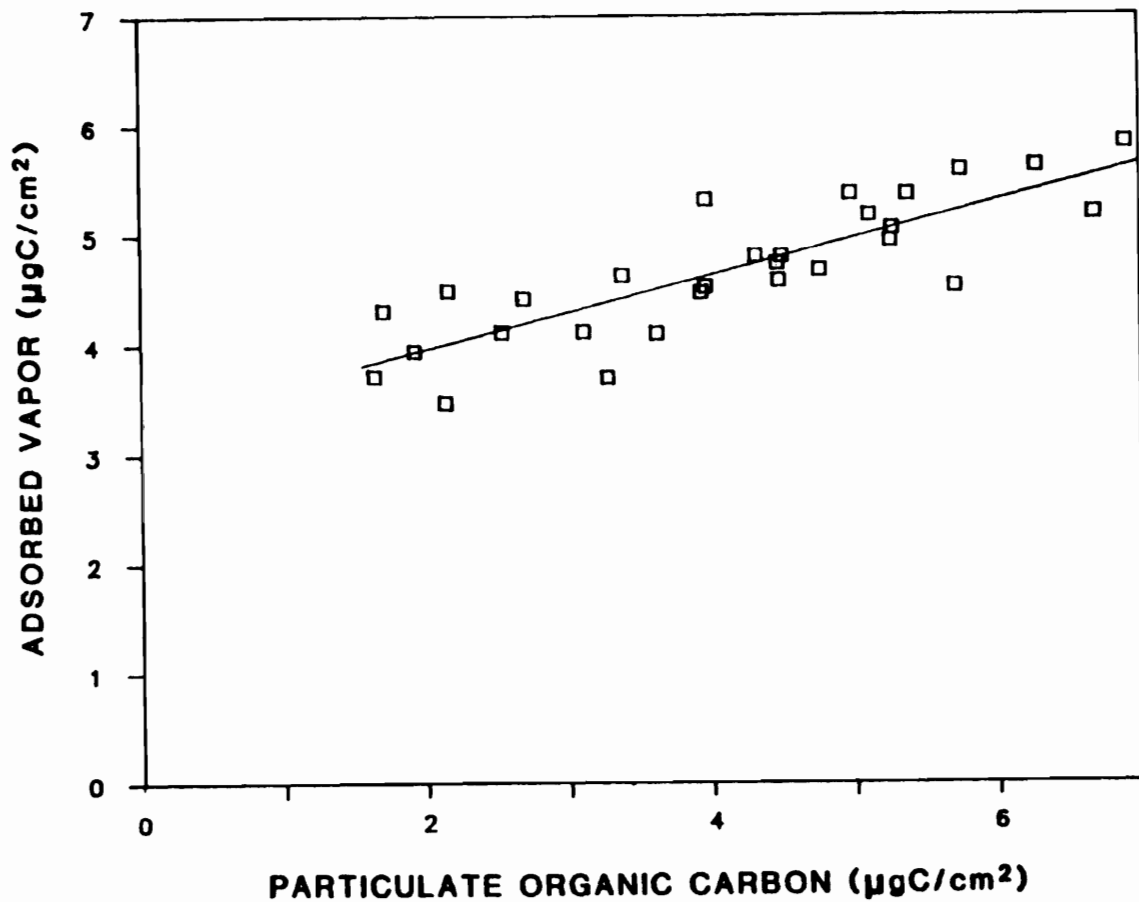


FIGURE 6.26

Figure 6.26. Adsorbed vapor as a function of particulate organic carbon loading ($\mu\text{gC}/\text{cm}^2$) for Carbonaceous Species Methods Comparison Study in situ carbon analyzer samples. The solid line is the linear least squares fit of Table 6.14. Adsorbed Vapor = $(3.3 \pm 0.4) + (0.34 \pm 0.09) \cdot \text{POC}$ ($R^2 = 69\%$).

TABLE 6.14. REGRESSION RESULTS FOR COMPARISON OF ADSORBED VAPOR AND PARTICULATE ORGANIC CARBON LOADINGS ($\mu\text{gC}/\text{cm}^2$).

Uncertainties are 95% confidence intervals. The number of samples comprising the regression is indicated by n, and R^2 is the percentage of the variance explained by the regression.

$$(\text{ADSORBED VAPOR}) = a + b (\text{PARTICULATE OC})$$

	a	b	R^2	n
FACE VELOCITY SAMPLER 20 cm/s	1.6 ± 1.0	0.43 ± 0.2	60%	17
FACE VELOCITY SAMPLER 40 cm/s	2.2 ± 1.2	0.25 ± 0.1	64%	16
TWO-PORT SAMPLER	2.7 ± 0.9	0.16 ± 0.08	51%	20
<u>IN SITU</u> SAMPLER	3.3 ± 0.4	0.34 ± 0.09	69%	29

Teflon filter is a good estimate of the adsorption on a quartz fiber front filter collected concurrently, (3) that longer collection periods will reduce the percentage of the collected material which is adsorbed vapor, (4) that it can take hours sampling at a constant concentration for gas phase organic carbon to reach equilibrium between the gas phase and the adsorbed phase on the sampling filter, (5) that adsorption contributes more to apparent organic carbon concentrations observed through quartz fiber filter collection in Glendora, California than in Portland, Oregon.

CHAPTER 7: GC/MS STUDY OF ORGANIC COMPOUNDS ON AEROSOL AND BACKUP FILTERS

INTRODUCTION

Whereas thermal-optical carbon analysis yields total organic carbon concentrations without any information about individual compounds, gas chromatography/mass spectroscopy (GC/MS) provides concentrations for many individual compounds at the expense of knowledge about the whole. The adaptation of a technique developed by Pankow and Isabelle (1982) and Greaves et al. (1985) allows organic compounds to be thermally desorbed directly from quartz fiber filters into the GC/MS system without solvent extraction. This technique decreases analysis time considerably. Two-port CSMCS samples were analyzed for specific organic compounds using this method in order to gain further insight into questions of secondary formation and sampling artifacts.

Secondary aerosol formation is believed to result from the gas phase oxidation of such precursors as olefins, cyclic olefins, di-olefins, and aromatics (Grosjean, 1977). Products are highly oxygenated difunctional compounds such as carboxylic acids, and the partitioning between particulate and gaseous phases is a function of vapor pressure (Junge, 1977). Because of the diurnal nature of photochemical activity, secondary formation products are expected to exhibit a strong diurnal variation. Vapor-particle partitioning concepts can also be applied

to the understanding of vapor adsorption of quartz fiber filters. Quartz fiber filters have a large surface area (see Chapter 6), and thus partitioning between the gas phase and the filter surface can lead to significant organic carbon artifacts during the filter collection of organic aerosol.

THERMAL DESORPTION/GAS CHROMATOGRAPHY/MASS SPECTROSCOPY

The quartz fiber filters collected in the two-port sampler during CSMCS in Glendora, California, were analyzed for specific organic compounds using thermal desorption/gas chromatography/mass spectroscopy (TD/GC/MS). Samples were thermally desorbed onto a 25 m long, 0.32 mm diameter fused silica capillary column with a 0.25 μm film thickness (Chrompack CP-SIL 8 CB) mounted in an HP 5790 gas chromatograph. The gas chromatograph is interfaced to a Finnigan 4000 mass spectrometer/data system as described by Pankow and Isabelle (1984).

In the analysis procedure, a 1 - 1.5 cm^2 section of the filter sample was placed in the desorption apparatus, and an internal standard was injected onto the filter. The desorber was purged with He at a rate of 5 ml/min for 5 min to remove solvent from the internal standard and ambient O_2 from the system. Filters were desorbed at 250 C for 20 minutes at a pressure of 30 psi, and target compounds were trapped at the head of the column by maintaining an oven temperature of -80 C. When desorption was complete, the GC oven was heated from -10 C to 320 C at a rate of 10 C/min. Mass spectra were obtained by scanning from 50 - 450 amu at 0.5 s/scan with an electron energy of 70 eV and the electron multiplier at 1300 V.

A calibration curve for each of the 119 target compounds was obtained by analyzing standards containing each compound in concentrations of 5, 20, and 50 ng/ μ l. These data were used to determine compound retention times and response factors. All three levels of standards were analyzed daily as a quality assurance measure. Positive identification was assigned only when the GC relative retention times and mass spectra matched those of the standards.

The filter samples were doped with internal standards to evaluate losses in thermal desorption, determine relative retention times, and facilitate quantitative analysis. The use of internal standards was particularly important because a build-up of polar compounds at the head of the column would degrade the peak shape, requiring that the column be shortened by 0.5 m every 5 or 6 runs to avoid loss of chromatographic resolution. The internal standards consisted of deuterated compounds from three major classes: alkanes (eicosane, D₄₂); acids and alcohols (decanoic acid, D₁₉ and hexadecanoic acid, D₃₁); and polycyclic aromatic hydrocarbons (PAH's) and PAH derivatives (naphthalene, D₈; acenaphthylene, D₁₀; fluorene, D₁₀; benzophenone, D₁₀; phenanthrene, D₁₀; fluoranthene, D₁₀; chrysene, D₁₂; and perylene, D₁₂).

RESULTS

Average concentrations for the front (QQF) and backup (QQB) filters of the QQ combination and for the backup filter (TQB) of the TQ combination are presented in Appendix B. Because of time constraints only a limited amount of exploratory data analysis was performed on the GC/MS data set.

Large concentrations of carboxylic acids were found on both front and backup filters and were present mostly as hexadecanoic, octadecanoic, and tetradecanoic acid. The lower vapor pressure acids (dodecanoic - octadecanoic) showed a substantial difference between day and night concentrations with elevated concentrations occurring during the day on both front and backup filters. One compound, hexadecanoic acid, was examined in more detail. A single-sided paired t-test comparing hexadecanoic acid concentrations found on QQ front and TQ backup filters indicated that QQ front filter concentrations were significantly larger with 95% confidence. The ratio of the means is about 1.6 indicating that hexadecanoic acid was present in significant quantities in particulate form. Due to a large variation in the means, TQB and QQB results were not significantly different but the ratio of their means is 2.7.

PAH's were found largely on the front filter, with a ratio of mean QQF to mean TQB of 3.6 ($QQF/QQB = 12.1$). A comparison of QQ front and backup filter averages with TQ backup filter averages for the three major compound classes of interest is given in Table 7.1. Ratios listed in Table 7.1 are from QQF, QQB, and TQB averages which exclude sample periods where TQ backups were missing. The mean concentration of PAH's on the TQ backups was substantially higher than the mean concentration on the QQ backups, suggesting that adsorption on the QQ front filter was far from equilibrium.

The dominant alkanes identified were tetracosane through nonacosane ($C_{24} - C_{29}$). As was the case for the PAH's, the QQ front filter alkane concentrations were much higher than the TQ backup filter concentrations, indicating that a substantial fraction of the material on the filter was in

TABLE 7.1. COMPARISON OF QQ FRONT AND BACKUP FILTERS WITH TQ BACKUPS FOR THE MAJOR COMPOUND CLASSES.

Values are in ng/m³. Periods for which there were no TQB results are excluded from the analysis.

	QQF	QQB	TQB	QQF/TQB	TQB/QQB
CARBOXYLIC ACIDS	163	43	75	2.2	1.8
PAH's AND ALKYL PAH's	6.7	0.6	1.8	3.6	3.1
ALKANES	58	11	13	4.4	1.1

particulate form. However, little difference was seen between TQ and QQ backup filter concentrations indicating that gas phase - adsorbed phase partitioning in the vicinity of the front filter had reached equilibrium, and TQ and QQ backup filters were therefore both exposed to ambient gas phase concentrations. One compound, tetracosane, was examined in more detail. Results of paired t-tests comparing QQF and TQB concentrations and comparing TQB and QQB concentrations agreed with the general conclusions above (QQF > TQB with 95% confidence but TQB and QQB are not significantly different). For tetracosane, QQF/TQB and TQB/QQB ratios are 4.1 and 1.1 respectively. In Table 7.2 QQ front (QQF) and TQ backup (TQB) filter results are averaged over all sampling periods for each alkane identified, and the QQF/TQB ratio is presented. Concentrations of pentadecane through heneicosane (C_{15} - C_{21}) were often below detection limits based on analysis of filter blanks. The QQF/TQB ratio increased as a function of carbon number for docosane through heptacosane (C_{22} - C_{27}) indicating an increasing particulate phase with decreasing vapor pressure as expected based on vapor-particle partitioning theory. However, the ratio declines between C_{27} and C_{29} . A desorption temperature of 250 C might be insufficient to efficiently remove these higher molecular weight compounds from the filter. Tricosane through nonacosane exhibited a diurnal variation on the QQ front filter with higher concentrations occurring at night. This might reflect a shift in the gas-particle partitioning. If concentrations remained constant, a decrease in temperature would cause a larger fraction of these organic compounds to be associated with the particulate phase.

TABLE 7.2. AVERAGES FOR ALKANES: QOF, TOB, AND QOF/TOB
(ng/m³)

Carbon No.	Compound	<u>QOF</u>	<u>TOB</u>	<u>QOF/TOB</u>
C15	pentadecane	0.2	0.2	1.4
C16	hexadecane	0.8	0.7	1.0
C17	heptadecane	0.02	0.3	0.1
C18	octadecane	0.4	1.1	0.4
C19	nonadecane	1.2	1.3	0.9
C20	eicosane	0.5	0.9	0.5
C21	heneicosane	0.9	1.2	0.8
C22	docosane	2.3	1.8	1.2
C23	tricosane	5.5	1.5	3.7
C24	tetracosane	10.1	2.5	4.1
C25	pentacosane	11.0	1.8	6.2
C26	hexacosane	7.7	0.7	11.8
C27	heptacosane	6.7	0.5	12.6
C28	octacosane	8.8	0.8	11.1
C29	nonacosane	8.4	1.2	7.2

A great deal of information can be derived from this expansive collection of data. This data set could contain valuable insights into sampling artifact and aerosol formation questions, and therefore an investigative analysis will continue.

**CHAPTER 8. SECONDARY FORMATION OF ORGANIC AEROSOL:
INVESTIGATION OF THE DIURNAL VARIATIONS OF
ORGANIC AND ELEMENTAL CARBON
IN THE LOS ANGELES BASIN**

INTRODUCTION

Although carbonaceous species comprise a large fraction of the urban aerosol (Shah et al., 1986), the relative contributions of primary and secondary organic components have long been disputed. Several investigators have used elemental carbon as a tracer for primary organic aerosol, but most studies have involved data with 6 to 24 hour averaging periods making it difficult if not impossible to observe the dynamics of aerosol formation. Strong correlations between OC and EC were observed in these studies. However, in certain cases the presence of secondary organic aerosol was suggested by either an increase in the OC/EC ratio with distance downwind from a major source region or a summertime average which was higher than the winter average at a given site.

Since secondary organic aerosol is a product in the general photochemical smog sequence, significant secondary organic aerosol formation should be accompanied by elevated ozone concentrations (see Chapter 3) and should correlate with other photochemically generated aerosols of local origin, such as nitrate. However, conditions which result in high ozone concentrations might not

be sufficient to generate secondary organic aerosol because aerosol formation will also depend upon the presence of organic precursors. The diurnal cycles of ozone and secondary organic aerosol are likely to be quite different when significant retention of pollutants has occurred overnight. A low bromine/lead ratio accompanied by higher than normal lead concentrations prior to the onset of morning traffic indicates the retention of pollutants from the previous day (Appel et al., 1979; Wesolowski et al., 1973). Because such information could prove useful in the interpretation of pollutant episodes it has been included in Appendix C.

EXPERIMENTAL

During the Southern California Air Quality Study an *in situ* carbon analyzer (see Chapter 4) was used to measure particulate organic and elemental carbon with approximately two-hour time resolution. From June 12 to July 29 and from August 17 to September 3, 1987, it was located at the Claremont site, at the eastern edge of the East Bauer Parking Lot at Claremont McKenna College in Claremont, California. During the fall study (November 6 - December 12, 1987) it was located at the Long Beach site, at Long Beach City College between the track and the McDonnell Douglas hangers.

The *in situ* carbon analyzer was situated in an air conditioned, Air Resources Board trailer which was maintained at a temperature of 25 ± 1 C. Two quartz fiber filters (Pallflex QAOT) mounted inside the instrument collected the fine (i.e., $d_p < 2.5 \mu\text{m}$) ambient aerosol and whatever vapor adsorbed on the filters. The coarse fraction was removed with a $2.5 \mu\text{m}$ cut-point Marple (1974) impactor

with an impactor surface composed of a fritted glass filter disk (Ace Glass, POR E) set flush into an aluminum plate and soaked in low vapor pressure vacuum pump oil to reduce bounce (Turner and Hering, 1987). It was necessary to change the quartz fiber filters about once every 3 to 4 weeks because a buildup of non-combustible material began to decrease the sensitivity of the transmittance measurement. In a parallel sampling port quartz fiber filters were preceded by a Teflon filter (Gelman, ringed Teflon, 2 μm pore) which removed particles. The parallel sampling port provided an estimate of the organic vapor adsorption artifact on the quartz fiber aerosol filters. Ambient air was sampled through a 2.5 cm diameter probe extending 90 cm above the roof and capped with a rain shield and insect screen. The sampling rate was 8.7 l/min in the summer and 8.9 l/min in the fall, and the sampling duration was varied from 40 to 200 minutes on the basis of air pollution forecasts and the instrument detection limits. The instrument generally operated on a two hour cycle in which aerosol was collected for 80 minutes followed immediately by in situ analysis for organic and elemental carbon by a thermal-optical technique (see Chapter 4).

An instrument blank and a three-peak internal calibration program were run every two to three days. The instrument blank analysis was a standard analysis without aerosol collection. The calibration program was identical to the standard analysis program except that a known amount of methane was automatically injected during each of the three distinct segments of the analysis. Because the instrument response differed by as much as 10% between these three conditions, appropriate response factors were incorporated into the data output. The analytical precision for the measurement of total aerosol carbon with the in situ

carbon analyzer is 3.1%, and the detection limit is 0.2 μgC . Comparable precision is expected for organic and elemental carbon, based on our experience with the laboratory carbon analyzer (Turpin and Huntzicker, 1988; Huntzicker et al., 1982; Johnson et al., 1981). However, since each analysis uses the whole sample, these values have not been determined.

The data treatment and quality control measures applied to the data were the same as those applied to the CSMCS data and have been discussed in Chapter 4. Instrument blanks for summer SCAQS data were not significantly different than zero with 95% confidence limits, but a small blank subtraction was required for fall SCAQS data. Consistency between the two sides of the analyzer was demonstrated in a set of experiments run during summer and fall periods in which both aerosol and vapor sampling ports were pre-filtered with a Teflon filter. In this configuration the analytical filters in both sides collect adsorbable organic vapor and should be equivalent. The two sides were statistically indistinguishable.

The sample analysis program has been written to facilitate a sensitivity study on the parameters which indirectly affect the OC-EC split. The most critical of these is the transit time between the quartz fiber filter and the FID. The laser signal responds immediately to the removal of material from the filter whereas the FID signal is delayed by the transit time. An accurate transit time estimate is needed to align the signals. The uncertainty associated with the transit time translates to 95% confidence levels of $\pm 0.5\%$ in OC and EC for the average SCAQS run.

The temperature dependence observed in the laser signal of the SCAQS blank and three-peak calibration runs was slightly greater than that observed during CSMCS. The laser signal decreased with increasing oven temperature resulting in a laser variation of 2 to 4% for SCAQS samples. The relationship between laser signal and oven temperature was path dependent as shown in Figure 8.1, and the method of correction applied to the data was discussed in Chapter 4. The correction resulted in a change of about $0.5 \mu\text{gC}/\text{m}^3$ on average in the calculated values of OC and EC (about 3% for OC and 10% for EC).

A data validation summary for the SCAQS in situ carbon analyzer data is provided in Appendix D. Figures 8.2 and 8.3 show optical absorbance vs. elemental carbon loading for August data and fall data. Graphs of this sort were used to identify outliers and also can give an estimate of the extinction coefficient of the elemental carbon ($b = \text{optical absorbance}/\text{elemental carbon loading}$) present on the filter. The extinction coefficient of elemental carbon on a quartz fiber filter is certainly not the same as the extinction coefficient of suspended elemental carbon, and whether or not the extinction coefficient is origin specific has not been satisfactorily resolved. The extinction coefficient appears to be about 0.6 and $0.5 \text{ cm}^2/\mu\text{gC}$ for August and fall data respectively. These values are considerably different than the extinction coefficient calculated by Gundel et al. (1984) from elemental carbon measurements made on quartz fiber filters collected in California, Michigan, Austria, and Yugoslavia ($b = 0.24 \text{ cm}^2/\mu\text{gC}$). This might result from a difference in the properties of the elemental carbon collected, or a difference in the analysis configuration such as use of a double sampling filter in the in situ carbon analyzer.

FIGURE 8.1

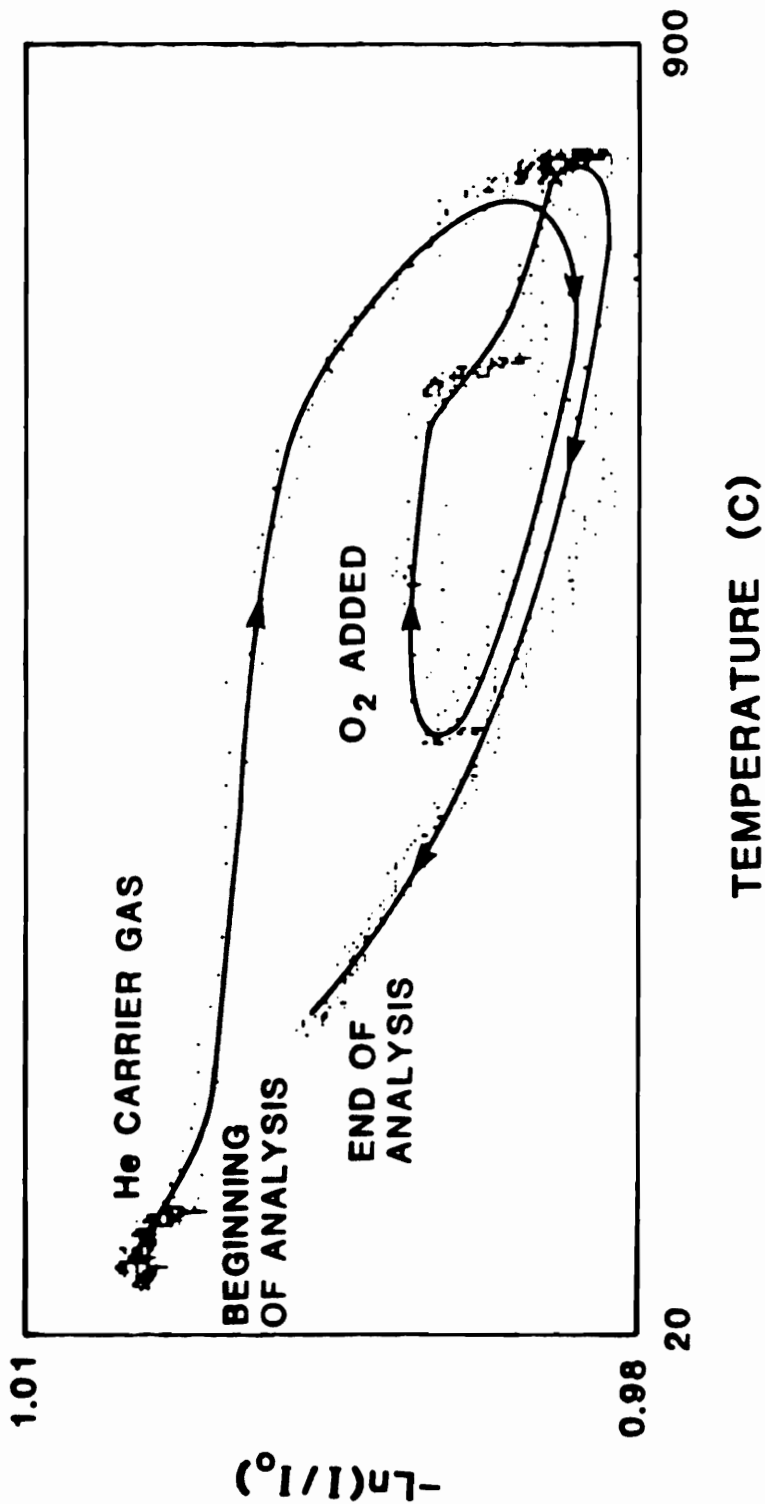


Figure 8.1. In situ carbon analyzer laser signal ($-\ln(I/I_0)$) as a function of oven temperature (C) for a typical Southern California Air Quality Study instrument blank analysis. Temperature dependence of laser is path dependent.

FIGURE 8.2

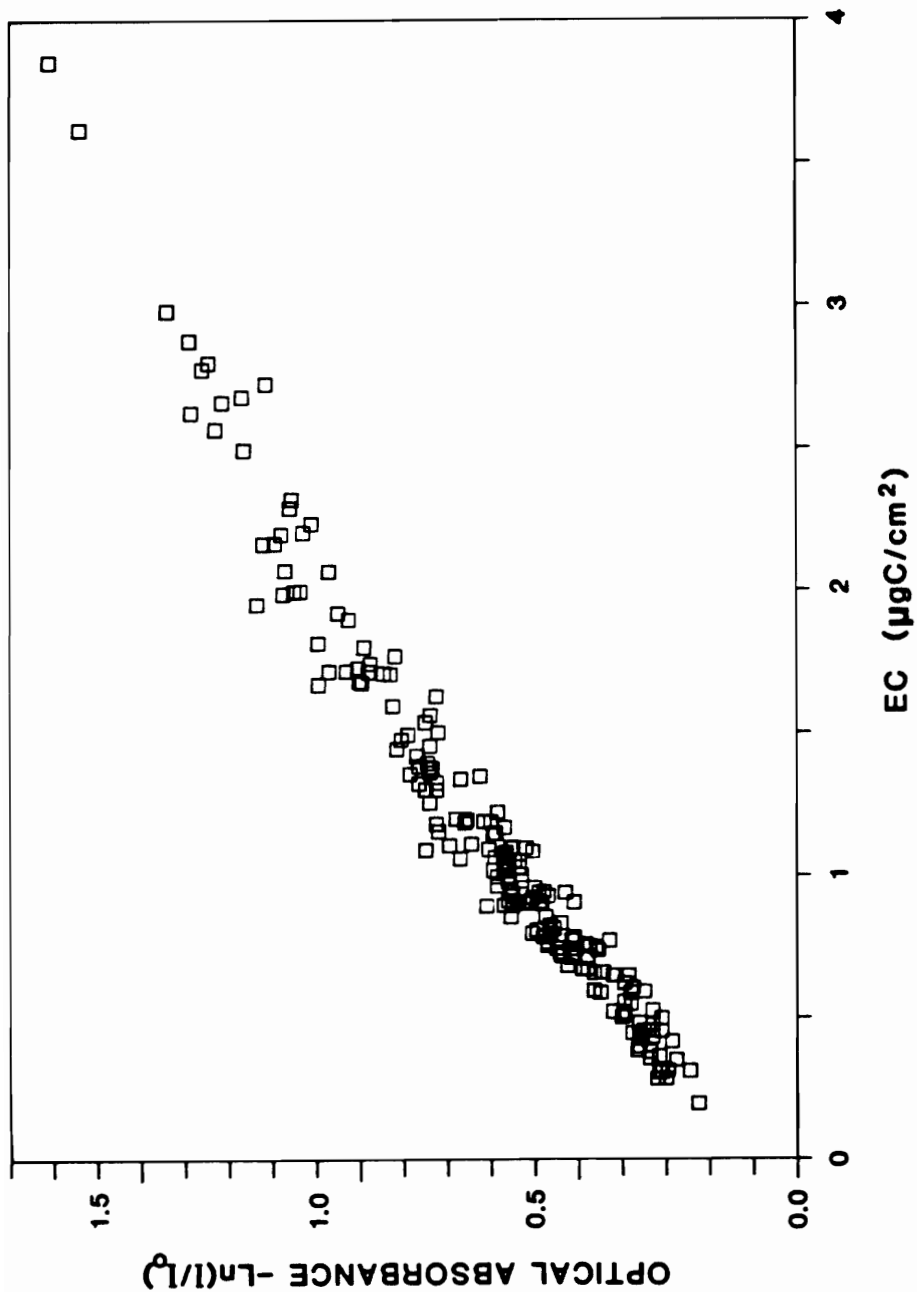


Figure 8.2. Optical absorbance ($-\ln(I/I_0)$) as a function of elemental carbon loading ($\mu\text{gC}/\text{cm}^2$) for August, 1987, Southern California Air Quality Study data.

FIGURE 8.3

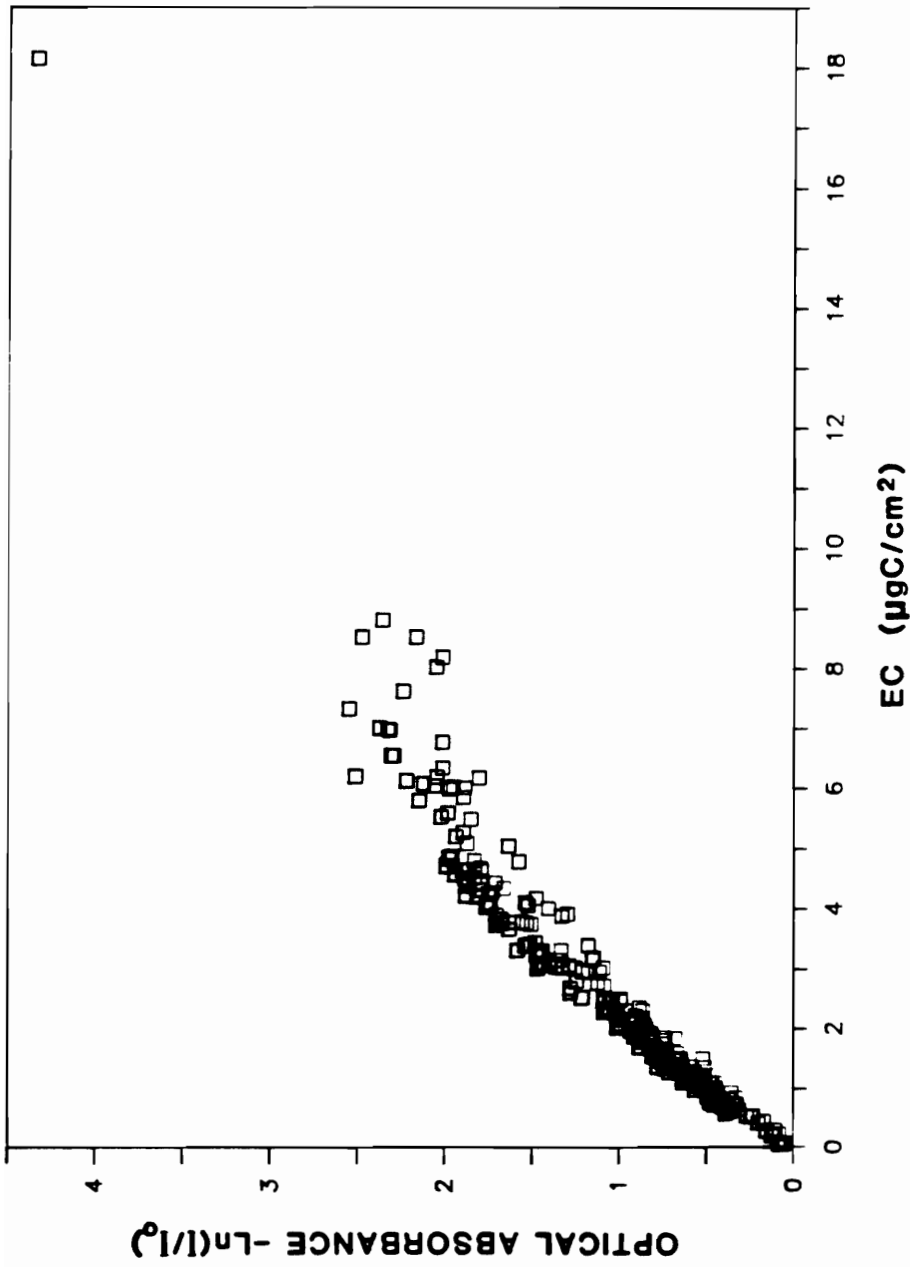


Figure 8.3. Optical absorbance ($-\ln(I/I_0)$) as a function of elemental carbon loading ($\mu\text{gC}/\text{cm}^2$) for November and December, 1987, Southern California Air Quality Study data.

The nights of November 8, 10, and 18 and December 2 were quite foggy, and enough water collected on the sampling filters to affect the optical transmittance. As the heating of the loaded filter began, the transmittance increased slightly. The remainder of the analysis proceeded normally. A similar phenomenon has been observed in the laboratory when filters doped with a sucrose - water solution were analyzed while wet. Thus it was concluded that the increase in the initial transmittance which occurred during analysis of samples from these dew and fog intensive periods was a result of the volatilization of water from the filter. The maximum transmittance observed after water volatilization but before carbon volatilization was taken to be the reference transmittance for the pyrolysis correction.

SCAQS METEOROLOGY

Wind trajectories in the Los Angeles basin are greatly influenced by the ocean. At night the flow is generally from the land to the ocean (land breeze), and during the day it is generally from the ocean to the land (sea breeze). In the summer, the sea breeze is strong, and the land breeze is quite weak; in the winter the opposite is true. A diagram of the Los Angeles Basin and the SCAQS sites with a few day-time wind trajectory lines typical of afternoon surface winds during July is given in Figure 8.4. As is evident in the diagram, the aged Long Beach air mass is typically transported through Claremont in the summer (Blumenthal et al., 1974).

In Claremont during the summer study the sea breeze (from the southwest) would occasionally blow continuously for 24 hours. However, the more typical

FIGURE 8.4

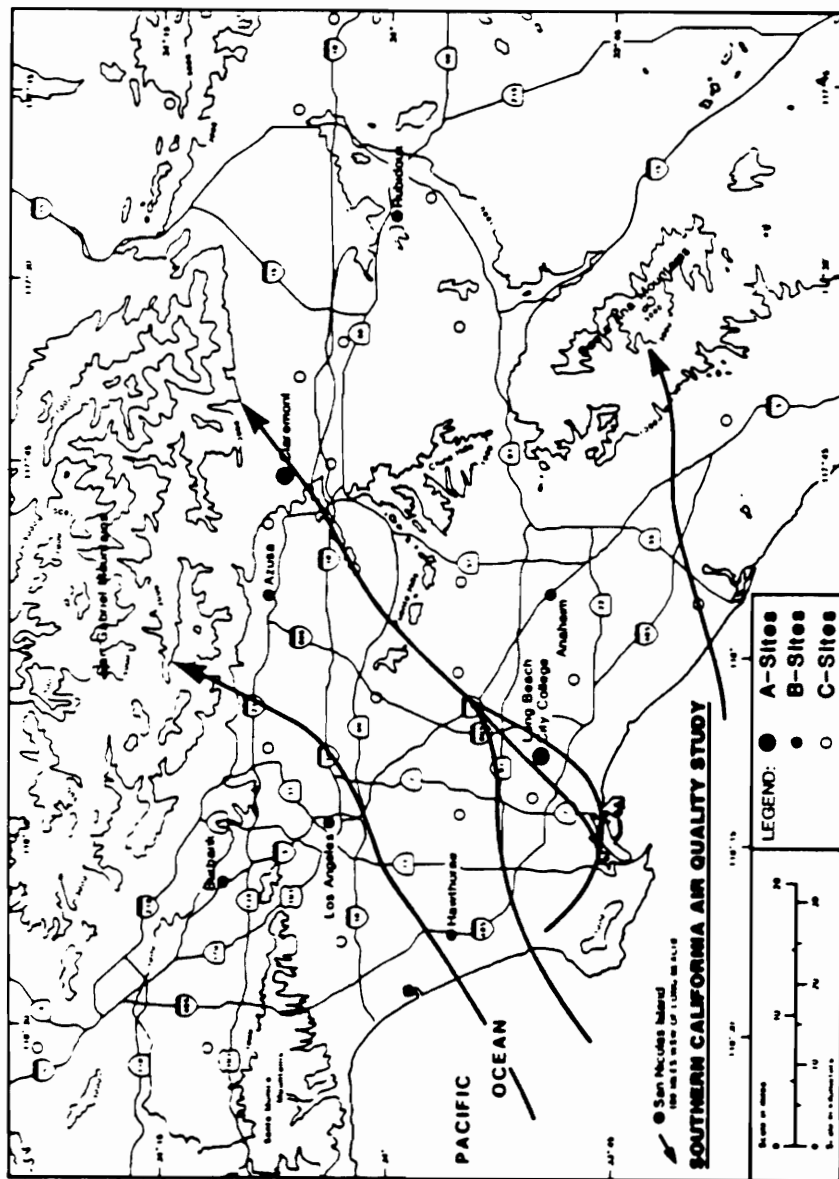


Figure 8.4. Schematic of the Los Angeles Basin showing Southern California Air Quality Study sampling sites and streamlines describing the most frequent afternoon surface winds during July (Blumenthal et al, 1974). The in situ carbon analyzer was located at the Claremont site during the summer study and at Long Beach City College in the fall.

situation was either a weak breeze from the northeast or no wind at all in the early to mid-morning with a strong sea breeze developing around mid-day. Atmospheric conditions changed very rapidly at the Long Beach site in the fall and resulted in drastic changes in aerosol concentrations over short time periods. On December 6, for example, the total particulate carbon concentration decreased from $75 \mu\text{gC}/\text{m}^3$ to $4 \mu\text{gC}/\text{m}^3$ within a 24 hour period. The wind often stopped or dropped significantly during fall nights.

The weather during the summer study was unusually cool. As a result, air quality was considerably better than is typical of Los Angeles Basin summers. As of the end of July there had been Stage I smog alerts in the basin on only 22 days, compared to 38 by July of 1986 and 53 in 1985. Stage I occurs when ozone concentrations have exceeded 20 pphm as an hourly average.

PRIMARY AND SECONDARY ORGANIC AEROSOL

Three-day plots of OC, EC, ozone, and meteorological information for all summer and fall sampling days are presented in Appendix E along with an explanation of the weather map symbols. Strong diurnal variations were evident in organic, elemental, and total carbon concentrations for both summer and fall data. In the summer, peak concentrations of OC and EC occurred during the daylight hours. However, in the fall the peaks occurred at night, and the maximum concentrations observed ($\text{TC}_{\text{max}} = 88 \mu\text{gC}/\text{m}^3$ on December 3) were two to three times the summer maxima ($\text{TC}_{\text{max}} = 36 \mu\text{gC}/\text{m}^3$ on June 24).

Each daily EC maximum in the summer occurred either around 0900 hours or 1500 hours (PDT), and the daily OC maxima were clustered around 1500 -

1700 hours as shown in the histograms of Figures 8.5 and 8.6. As a result, most of the summer data fell into two categories: (1) EC and OC peak together around 1500 - 1700 hours, and (2) EC peaks around 0900 hours and OC peaks around 1500 - 1700 hours. Elemental carbon is a tracer for primary, combustion-generated organic aerosol, a high correlation between organic and elemental carbon indicates that the organic and elemental carbon are from a common origin. The coefficients of determination (R^2) between OC and EC for several type (1), type (2), and fall days are given in Table 8.1. The coefficient of determination was 69% for the set of samples comprising all type (1) days and in the range of 80 - 95% for the period of July 14 - 17. For the fall data an R^2 of 80% was observed. In contrast, for the set of samples comprising type (2) days OC and EC were poorly correlated ($R^2 = 30\%$), indicating different origins for OC and EC during these periods. Three episodes of type (2) days were encountered during the study: July 11 - 13, July 25 - 29, and August 27 - 31.

Figure 8.7 shows OC, EC, ozone, and b_{scat} for August 25 - 31, and Table 8.2 summarizes some additional information about this period. The ozone and b_{scat} values in Figure 8.7 are averaged over the collection periods for OC and EC. On Tuesday, August 25 and Wednesday, August 26 the air was relatively unstable, and the pollutant concentrations were low. Between August 27 and August 29 a high pressure ridge was building. Ozone concentrations built to a Friday, August 28 peak of 29 pphm, and the visual range decreased daily reaching a low of 9 km on Saturday, August 29. During this period strong temperature inversions developed, and several Stage I smog alerts were in affect in the basin. A weak disturbance developed in the high pressure ridge on Sunday, August 30,

FIGURE 8.5

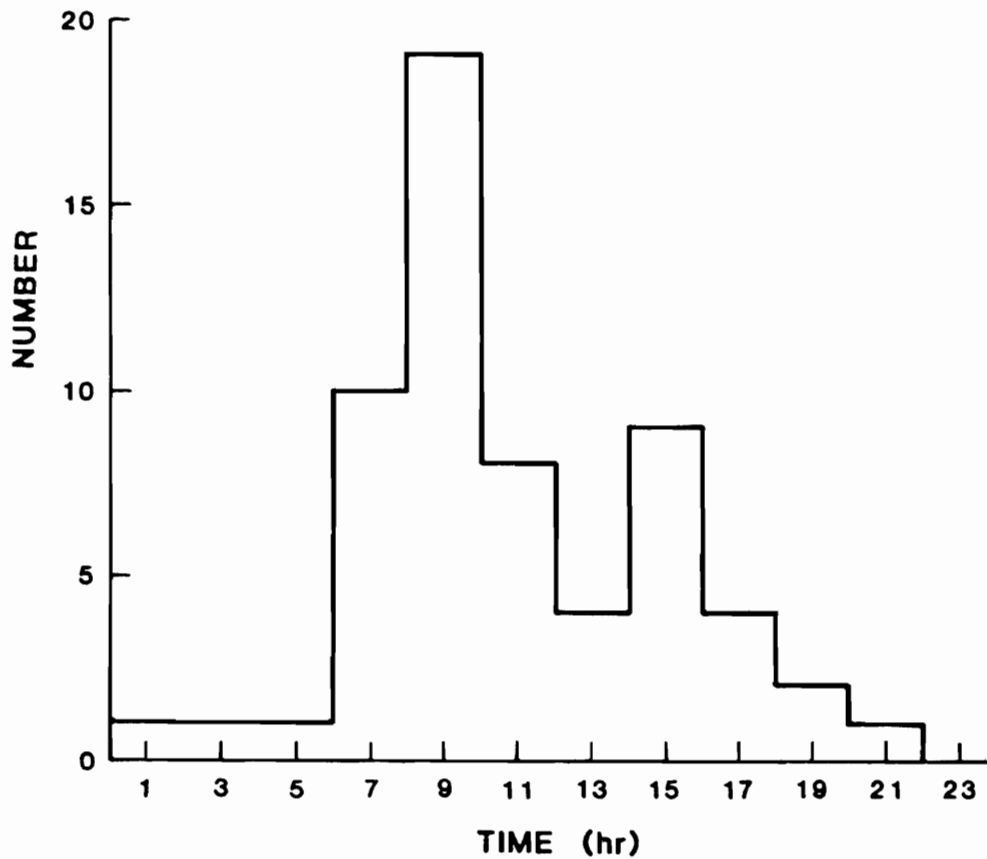


Figure 8.5. Histogram of time of daily particulate elemental carbon maximum at Claremont, California for Southern California Air Quality Study summer data, 1987. Time is Pacific Daylight time (PDT).

FIGURE 8.6

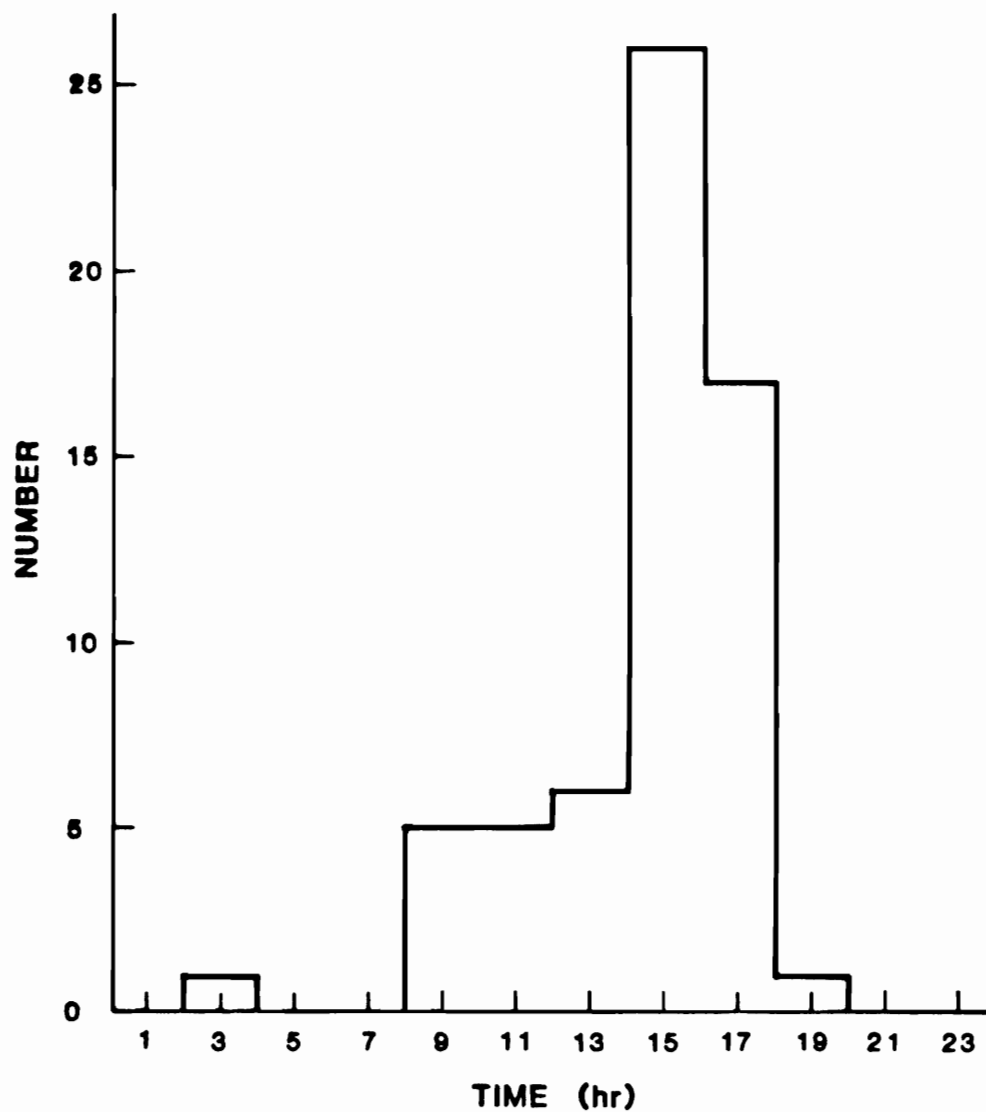


Figure 8.6. Histogram of time of daily particulate organic carbon maximum at Claremont, California for Southern California Air Quality Study summer data, 1987. Time is Pacific Daylight Time (PDT).

**TABLE 8.1. COEFFICIENTS OF DETERMINATION (R²)
FOR SELECTED SCAQS DATA**

Dates	Type	R ²
All	(1)	69%
All	(2)	30%
All	fall	80%
July 11	(2)	65%
July 12	(2)	36%
July 13	(2)	33%
July 14	(1)	87%
July 15	(1)	95%
July 16	(1)	87%
July 17	(1)	80%
August 25	(1)	89%
August 26	(?)	72%
August 27	(2)	50%
August 28	(2)	38%
August 29	(2)	0%
August 30	(2)	24%
August 31	(2)	28%
November 16	fall	72%
November 17	fall	80%
November 18	fall	91%
November 19	fall	81%

FIGURE 8.7

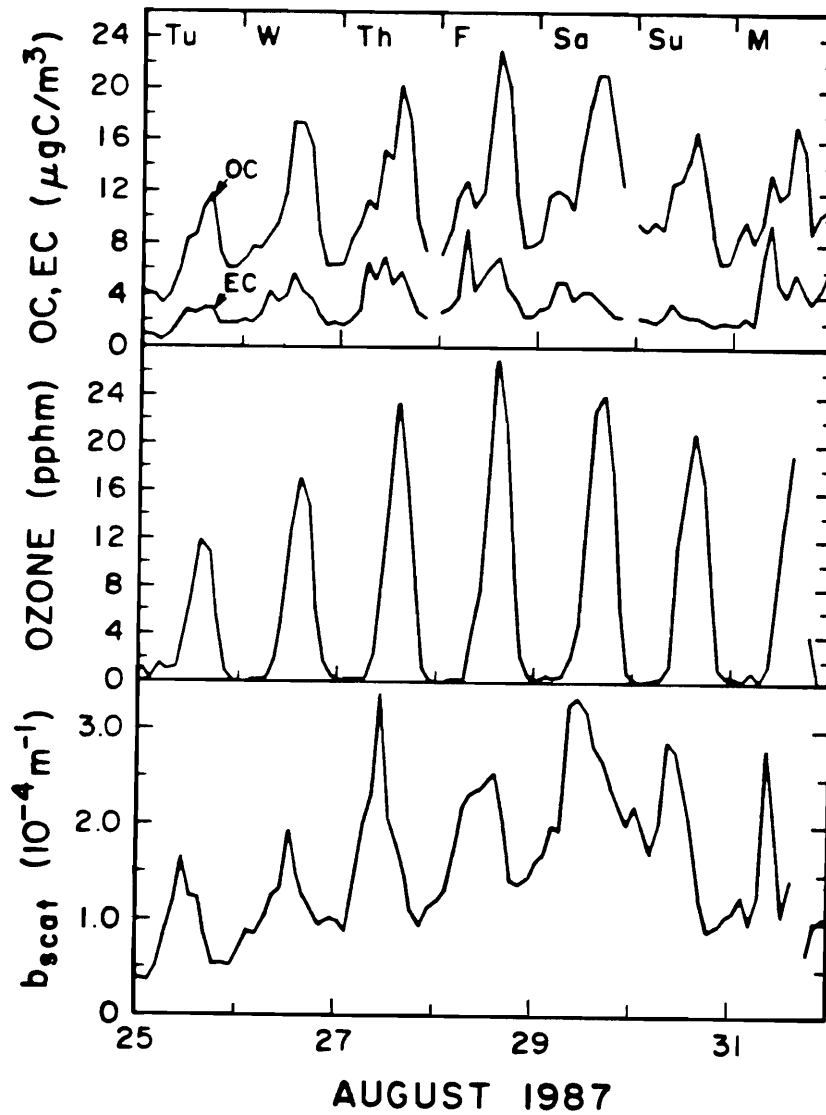


Figure 8.7. Concentrations of organic and elemental carbon ($\mu\text{gC}/\text{m}^3$), ozone (pphm) and b_{scat} (10^{-4} m^{-1}) for August 25-31, 1987 at Claremont, California. Ozone and b_{scat} are averaged to correspond with the 80 minute collection periods of the *in situ* carbon analyzer, and data are plotted at the midpoints of their averaging periods. Time is Pacific Daylight Time (PDT).

TABLE 8.2. SUMMARY DATA FOR AUGUST 25 - 31.

August		minimum visual range (km)	peak ozone (pphm)	peak organic carbon ($\mu\text{gC}/\text{m}^3$)	peak elemental carbon ($\mu\text{gC}/\text{m}^3$)	descriptive meteorology
25	Tue	22	13	12	3	unstable
26	Wed	20	17	17	6	unstable
27	Thu	10	24	20	7	high pres. ridge building
28	Fri	14	29	23	9	high pres. ridge building
29	Sat	9	24	21	5	high pres. ridge building
30	Sun	14	21	17	3	weak disturbance in ridge
31	Mon	16	21	17	10	afternoon: thin cloud cover

and a few high cirrus clouds were visible over the site on Monday. Late Monday afternoon a thin layer of clouds covered the site.

August 25 (Tuesday) and 26 (Wednesday) were type (1) days, and August 27 - 31 were type (2) days. Coefficients of determination between OC and EC for the August 25 - 31 period are shown in Figure 8.8. OC and EC profiles on August 25 and 26 were quite similar, and strong correlations were observed between OC and the primary tracer, EC ($R^2 = 89\%$ and 72% respectively). As ozone concentrations built and the temperature inversion strengthened, the profiles of OC and EC became less similar. The coefficients of determination (R^2) between OC and EC were 50% , 38% , 0% , 24% , and 28% on August 27 - 31 respectively.

On August 27 (Thursday) and August 28 (Friday) elemental carbon concentrations peaked in the morning, probably as a result of the accumulation of fresh, local emissions. Daily minimum OC/EC ratios were 1.7 ± 0.1 and 1.4 ± 0.1 on August 27 and 28, respectively, and occurred around 0700 hours (PDT) on both days. In the afternoon the EC concentration decreased significantly, and the OC concentration increased significantly, reaching its maximum concentration around 1500 hours (PDT), about the same time as the peak ozone concentration. The OC/EC ratio reached a maximum of 4.1 ± 0.3 on Thursday and 4.6 ± 0.4 on Friday at about 1700 hours (PDT). The additional organic carbon, which cannot be explained by common origin with elemental carbon, was probably of photochemical origin (secondary organic aerosol).

Although OC and EC were only poorly correlated on Friday, August 28 ($R^2 = 38\%$), they were not correlated at all on Saturday, August 29 ($R^2 = 0.0\%$).

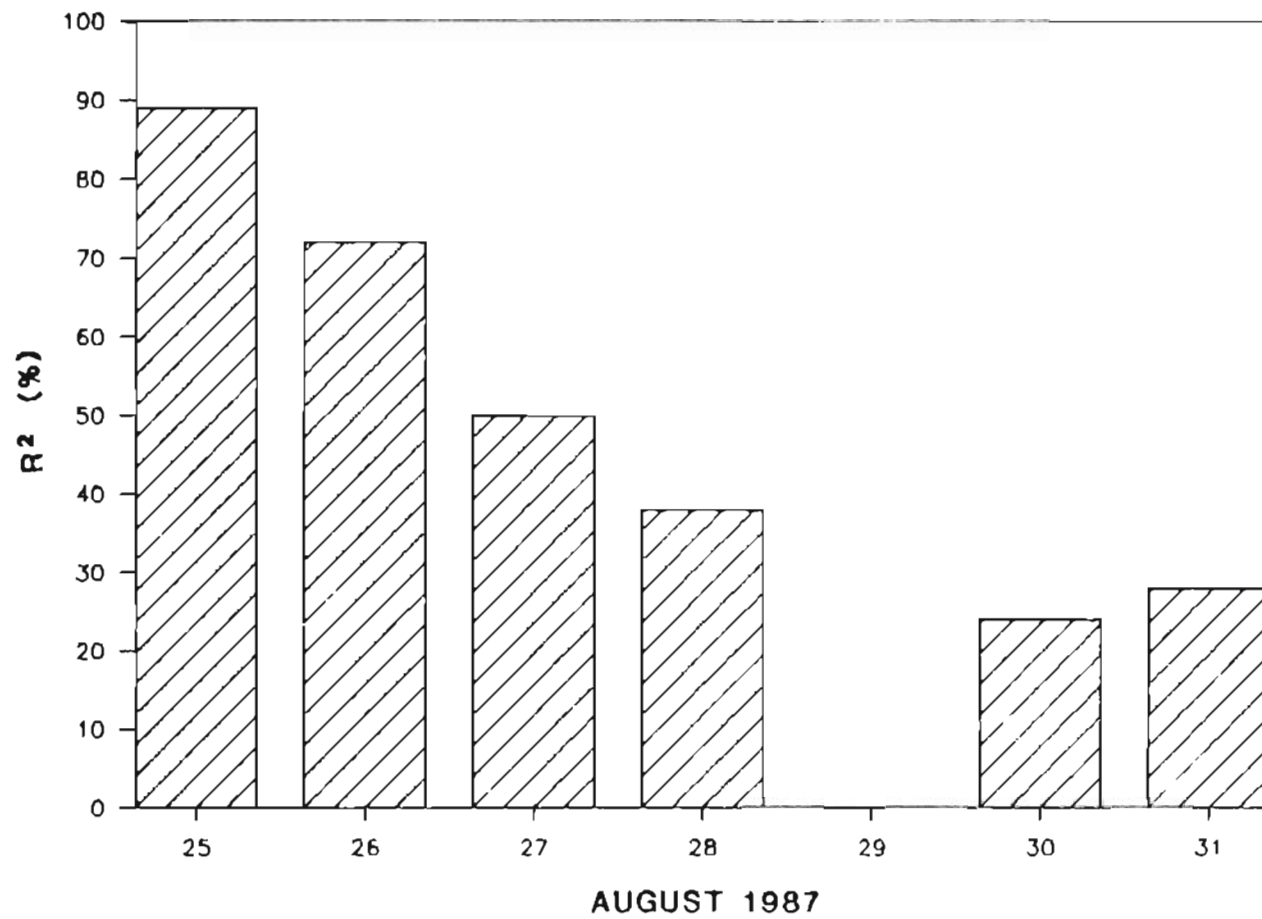


Figure 8.8. Coefficients of determination (R^2) between organic and elemental carbon concentrations on August 25-31, 1987 at Claremont, California.

FIGURE 8.8

The OC/EC ratio reached 7.0 ± 0.8 at 1700 hours (PDT) on Saturday and 7.3 ± 1.0 at 1500 hours (PDT) on Sunday, and OC peaked at about the same time as the ozone concentration on both days. On other weekends OC/EC ratios as high as 14 were observed. Thus, the contribution of secondary organic aerosol appears to be highest on weekends. This difference probably relates to a change in the geographical and temporal distributions of emissions of secondary organic aerosol precursors on weekends relative to weekdays.

As shown in Figure 8.7, the principal peak in the daily light scattering profiles of August 26, 27, 30, and 31 occurred at about the same time as the elemental carbon peak and, with the exception of August 26, the peak OC concentration on those days lined up with a shoulder to the right of the b_{scat} peak. Alignment of the b_{scat} and EC peaks suggests that primary carbonaceous aerosol contributed significantly to visibility reduction on these days. On August 28 and 29 the b_{scat} peak lined up with the OC peak in the afternoon, and a left shoulder was evident in the b_{scat} data which aligned with the morning EC peak. Thus, in this episode, when secondary organic aerosol concentrations were particularly high, secondary organic aerosol appeared to contribute significantly to visibility reduction. Knowledge about the importance of other light-scattering aerosols is needed to draw more definite conclusions about the importance of organic aerosol in visibility reduction.

The contributions of primary and secondary sources to the ambient organic aerosol were estimated for Friday, August 28, a day when conditions for secondary formation were good. The first estimate was made by assuming that

the primary aerosol could be described by the OC/EC ratio at the time of the peak EC concentration on the day in question. This gave a primary ratio of 1.4 ± 0.1 . The primary and secondary organic carbon concentrations which resulted are shown in Figure 8.9. The primary component of the aerosol reached a maximum concentration of $13 \mu\text{gC}/\text{m}^3$ at about 0700 hours (PDT). The maximum reached by the secondary component was $14 \mu\text{gC}/\text{m}^3$ at 1700 hours (PDT); this corresponded to about 69% of the organic aerosol present at that time. Over a 24 hour period secondary sources contributed approximately 55% of the organic aerosol. The second estimate assumes a primary OC/EC ratio of 2.4, which was calculated from a comprehensive emissions inventory for the Los Angeles Basin (Gray, 1986). (The carbon measurements which form the emissions inventory come from a variety of sources, and therefore it was not possible to correct the measurements for organic sampling artifacts.) The estimated primary and secondary OC concentrations are shown in Figure 8.10. In this estimate, primary OC dominated except in the late afternoon. The secondary component reached a maximum of $10 \mu\text{gC}/\text{m}^3$ at about 1700 hours (PDT) accounting for roughly 48% of the aerosol.

These methods of estimating primary and secondary contributions assume that the primary ratio is invariant over the course of the day. Emissions ratios vary considerably from source to source, and therefore the primary ratio will be influenced by meteorology, diurnal and seasonal fluctuations in emissions, and the influence of local sources. Because of the sea breeze the inland sites like Claremont receive a more representative mixture of sources than sites nearer the coast. However, the variability of the primary ratio is not known.

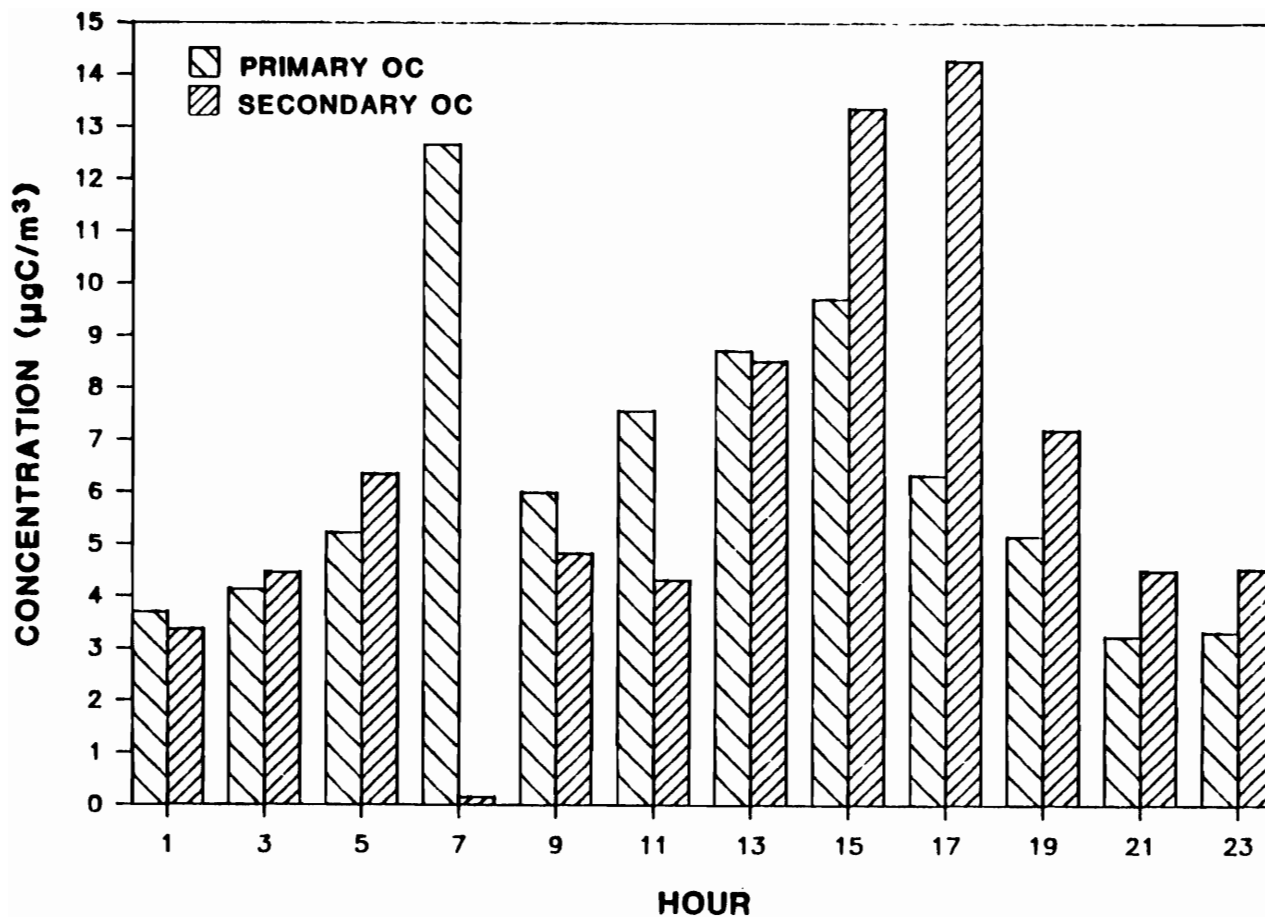


Figure 8.9. Estimates of primary and secondary organic aerosol ($\mu\text{gC}/\text{m}^3$) for August 28, 1987 at Claremont, California assuming a primary organic/elemental carbon ratio of 1.4. Time is Pacific Daylight Time (PDT). The ambient organic/elemental carbon ratio at the time of the peak elemental carbon concentration (0700 hours) was taken to be the primary ratio.

FIGURE 8.9

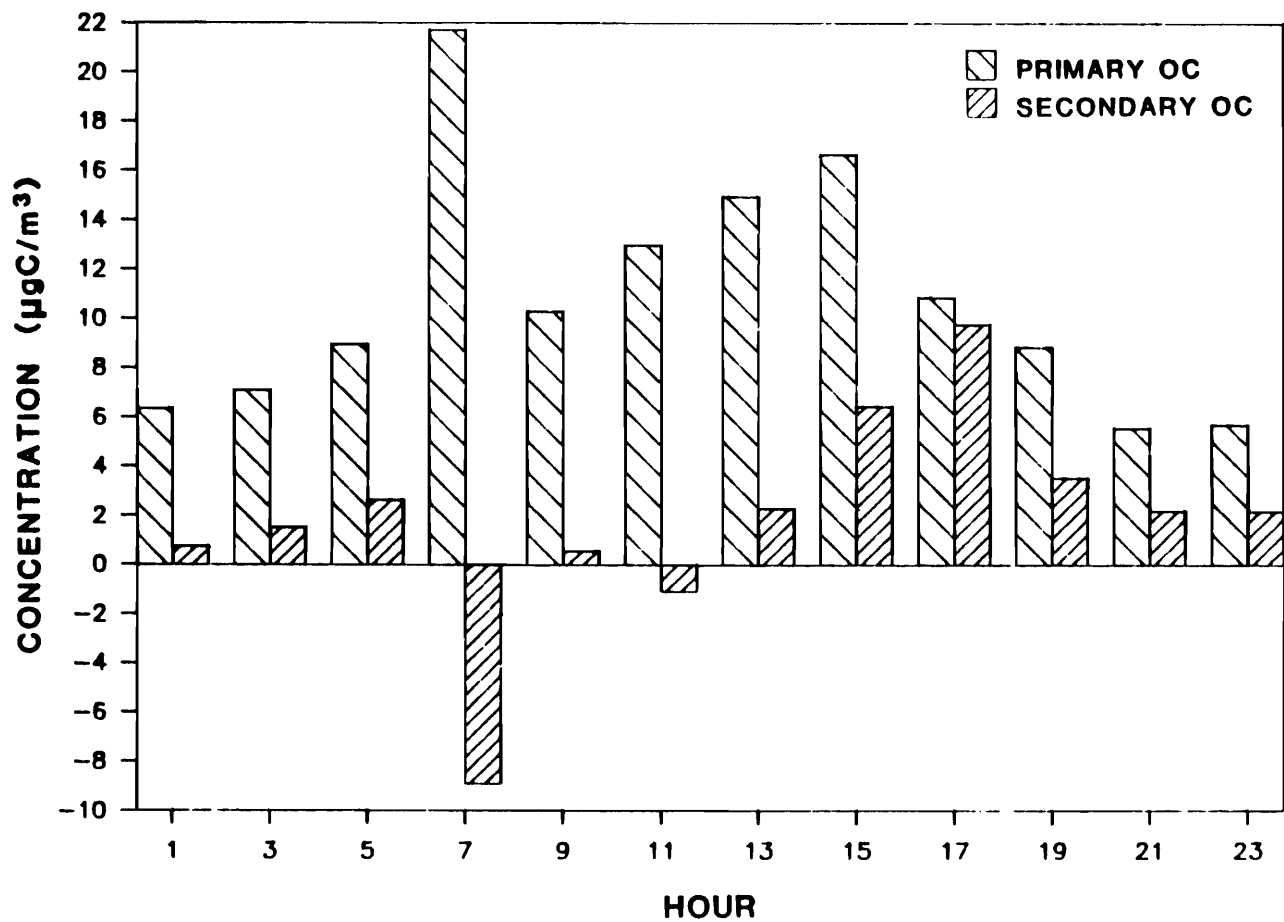


Figure 8.10. Estimates of primary and secondary organic aerosol ($\mu\text{gC}/\text{m}^3$) for August 28, 1987 at Claremont, California assuming a primary organic/elemental carbon ratio of 2.4. Time is Pacific Daylight Time (PDT). The primary organic/elemental carbon ratio was calculated from a comprehensive Los Angeles Basin emissions inventory.

FIGURE 8.10

Figure 8.11 shows OC and EC for November 17 - 19, and Table 8.3 summarizes additional information. In contrast to the summer, the wind flow at the Long Beach site in the fall did not follow a standard daily pattern except that the air tended to be fairly still at night. From November 17 through 19 the air was unstable, and there was no stagnation. Ozone and b_{scat} were low except from about 1900 hours (PST) on November 17 to 1000 hours (PST) on November 18, when b_{scat} was elevated. The highest OC and EC concentrations of the three day period were observed during this period of high light scattering.

The lack of sun on Tuesday, low ozone concentrations, and an unstable air mass suggest that photochemical activity, including secondary formation of organic aerosol, should have been minimal during this period. The OC and EC profiles were quite similar, and the coefficients of determination between OC and EC were 80%, 91%, and 81% for November 17, 18, and 19 respectively. OC/EC ratios, shown in Figure 8.12, varied from 1.4 ± 0.1 to 3.0 ± 0.5 . As in the summer, the minimum ratios of OC/EC occurred between 0700 and 0900 hours (PST). The OC/EC ratio on each of these days was relatively constant except for the dip which occurred between 0700 and 0900 hours (PST). This dip could have resulted from the infusion of a large quantity of fresh emissions due to morning traffic followed by some gas-to-particle conversion later in the day. Alternatively, it could have resulted from a diurnal variation in the source contributions to the Long Beach receptor site which would produce a diurnal variation of the primary OC/EC ratio. For November 17 this suggests that the primary ratio would be about 1.4 - 1.5 at 0700 hours and about 2.4 at 1700 hours.

FIGURE 8.11

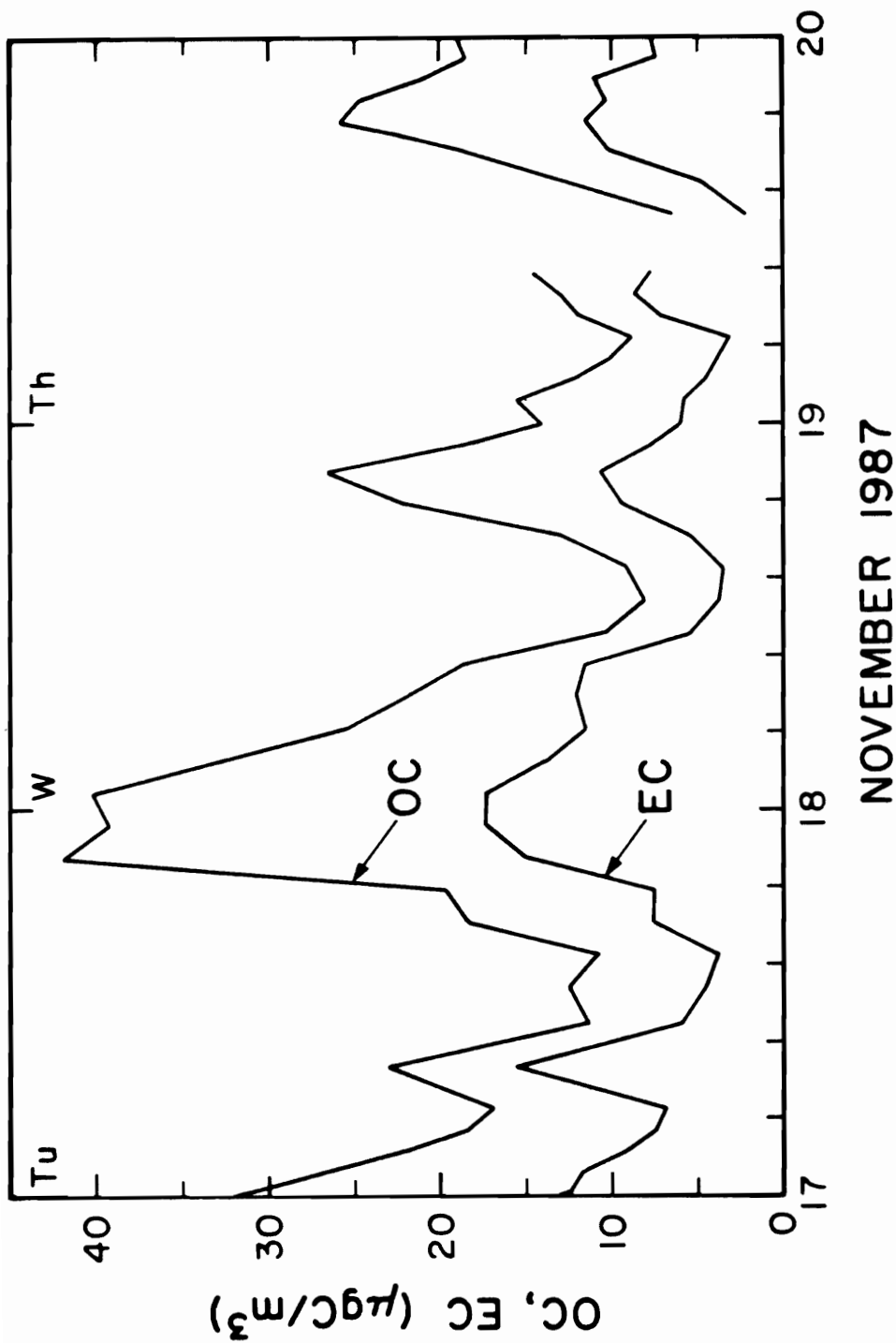


Figure 8.11. Concentrations of organic and elemental carbon ($\mu\text{gC}/\text{m}^3$) for November 17-19, 1987 at Long Beach, California. Data are 80 minute averages, plotted at the midpoints of their averaging periods. Time is Pacific Standard Time (PST).

TABLE 8.3. SUMMARY DATA FOR NOVEMBER 17 - 19.

November		minimum visual range (km)	peak ozone (pphm)	peak organic carbon ($\mu\text{gC}/\text{m}^3$)	peak elemental carbon ($\mu\text{gC}/\text{m}^3$)	wind dir.	descriptive meteorology
17	Tue	18	1	42	17	NW	overcast all day intermittent drizzle
18	Wed	15	3*	40	17	variant	morning coastal surface inversion
19	Thu	39	*	26	11	variant	

* Ozone data were not available after noon on November 18.

FIGURE 8.12

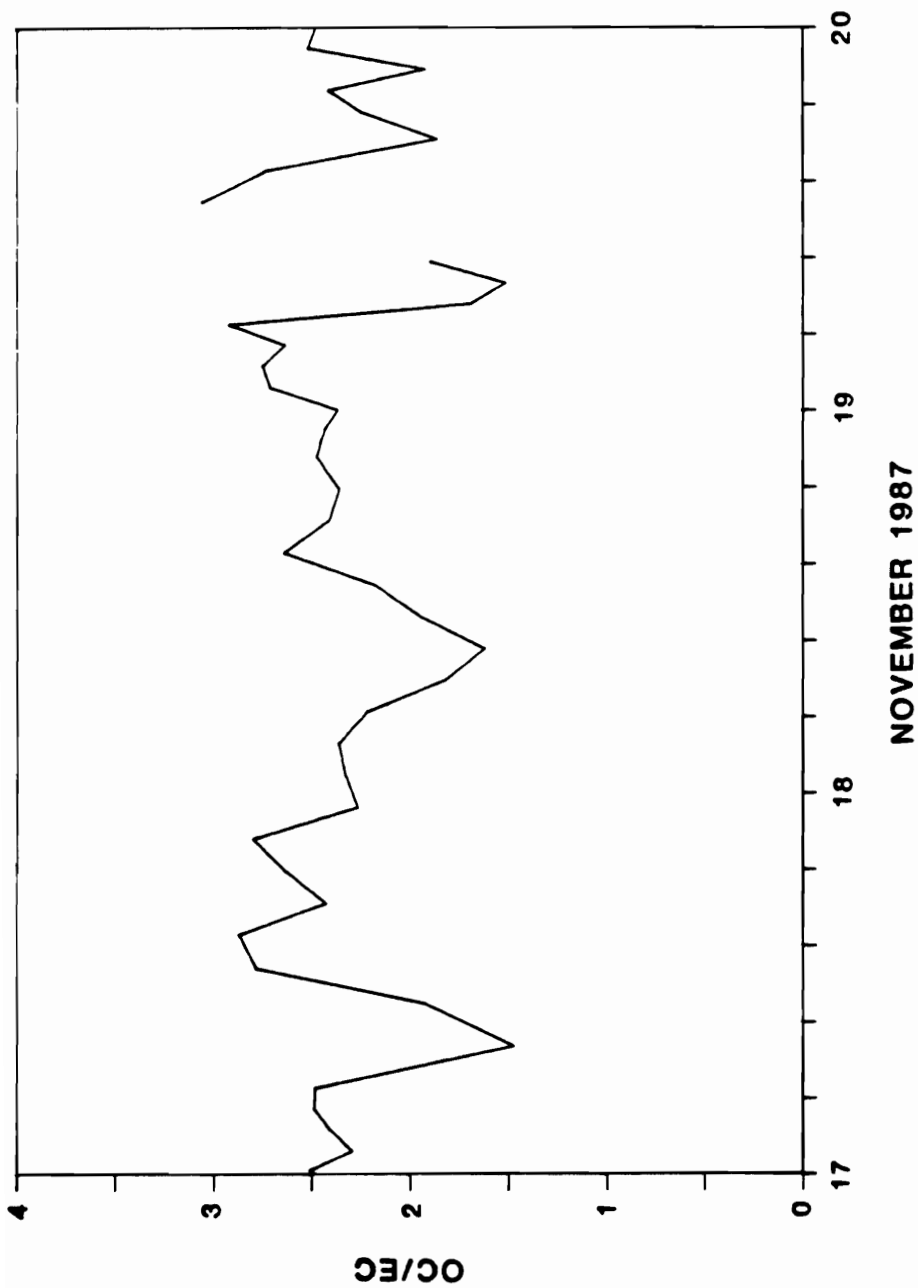


Figure 8.12. Ratios of organic to elemental carbon at Long Beach, California on November 17-19, 1987. Organic and elemental carbon concentrations are 80 minute averages, and their ratios are plotted at the midpoints of these averaging periods. Time is Pacific Standard Time (PST).

If the diurnal profile of the OC/EC ratio at Long Beach represents the variation in the primary OC/EC ratio and if it can be applied to the Claremont summer aerosol, an estimate of $10 \mu\text{gC}/\text{m}^3$ of secondary organic aerosol at 1700 hours (PDT) on August 28 would result. Under this set of assumptions secondary sources represent about 48% of the organic aerosol on August 28 at the time of day when their contribution is greatest, and primary organic aerosol dominates throughout the rest of the day. Primary and secondary organic aerosol estimates are shown in Figure 8.13. On August 28 the peak ozone concentration occurs at about 1540 hours, and the peak concentration of secondary organic aerosol occurs at about 1700 hours suggesting a time lag of 1.5 ± 1.0 hours between ozone formation and the formation of secondary organic aerosol.

CONCLUSION

A data base of time-resolved, particulate organic and elemental carbon values now exists for an extended period of summer and fall days during which supporting measurements are abundant. This information should prove useful for analyzing organic aerosol chemistry in the Los Angeles Basin with appropriate time resolved advection - diffusion - chemical reaction models. Preliminary examination of the in situ analyzer data for organic and elemental carbon has shown the existence of summer days on which the correlation between OC and EC, a tracer of primary combustion generated aerosol, is quite high. It has also identified three multiple day episodes during which OC - EC correlations were quite low, and secondary formation contributed significantly to organic aerosol concentrations. At the height of the August 27 - 31 episode secondary

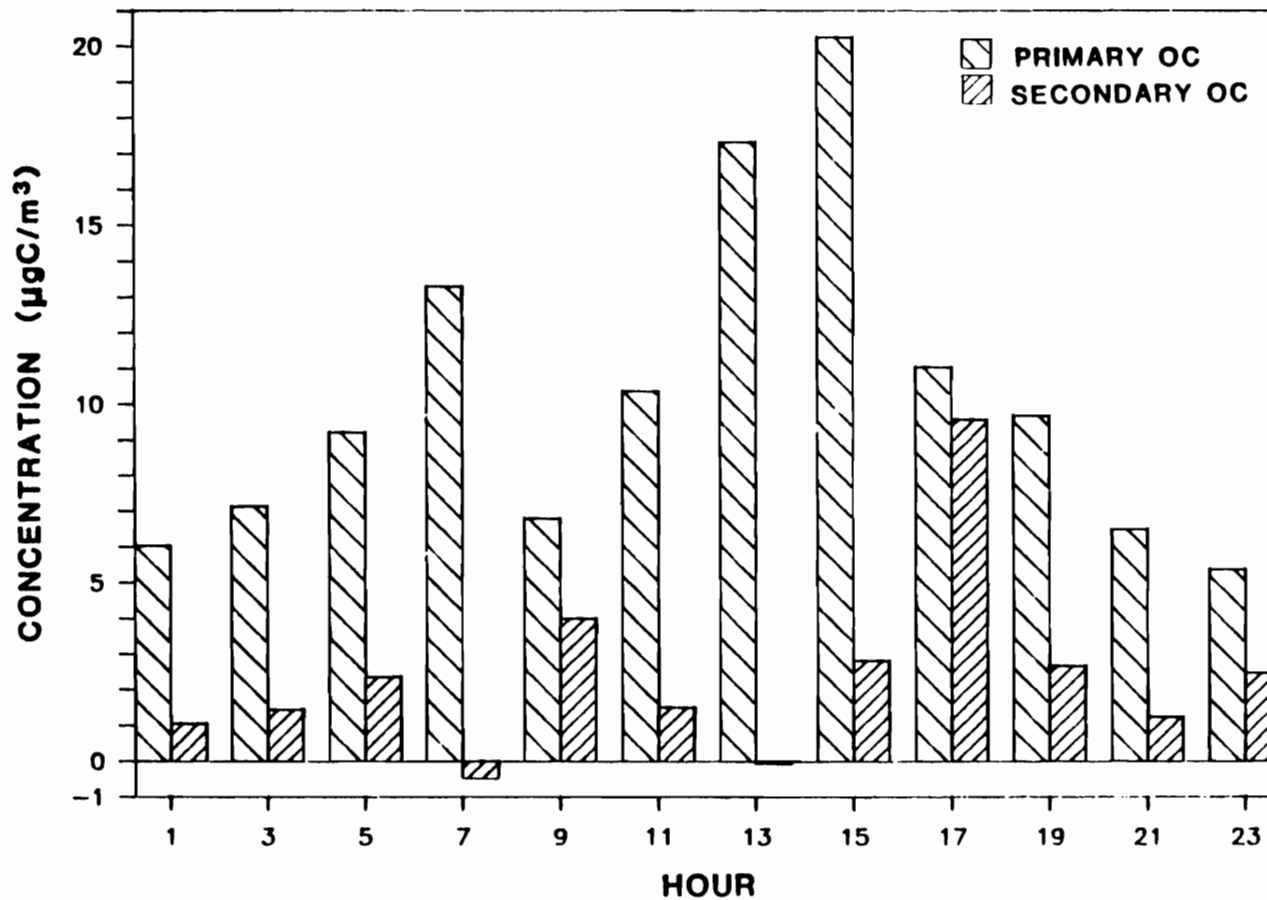


Figure 8.13. Estimates of primary and secondary organic aerosol ($\mu\text{gC}/\text{m}^3$) for August 28, 1987 at Claremont, California assuming that the ambient organic/elemental carbon ratio at Long Beach, California on November 17 describes the primary organic/elemental carbon ratio at Claremont, California on August 28. Time is Pacific Standard Time (PST).

FIGURE 8.13

formation accounted for 45 - 70% of the organic aerosol at 1700 hours (PDT). A better understanding of the diurnal variation of the primary OC/EC ratio is needed to determine whether or not secondary formation contributed significantly to organic aerosol concentrations over the 24 hour period.

CHAPTER 9. SUMMARY AND CONCLUSIONS

SUMMARY

Elevated particulate concentrations in urban areas result not only from direct particulate emissions but also from the condensation of products of gas phase, photochemical reactions. Aerosols emitted directly as particles are known as primary whereas those formed in the atmosphere are referred to as secondary. Although carbonaceous species comprise a large fraction of the urban aerosol, the contributions of primary and secondary sources to the carbonaceous aerosol are not well understood. The development of an effective air pollution control strategy requires an understanding of these sources. The goal of this research was to establish a method of identifying primary and secondary organic aerosol in Los Angeles through the use of time-resolved organic and elemental carbon measurements.

Because of the need to obtain improved time-resolution, low detection limits, and minimal influence from sampling artifacts, development of an in situ carbon analyzer continued, and a series of laboratory experiments were conducted to characterize the instrument. Sample handling uncertainties and volatilization losses during storage were eliminated by combining the sampling function of a

conventional filter sampler with the analytical function of a thermal-optical carbon analyzer. The instrument has an analytical precision of 3.1% (total particulate carbon) and a detection limit of 0.2 μg . Ambient carbon concentrations measured with the in situ carbon analyzer compared favorably with manual sampling and laboratory thermal-optical carbon analysis, and with the Ford Motor Company photoacoustic spectrometer data.

Two sampling artifacts which complicate the measurement of organic aerosol on quartz fiber filters are: (1) adsorption of organic vapors on the sampling filters and (2) volatilization of particulate material from the sampling filter. Experiments were conducted during the Carbonaceous Species Methods Comparison Study (CSMCS) and the Southern California Air Quality Study (SCAQS) in the Los Angeles Basin to assess the importance of these two artifacts. The results were consistent with those obtained by McDow and Huntzicker (1989) in Portland, Oregon. They suggest that (1) at the loadings of interest adsorption is the dominant artifact in the sampling of organic aerosol, (2) the organic carbon collected on a quartz fiber filter behind a Teflon filter is a good estimate of the adsorption on a quartz fiber front filter collected concurrently, (3) using longer collection periods will reduce the percentage of the collected material which is adsorbed vapor, and (4) during ambient sampling, gas phase organic compounds are frequently not in equilibrium between the gas phase and the adsorbed phase on the sampling filter. The in situ carbon analyzer minimizes volatilization by keeping collection periods short and burning collected material off the sampling filter before each subsequent collection. Correction for the adsorption artifact is accomplished by using two parallel sampling and analysis

systems. The aerosol side contains two quartz fiber filter disks, and the vapor side contains a Teflon filter followed by two quartz fiber filter disks. The particulate organic carbon concentration is obtained by subtracting the concentration on the vapor-side quartz filter disks (behind the Teflon filter) from the concentration on the aerosol-side quartz filter disks.

One set of quartz fiber filters collected in a manual sampler during CSMCS was also analyzed for specific organic compounds by direct thermal desorption/gas chromatography/mass spectroscopy to gain further insight into secondary formation and sampling artifacts. Little adsorption of gas-phase alkanes and polycyclic aromatic hydrocarbons (PAHs) was observed, whereas adsorption of gas-phase carboxylic acids contributed significantly to apparent concentrations of carboxylic acids on quartz fiber front filters.

Because elemental carbon is a good tracer for primary organic aerosol, many investigators have used the correlation between organic carbon (OC) and elemental carbon (EC) or the OC/EC ratio to investigate secondary organic aerosol formation. Ambient ratios greater than those observed for primary aerosol are considered indicative of secondary formation. Quantitative analysis requires an estimate of the primary OC/EC ratio and usually assumes that this ratio is constant. The assumption of a constant ratio would be valid if the source contributions at the site were relatively constant, and this assumption is best in areas where the contributions of local sources are small. Nevertheless, little is known about the variability of the primary ratio.

A preliminary study of secondary formation was conducted using 4 hour data from a 1984 Los Angeles Basin field study and a constant primary ratio

estimate. The analysis suggested that secondary formation contributed roughly half of the organic aerosol in the Los Angeles Basin during mid-day, summer conditions. However, all samples were collected at mid-day in the summer, when photochemical activity was at a maximum, and therefore no internal verification of the primary ratio estimate could be made.

Ambient organic and elemental carbon concentrations were measured with two hour time resolution at Glendora, California (1986) during CSMCS, at Claremont, California (1987) during the SCAQS summer session, and at Long Beach, California (1987) during the SCAQS fall session. Sampling included both days with high photochemical activity and days with low photochemical activity. Strong diurnal variations were evident in organic, elemental, and total carbon concentrations for both summer and fall data. In the summer, peak concentrations occurred during the daylight hours. However, in the fall the peaks occurred at night, and the maximum concentrations observed (max. total carbon = $88 \mu\text{gC}/\text{m}^3$ on December 3, 1987) were two to three times the summer maxima (max. total carbon = $36 \mu\text{gC}/\text{m}^3$ on June 24, 1987).

The summer SCAQS sampling days fell into two distinct categories (type (1) and type (2)). The coefficient of determination (R^2) between OC and EC was 69% for the set of samples comprising all type (1) days and in the range of 80 - 95% for the period of July 14 - 17. This is comparable to that observed in the fall ($R^2 = 80\%$). In contrast, for the set of samples comprising type (2) days OC and EC were poorly correlated ($R^2 = 30\%$), indicating a different origins for organic and elemental carbon on those days. Much of the organic carbon was

probably of photochemical origin. Three episodes of secondary organic aerosol formation were identified: July 11 - 13, July 25 - 29, and August 27 - 31, 1987.

The diurnal profiles of organic and elemental carbon also provided evidence of secondary formation on these days. On type (1) and fall days OC and EC profiles were quite similar. August 28, 1987 is an example of a type (2) day. On this day the maximum EC concentration and the minimum OC/EC ratio occurred around 0700 hours. The organic aerosol at this time was probably entirely primary. Then, the EC concentration decreased significantly, and the OC concentration increased significantly, reaching its maximum concentration around 1500 hours (PDT), about the same time as the ozone concentration peaked. Ozone is an indicator of photochemical activity. The additional organic carbon, which cannot be explained by common origin with elemental carbon, is probably secondary aerosol.

An estimate of the contributions of primary and secondary organic aerosol requires an understanding of the nature of the primary ratio. Primary and secondary organic aerosol contributions were calculated for August 28, 1987 using three scenarios for the primary ratio. In case (1) it was assumed that the organic aerosol was entirely primary when the peak EC concentration occurred (0700 hours), and the primary ratio was constant and equal to the ambient ratio at 0700 hours. In case (2) the primary ratio was estimated from a comprehensive emissions inventory for the Los Angeles basin. It was assumed to be constant also. In case (3) it was assumed that the primary ratio varied diurnally, and the Claremont aerosol resembled the composition of the aged Long Beach aerosol upwind. For all three cases the calculated secondary organic aerosol

concentration peaked at 1700 hours, and it comprised 48 to 69% of the organic aerosol present at that time. However, for case (1) secondary organic aerosol contributed about 55% of the organic aerosol over the 24 hour period, whereas for cases (2) and (3) secondary organic aerosol concentrations were only significant near 1700 hours and were negligible during rest of the day.

CONCLUSIONS

A data base of time-resolved, particulate organic and elemental carbon values now exists for an extended period of summer and fall days during which supporting measurements are abundant. These data suggest that secondary formation of organic aerosol does occur in the ambient Los Angeles Basin atmosphere and can be responsible for at least half of the organic aerosol in the late afternoon when conditions for secondary formation are favorable. However, the importance of secondary organic aerosol over a 24 hour average has not yet been determined. Accurate estimates of primary and secondary organic aerosol concentrations will require a better understanding of the primary OC/EC ratio.

RECOMMENDATIONS

- 1) Correction for the vapor adsorption artifact in the filter collection of organic aerosol should be accomplished by subtracting the organic carbon concentration on the Teflon-quartz backup filter from the quartz fiber front filter sample collected concurrently.
- 2) During thermal carbon analysis the proper division of total carbon into organic and elemental carbon fractions requires that the pyrolytic conversion of

organic to elemental carbon which occurs during the analysis be taken into consideration.

- 3) Because of the diurnal nature of photochemistry, investigations of secondary organic aerosol formation should be conducted using data with at least two hour time resolution.
- 4) Such investigations should include both periods of high and periods of low photochemical activity in order to provide internal estimates of the primary OC/EC ratio.
- 5) Further investigation into the variability of the primary OC/EC ratio is needed. This can be accomplished by examination of fall SCAQS data and type (1) summer SCAQS data and checked by estimating the time-resolved primary ratio for these days with the time-resolved source contributions. The source contributions can be determined by using a chemical element balance technique and an emissions inventory.
- 6) With this understanding of the primary ratio, primary and secondary organic carbon concentrations should be calculated for the SCAQS data sets.
- 7) The correlation of secondary OC with ozone, an indicator of photochemical activity, and nitrate, another secondary aerosol, should be examined further.
- 8) Exploratory analysis techniques such as factor analysis should be used to identify the conditions in which secondary formation of organic aerosol occurs in the Los Angeles Basin.
- 9) This time-resolved data should be used with the supporting data available to analyze organic aerosol chemistry using time-resolved advection - diffusion - chemical reaction models.

REFERENCES

- Adams, K. M. (1988). Appl. Opt. 27:4052-4056.
- Adams, K. M., Davis, L. I., Jr., Japar, S. M., Finley, D. R., and Cary, R. A. (1989b). Atmos. Environ. (submitted).
- Adams, K. M., Davis, L. I., Jr., Japar, S. M., and Pierson, W. R. (1989a). Atmos. Environ. 23:693.
- Adams, K. M., Japar, S. M., and Pierson, W. R. (1986). Atmos. Environ. 20:1211-1215.
- Appel, B. R., Colodny, P., and Wesolowski, J. J. (1976). Environ. Sci. Technol. 10:359-363.
- Appel, B. R., Hoffer, E. M., Kothny, E. L., Wall, S. M., Haik, M., and Knights, R. L. (1979). Environ. Sci. Technol. 13:98-104.
- Benner, W. H., Hansen, A. D. A., Gundel, L. A., and Novakov, T. (1984). Sci. Total Environ. 36:271-276.
- Blumenthal, D. L., Smith, T. B., White, W. H., Marsh, S. L., Ensor, D. S., Husar, R. B., McMurry, P. S., Heisler, S. L., and Owens, P. (1974). Three-Dimensional Pollutant Gradient Study 1972-1973 Program. California Air Resources Board, MRI 74 FR-1262, p. 78.
- Brunauer S., Emmet P. H., and Teller E. (1938). J. Am. Chem. Soc. 60:309-319.
- Cadle, S. H., Groblicki, P. J., and Mulawa, P. A. (1983). Atmos. Environ. 17:593-600.
- Cass, G. R., Boone, P. M., and Macias, E. S. (1982). In Particulate Carbon: Atmospheric Life Cycle (G. T. Wolff and R. L. Klimisch, eds.). Plenum Press, New York, pp. 207-243.
- Chatfield, C. (1983). Statistics for Technology. Chapman and Hall, New York, pp. 157-158.
- Cheng, Y. S., and Yeh, H. C. (1979). Environ. Sci. Technol. 13:1392-1396.

Chu, L. C., and Macias, E. S. (1981). In Atmospheric Aerosol: Source/Air Quality Relationships (E. S. Macias and P. K. Hopke, eds.). American Chemical Society, Washington, D.C., pp. 251-268.

Conklin, M. H., Cass, G. R., Chu, L. -C., and Macias, E. S. (1981). In Atmospheric Aerosol: Source/Air Quality Relationships (E. S. Macias and P. K. Hopke, ed.). American Chemical Society, Washington, D.C., pp. 235-250.

Countess, R. J. (1989). Aerosol Sci. Technol. (in press).

Cronn, D., and Crittenden, A. L. (1975). Environ. Sci. Technol. 9:838-845.

Esman, N. A., Ziegler, P., and Whitfield, R. (1978). J. Aerosol Sci. 9:547-556.

Friedlander, S. K. (1973). Environ. Sci. Technol. 7:235-240.

Gartrell, G., and Friedlander, S. K. (1975). Atmos. Environ. 9:279-299.

Gray, H. A. (1986). Control of Atmospheric Fine Primary Carbon Particle Concentrations, EOL Report No. 23 Environmental Quality Laboratory, California Institute of Technology, Pasadena, CA 91125, pp. 103-108.

Gray, H. A., Cass, G. R., Huntzicker, J. J., Heyerdahl, E. K., and Rau, J. A. (1984). Sci. Total Environ. 36:17-25.

Gray, H. A., Cass, G. R., Huntzicker, J. J., Heyerdahl, E. K., and Rau, J. A. (1986). Environ Sci. Technol. 20:580-582.

Greaves, R. C., Barkley, R. M., and Sievers, R. E. (1985). Analyt. Chem. 57:2807-2815.

Groblicki, P.J., and Nebel, G.J. (1971). In Chemical Reactions in Urban Atmospheres (C.S. Tuesday, ed.). American Elsevier Publishing Co., New York, pp. 241-263.

Grosjean, D. (1977). Ozone and Other Photochemical Oxidants, Ch. 3. National Academy of Sciences, Washington, D.C.

Grosjean, D. (1984). Sci. Total Environ. 32:133-145.

Grosjean, D., and Friedlander, S. K. (1975). J. Air Pollution Control Assoc. 25:1038-1044.

Grosjean, D., VanCauwenberghe, K., Schmid, J. P., Kelley, P. E., and Pitts, J. N. (1978). Environ. Sci. Technol. 12:313-317.

Gundel, L. A., Dod, R. L., Rosen, H., and Novakov, T. (1984). Sci. Total Environ. 36:197-202.

Heisler, S. L., and Friedlander, S. K. (1977). Atmos. Environ. 11:157-168.

Hidy, G. M., and Friedlander, S. K. (1971). In Proceedings of the Second International Clean Air Congress (H.M. Englund and W.T. Beery, eds.). Academic Press, New York, pp. 391-404.

Hogan, A., Ahmed, N., Black, J., and Barnard, S. (1985). J. Aerosol Sci. 16:391-397.

Huntzicker, J. J., Heyerdahl, E. K., Rau, J.A., Griest, W. H., and MacDougall, J. (1986). Air Pollution Control Assoc. 36:705-709.

Huntzicker, J. J., Johnson, R. L., Shah, J. J., and Cary, R. A. (1982). In Particulate Carbon: Atmospheric Life Cycle (G. T. Wolff and R. L. Klimisch, eds.). Plenum, New York, pp. 79-88.

Japar, S. M., Szkarlat, A. C., and Pierson, W. R. (1984). Sci. Total Environ. 36:121-130.

Johnson, R. L., Shah, J. J., Cary, R. A., and Huntzicker, J. J. (1981). In ACS Symposium Series No. 167: Atmospheric Aerosol: Source/Air Quality Relationships, (E. S. Macias and P. K. Hopke, eds.), American Chemical Society, Washington, D.C., pp. 223-233.

Junge, C. E. (1977). In Fate of Pollutants in the Air and Water Environments, (I. H. Suffet, ed.), John Wiley & Sons, New York, pp. 7-25.

King, J. A., Shair, F. H., and Reible, D. D. (1987). Atmos. Environ 21:53-59.

Knights, R. L., Cronn, D. R., and Crittenden, A. L. (1975). Paper No. 3 presented at 1975 Pittsburgh Conference on Analytical Chemistry and Applied Spectroscopy, Cleveland, Ohio, March 3.

Ligocki, M. P. (1986). The Scavenging of Atmospheric Trace Organic Compounds by Rain. Ph.D. Thesis, Oregon Graduate Center, Beaverton, Oregon, 97006.

Marple, V. A., and Liu, B. Y. H. (1974). Environ. Sci. Technol. 8:648-654.

Marple, V. A., and Liu, B. Y. H. (1975). J. Colloid Interface Sci. 53:31-34.

- McDow, S. R. (1986). The Effect of Sampling Procedures on Organic Aerosol Measurement. Ph.D. Thesis, Oregon Graduate Center, Beaverton, OR 97006.
- McDow, S. R. and Huntzicker, J. J. (1989). Vapor Adsorption Artifact in the Sampling of Organic Aerosol: Face Velocity Effects. Atmos. Environ. (in press).
- McMurry, P. H., and Grosjean, D. (1985). Atmos. Environ. 19:1445-1451.
- Neiburger, M., Edinger, J. G., and Bonner, W. D. (1982). Understanding Our Atmos. Environ. W. H. Freeman and Co., San Francisco, pp. 385-391.
- Novakov, T. (1982). In Particulate Carbon: Atmospheric Life Cycle (G. T. Wolff and R. L. Klimisch, eds.). Plenum Press, New York, pp. 19-41.
- O'Brien, R.J., Holmes, J.R., and Bockian, A.H. (1975). Environ. Sci. Technol. 9:568-576.
- Pankow, J. F. (1987). Atmos. Environ. 21: 2275-2283.
- Pankow, J. F., and Isabelle, L. M. (1982). J. Chromatog. 237: 25-39.
- Pankow, J. F., and Isabelle, L. M. (1984). Anal. Chem. 56: 2997-2999.
- Pao, Y. -H., ed. (1977). Optoacoustic Spectroscopy and Detection. Academic Press, New York.
- Rosencwaig, A. (1980). In Chemical Analysis: A Series of Monographs on Analytical Chemistry and Its Applications, Volume 57 (P. J. Elving and J. D. Winefordner, eds., I. M. Kolthoff, ed. emeritus). John Wiley and Sons, New York.
- Shah, J. J., Johnson, R. L., Heyerdahl, E. K., and Huntzicker, J. J. (1986). J. Air Pollution Control Assoc. 36:254-257.
- Stern, J. E., Flagan, R. C., Grosjean, D., and Seinfeld, J. H. (1987). Environ. Sci. Technol. 21:1224-1231.
- Terhune, R. W., and Anderson, J. E. (1977). Opt. Lett. 1:70-72.
- Turner, J. R., and Hering, S. V. (1987). J. Aerosol Sci. 18:215-224.
- Turpin, B. J., and Huntzicker, J. J. (1988). ARB Report, Contract A5-149-32 California Air Resources Board, Sacramento, CA 95812, pp. 90,94.
- Wesolowski, J. J., John, W., and Kaifer, R. (1973) In Trace Elements in the Environment: Advances in Chemistry Series No. 123 (E. L. Kothny, ed.). American Chemical Society, Washington, D.C., pp. 1-16.

Whitby, K. T., Husar, R. B., and Liu, B. Y. H. (1972). J. Colloid Interface Sci. 39:117-204.

Wolff, G. T., Countess, R. J., Groblicki, P. J., Ferman, M. A., Cadle, S. H., and Muhlbaier, J. L. (1981). Atmos. Environ. 15:2485-2502.

Wolff, G. T. Groblicki, P. J., Cadle S. H., and Countess, R. J. (1983). In Particulate Carbon: Atmospheric Life Cycle (G. T. Wolff and R. L. Klimisch, eds.). Plenum Press, New York, pp. 297-315.

Yamasaki H., Kuwata K., and Miyamoto H. (1982). Environ. Sci. Technol. 16:189-194.

**APPENDIX A. FORD PHOTOACOUSTIC AND OGC THERMAL-OPTICAL
ELEMENTAL CARBON DATA USED FOR INTERCOMPARISON.**

TABLE A.1.

Date 1987	FORD			OGC		
	Start Time	Stop Time	Conc. ug/m ³	Conc. ug/m ³	Start Time	Stop Time
6-19	0207	0356	2.60	2.36	0223	0344
	0616	0756	3.29	3.17	0623	0744
	0808	0954	5.05	4.78	0823	0944
	1206	1355	3.07	2.69	1223	1344
	1407	1553	2.39	2.18	1423	1544
	1808	1957	1.89	1.85	1823	1944
	2005	2155	2.32	1.85	2024	2145
6-24	0205	0354	1.61	1.51	0221	0342
	0626	0750	2.53	2.29	0621	0742
	0805	0949	3.36	3.35	0821	0942
	1208	1355	5.26	5.92	1221	1342
	1407	1554	5.75	6.55	1421	1542
	1814	1956	2.55	2.98	1821	1942
6-25	0210	0357	2.41	1.76	0222	0343
7-13	0207	0357	0.82	1.20	0221	0342
	0809	0959	5.76	6.81	0821	0942
	1205	1354	3.77	3.95	1221	1342
	1405	1552	4.47	5.13	1421	1542
	1815	1957	2.20	2.25	1821	1942
	2022	2140	1.77	2.28	2021	2142
	2207	2353	1.79	2.30	2221	2342
7-14	0208	0357	2.09	2.31	0221	0342
	0605	0755	2.61	3.02	0621	0742
	0805	0952	3.79	4.57	0821	0942
	1435	1548	5.73	6.62	1421	1542
	2012	2156	1.49	2.26	2021	2142
	2213	2354	1.06	1.62	2221	2342
	7-15	0207	0358	1.44	2.01	0221
0608		0757	1.85	2.54	0621	0742
0806		0956	2.00	3.37	0821	0942
1206		1355	2.99	4.15	1221	1342
1404		1552	3.42	4.90	1421	1542
2011		2155	1.69	2.39	2021	2142
8-27		0208	0355	2.29	2.03	0219
	1204	1351	6.14	4.73	1219	1340
	1359	1549	7.88	5.80	1419	1540
	1809	1957	3.09	2.65	1819	1940
	2011	2155	2.39	2.22	2019	2140

TABLE A.1, cont.

Date 1987	FORD			OGC		
	Start Time	Stop Time	Conc. ug/m3	Conc. ug/m3	Start Time	Stop Time
8-28	0209	0356	2.94	2.95	0219	0340
	0620	0741	8.03	9.05	0619	0740
	0811	0955	4.92	4.28	0819	0940
	1208	1351	6.91	6.23	1219	1340
	2006	2154	2.09	2.31	2019	2140
	2205	2351	2.41	2.37	2219	2340
	8-29	0205	0355	3.48	3.14	0219
0808		0955	3.73	3.60	0819	0940
1209		1354	4.20	4.27	1219	1340
1411		1552	4.07	3.63	1419	1540
1812		1955	2.76	2.40	1819	1940
2011		2153	2.19	2.27	2019	2140
9-02	0204	0355	1.43	0.71	0223	0344
	0613	0748	4.38	4.45	0628	0744
	0805	0955	3.60	2.80	0826	0946
	1207	1355	2.55	0.78	1224	1344
	1816	1955	3.71	2.53	1821	1941
	2005	2153	4.21	3.39	2020	2140
9-03	0206	0356	2.55	1.93	0219	0340
	0609	0756	8.19	6.81	0619	0740
	1207	1354	4.48	3.37	1219	1340

APPENDIX B: GC/MS RESULTS

TABLE B.1. GRAND AVERAGES (ng/m³)

	---- QQF ----		---- QQB ----		---- TQB ----	
	mean	std dev	mean	std dev	mean	std dev
Carboxylic acids						
hexanoic	4.3	2.9	0.3	0.6	0.5	0.7
heptanoic	10.8	7.4	0.2	0.3	0.5	0.5
octanoic	6.9	3.6	0.7	0.8	1.1	1.0
nonanoic	4.9	2.4	0.1	0.3	0.3	0.6
decanoic	3.1	1.3	0.3	0.5	0.6	0.8
undecanoic	1.3	0.7	0.3	0.4	0.5	0.6
dodecanoic	6.2	3.2	4.3	2.3	4.1	2.7
tridecanoic	2.3	2.9	0.8	0.9	1.2	0.9
tetradecanoic	16.0	8.0	7.3	11.7	9.9	10.7
pentadecanoic	7.6	6.0	3.3	4.6	4.6	4.7
hexadecanoic	60.1	32.6	13.1	19.8	36.9	34.4
octadecanoic	53.1	28.3	5.8	9.9	21.6	44.8
PAHs and Alkyl PAH's						
naphthalene	0.9	1.0	0.2	0.6	0.8	2.0
2-methylnaphthalene	0.4	0.3	0.06	0.2	0.2	0.4
1-methylnaphthalene	0.3	0.2	0.03	0.1	0.07	0.2
biphenyl	0.5	0.6	0.0	0.0	0.1	0.5
2,6-dimethyl- naphthalene	0.1	0.07	0.03	0.03	0.04	0.07
1,3+1,6-dimethyl- naphthalene	0.1	0.08	0.03	0.07	0.1	0.2
acenaphthylene	0.09	0.04	0.00	0.01	0.02	0.03
fluorene	0.07	0.05	0.00	0.01	0.03	0.03
phenanthrene	0.6	0.4	0.2	0.1	0.3	0.3
anthracene	0.09	0.06	0.03	0.03	0.04	0.04
2-methylphenanthrene	0.09	0.04	0.00	0.01	0.02	0.03
1-methylphenanthrene	0.10	0.04	0.01	0.02	0.04	0.04
fluoranthene	0.3	0.1	0.08	0.04	0.11	0.07
pyrene	0.29	0.09	0.07	0.03	0.08	0.05
benz[a]anthracene + chrysene	0.4	0.1	0.05	0.03	0.10	0.07
benzo[b+j+k]fluoranthene	2.4	2.0	0.01	0.01	0.08	0.07
benzo[e]pyrene	0.9	0.6	0.00	0.00	0.01	0.02
benzo[a]pyrene	0.2	0.3	0.00	0.00	0.00	0.00

TABLE B.1. GRAND AVERAGES (ng/m³; cont.)

	---- QQF ----		---- QQB ----		---- TQB ----	
	mean	std dev	mean	std dev	mean	std dev
Alkanes						
pentadecane	0.2	0.3	0.09	0.3	0.2	0.5
hexadecane	0.8	2.0	0.9	1.3	0.7	1.4
heptadecane	0.0	0.0	0.0	0.0	0.3	0.9
pristane	0.02	0.05	0.02	0.06	0.1	0.4
octadecane	0.4	0.4	0.7	0.7	1.1	1.9
nonadecane	1.3	1.6	0.8	0.9	1.3	2.1
eicosane	0.5	1.2	0.4	0.7	0.9	1.7
heneicosane	1.0	0.7	0.7	0.8	1.2	1.1
docosane	2.3	1.6	1.4	1.6	1.8	2.1
tricosane	5.5	5.1	1.9	1.4	1.5	1.2
tetracosane	10.1	9.2	2.8	2.5	2.5	2.3
pentacosane	11.0	8.4	1.6	1.1	1.8	1.8
hexacosane	7.7	7.0	0.8	0.6	0.7	0.7
heptacosane	6.7	4.5	0.5	0.5	0.5	0.6
octacosane	8.8	7.7	0.3	0.4	0.8	1.5
nonacosane	8.4	4.9	0.4	0.5	1.2	3.1
Heterocyclic Compounds						
dibenzofuran	0.2	0.2	0.04	0.06	0.1	0.2
dibenzothiophene	0.05	0.04	0.04	0.08	0.03	0.05
quinoline	1.6	1.4	0.9	1.7	0.7	1.2
methylquinolines	2.2	2.5	1.5	2.1	0.9	1.3
PAH Ketones and Quinones						
1-indanone	0.4	0.4	0.1	0.2	0.02	0.06
benzothiazole	0.04	0.08	0.2	0.4	0.3	0.8
2-coumaranone	0.5	0.5	0.02	0.04	0.01	0.04
1,3-indanedione	1.1	1.1	0.5	1.0	0.4	0.5
coumarin	0.3	0.2	0.2	0.1	0.2	0.2
9-fluorenone	0.6	0.6	0.1	0.2	0.3	0.5
xanthone	0.1	0.1	0.06	0.06	0.09	0.08
9,10-anthdione	0.7	0.4	0.4	0.6	0.3	0.3
benzanthrone	0.1	0.1	0.02	0.03	0.03	0.03
7,12-benz[a]adione	0.03	0.07	0.0	0.0	0.0	0.0
Phthalate Esters						
diethyl	0.7	1.3	4.4	5.5	6.3	11.4
dibutyl	16.3	12.4	14.5	8.1	21.4	10.1
butylbenzyl	6.3	3.0	1.1	1.5	5.1	3.4
2-ethylhexyl	106.8	50.5	4.0	9.4	51.6	38.6
dioctyl	1.7	0.9	0.3	0.3	0.6	0.3

TABLE B.1. GRAND AVERAGES (ng/m³; cont.)

	---- QF ----		---- QB ----		---- TQ ----	
	mean	std dev	mean	std dev	mean	std dev
Methyl Alkanoic Esters						
dodecanoate	0.0	0.0	0.06	0.05	0.02	0.03
tetradecanoate	0.02	0.06	0.08	0.05	0.06	0.07
hexadecanoate	0.2	0.2	0.5	0.5	0.3	0.3
octadecanoate	0.6	0.6	0.3	0.3	0.5	0.4
eicosanoate	0.04	0.05	0.01	0.02	0.04	0.04
Alcohols						
dodecanol	3.0	3.5	1.7	2.5	1.1	1.6
tetradecanol	0.4	0.8	1.6	2.0	0.4	0.8
Miscellaneous						
tributylphosphate	7.5	11.4	1.3	0.9	3.6	1.6
dioctyl adipate	3.8	3.0	0.2	0.3	2.4	2.5
cholestane	0.3	0.4	0.05	0.1	0.02	0.06
dibutylcresol	0.4	0.8	1.6	1.6	0.6	1.4
pristanone	0.0	0.0	0.4	1.2	0.0	0.0

TABLE B.2. DAYTIME AVERAGES CSMCS GC/MS (ng/m³)

	-- QQF DAY --		-- QQB DAY --	
	mean	std dev	mean	std dev
Carboxylic acids				
hexanoic	5.3	3.0	0.3	0.6
heptanoic	7.8	5.8	0.3	0.2
octanoic	6.4	4.0	0.3	0.7
nonanoic	4.4	2.3	0.0	0.0
decanoic	2.9	1.2	0.3	0.9
undecanoic	1.6	0.7	0.3	0.4
dodecanoic	10.6	13.4	18.4	46.2
tridecanoic	2.6	2.9	1.5	1.3
tetradecanoic	25.1	17.5	12.8	23.7
pentadecanoic	10.3	6.2	4.3	3.1
hexadecanoic	74.8	33.1	20.2	29.7
octadecanoic	66.1	42.9	1.9	2.7
PAHs and Alkyl PAHs				
naphthalene	1.3	1.3	0.0	0.0
2-methylnaphthalene	0.6	0.4	0.0	0.0
1-methylnaphthalene	0.3	0.3	0.0	0.0
biphenyl	0.6	0.7	0.0	0.0
2,6-dimethylnaphthalene	0.15	0.05	0.02	0.03
1,3+1,6-dimethyl- naphthalene	0.21	0.08	0.03	0.07
acenaphthylene	0.11	0.06	0.0	0.0
fluorene	0.08	0.05	0.00	0.01
phenanthrene	0.6	0.4	0.2	0.2
anthracene	0.10	0.05	0.03	0.03
2-methylphenanthrene	0.11	0.03	0.00	0.01
1-methylphenanthrene	0.11	0.03	0.01	0.02
fluoranthene	0.31	0.09	0.09	0.04
pyrene	0.31	0.09	0.07	0.03
benz[a]anthracene + chrysene	0.44	0.09	0.04	0.03
benzo[b+j+k]fluoranthene	1.7	2.0	0.01	0.01
benzo[e]pyrene	0.5	0.6	0.0	0.0
benzo[a]pyrene	0.05	0.08	0.0	0.0

TABLE B.2. DAYTIME AVERAGES CSMCS GC/MS. (ng/m³; cont.)

	-- QQF DAY --		-- QQB DAY --	
	mean	std dev	mean	std dev
Alkanes				
pentadecane	0.4	0.5	0.09	0.3
hexadecane	0.5	1.9	0.6	1.3
heptadecane	0.0	0.0	0.0	0.0
pristane	0.0	0.0	0.0	0.0
octadecane	0.3	0.4	0.6	0.6
nonadecane	0.9	1.7	0.6	0.9
eicosane	0.5	1.2	0.3	0.6
heneicosane	0.8	0.9	0.6	0.8
docosane	1.6	1.2	1.2	1.6
tricosane	2.5	1.8	1.7	1.5
tetracosane	5.1	3.2	2.5	2.5
pentacosane	6.3	3.0	1.7	1.4
hexacosane	3.5	2.1	0.6	0.6
heptacosane	3.7	1.6	0.3	0.4
octacosane	4.3	3.6	0.2	0.2
nonacosane	5.4	2.9	0.2	0.3
Heterocyclic Compounds				
dibenzofuran	0.3	0.2	0.04	0.06
dibenzothiophene	0.05	0.05	0.04	0.08
quinoline	1.4	1.1	0.6	0.9
methylquinolines	1.3	0.8	1.2	1.5
PAH Ketones and Quinones				
1-indanone	0.7	0.9	0.0	0.0
benzothiazole	0.03	0.08	0.0	0.0
2-coumaranone	1.2	1.3	0.01	0.03
1,3-indanedione	2.1	1.7	0.3	0.7
coumarin	0.4	0.2	0.2	0.1
9-fluorenone	0.5	0.6	0.08	0.2
xanthone	0.1	0.1	0.06	0.04
9,10-anthdione	0.7	0.4	0.3	0.5
benzanthrone	0.05	0.07	0.0	0.0
7,12-benz[a]adione	0.0	0.0	0.0	0.0
Phthalate Esters				
diethyl	0.5	0.6	3.9	5.4
dibutyl	16.4	15.7	11.7	7.3
butylbenzyl	8.5	2.1	1.8	2.0
2-ethylhexyl	149.9	26.9	0.4	1.1
dioctyl	2.2	1.0	0.3	0.2

TABLE B.2. DAYTIME AVERAGES CSMCS GC/MS. (ng/m³; cont.)

	-- QQF DAY --		-- QQB DAY --	
	mean	std dev	mean	std dev
Methyl Alkanoic Esters				
dodecanoate	0.0	0.0	0.07	0.05
tetradecanoate	0.02	0.06	0.06	0.05
hexadecanoate	0.2	0.2	0.5	0.5
octadecanoate	0.8	0.6	0.3	0.3
eicosanoate	0.04	0.05	0.02	0.02
Alcohols				
dodecanol	1.9	2.0	1.7	2.9
tetradecanol	0.3	0.8	1.0	2.1
Miscellaneous				
tributylphosphate	2.5	1.8	1.5	0.7
dioctyl adipate	4.0	3.0	0.06	0.1
cholestane	0.1	0.3	0.06	0.2
dibutylcresol	0.8	0.9	2.1	1.5
pristanone	0.0	0.0	0.0	0.0

TABLE B.3. NIGHTTIME AVERAGES CSMCS GC/MS (ng/m³)

	-- QQF NIGHT --		-- QQB NIGHT--	
	mean	std dev	mean	std dev
Carboxylic acids				
hexanoic	2.9	1.2	0.2	0.4
heptanoic	9.3	7.6	0.1	0.2
octanoic	5.8	2.4	0.5	0.6
nonanoic	4.7	2.1	0.2	0.3
decanoic	2.6	1.7	0.4	0.6
undecanoic	1.1	0.6	0.2	0.3
dodecanoic	5.3	1.8	3.5	2.1
tridecanoic	1.3	0.5	0.5	0.3
tetradecanoic	14.9	4.8	9.5	12.5
pentadecanoic	6.0	3.0	2.3	4.9
hexadecanoic	54.9	30.3	10.4	21.3
octadecanoic	55.5	26.2	6.4	11.1
PAHs and Alkyl PAHs				
naphthalene	0.4	0.7	0.3	0.7
2-methylnaphthalene	0.3	0.3	0.08	0.2
1-methylnaphthalene	0.1	0.2	0.05	0.1
biphenyl	0.2	0.3	0.04	0.1
2,6-dimethylnaphthalene	0.06	0.05	0.02	0.02
1,3+1,6-dimethyl- naphthalene	0.2	0.2	0.01	0.02
acenaphthylene	0.07	0.03	0.01	0.01
fluorene	0.05	0.05	0.01	0.01
phenanthrene	0.4	0.2	0.2	0.1
anthracene	0.06	0.03	0.03	0.02
2-methylphenanthrene	0.07	0.04	0.01	0.01
1-methylphenanthrene	0.08	0.04	0.01	0.01
fluoranthene	0.2	0.08	0.06	0.03
pyrene	0.2	0.08	0.05	0.03
benz[a]anthracene + chrysene	0.4	0.2	0.04	0.02
benzo[b+j+k]fluoranthene	2.1	1.0	0.01	0.01
benzo[e]pyrene	1.0	0.5	0.0	0.0
benzo[a]pyrene	0.3	0.4	0.0	0.0

TABLE B.3. NIGHTTIME AVERAGES CSMCS GC/MS. (ng/m³; cont.)

	-- QQF NIGHT --		-- QQB NIGHT--	
	mean	std dev	mean	std dev
Alkanes				
pentadecane	0.2	0.2	0.03	0.1
hexadecane	0.3	0.8	0.6	0.8
heptadecane	0.0	0.0	0.0	0.0
pristane	0.02	0.06	0.02	0.07
octadecane	0.3	0.2	0.5	0.4
nonadecane	0.8	0.7	0.6	0.5
eicosane	0.0	0.0	0.2	0.5
heneicosane	0.7	0.4	0.2	0.4
docosane	2.0	1.7	0.7	0.6
tricosane	5.8	5.6	1.3	0.9
tetracosane	10.9	10.1	1.8	1.4
pentacosane	11.9	9.4	1.0	0.8
hexacosane	8.9	7.5	0.6	0.6
heptacosane	7.7	5.1	0.3	0.5
octacosane	9.1	8.5	0.3	0.4
nonacosane	8.9	6.7	0.3	0.5
Heterocyclic Compounds				
dibenzofuran	0.1	0.07	0.04	0.06
dibenzothiophene	0.03	0.02	0.01	0.01
quinoline	1.8	1.6	0.6	1.7
methylquinolines	2.8	2.7	0.9	1.9
PAH Ketones and Quinones				
1-indanone	0.3	0.4	0.2	0.2
benzothiazole	0.06	0.09	0.2	0.5
2-coumaranone	0.3	0.3	0.03	0.04
1,3-indanedione	0.6	0.9	0.5	0.9
coumarin	0.2	0.1	0.1	0.09
9-fluorenone	0.3	0.2	0.1	0.2
xanthone	0.08	0.04	0.05	0.05
9,10-anthdione	0.6	0.4	0.3	0.5
benzanthrone	0.2	0.09	0.02	0.03
7,12-benz[a]adione	0.1	0.1	0.0	0.0
Phthalate Esters				
diethyl	0.7	1.4	3.6	4.4
dibutyl	15.2	7.1	15.6	7.7
butylbenzyl	4.5	1.5	0.3	0.4
2-ethylhexyl	66.5	15.1	5.2	10.4
dioctyl	1.6	0.8	0.3	0.4

TABLE B.3. NIGHTTIME AVERAGES CSMCS GC/MS. (ng/m³; cont.)

	-- QQF NIGHT --		-- QQB NIGHT--	
	mean	std dev	mean	std dev
Methyl Alkanoic Esters				
dodecanoate	0.06	0.2	0.04	0.03
tetradecanoate	0.01	0.02	0.06	0.04
hexadecanoate	0.2	0.2	0.3	0.2
octadecanoate	0.2	0.2	0.2	0.09
eicosanoate	0.02	0.04	0.00	0.01
Alcohols				
dodecanol	2.9	3.9	1.6	2.6
tetradecanol	1.03	1.07	1.5	0.9
Miscellaneous				
tributylphosphate	10.6	12.0	0.8	0.8
dioctyl adipate	3.6	3.3	0.2	0.3
cholestane	0.4	0.4	0.0	0.0
dibutylcresol	0.0	0.0	1.3	0.9
pristanone	0.0	0.0	0.8	1.7

APPENDIX C. SCAQS BROMINE AND LEAD CONCENTRATIONS

INTRODUCTION

The diurnal cycles of ozone and secondary organic aerosol are likely to be quite different when significant retention of pollutants has occurred overnight. Retained ozone is likely to be depleted at night through scavenging by NO (King et al., 1987), whereas secondary aerosol concentrations can remain elevated for many days. The following morning the NO₂ generated from ozone scavenging is likely to photolyze, producing additional ozone. Likewise, secondary aerosol generated on that day adds to that which was retained from previous days.

The bromine to lead ratio (Br/Pb) is a measure of the age of an air mass when motor vehicles are the major source (Appel et al., 1979; Wesolowski et al., 1973). The anti-knock gasoline additive, tetraethyl lead, along with lead scavenger additives, ethylene dibromide and ethylene dichloride, form lead halide particles (e.g., PbBrCl) in motor vehicle exhaust. The PbBrCl loses bromine in the atmosphere yielding a Br/Pb ratio which decreases with the age of the particle. The atmospheric concentrations of bromine and lead have decreased substantially since the introduction of unleaded gasoline, but the Br/Pb exhaust ratio has not changed considerably. In 1970, Wesolowski estimated that ratio to be 0.39. Based on the Los Angeles emissions inventory of Gray (1986) if 20% of the automobile fleet ran on leaded gasoline the exhaust ratio would remain 0.39. A low Br/Pb ratio accompanied by higher than normal lead concentrations prior to the onset of morning traffic indicates the retention of pollutants from the

previous day. Such information could prove useful in the interpretation of pollutant episodes.

EXPERIMENTAL

A manual sampler was used to collect ambient aerosol at a flow rate of 25 l/min between 0000 hours and 0500 hours daily on a Teflon filter (Gelman, ringed 2 μm pore, 47 mm) for analysis by X-ray fluorescence (XRF) for bromine and lead. The filter was downstream of a 2.5 μm cut-point impactor and was masked to 2.99 cm^2 to assure adequate loading. XRF analysis was performed by NEA, Inc. in Beaverton, Oregon. The average lead and bromine concentrations on the field blanks were subtracted from each sample. Because lead contamination was found on one blank, a measurement was made in the unexposed section of each sample filter to check for contamination. None was found. Uncertainties for bromine, lead, and Br/Pb were 8.6%, 7.5%, and 11.1% respectively, and detection limits were 0.2 ng/m^3 for bromine and 0.1 ng/m^3 for lead.

RESULTS

Plots of lead and Br/Pb for June, July, August, and Fall data are shown in Figures C.1 - C.4. The horizontal line is the average which was computed separately for summer data and for fall data. Concentrations of lead fall between 0.01 to 1.0 $\mu\text{g}/\text{m}^3$. In comparison, Hidy and Friedlander (1971) reported lead concentrations in Los Angeles ranging between 1.6 and 8 $\mu\text{g}/\text{m}^3$ between 1960 and 1966. The lower concentrations are probably the direct result of the

FIGURE C.1

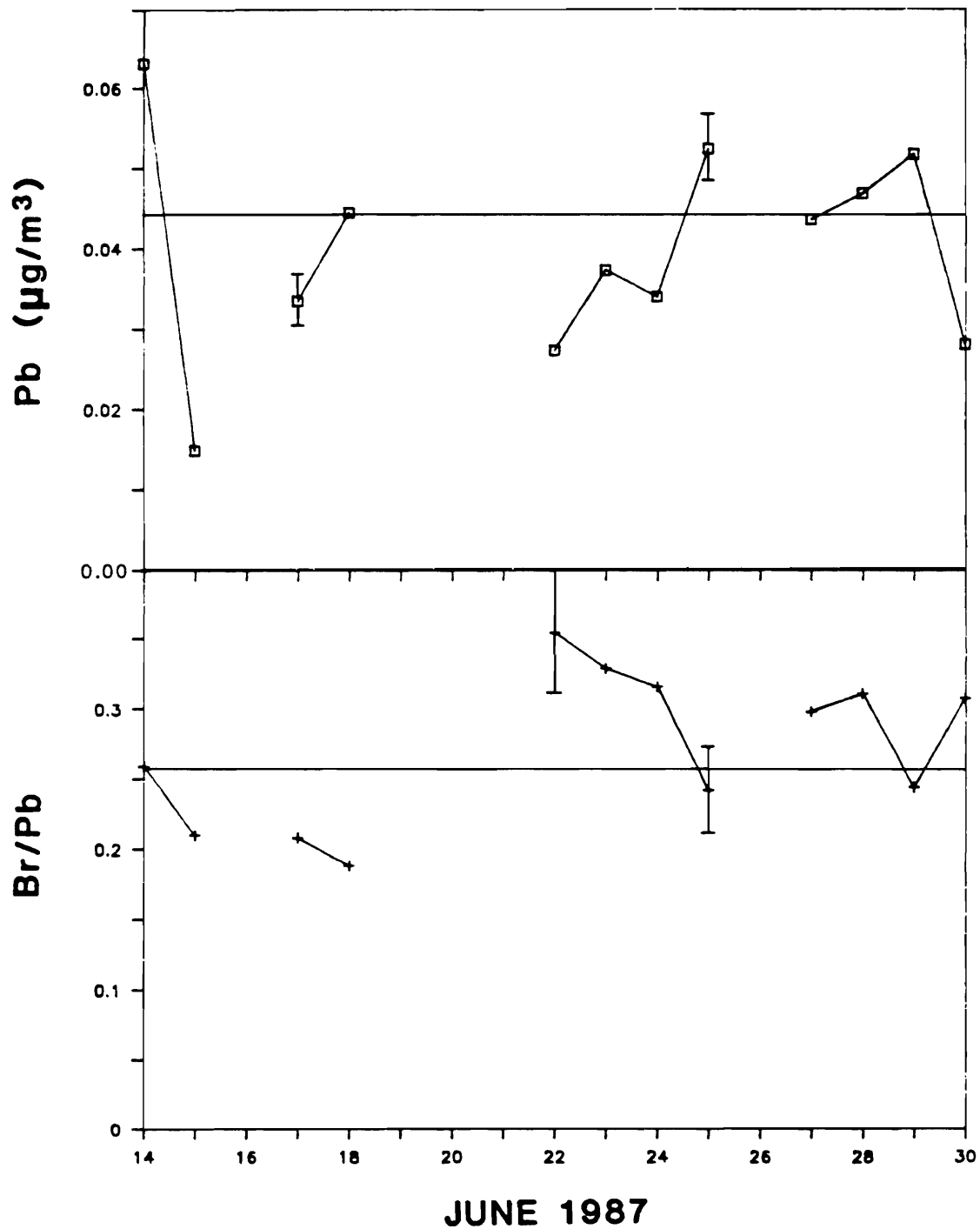


Figure C.1. Lead concentrations ($\mu\text{g}/\text{m}^3$) and bromine/lead ratios for particles under $2.5 \mu\text{m}$ in diameter at Claremont, California, June 1987. The horizontal line is the average computed for the summer data.

FIGURE C.2

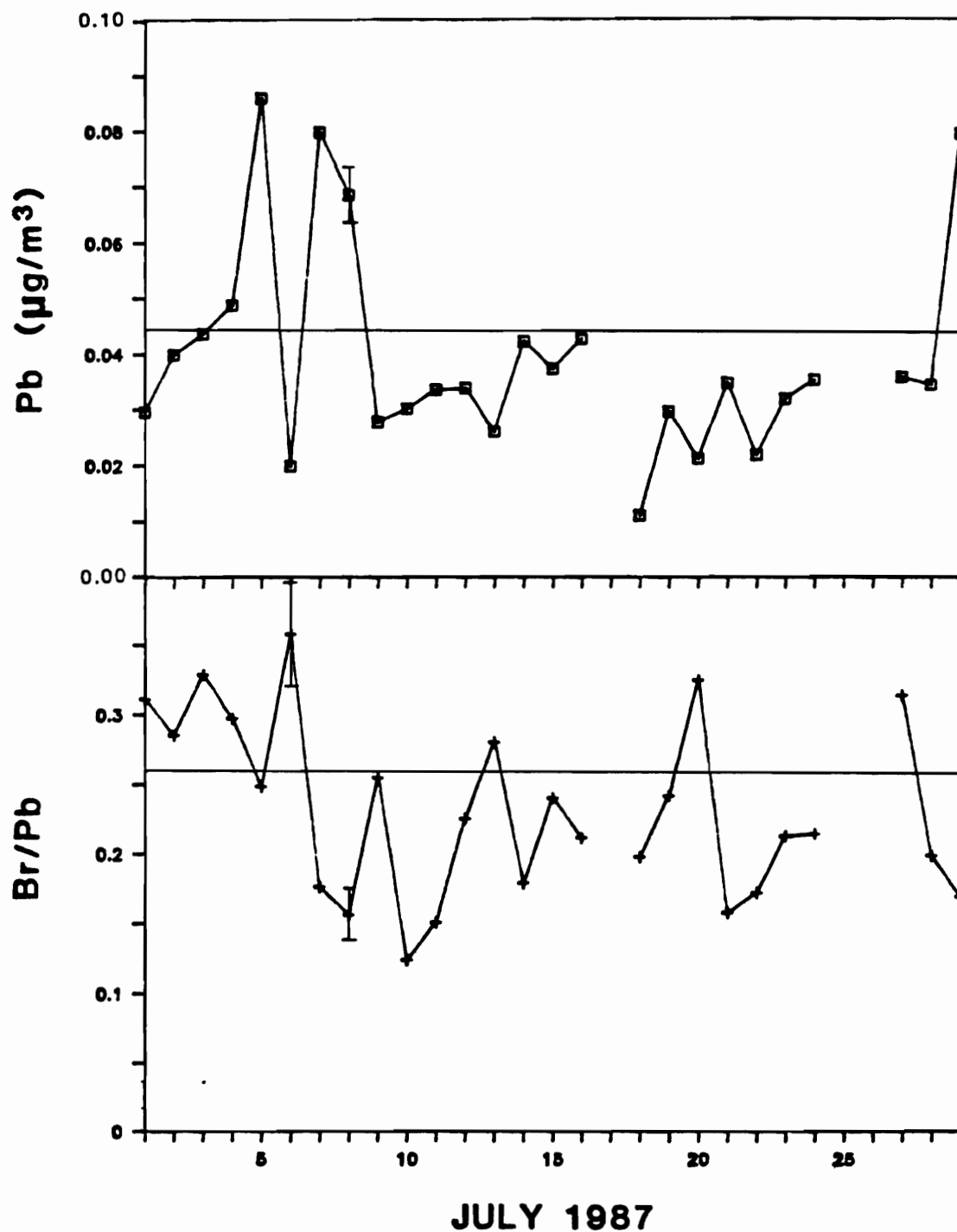


Figure C.2. Lead concentrations ($\mu\text{g}/\text{m}^3$) and bromine/lead ratios for particles under $2.5 \mu\text{m}$ in diameter at Claremont, California, July 1987. The horizontal line is the average computed for the summer data.

FIGURE C.3

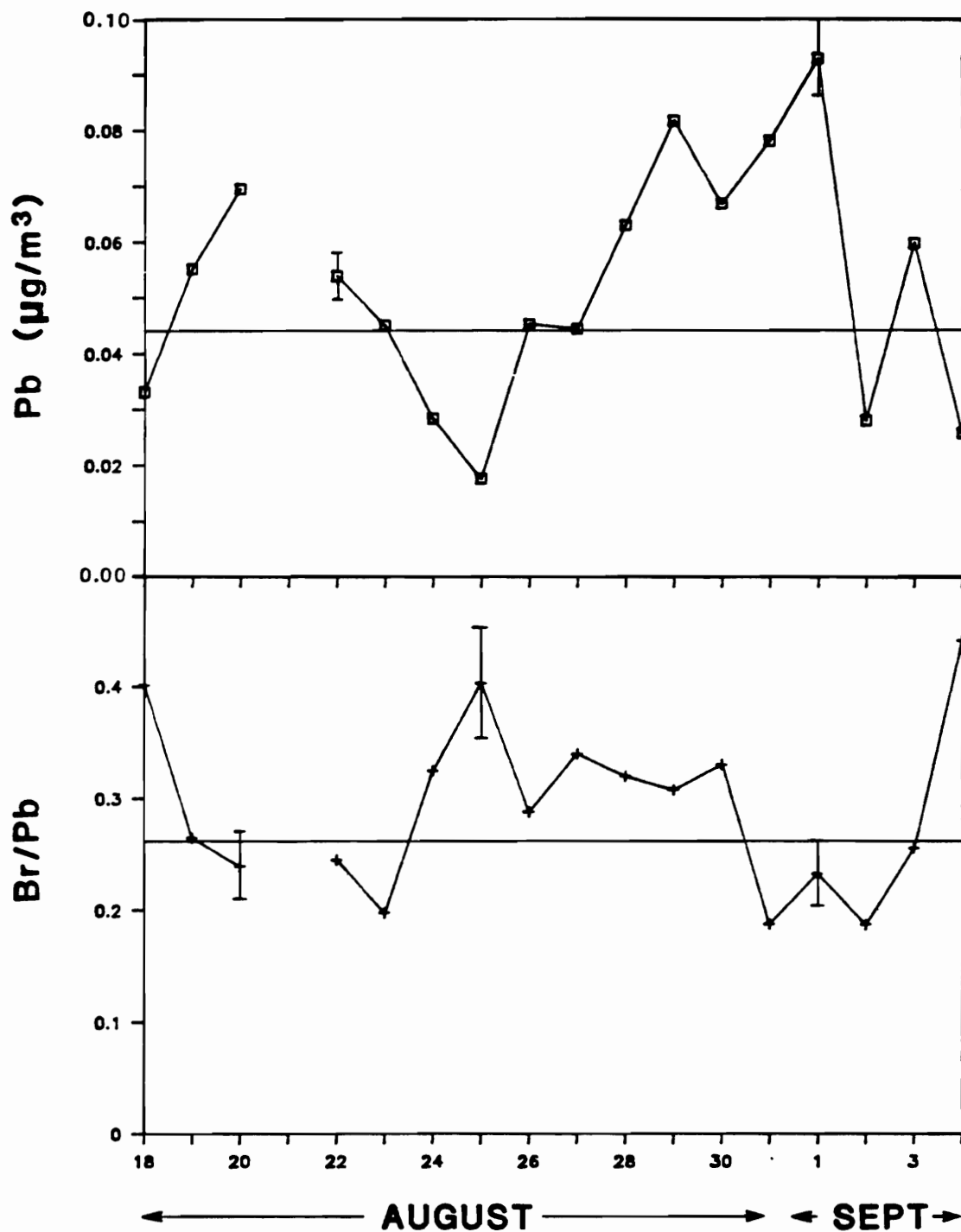


Figure C.3. Lead concentrations ($\mu\text{g}/\text{m}^3$) and bromine/lead ratios for particles under $2.5 \mu\text{m}$ in diameter at Claremont, California, August and September, 1987. The horizontal line is the average computed for the summer data.

FIGURE C.4

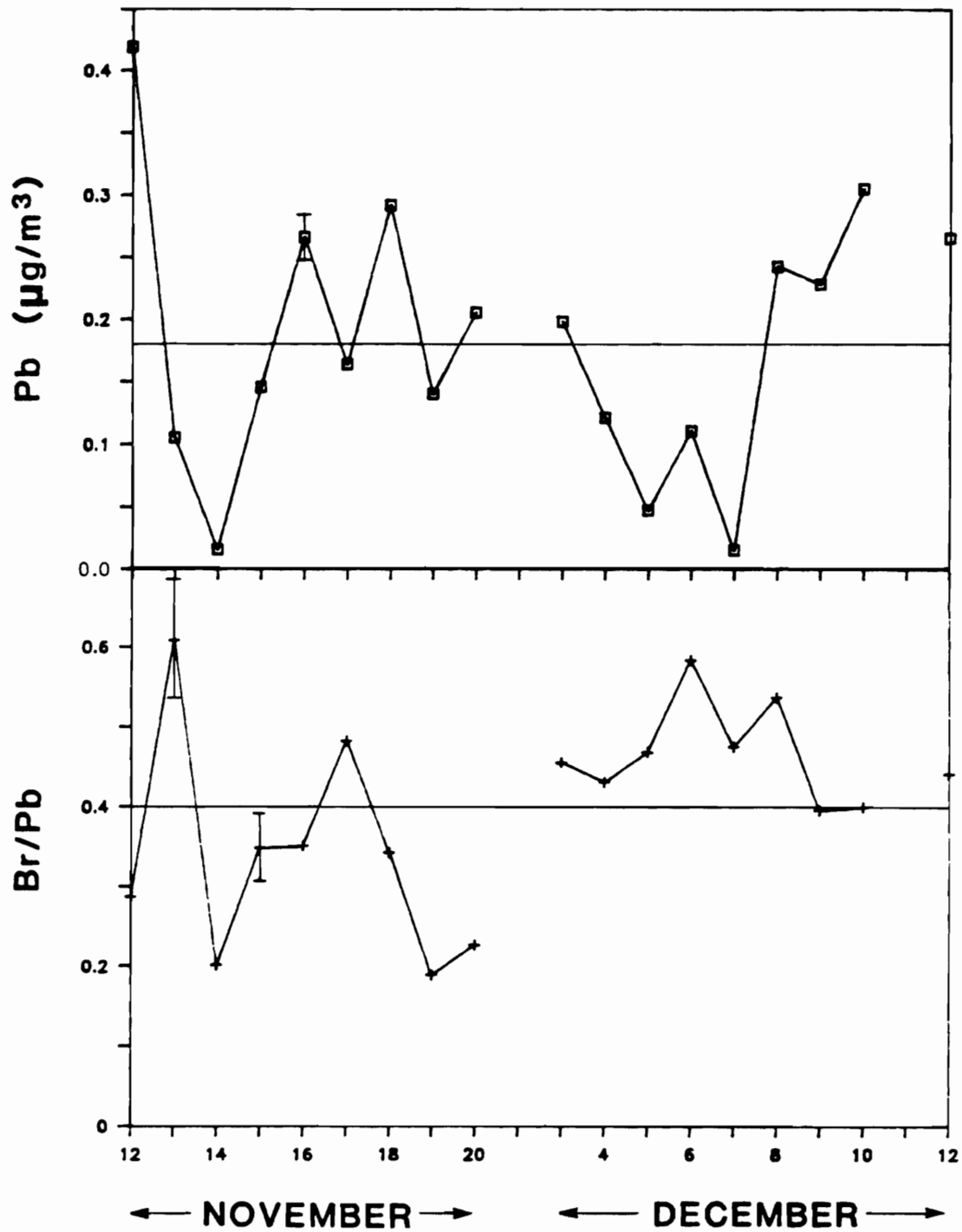


Figure C.4. Lead concentrations ($\mu\text{g}/\text{m}^3$) and bromine/lead ratios for particles under $2.5 \mu\text{m}$ in diameter at Long Beach, California, November and December, 1987. The horizontal line is the average computed for the fall data.

conversion of a large fraction of the automobile fleet to unleaded fuel. Average concentrations of bromine, lead, and Br/Pb are substantially higher at Long Beach in the fall than at Claremont in the summer. Higher concentrations are to be expected in a source-dominated area like Long Beach. Note that Long Beach Br/Pb ratios are often much higher than the estimated exhaust ratio. This is probably due to the contribution of the marine aerosol which contains bromine. The days in which lead concentrations and Br/Pb ratios indicate retention from previous days are listed in Table C.1.

TABLE C.1. RETENTION OF POLLUTANTS FROM PREVIOUS DAYS AS INDICATED BY LEAD AND BR/PB

Parentheses indicate days in which the criteria were satisfied but the lead concentration or Br/Pb ratio fell within one standard error of the mean.

June 25, 28

July 5, 7, 8, 29

August 20, 22, 31 (23)

September 1, 3

November 12, 16, 18 (20)

December (9, 10)

APPENDIX D: DATA VALIDATION TESTS FOR SCAQS IN SITU DATA

This appendix defines specific data validation checks which have been performed on the in situ carbon data collected by the Oregon Graduate Center and suggests others which could be done. Validation codes and comments are included. All measurements are valid (V1) unless otherwise noted. Data which are qualified (Q1) or suspect (S1) were included in the graphs of Appendix E and the table of Appendix D, but suspect data were not used in the data interpretation.

LEVEL I VALIDATIONS:

The individual analyses were all examined for unusual behavior. Throughout each analysis the transmittance of He-Ne laser light through the filter, the oven temperature, and the flame ionization detector (FID) signal were all plotted. By examining these plots samples with elemental carbon loadings too low to quantitatively determine the organic carbon (OC) - elemental carbon (EC) split and samples which overloaded the FID were identified, and these data were removed from the data set. On four fall nights enough water vapor collected on the sampling filters to affect the optical transmittance. A correction was made for this affect. This and all other unusual behavior are reported in the validation comments in Table D.1.

Total carbon (TC), OC, and EC concentrations were entered into the spreadsheet individually, and the sums (OC+EC) were compared to the entered

TABLE D.1. LEVEL I VALIDATION

Date	Start	Through	Code	Comments
19-June	18:23	19:44	S1(OC,EC)	OC/EC split suspect
30-June	15:19	17:40	S1(OC,EC)	outlier, split vs EC
30-June	18:19	20:40	S1(OC,EC)	outlier, split vs EC
4-July	21:24	23:45	S1(OC,EC)	outlier, split vs EC
5-July	00:24	02:45	S1(OC,EC)	outlier, split vs EC
5-July	03:24	05:45	S1(OC,EC)	outlier, split vs EC
19-July	06:32	11:52	S1(O,E,TC)	very brief signal overload possible
16-July	22:21	23:42	S1(OC,EC)	uncertainty in split due to low loading
17-Jul	00:21	07:42	I1(OC,EC)	loading too low to get good OC-EC split
23-Aug	14:19	15:40	S1(OC,EC)	uncert. spl., low load.
25-Aug	04:19	05:40	S1(OC,EC)	outlier, split vs EC uncert. spl., low load.
1-Sept	22:23	23:44	S1(OC,EC)	uncert. spl., low load.
2-Sept	00:23	01:44	S1(OC,EC)	uncert. spl., low load.
2-Sept	02:23	03:44	S1(OC,EC)	uncert. spl., low load.
2-Sept	12:24	13:44	S1(OC,EC)	uncert. spl., low load.
2-Sept	14:23	15:43	S1(OC,EC)	uncert. spl., low load.
8-Nov	04:00	05:21	Q1(OC,EC)	water vapor affected laser, correction made
10-Nov	23:21	00:02	Q1(OC,EC)	water vapor (see above)
16-Nov	05:50	09:21	S1(OC,EC)	heavy loading, OC/EC split inaccurate
18-Nov	02:24	03:45	Q1(OC,EC)	water vapor (see above)
2-Dec 20:19 - 3-Dec 13:43			Q1(OC,EC)	water vapor (see above)
3-Dec 18:19 - 5-Dec 21:41			S1(O,E,TC)	adsorbed vapor estimate is high (by < 10%) therefore total OC fine, but particulate OC (OC-ads.vap) is low
8-Dec	00:35	09:41	S1(O,E,TC)	ads. vap. (see above)

TC values to check for typographical errors and errors in spreadsheet data manipulations. Graphs of optical absorbance vs elemental carbon loading (μg) prepared for each study month, and graphs of the OC-EC split time vs EC loading were used to identify outliers. Monthly graphs of the data were also visually inspected to screen for unusual temporal behavior.

LEVEL II VALIDATION:

A comparison of OGC and Ford elemental carbon concentrations for summer intensives has been performed. Two hour averages of Ford's photoacoustic spectrophone data were compared with 80 minute average concentrations from the OGC carbon analyzer. Care was taken only to include samples with identical midpoints to minimize scatter resulting from the difference in sampling times. The agreement was quite good, and a t-test showed no significant difference between the two sets with 95% confidence intervals. No outliers were observed.

Comparisons with other elemental carbon and particulate total carbon (corrected for adsorption) data sets should be performed although it should be remembered that large disagreement between methods exists as evidenced in the Carbonaceous Species Method Comparison Study. A plot of EC vs CO would also be a useful check because EC and CO are both primary combustion products.

APPENDIX E. SCAQS ORGANIC CARBON, ELEMENTAL CARBON, AND OZONE CONCENTRATIONS WITH METEOROLOGICAL DATA AT CLAREMONT, CALIFORNIA, JUNE 12 - SEPTEMBER 2, 1987 AND AT LONG BEACH, CALIFORNIA, NOVEMBER 6 - DECEMBER 13, 1987.

The meteorological symbols used throughout this appendix are described in Figures E.1 - E.4 and are taken from Neiburger et al. (1982). Changes in wind direction are indicated by a symbol positioned at the time the change in direction occurred. The wind direction arrow extends toward the direction from which the wind is blowing. Visibility is indicated in kilometers and is omitted when visibility is greater than 16 km. The current air temperature and temperature of dewpoint are provided in Fahrenheit.

Data are plotted in three day segments on a horizontally divided graph in Figures E.5 - E.32. Organic carbon (OC) and elemental carbon (EC) concentrations ($\mu\text{gC}/\text{m}^3$) are plotted in the lower section at the mid-point of each sampling period. One hour average ozone concentrations (pphm) are plotted in the upper section at the mid-point of each sampling period. The federal standard for ozone is 12 pphm as a one hour average, and a first stage smog alert is called at one hour average ozone concentrations above 20 pphm.

FIGURE E.1



EXPLANATION OF SYMBOLS

N	Total amount of cloud cover (see Figure D 2)
dd	True direction from which wind is blowing Plotted as the shaft of an arrow extending from the circle toward the direction from which the wind is blowing
ff	Wind speed plotted as feathers and half-feathers representing 10 and 5 knots, respectively, on the shaft of the wind direction arrow (see Figure D 3)
VV	Visibility in kilometers. Values higher than 16 km (10 miles) are omitted from map
ww	Present weather coded in symbols taken from Figure D.4.
RH	Relative humidity in %.
TT	Current air temperature in Fahrenheit.
T _d T _d	Temperature of dewpoint in Fahrenheit

Figure E.1. Explanation of meteorological symbols.

FIGURE E.2

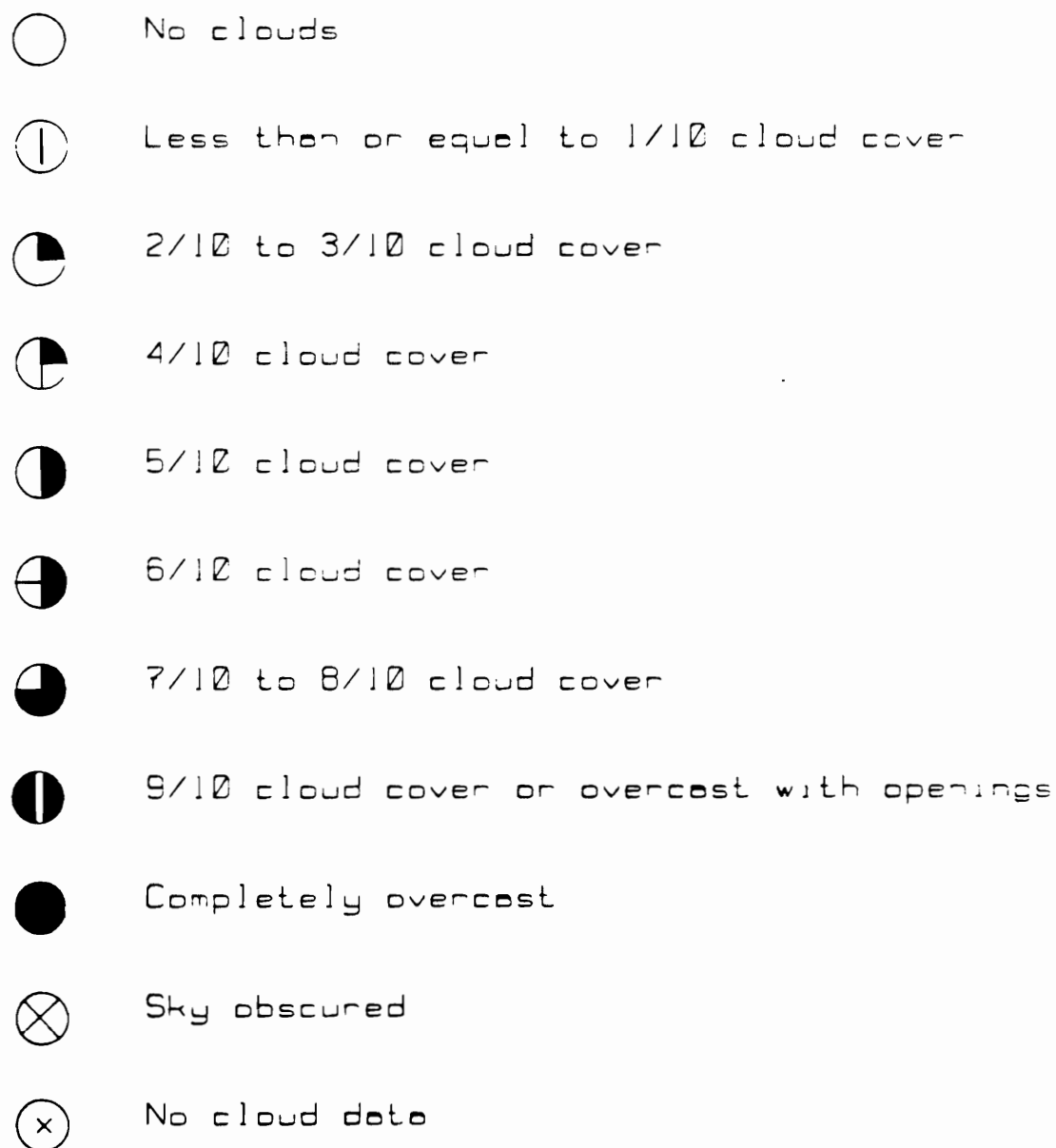
**Figure E.2. Total amount of sky coverage (N).**

FIGURE E.3








	KNOTS	MILES/HOUR (statute)	KILOMETERS/HOUR
	Calm	Calm	Calm
	1-2	1-2	2-4
	3-7	3-8	5-13
	8-12	9-14	14-23
	13-17	15-20	24-32
	18-22	21-25	33-41
	23-27	26-31	42-50

Figure E.3. Wind speed symbols (ff).

FIGURE E.4

- , Intermittent drizzle (not freezing). slight
at time of observation
- ,, Continuous drizzle (not freezing). slight
at time of observation
- ,, Intermittent drizzle (not freezing) moderate
at time of observation
- ,, Continuous drizzle (not freezing). moderate
at time of observation
- ,, Intermittent drizzle (not freezing). heavy
at time of observation
- Intermittent rain (not freezing). slight
at time of observation
- Continuous rain (not freezing). slight
at time of observation
- Continuous rain (not freezing). moderate
at time of observation
- Intermittent rain (not freezing). heavy
at time of observation

Figure E.4. Precipitation symbols (present weather (ww)).

FIGURE E.5

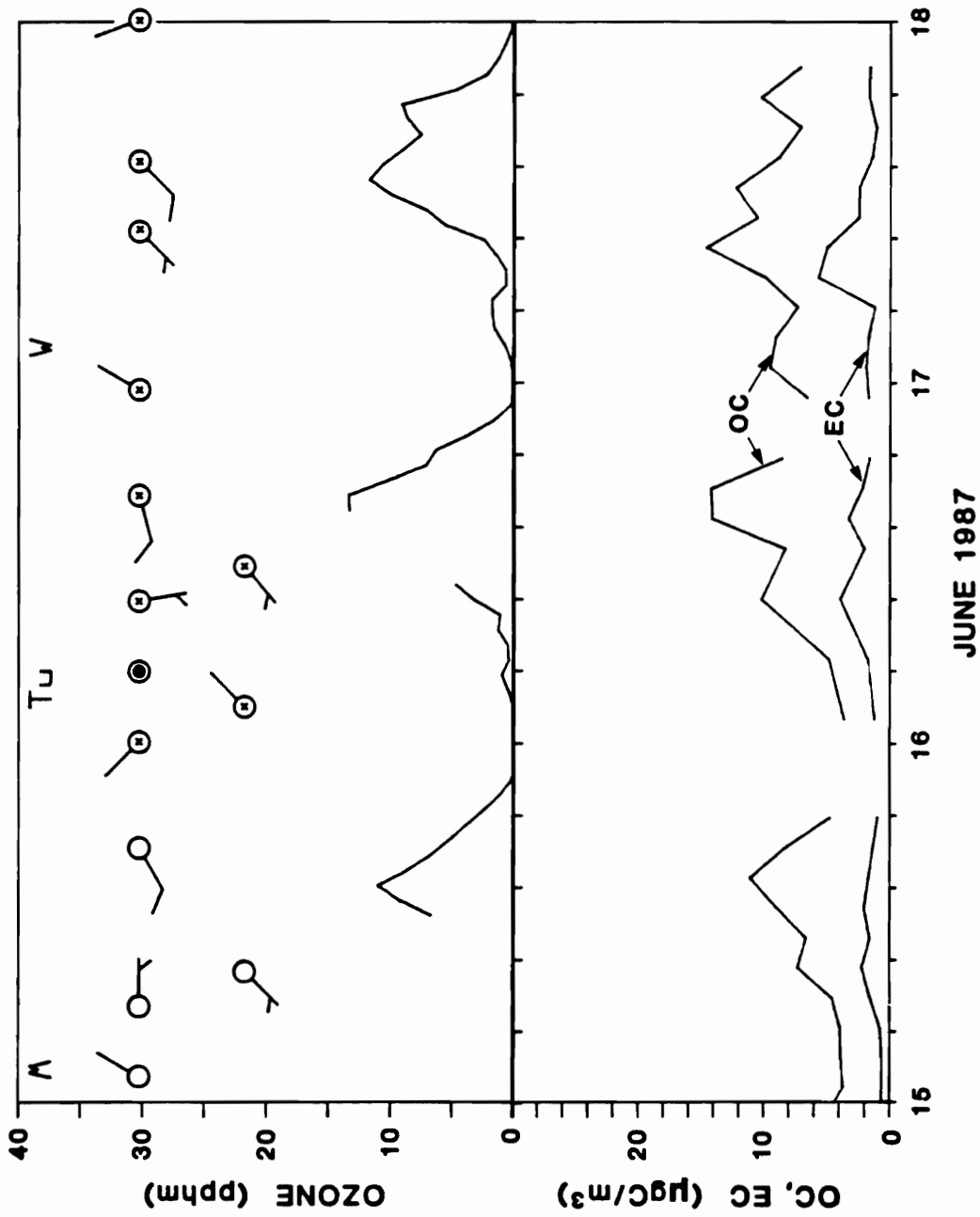


Figure E.5. OC, EC, ozone and meteorological data June 15-17, 1987 in Claremont, California. (Ozone data were not available between 0000 and 1200 hours, June 15.)

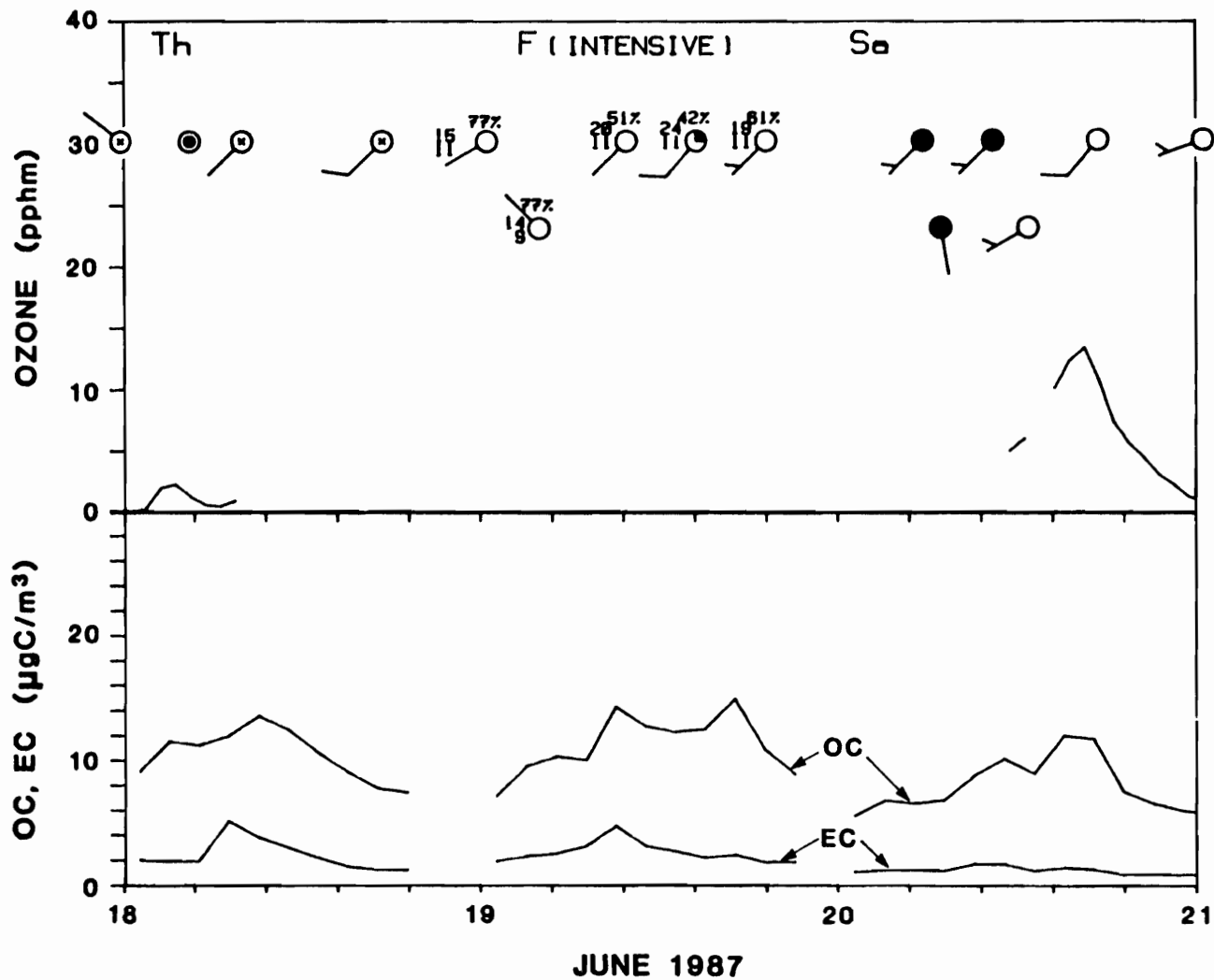


Figure E.6. OC, EC, ozone and meteorological data June 18-20, 1987 in Claremont, California. (Ozone data were not available between 0800 hours, June 18 and 1000 hours, June 20.)

FIGURE E.6

FIGURE E.7

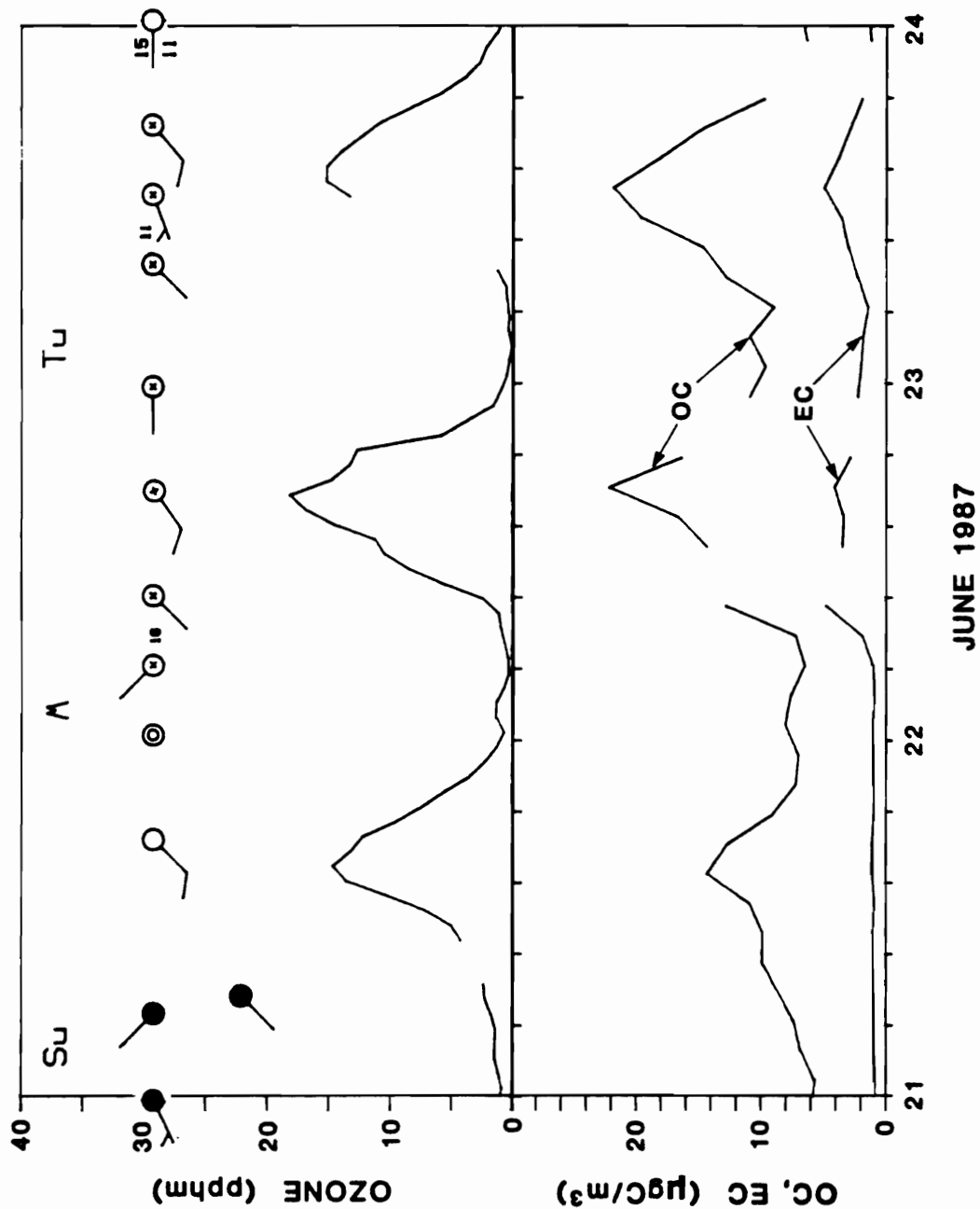


Figure E.7. OC, EC, ozone and meteorological data June 21-23, 1987 in Claremont, California.

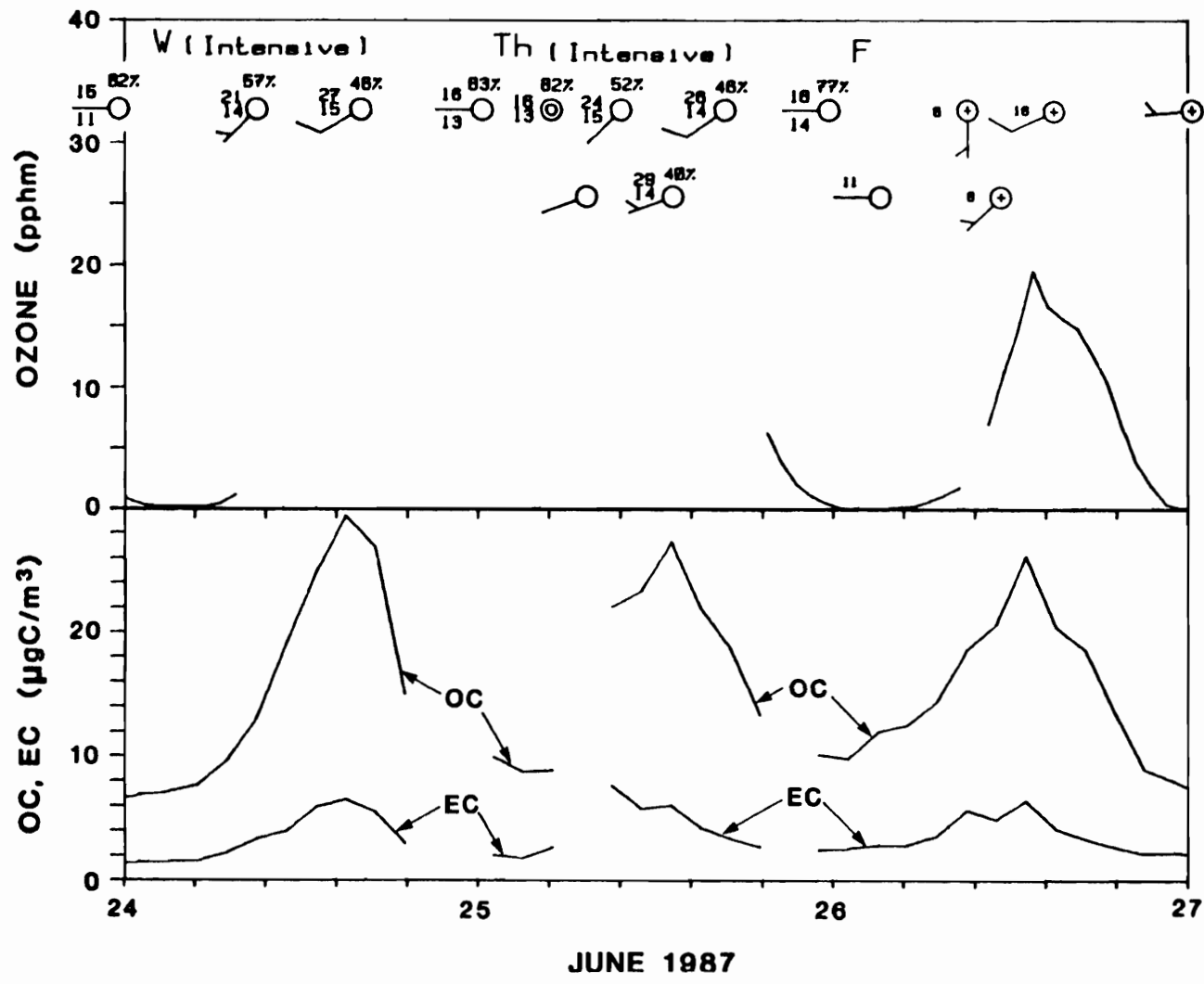


Figure E.8. OC, EC, ozone and meteorological data June 24-26, 1987 in Claremont, California. (Ozone data were not available between 0800 hours, June 24 and 1800 hours, June 25.)

FIGURE E.8

FIGURE E.9

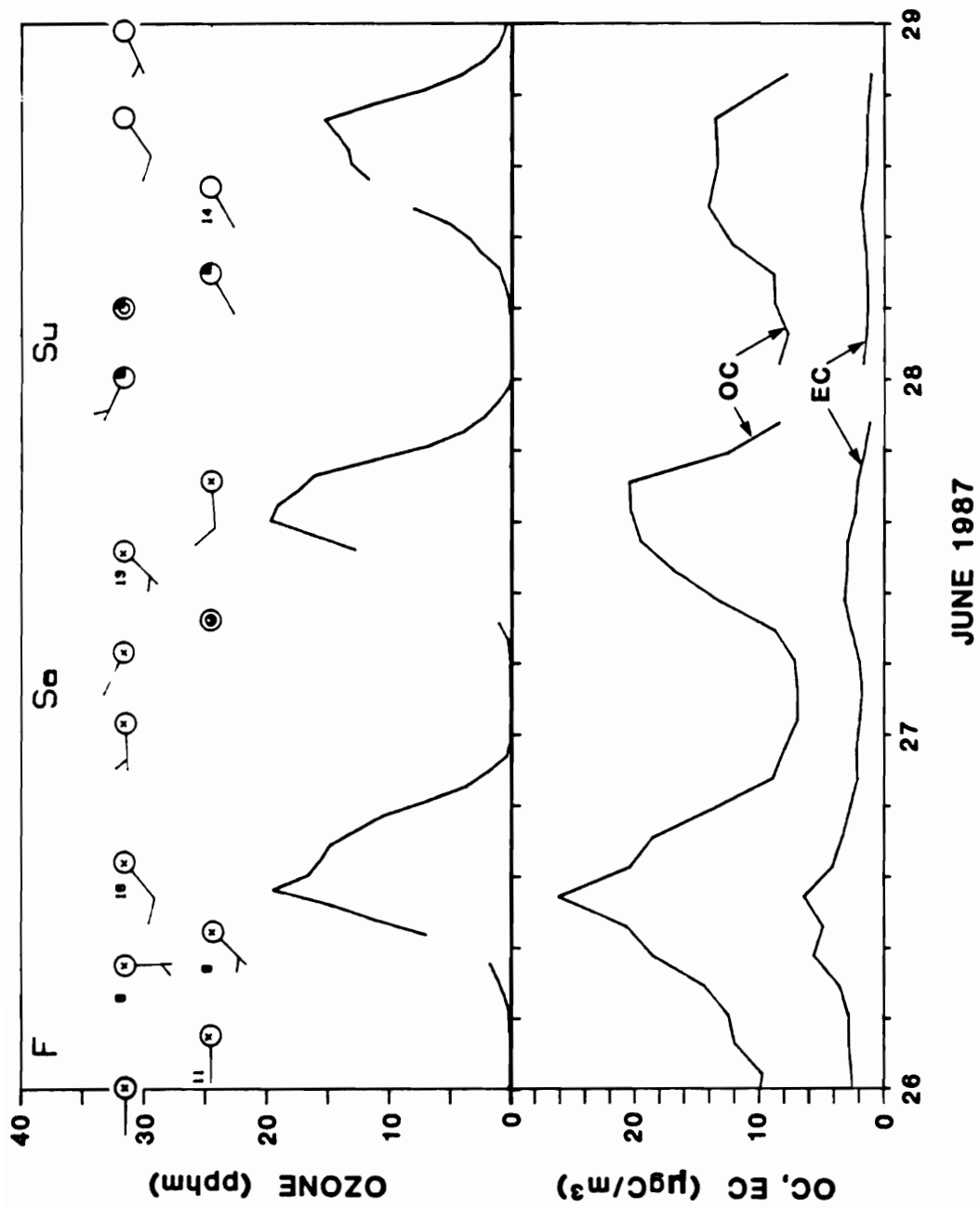
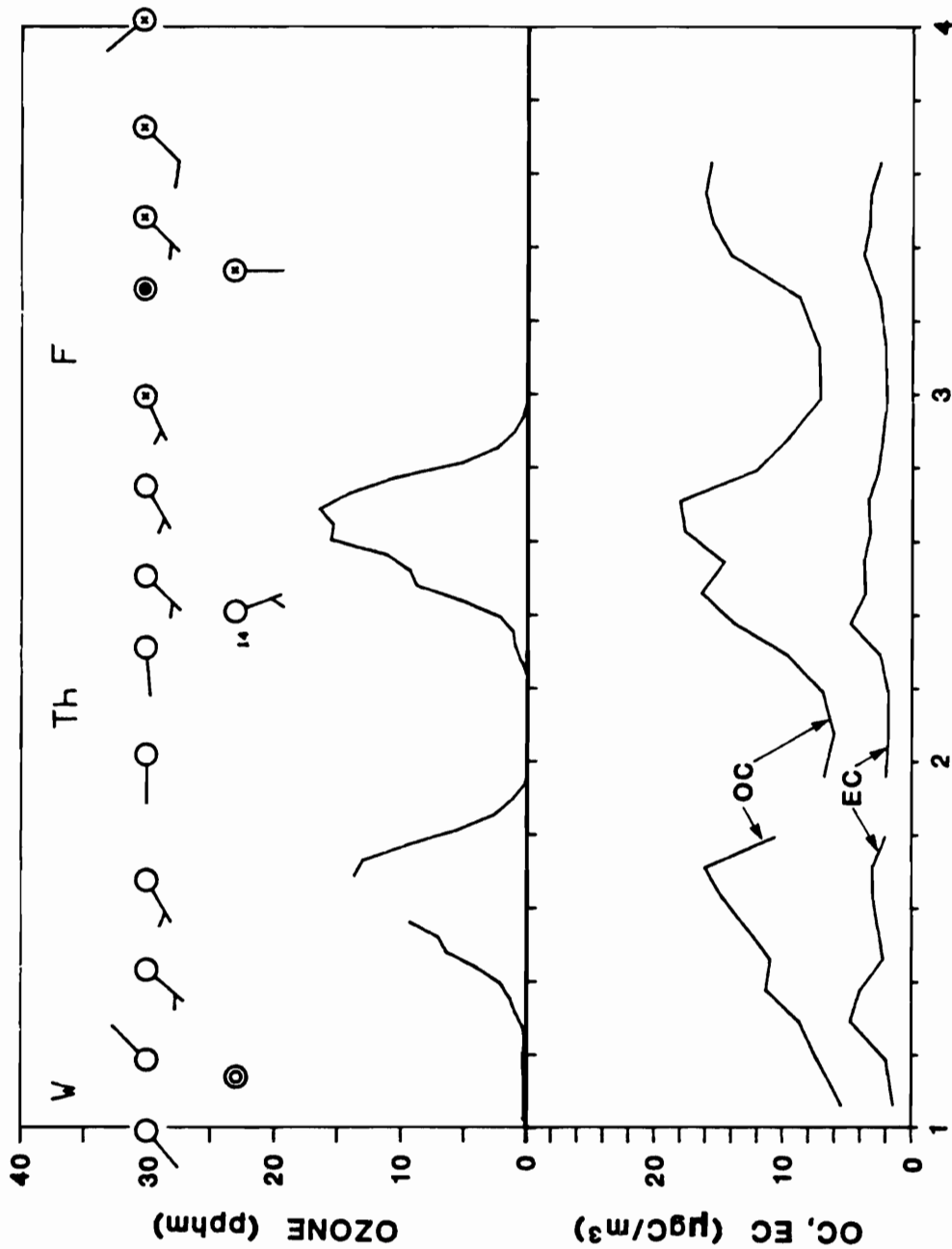


Figure E.9. OC, EC, ozone and meteorological data June 26-28, 1987 in Claremont, California.

FIGURE E.10



JULY 1987

Figure E.10. OC, EC, ozone and meteorological data July 1-3, 1987 in Claremont, California. (Ozone data were not available between 0100 hours, July 3 and 0000 hours, July 4.)

FIGURE E.11

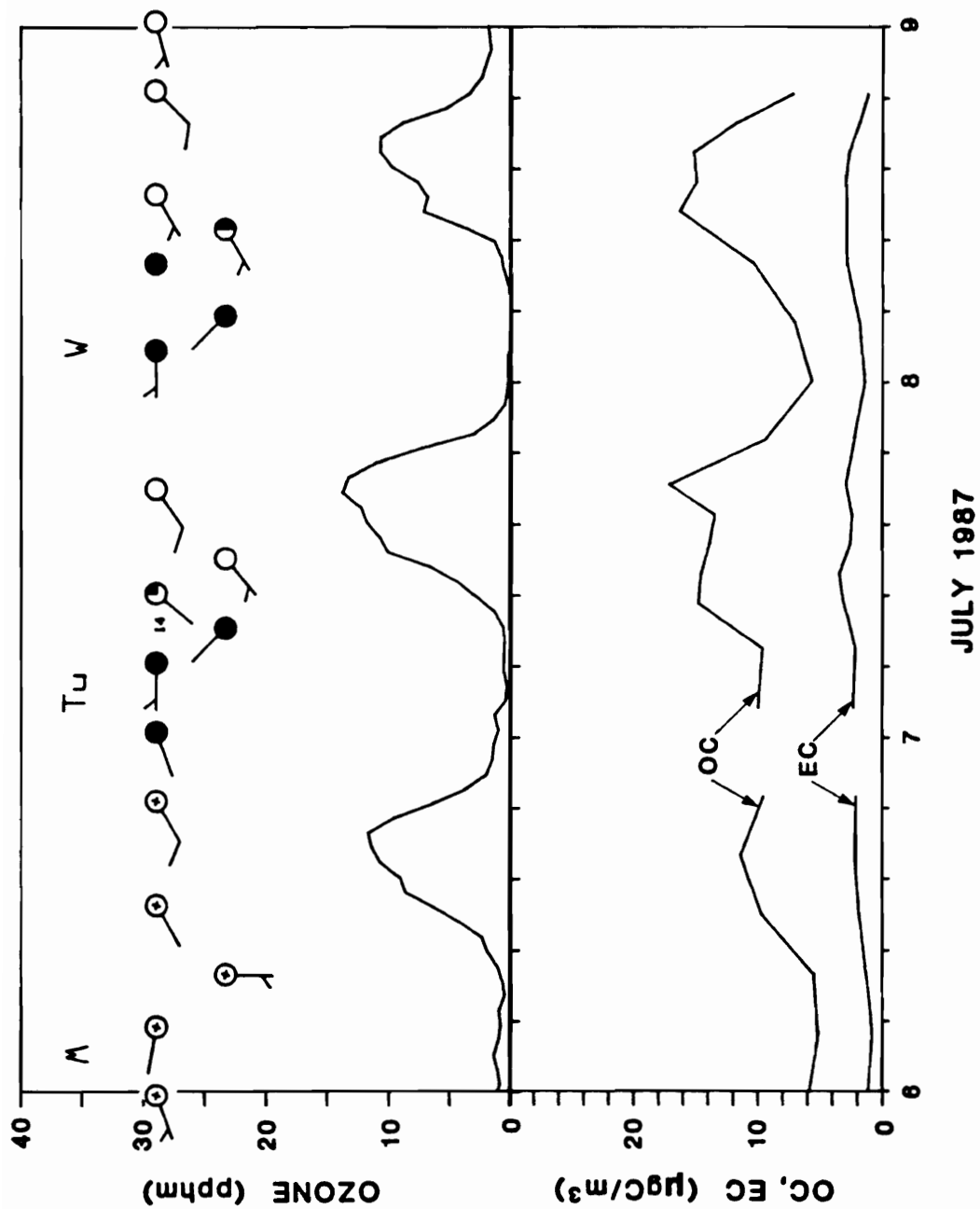


Figure E.11. OC, EC, ozone and meteorological data July 6-8, 1987 in Claremont, California.

FIGURE E.12

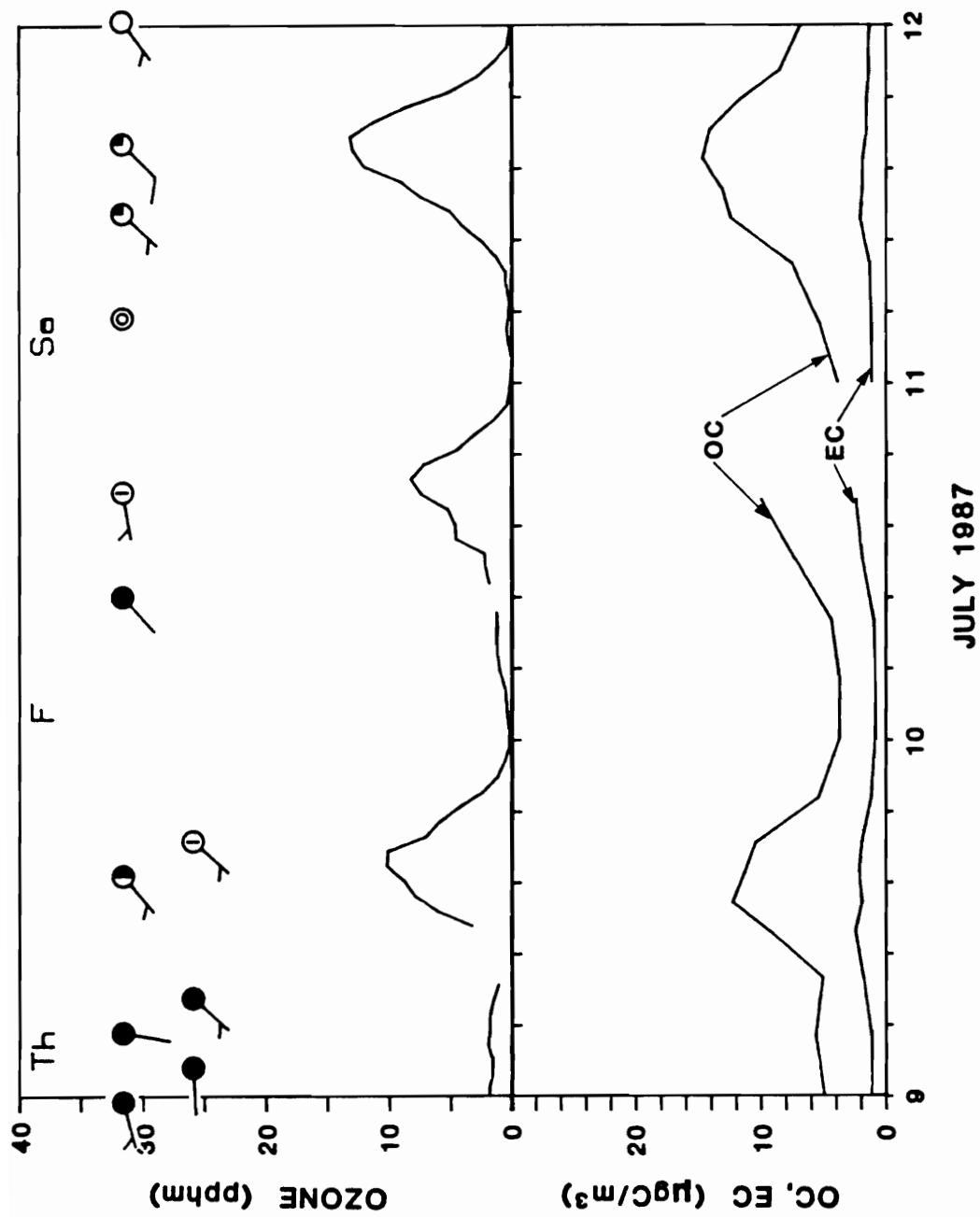


Figure E.12. OC, EC, ozone and meteorological data July 9-11, 1987 in Claremont, California.

FIGURE E.13

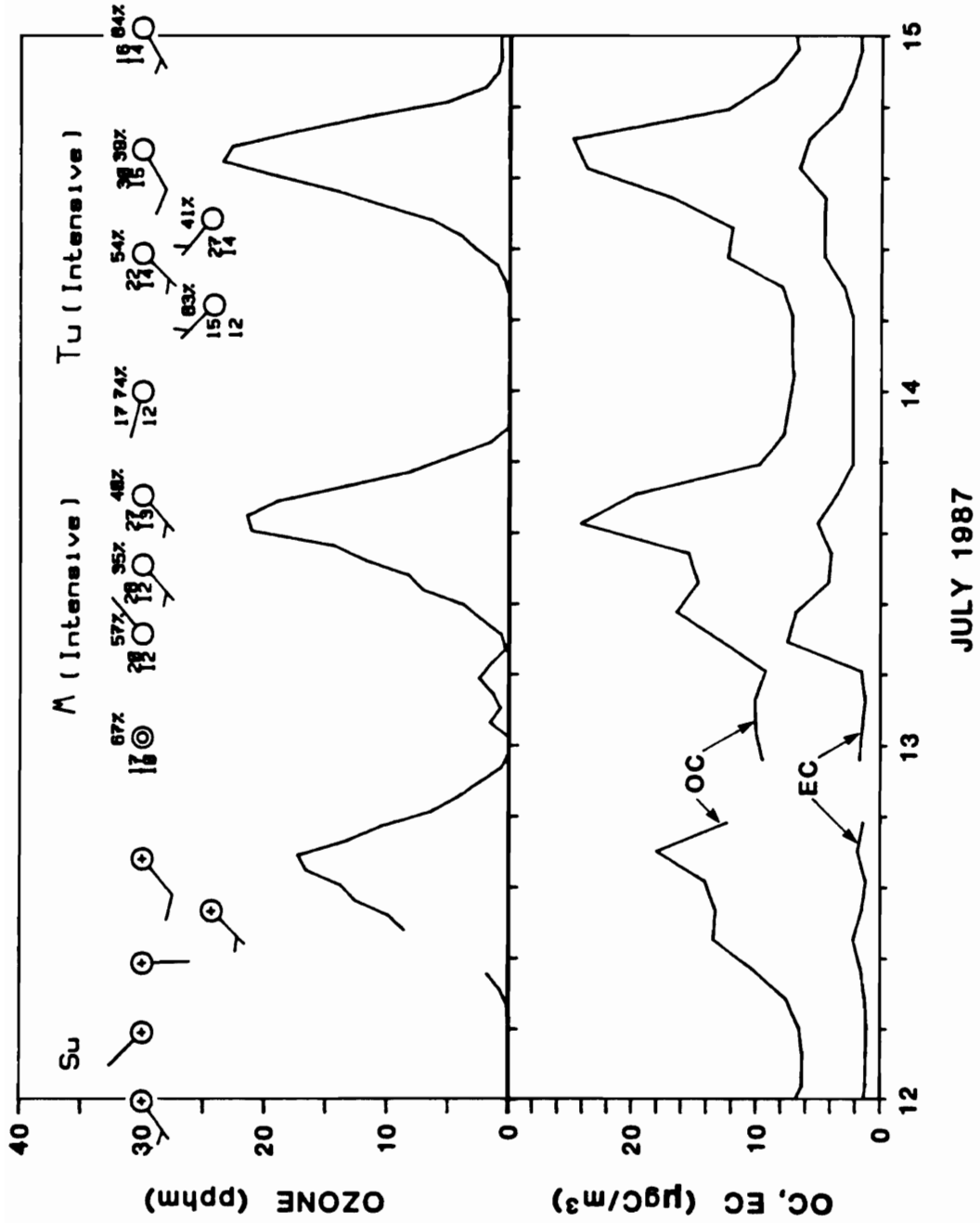


Figure E.13. OC, EC, ozone and meteorological data July 12-14, 1987 in Claremont, California.

FIGURE E.14

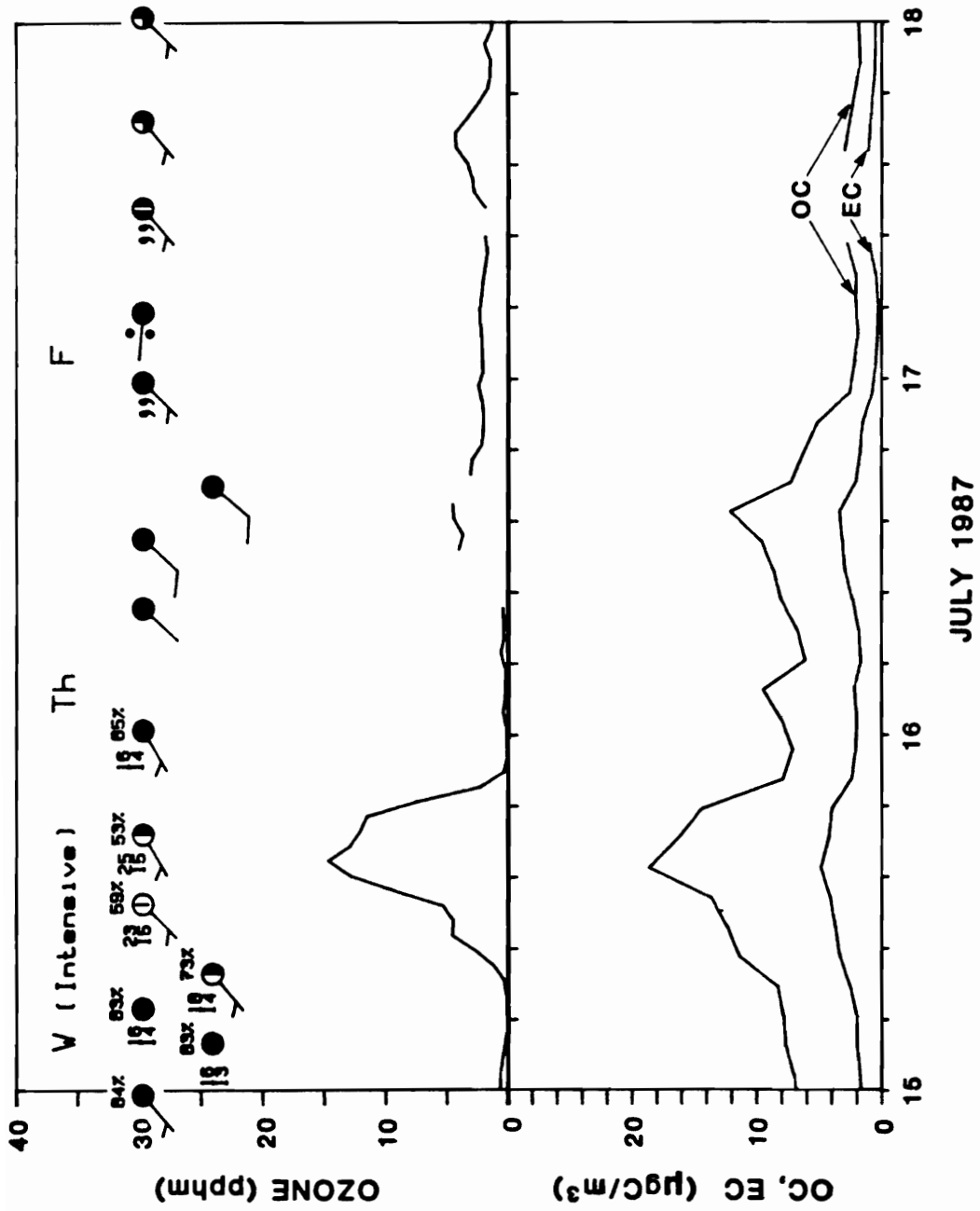


Figure E.14. OC, EC, ozone and meteorological data July 15-17, 1987 in Claremont, California.

FIGURE E.15

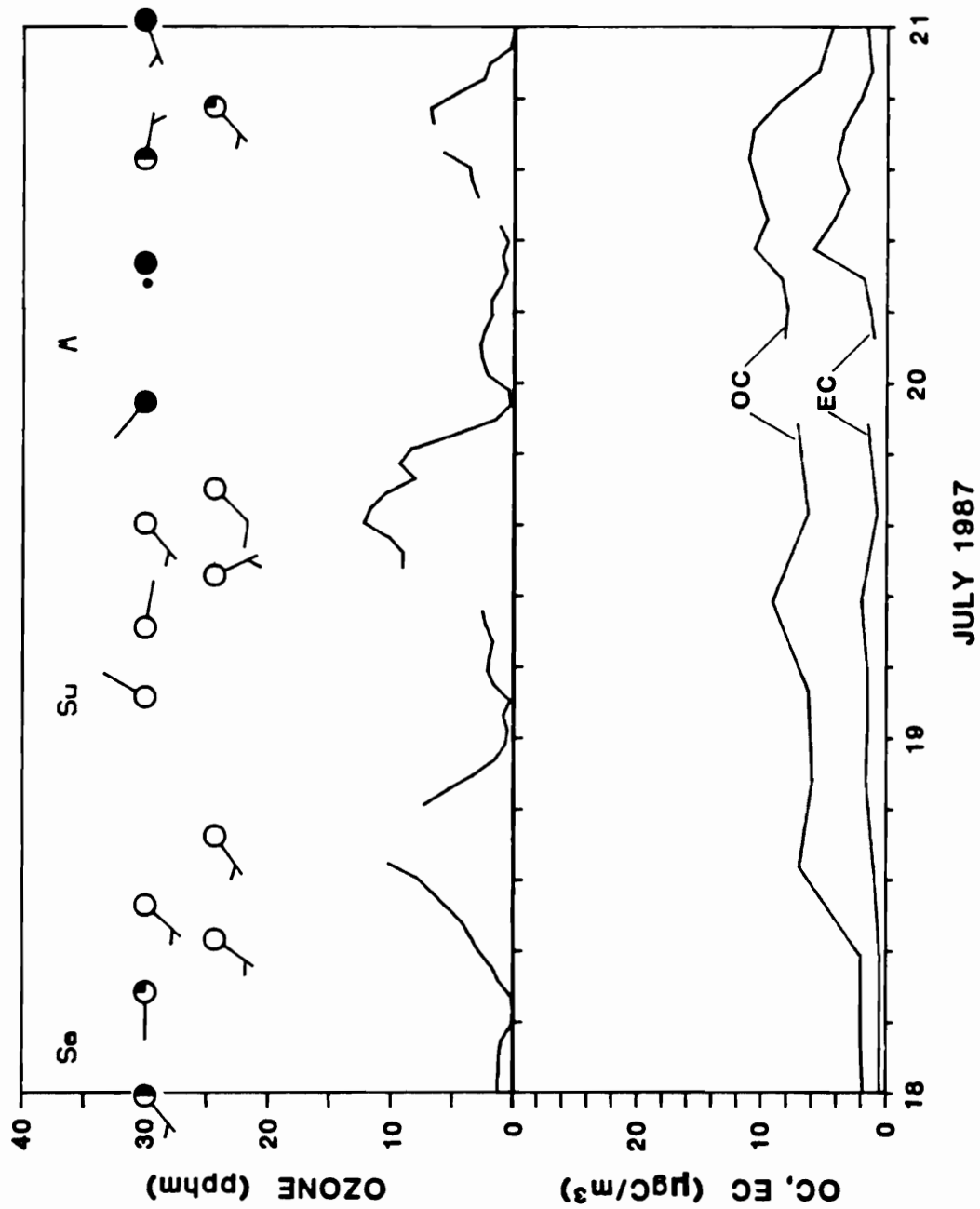


Figure E.15. OC, EC, ozone and meteorological data July 18-20, 1987 in Claremont California.

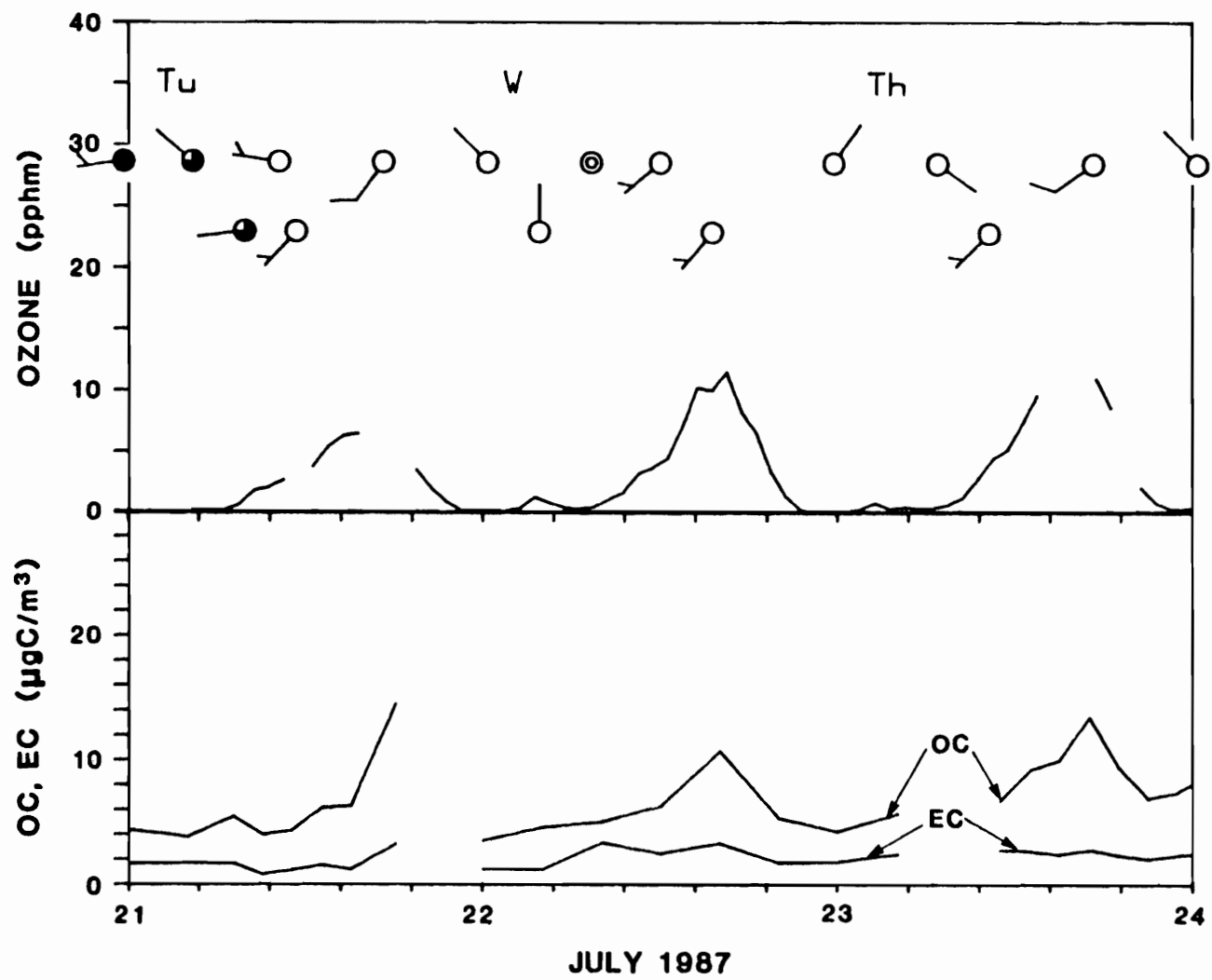


Figure E.16. OC, EC, ozone and meteorological data July 21-23, 1987 in Claremont, California.

FIGURE E.16

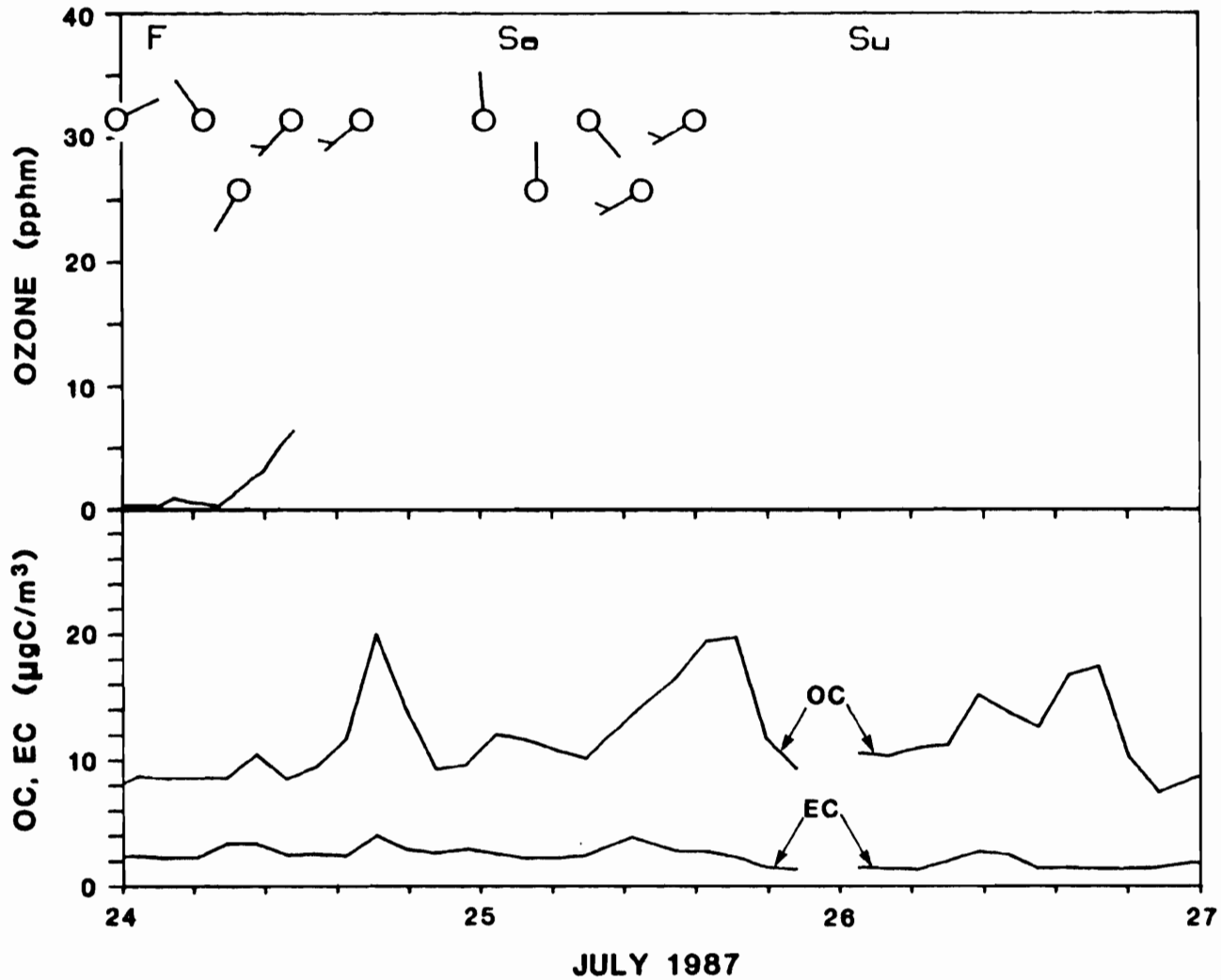


Figure E.17. OC, EC, ozone and meteorological data July 24-26, 1987 in Claremont, California. (Ozone data were not available between 1200 hours, July 24 and 0000 hours, July 27.)

FIGURE E.18

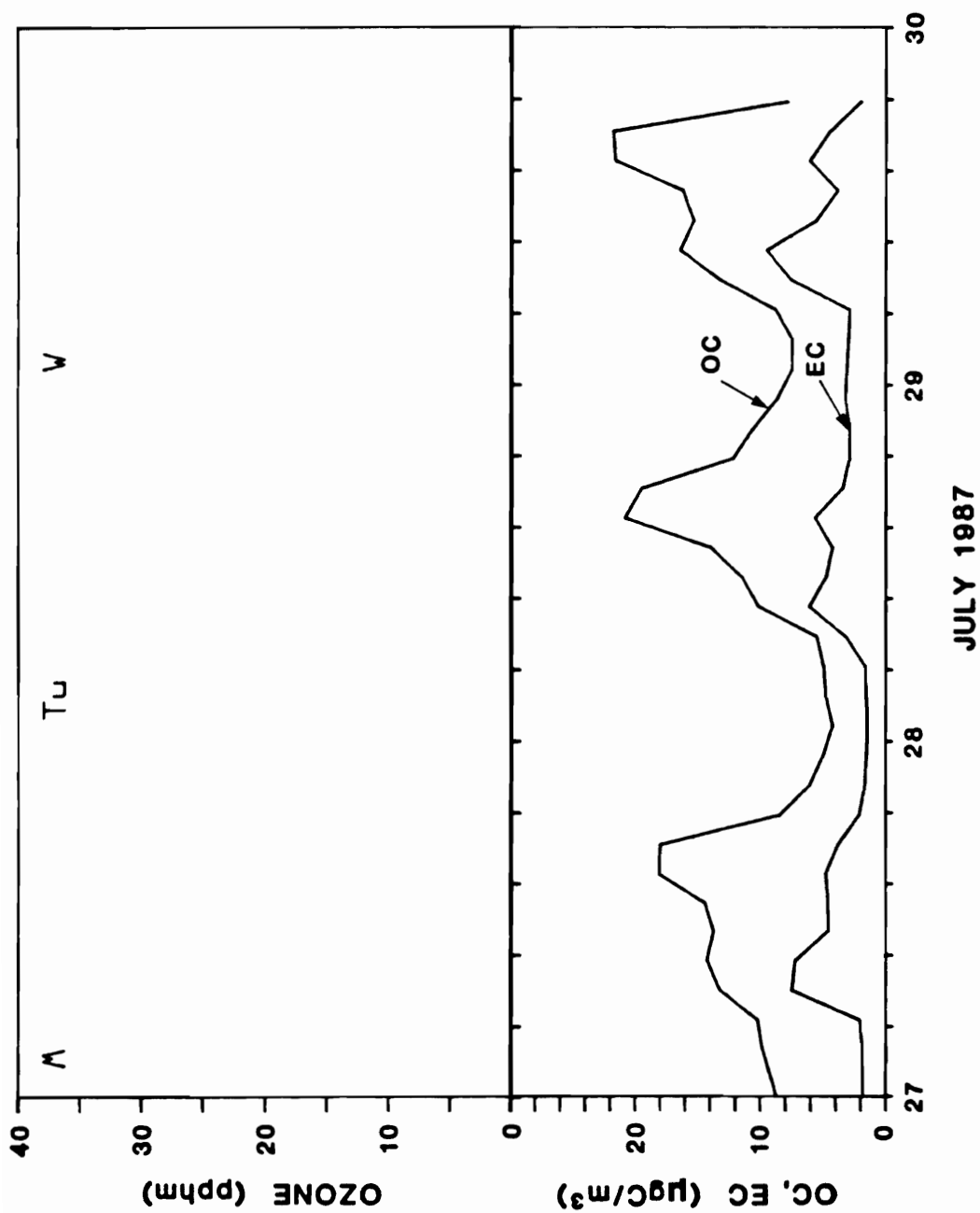


Figure E.18. OC, EC, ozone and meteorological data July 27-29, 1987 in Claremont, California. (Ozone concentrations were not available during this period.)

FIGURE E.19

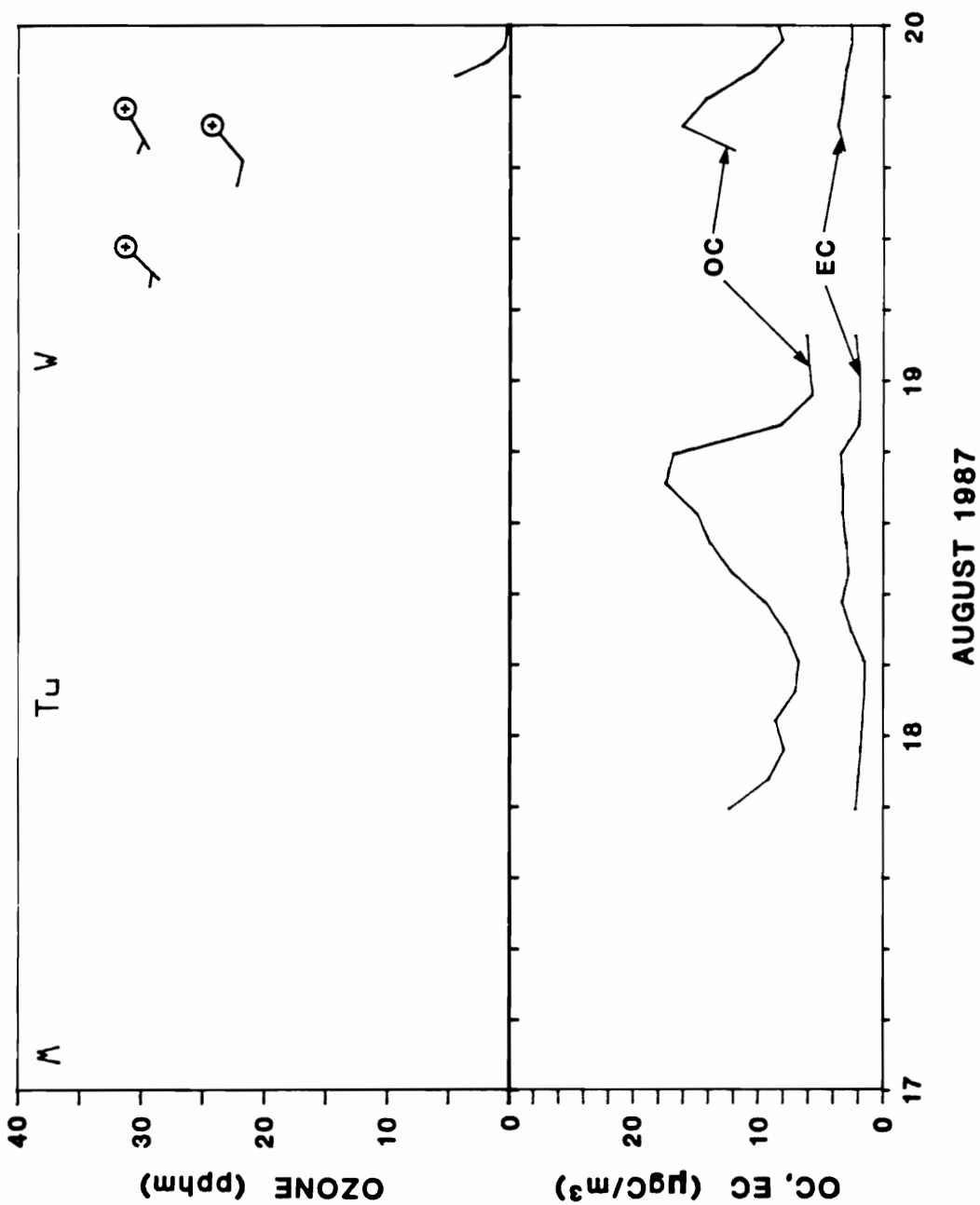


Figure E.19. OC, EC, ozone and meteorological data August 17-19, 1987 in Claremont, California. (Ozone data were not available between 0000 hours, Aug. 17 and 1900 hours, Aug. 19.)

FIGURE E.20

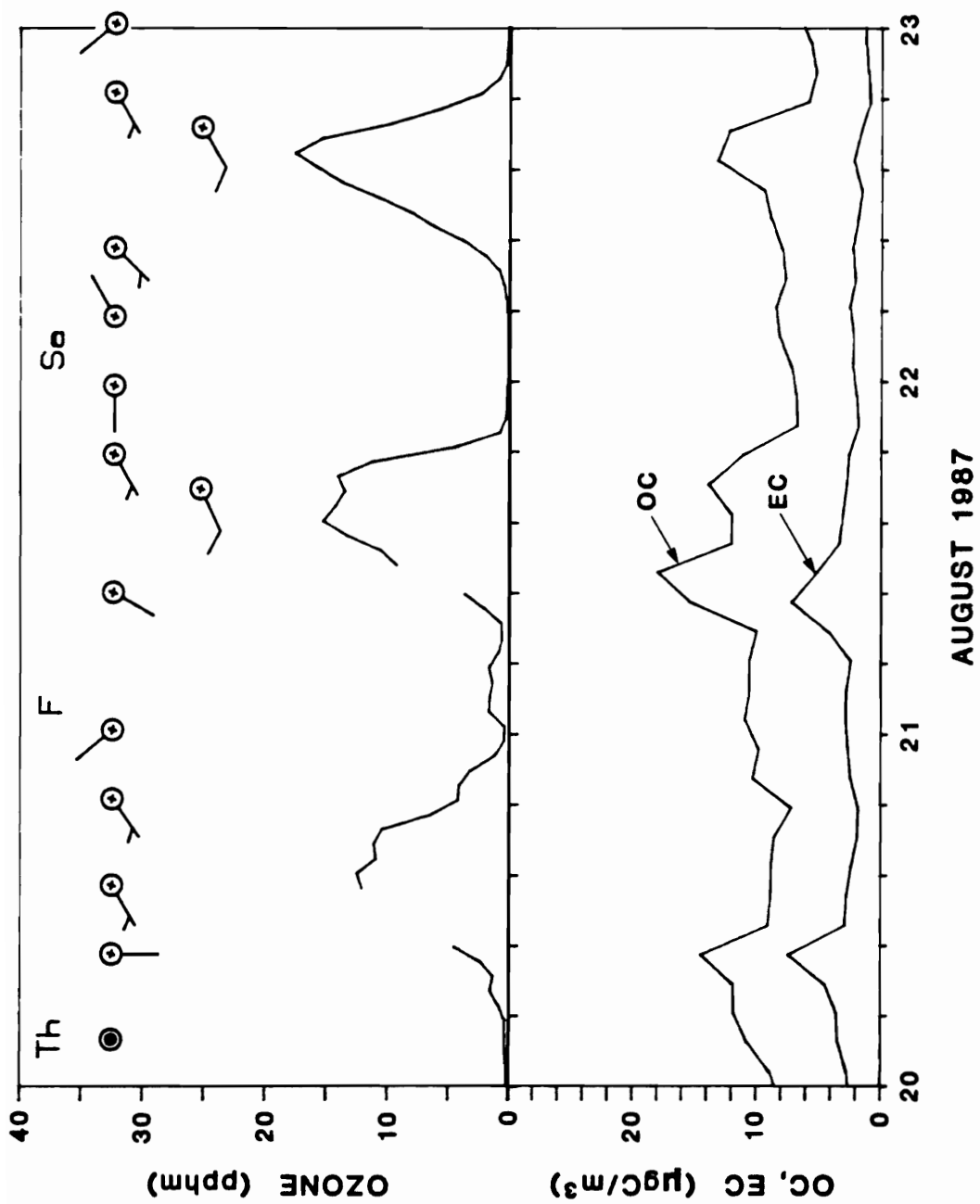


Figure E.20. OC, EC, ozone and meteorological data August 20-22, 1987 in Claremont, California.

FIGURE E.21

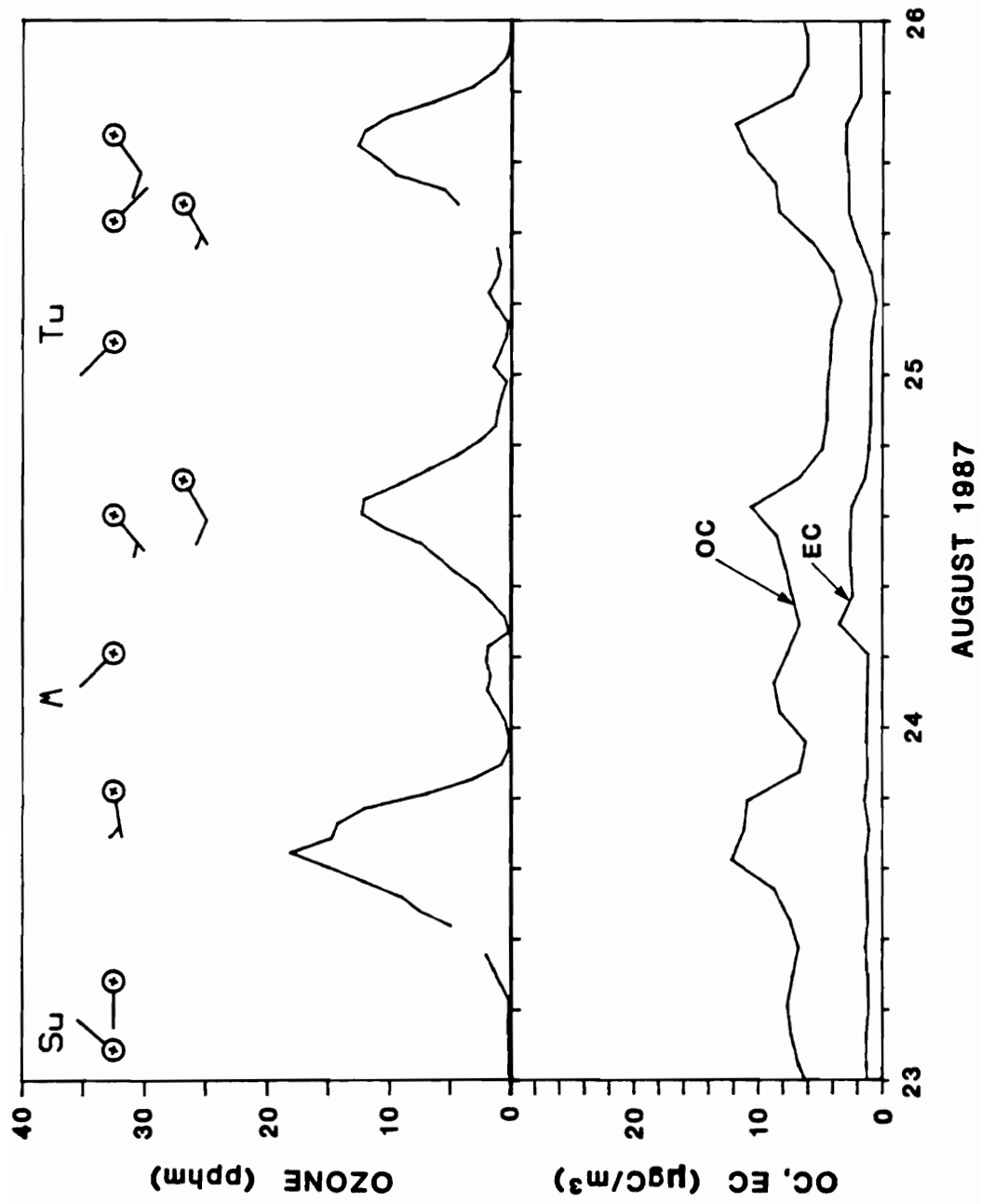


Figure E.21. OC, EC, ozone and meteorological data August 23-25, 1987 in Claremont, California.

FIGURE E.22

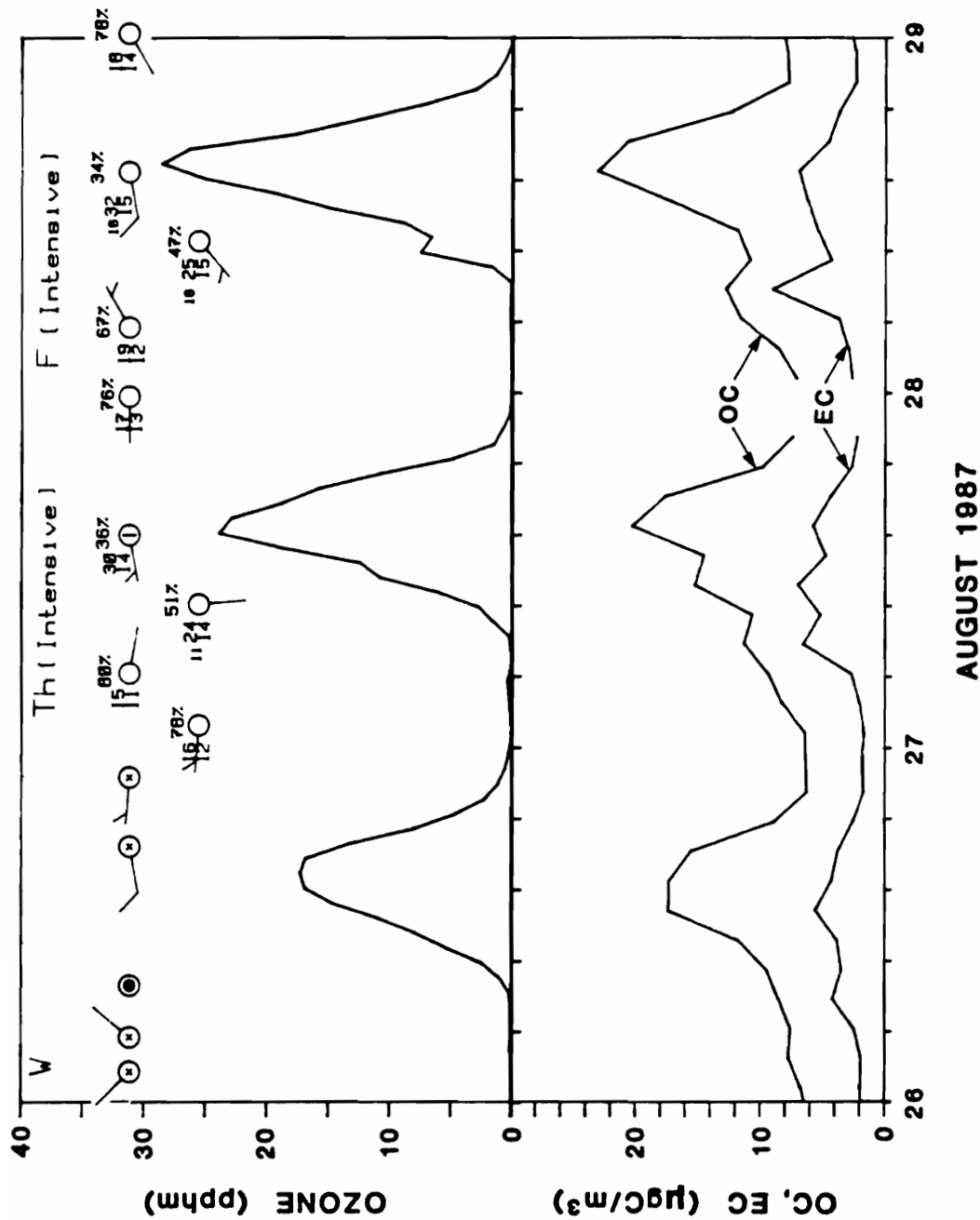


Figure E.22. OC, EC, ozone and meteorological data August 26-28, 1987 in Claremont, California.

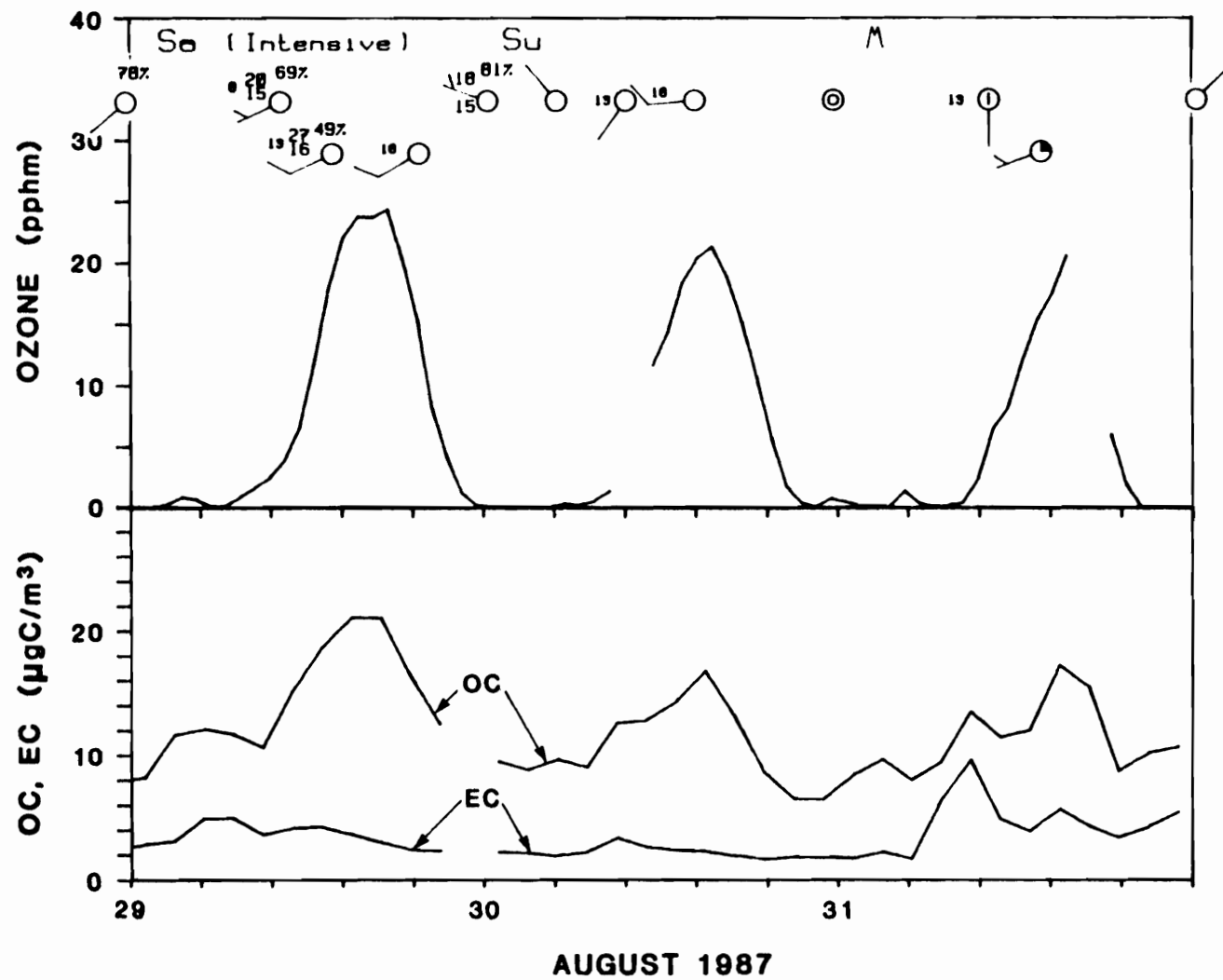


Figure E.23. OC, EC, ozone and meteorological data August 29-31, 1987 in Claremont, California.

FIGURE E.23

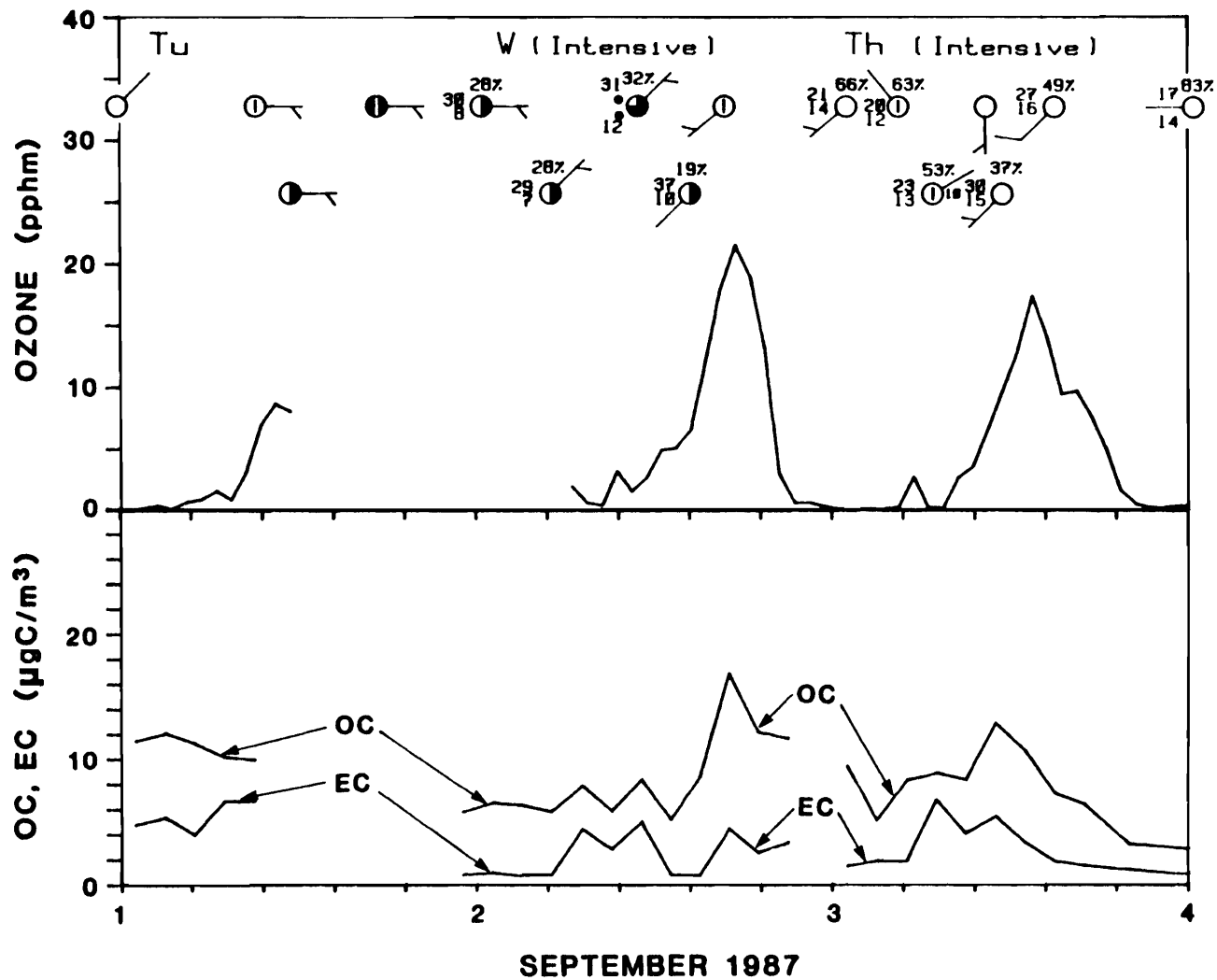


Figure E.24. OC, EC, ozone and meteorological data September 1-3, 1987 in Claremont, California. (Ozone data were not available between 1200 hours, Sept. 1 and 0500 hours, Sept. 2.)

FIGURE E.24

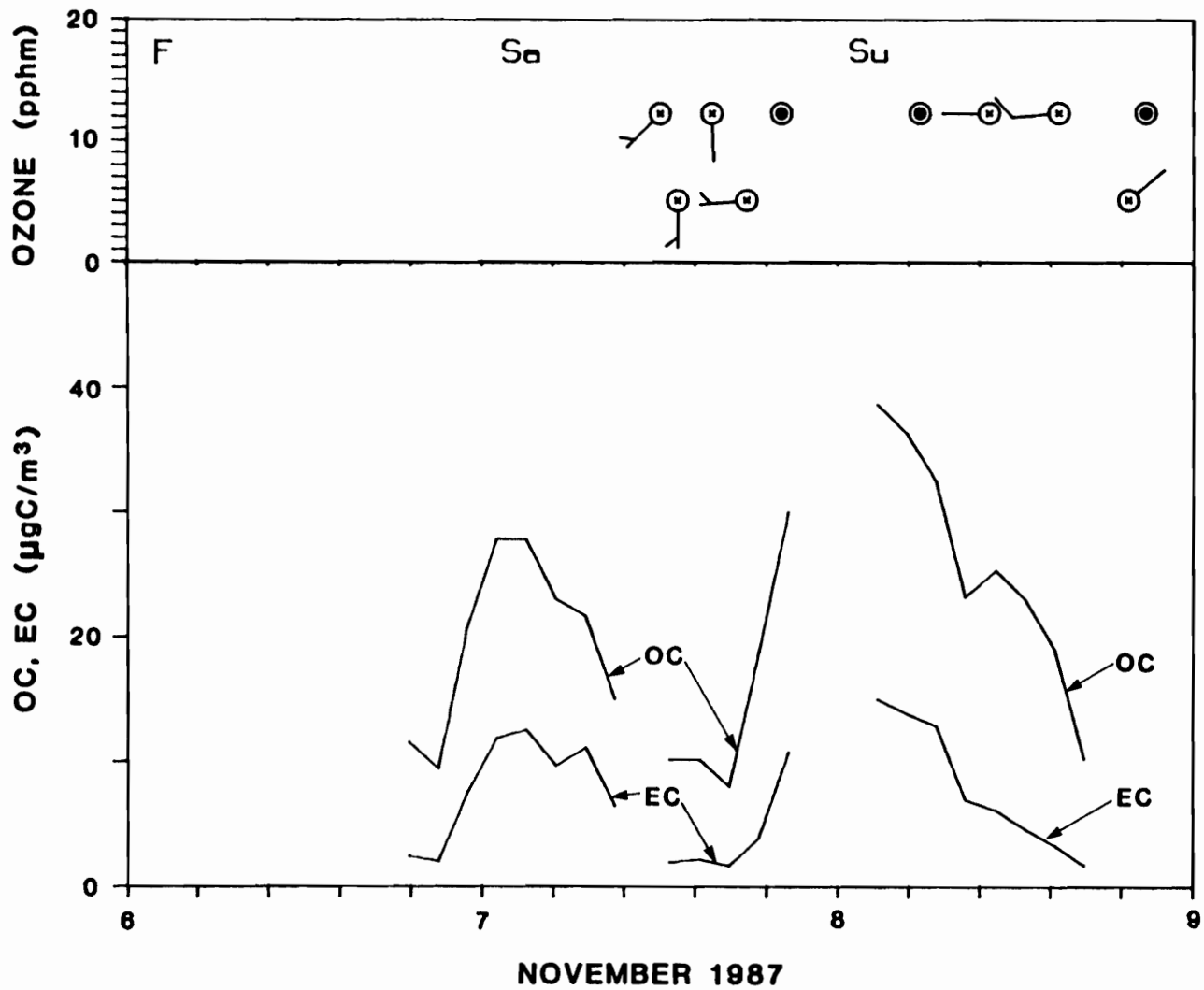


Figure E.25. OC, EC, ozone and meteorological data November 6-8, 1987 in Long Beach, California. (Ozone data were not available during this period.)

FIGURE E.26

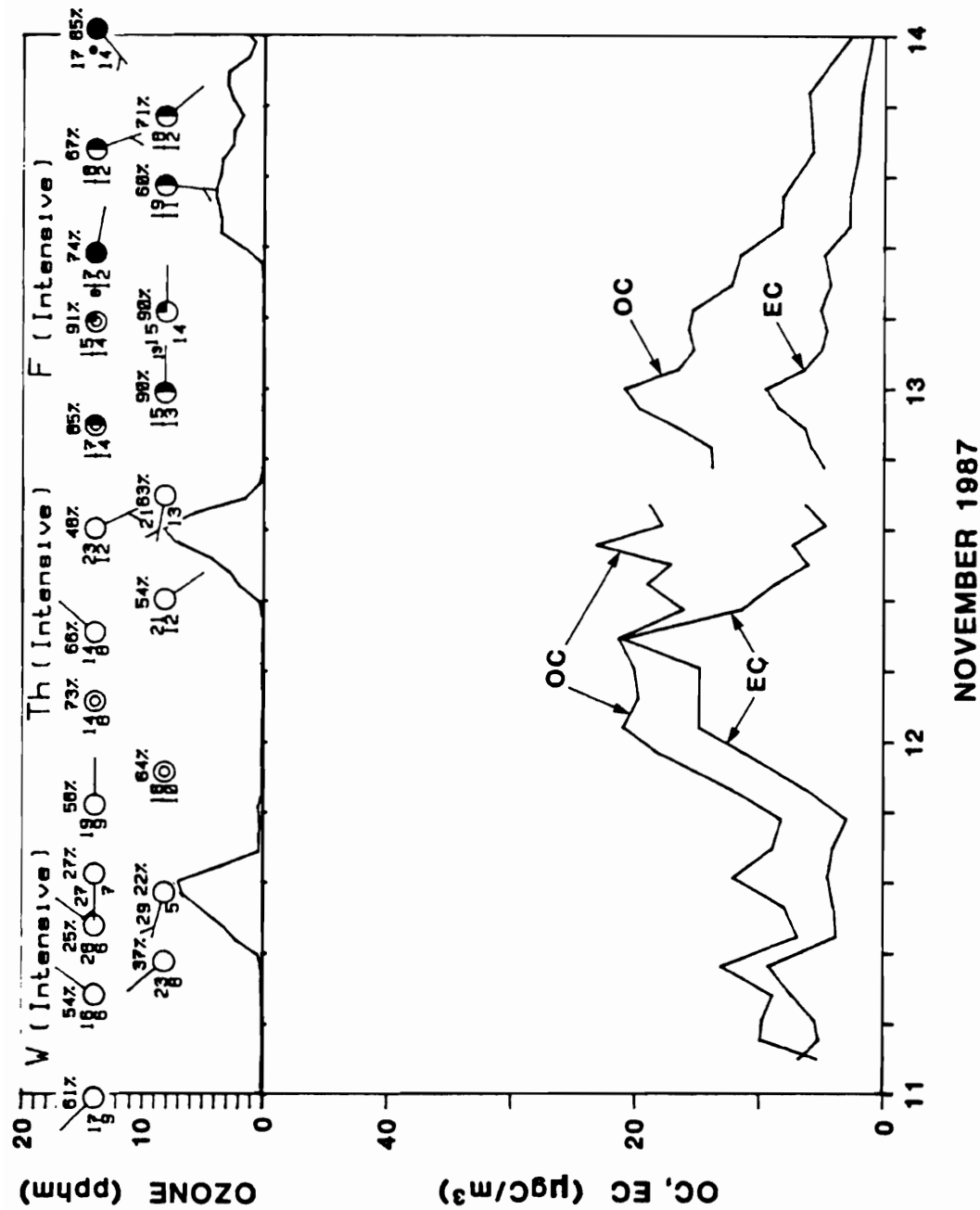


Figure E.26. OC, EC, ozone and meteorological data November 11-13, 1987 in Long Beach, California.

FIGURE E.27

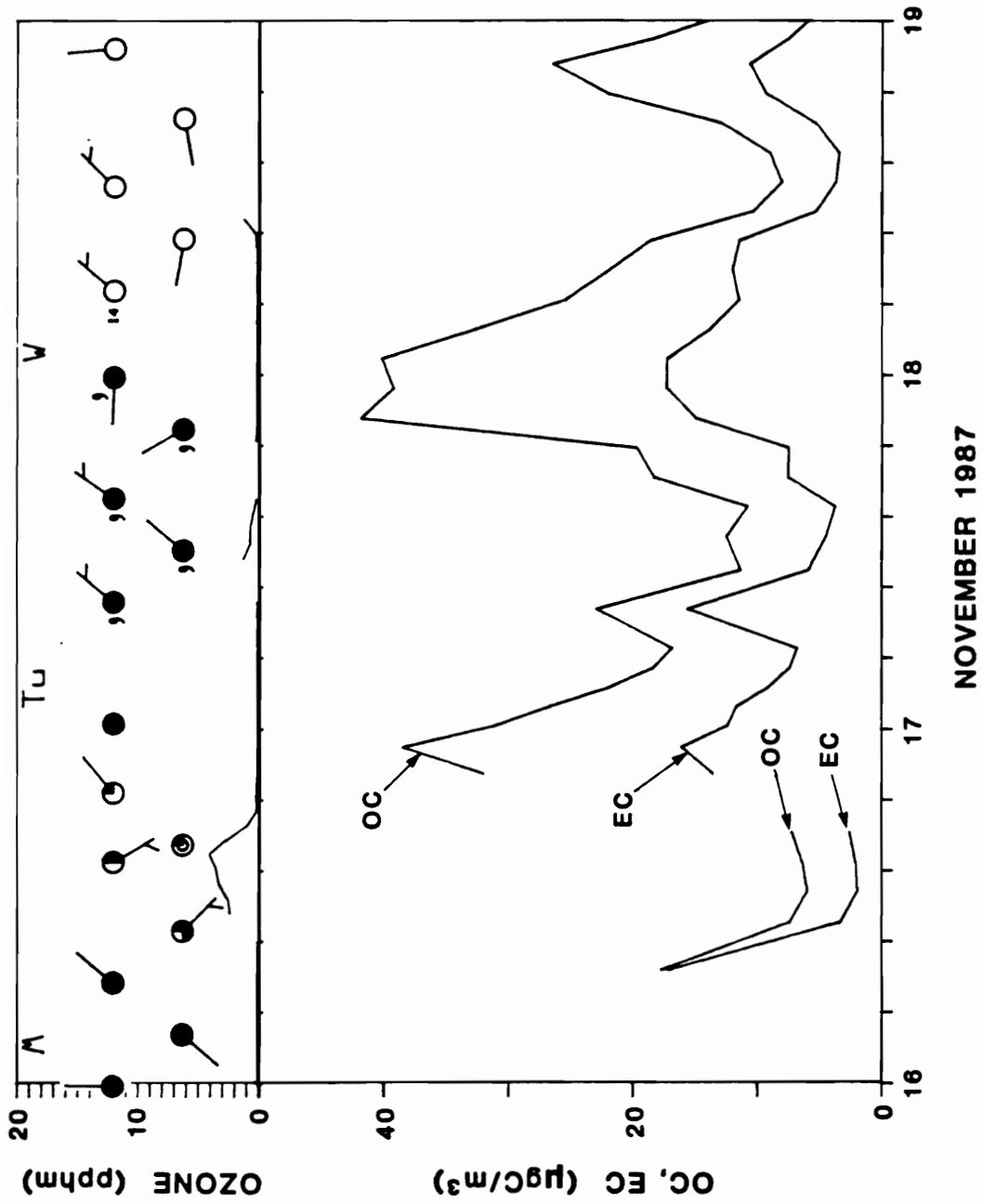


Figure E.27. OC, EC, ozone and meteorological data November 16-18, 1987 in Long Beach, California. (Ozone data were not available between 1300 hours, Nov. 18 and 0000 hours, Nov. 19.)

FIGURE E.28

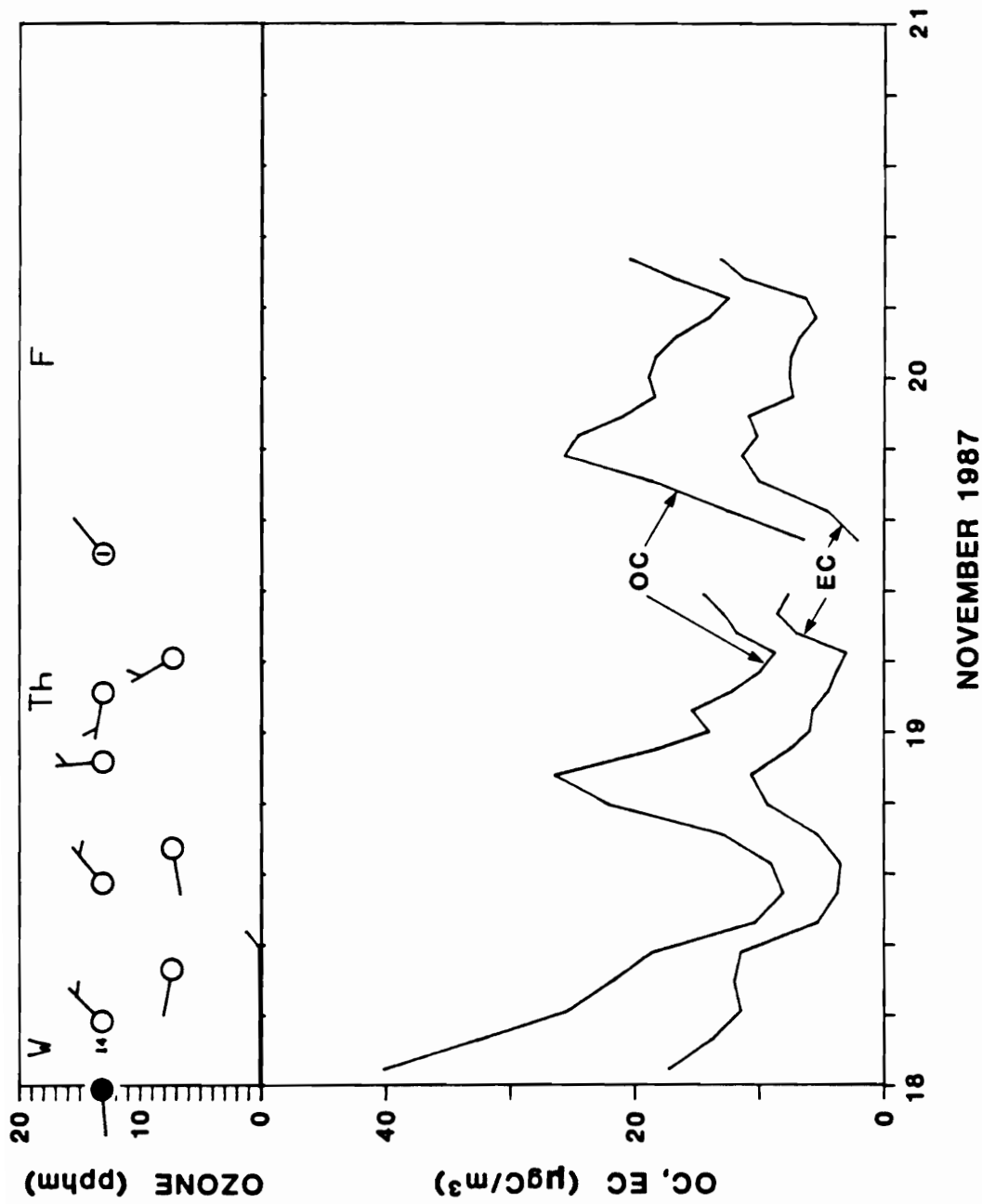
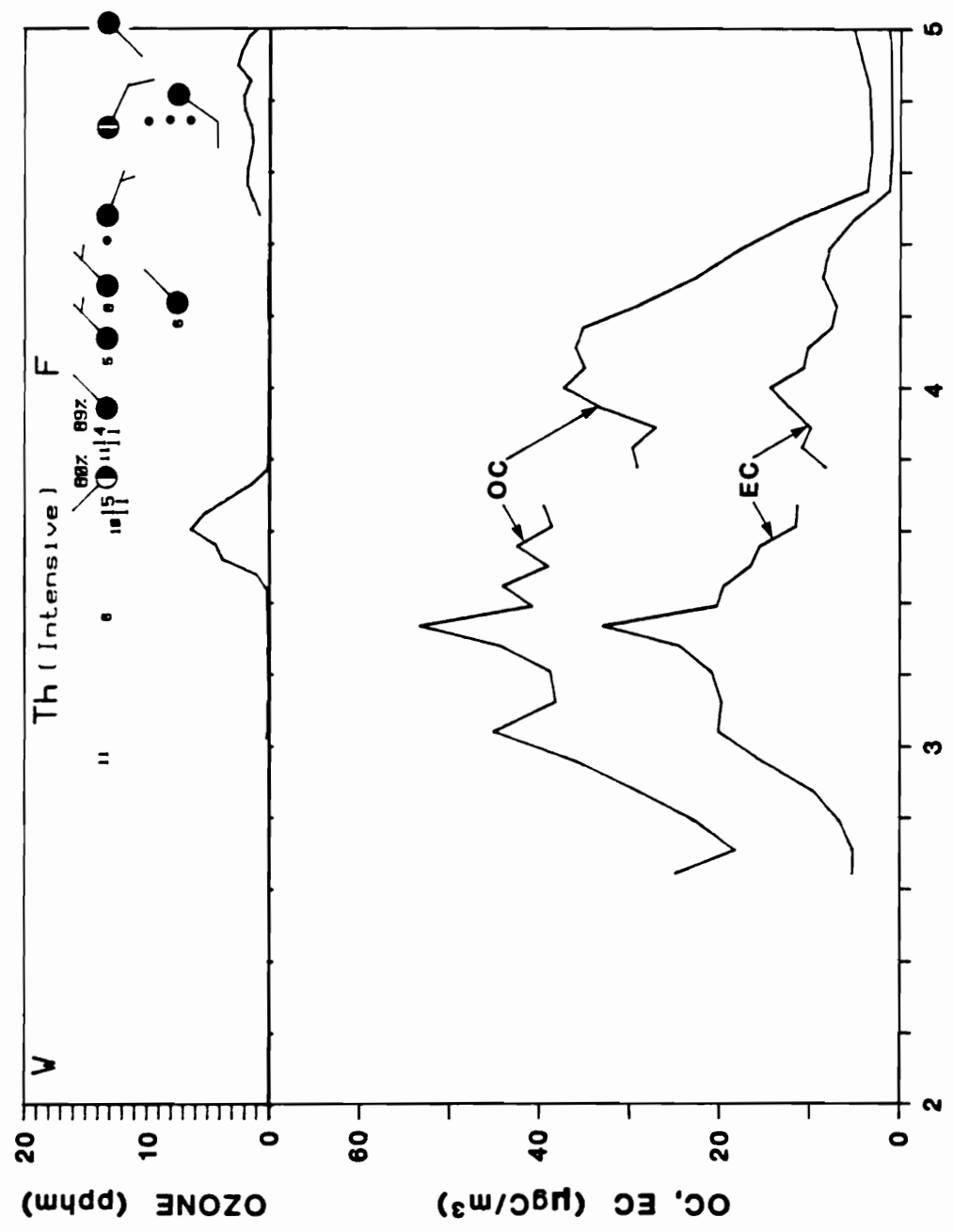


Figure E.28. OC, EC, ozone and meteorological data November 18-20, 1987 in Long Beach, California. (Ozone data were not available between 1300 hours, Nov. 18 and 0000 hours, Nov. 21.)

FIGURE E.29



DECEMBER 1987

Figure E.29. OC, EC, ozone and meteorological data December 2-4, 1987 in Long Beach, California. (Ozone data were not available between 0000 hours and 2300 hours, Dec. 2.)

FIGURE E.30

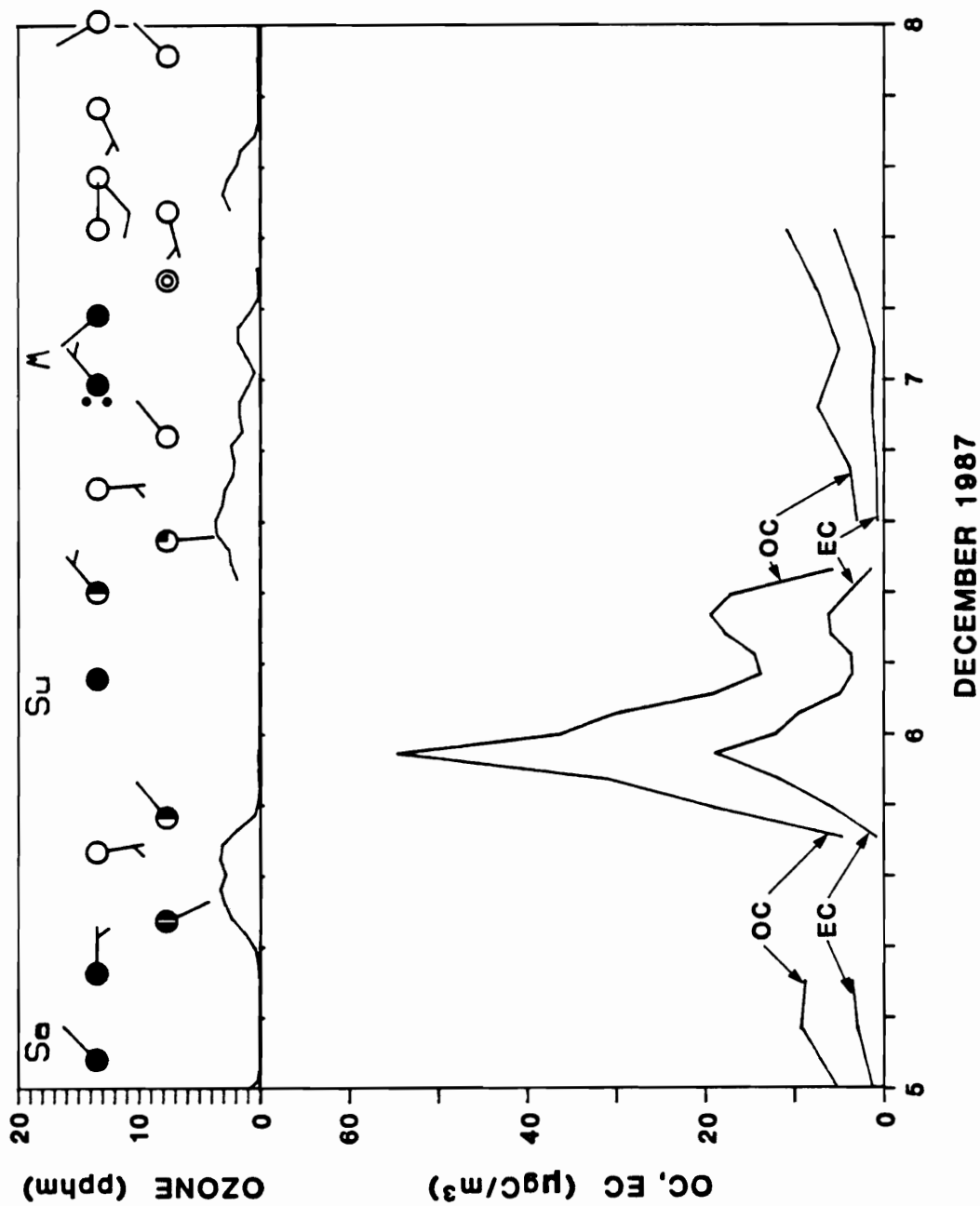
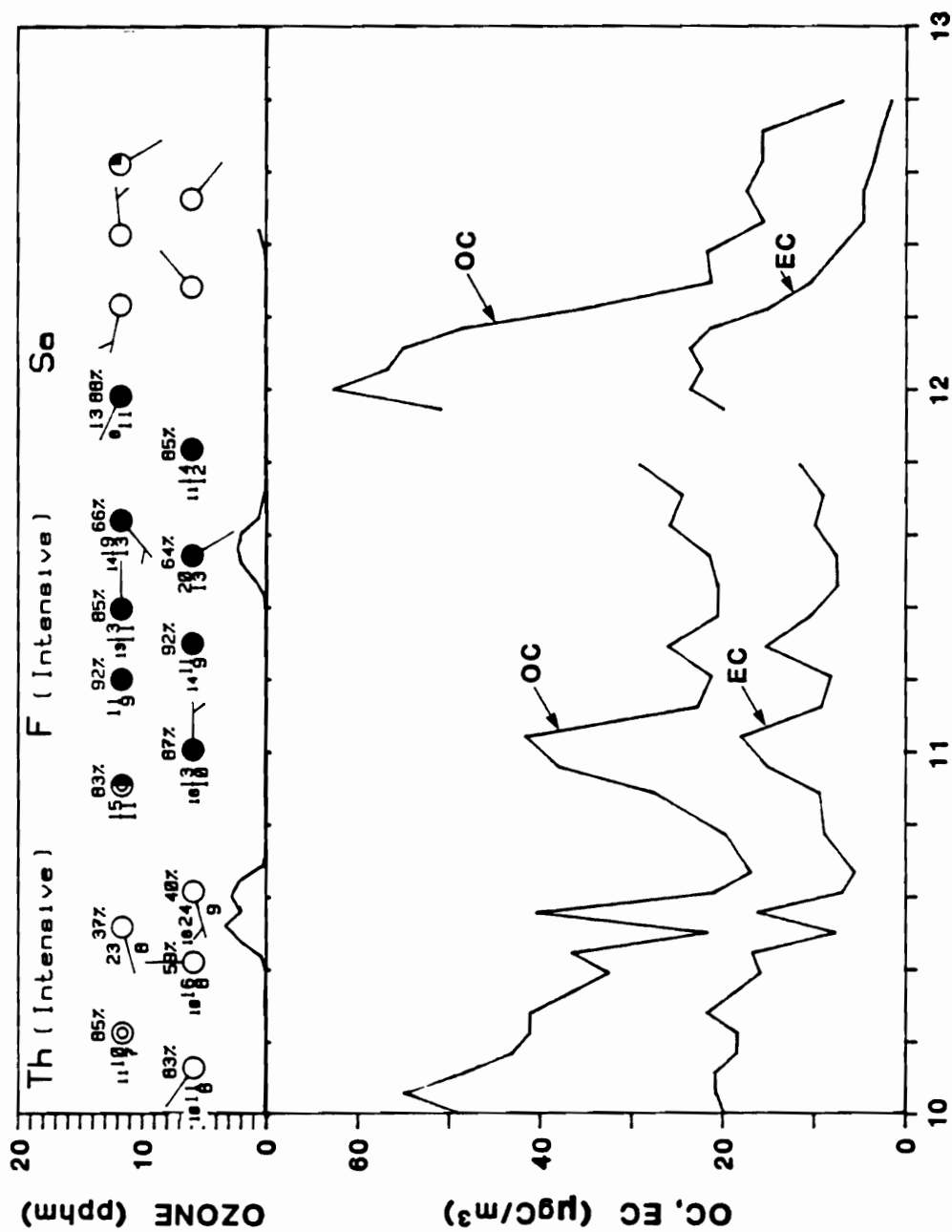


Figure E.30. OC, EC, ozone and meteorological data December 5-7, 1987 in Long Beach, California

FIGURE E.32



DECEMBER 1987

Figure E.32. OC, EC, ozone and meteorological data December 10-12, 1987 in Long Beach, California. (Ozone data were not available between 1100 hours, Dec. 12 and 0000 hours, Dec. 13.)

BIOGRAPHICAL NOTE

The author was born 30 September 1962, in San Diego, California. In 1964 she moved to Washington State, and she lived in Lakota Beach, Washington from 1967 to 1980. She graduated from the Annie Wright School in Tacoma and received her Bachelor of Science at the California Institute of Technology in June 1984. While an undergraduate, the author received a Beckman Internship to work one summer for the Secretary of State of Washington State and a Student Undergraduate Research Fellowship for work she conducted in Southwest Africa/Namibia. She conducted air pollution research in the laboratory of Dr. Glen Cass in 1984. Upon graduation she received a graduate scholarship from the College Women's Club of Pasadena.

The author came to the Oregon Graduate Center in September 1984 and completed the requirements for the degree Doctor of Philosophy in June 1989. She was the teaching assistant for a course in atmospheric chemistry and physics in 1985, and in 1986 she received a Northwest Air Pollution Control Association Scholarship. She participated in the Carbonaceous Species Methods Comparison Study and the Southern California Air Quality Study in the process of conducting her research.

The author is married to David C. Younge, a musician and writer, and she has competed in the World Championships and the World University Games as a member of the United States fencing team.

She will remain at the Oregon Graduate Center with a postdoctoral position.

PUBLICATIONS

Hering, S. V., Appel, B. R., Cheng, W., Salaymeh, F., Cadle, S. H., Mulawa, P. A., Cahill, T. A., Eldred, R. A., Surovik, M., Fitz, D., Howes, F. E., Knapp, K. T., Stockburger, L., Turpin, B. J., Huntzicker, J. J., Zhang, X. -Q., and McMurry, P. H. "Comparison of Sampling Methods for Carbonaceous Aerosols in Ambient Air", Aerosol Sci. Technol. (in press 1989).

Turpin, B. J., Cary, R. A., and Huntzicker, J. J. "An In Situ, Time-Resolved Analyzer for Aerosol Organic and Elemental Carbon", Aerosol Sci. Technol. (in press 1989).

Turpin, B. J. (1984). "Cross-Cultural Attitudes Toward the Use of Reclaimed Water in SWA-Namibia", Munger Africana Library Notes 72:5-12.

Turpin, B. J., Huntzicker, J. J., and Adams, K. M. "Intercomparison of Photoacoustic and Thermal-Optical Methods for the Measurement of Atmospheric Elemental Carbon", Atmos. Environ. (in press 1989).

Turpin, B. J., and Huntzicker, J. J. (1989). "In Situ Measurement of Aerosol Organic and Elemental Carbon: Southern California Air Quality Study", California Air Resources Board Report, A732-072.

Turpin, B. J., Huntzicker, J. J., Larson, S. M., and Cass, G. R. "An Investigation of Los Angeles Mid-Day Particulate Carbon" (in preparation 1989).

Turpin, B. J., and Huntzicker, J. J. "Organic Aerosol Sampling Artifacts: A Los Angeles Area Field Study" (in preparation 1989).

Turpin, B. J., and Huntzicker, J. J. (1988). "Sampling and Analysis of Organic Aerosol: Carbonaceous Species Methods Comparison Study", California Air Resources Board Report, A5-149-32.

Turpin, B. J., and Huntzicker, J. J. "Secondary Formation of Organic Aerosol in the Los Angeles Basin: Investigation of the Diurnal Variations of Organic and Elemental Carbon", Proceedings AWMA Annual Meeting, Anaheim, California, June 1989, paper 89-153.3 (in preparation for Atmos. Environ. 1989).